

ADVANCING TOWARDS BIOMASS-DERIVED SYNGAS FERMENTATION

EVALUATION OF PROCESS PARAMETERS AND GAS COMPOSITION EFFECTS

Zur Erlangung des akademischen Grades einer
DOKTORIN DER INGENIEURWISSENSCHAFTEN (DR.-ING.)

von der KIT-Fakultät für Chemieingenieurwesen und Verfahrenstechnik des
Karlsruher Instituts für Technologie (KIT)

genehmigte

DISSERTATION

von

M. Sc Alba Infantes-López
aus Mataró (Barcelona), Spain

Tag der mündlichen Prüfung: 14.08.2020

Erstgutachter: Prof. Dr. Christoph Syldatk

Zweitgutachter: Prof. Dr. Nicolaus Dahmen

Zweitgutachterin: Dr. Anke Neumann



This document is licensed under a Creative Commons Attribution-ShareAlike 4.0 International License (CC BY-SA 4.0): <https://creativecommons.org/licenses/by-sa/4.0/deed.en>

“Le rêve c’est tout – la technique, ça s’apprend.”

Dreams are everything, technique can be learned.

Jean Tinguely

PREAMBLE

Parts of this thesis have been published as peer reviewed research articles. They describe the main findings of my work. At the end of any applicable paragraph a reference note states the publication in which the content has been previously published. The text of these paragraphs is partially identical to the content of the publications. Layout, citation style, figures and formatting have been modified and adjusted to the style of this dissertation. Chapters that contain contents of previously published work are as follows:

Chapters with the heading “General procedures for STR experiments”, “Impact of medium components and process parameters”, the discussion and the conclusion include content of the publication

Infantes, A., Kugel, M., and Neumann, A. (2020). Evaluation of media components and process parameters in a sensitive and robust fed-batch syngas fermentation system with *Clostridium ljungdahlii*. *Fermentation*. 6(2), 61. DOI: 10.3390/fermentation6020061.

Chapters with the heading “Evaluation of beech wood and lignin derived syngas”, the discussion and the conclusion include content of the submitted work for publication

Liakakou, E. T., Infantes, A., Neumann, A., and Vreugdenhil, B. J. (2020). Connecting lignin gasification with syngas fermentation.

Chapters with the heading “Impact of syngas composition and impurities”, the discussion and the conclusion include content of the publication

Infantes, A., Kugel, M., Raffelt, K. and Neumann, A. (2020). Side-by-side comparison of clean and biomass-derived, impurity-containing syngas as substrate for acetogenic fermentation with *Clostridium ljungdahlii*. *Fermentation*. 6(3), 84. DOI: 10.3390/fermentation6030084.

Chapters with the heading “Sequential cultivation for acetogenic fermentation from oxygen-containing waste gas” include content of the publication

Mohr, T., Infantes, A., Biebinger, L., de Maayer, P., and Neumann, A. (2019). Acetogenic Fermentation From Oxygen Containing Waste Gas. *Front. Bioeng. Biotechnol.* 7, 433. DOI:10.3389/fbioe.2019.00433.

ACKNOWLEDGMENTS

I would like to thank all those who have contributed towards the realization of this doctoral thesis.

I especially, and sincerely thank Prof. Dr. Christoph Syldatk for giving me the opportunity to work and pursue my research at his group. To my supervisor Dr. Anke Neumann, thanks for the incredible support you have given me through my years at TeBi. Thanks for the constructive critics and ideas, and for the uncountable times we discussed together – you always helped me look at my results with a better light.

I want to thank all students who worked with my and supported my research. You have all played a very important part on my thesis, and from each of you, I learned something. They are: Phillip Lemke, Nahla Isso and Laura Merker: thanks for your positivism and involvement; Karoline Haack and Laura Herrmann, a huge thank you to both for your commitment, organization and extremely professional approach to the experiments. Jennifer Reichert, thanks so much for helping with the analytics! Lars Biebinger, I thank the half of you I supervised for your contribution towards our shared paper! It was a pleasure working with you. To Lorenzo Wormer, I will be forever grateful for the amount of effort you put towards your Bachelor thesis. Thanks for your commitment, even when not everything went smooth. Last, but not least, Ana B. Torres Martínez: Santificado sea el Infors! Millones de gracias por estar ahí. Thanks for infusing good mood! And for our Mexican Spanish – European Spanish discussions, I will always remember this!

To all my PhD colleagues at TeBi, past and present: You are truly the best people one could wish to be surrounded while pursuing a PhD. Special mention must be made to the members of our beloved Mädchenbüro: Olga, thanks for always listening when I needed someone to talk to. Rebecca, thanks for your authenticity! You never failed to make me smile! Caro, thanks for your valuable comments and advice, and for being my thesis mentor! Fei, you are a fountain of positivism! Also: Marcus, sin ti hubiera olvidado mi español. Gracias por estar siempre ahí!

Stefan, Olli and Sascha: thanks for making me feel so welcome, and thanks for introducing me to TeBi and PhD student life!

To the technicians team, past and present: Laura, Pascal, Delphine, Sandra, Elke and Daniela: thanks for taking care of the equipment, thanks for your support, and for teaching me. To Michaela: I could not have done this thesis without you. Thanks for the invaluable support, for making sure the fermenters were always in shape, for all your pieces of advice, and for answering all my questions.

To Habibu, Katrin, Jens and Ulrike: I hugely appreciate the discussions we have had, and all your contributions during these years. Thanks for challenging my assumptions, and questioning my theories, you made a better scientist of me!

To Beate and Susanne: thanks for being there, for always being ready to help and give advice, and for the nice conversations we have had.

Finalment, he d'agrair a tots els de Mataró (i rodalies) per creure en mi, per aguantar-me durant aquests anys de doctorat, i per fer-me sentir sempre a casa: gràcies per ser-hi!

Lluc: gràcies per acompanyar-me, sempre i en tot. Ets el pilar que m'ha sostingut tantes vegades.

A mi familia: os lo debo todo.

LIST OF PUBLICATIONS

Peer reviewed original research papers

Mohr, T.*, **Infantes, A. ***, Biebinger, L., de Maayer, P., and Neumann, A. (2019). Acetogenic Fermentation From Oxygen Containing Waste Gas. *Front. Bioeng. Biotechnol.* 7, 433. DOI:10.3389/fbioe.2019.00433

***Co-first authorship**

Infantes, A., Kugel, M., and Neumann, A. (2020). Evaluation of media components and process parameters in a sensitive and robust fed-batch syngas fermentation system with *Clostridium ljungdahlii*. *Fermentation*. 6(2), 61. DOI: 10.3390/fermentation6020061

Infantes, A., Kugel, M., Raffelt, K., and Neumann, A. (2020). Side-by-side comparison of clean and biomass-derived, impurity-containing syngas as substrate for acetogenic fermentation with *Clostridium ljungdahlii*. *Fermentation*. 6(3), 84. DOI: 10.3390/fermentation6030084

Liakakou, E. T.*, **Infantes, A.***, Neumann, A., Vreugdenhil, B. J., and Liakakou, E. T. Connecting lignin gasification with syngas fermentation. PREPRINT DOI: 10.31224/osf.io/9f5pj
Submitted for publication (2020)

***Co-first authorship**

Conference Talk

Infantes, A., Neumann, A. (2019). Syngas Fermentation. EUBCE Workshop, Advanced biofuel production with energy system integration. EUBCE 2019, 27th European Biomass Conference & Exhibition

Conference Posters

Infantes A., Merker L., Reichart, J., Syldatk C. and Neumann A. Combining ABE and syngas fermentations for biobased fuels and chemicals. Annual Conference 2018 of the Association for General and Applied Microbiology (VAAM Jahrestagung)

Infantes, A., Zwick, M., Stoll, I. K., Boukis, N., Oswald, F. and Neumann, A. Syngas Fermentation at Elevated Pressure. ProcessNet-Jahrestagung und 33. DECHEMA-Jahrestagung der Biotechnologen 2018. DOI: 10.1002/cite.201855330

Infantes A., Zwick M., Herrmann L., Torres A., Syldatk C. and Neumann A. Evaluation of “Impure” Syngas from the Karlsruhe Bioliq® Plant and Other Sources as Substrate in Syngas Fermentation. C1net Conference 4, 2019

Infantes, A., Wormer, L. and Neumann, A. Effect of CO or syngas overpressure on growth and product formation of *Clostridium ljungdahlii*. Annual Conference 2019 of the Association for General and Applied Microbiology (VAAM Jahrestagung)

Infantes A., Kugel M., Neumann, A. Evaluation of “Impure” Syngas derived from Biomass Gasification as Substrate for Syngas Fermentation. Annual Conference 2020 of the Association for General and Applied Microbiology (VAAM Jahrestagung)

ABSTRACT

The need for renewed efforts to transition from a petroleum-based economy towards a more bio-based economy is becoming ever more evident. If fossil resources continue to be the main source of fuel and bulk chemicals, it will become increasingly difficult to tackle problems such as climate change. In order to achieve a long-term sustainable development, renewable energy and biomass sources need to be the focus of research efforts. Biomass from renewable or waste sources can be gasified to generate syngas, which is mainly composed of H₂, CO₂ and CO. Impurities can be present, and will depend on the gasification technology used and the source of the biomass. Syngas, as well as CO-rich gases, can also be a by-product of industrial processes, like steel-mills. A highly specialized group of anaerobic, autotrophic bacteria, known as acetogens, can use these gases as fermentation substrate. The syngas is metabolized via the reductive acetyl-CoA pathway, also known as Wood-Ljungdahl pathway. In this work, *Clostridium ljungdahlii* was the organism of choice, since it is considered a model acetogen, is widely studied and well-characterized. The carbon in the gaseous substrate is fixed into acetate and ethanol, in the case of *C. ljungdahlii*, but other products like butyrate or 2,3-butanediol can be produced with different organisms. These can be used as renewable bulk chemicals and commodities in present value-added chains. Therefore, the fermentation of industrial waste gases turns otherwise worthless side-products into worthy substrates, as well as helping reduce the amount of CO₂ released into the atmosphere. Biomass gasification coupled with syngas fermentation technology allows to overcome the food versus fuel dilemma, since lignin-containing waste can be used and the lignocellulosic components will also be converted. Furthermore, even if syngas has been used in chemical processes like Fischer-Tropsch (FT) for decades, bacteria are much more tolerant to varying ratios of CO/H₂ and impurities, and the conversion conditions are much milder, and thus can be more energy-efficient compared to the high pressures (up to 300 bar) and temperatures (up to 350 °C) needed for the FT process.

Firstly, for syngas fermentation to be successful as a widespread technology, it needs to be optimized and its economic and bioenergetic constraints need to be addressed. A deep understanding of which parameters play a significant role in the fermentation outcome is needed. Some factors that can impact the productivity and product ratios are the availability of the substrate, which is influenced by the gas flow, the availability of nutrients in the medium, the pH and the temperature. These parameters were tested in this thesis in a bench-top, stirred tank reactor (STR), in fed-batch operation. The focus was the effect of supplementing the medium with higher amounts of yeast extract and cysteine, decreasing the pH, and a combination of lower pH and lower gas flow. The results are presented in chapter 4.1. After achieving maximum substrate consumption, the culture inevitably

collapses, with H₂ consumption coming to a halt, and eventually also CO. It could be seen that this was not improved by higher amounts of yeast extract or cysteine, so that a nutrient deficiency could be ruled out as the cause of the culture collapse. The lowering of the pH caused a lowering in the molar acetate to ethanol ratio during the maximum gas consumption phase of the culture. This was not so when the whole run was taken into consideration, since lower pH caused a lower biomass formation overall, resulting in lower productivities and titers. The combination of lower pH and gas flow produced the highest ethanol to acetate ratio, 0.25 mol of ethanol per mol of acetate, almost doubling that of the control, although at the expense of the lowest productivity, 0.12 g/L·h. The fermentation system used proved to be a valuable tool for screening purposes, since it could successfully detect not only differences in product formation, but also small variations in gas consumption.

Secondly, for the integration of biomass gasification and syngas fermentation technology, the tolerance towards impurities needs to be studied in detail to determine which level of syngas cleaning is needed for the process to be viable, while avoiding excessive costs. The combined effect of different syngas compositions and its impurities must be accounted for as well. Despite this being widely acknowledged, most of the studies found in literature are focused on clean, impurity-free syngas, or examine one single inhibitory compound at a time. Having established that the fermentation system here presented is a robust screening tool, different biomass-derived syngases were examined. This is presented in chapters 4.2 and 4.3 of this work. In cooperation with Prof. Dr. Nicolaus Dahmen, syngas from the gasification of straw at the Bioliq[®] plant at the KIT, Karlsruhe, was fermented at two different gas flows. Within the framework of Ambition, a Horizon2020 Project, and in cooperation with TNO Energy Transition, Biomass & Energy Efficiency Unit, Petten, the Netherlands, two further biomass-derived syngases were tested, one obtained from the gasification of beech wood, and the second, from gasified lignin. For each biomass-derived syngas, the same conditions were used to test an impurity-free syngas of the same composition. The performance of these fermentations, in terms of growth, product formation and gas consumption were compared. Additionally, four other clean syngas compositions were evaluated as fermentation substrates. From those, two of them were based on the syngas composition obtained at the gasification plant of ENEA (Italian National Agency for New Technologies, Energy and Sustainable Economic Development), Research Centre of Trisaia, Italy; and LNEG (National Laboratory of Energy and Geology), Amadora, Portugal. The systematic, side-by-side comparison of the biomass-derived, and the commercial, impurity-free syngases highlighted the complex synergistic effects at play. If only the gas composition is considered, the results cannot replicate what is seen with real, biomass-derived syngases: the presence of impurities had a greater impact on the fermentation than the gas composition. In all cases, when impurities were present, lower productivities were achieved, but the acetate to ethanol molar ratio decreased, signaling a shift

towards a higher ethanol production. No growth inhibition was observed with any biomass-derived syngas, even if the maximum biomass concentration achieved tended to be slightly lower than with impurity-free syngas. Again, this STR fermentation system was found to be a successful screening tool for a first evaluation of biomass-derived syngases. A general overview for all fermentations of the substrate usage and fixation ratios, as well as a comparison between the maximum theoretical amount of acetate and the amount produced is given in chapter 4.4.

A further constraint of syngas fermentation technology is the limitation posed by the low biomass concentration and productivities that can be achieved. Due to the gaseous nature of the substrate, its availability is constrained by the gas-liquid mass-transfer limitation of the poorly soluble CO and H₂. In an STR configuration, the volumetric power input needed to increase the gas-liquid mass transfer is deemed too high for industrial applications, and other configurations, like bubble columns or gas-lift reactors are preferred. With those systems, the liquid height needed at industrial scale will cause the hydrostatic pressure to increase, and thus the solubility of the gases is enhanced. In chapter 4.5 of this thesis, the effect of increased pressures of syngas, CO₂/H₂ and pure CO on growth and product formation on *C. ljungdahlii* was investigated, using a batch system. Besides, changes in the relative gene expression were analyzed using qPCR for the CO₂/H₂ cultures, to assess whether pressure had an impact in the transcriptional regulation of the cells. The cultivation system was improved and adapted to higher pressures by testing different pressure-resistant cultivation vessels: stainless-steel bottles, and glass tubes incorporating a mounted gauge. With these, experiments with pressures up to 5 bar (absolute) could be performed. With increasing syngas pressure, increasingly high maximum biomass concentrations were achieved, although a lag-phase was observed for all pressures above 1 bar (absolute). The biomass concentration decreased towards the end, and the end biomass concentration was equivalent in all cases. A slight increment in the final acetate concentration of 1 g/L at 1.5 bar and 2.5 bar, and 2 g/L at 2 bar was observed when compared to 1 bar, where 11 g/L were measured. Ethanol, contrarily, decreased from 2.6 g/L at 1 bar to 0.9 – 1.1 g/L at increased pressures. When exposed to CO₂/H₂ at 5 bar, the culture did not grow, and its acetate production was reduced a 54 % when compared to 1 bar. On pure CO, both cultures performed nearly identically: neither the culture at 1 bar nor the one at 5 bar showed any growth, and only a very limited acetate production of 2.7 g/L was detected. Regarding gene expression, no significant changes were observed, indicating that, under the pressure tested, the regulation of gene expression of *C. ljungdahlii* is equivalent to that of atmospheric pressure.

Finally, due to the anaerobic nature of *C. ljungdahlii*, a potential contamination of the syngas with oxygen will have an inhibitory effect, with the subsequent negative impact on the process. In chapter 4.6, and as a joint project with Dr. Teresa Mohr, a sequential culture approach was deployed

to enable acetogenic fermentation on oxygen-containing waste gases. *Parageobacillus thermoglucosidasius*, a facultative anaerobic thermophile, was used to remove the oxygen from a 50 % air/50 % CO mixture. When both O₂ and CO were consumed, the headspace consisted of mainly H₂ and CO₂, with leftover N₂. *C. ljungdahlii* was subsequently inoculated, obtaining 0.52 mmol of acetate, which corresponds to 63 % of the theoretical maximum, considering the initial amount of CO.

As a final overview, the following topics were investigated on this thesis:

- Evaluation of a fed-batch system for the study of media and process parameters influence on syngas fermentation.
- Effect of biomass-derived syngas containing impurities and various gas compositions on growth and product formation of *C. ljungdahlii*.
- Impact of increased substrate pressure on batch cultures of *C. ljungdahlii*, and effect on gene expression.
- Establishment of a sequential cultivation for acetogenic fermentation following oxygen removal.

ZUSAMMENFASSUNG

Die Notwendigkeit des Übergangs von einer erdölbasierten Wirtschaft hin zu einer biobasierten Wirtschaft wird immer deutlicher. Das Beibehalten fossiler Rohstoffe als Hauptquelle für Chemikalien und Treibstoffe wird die Lösung von Problemen, wie dem menschengemachten Klimawandel, immer schwieriger gestalten. Um eine langfristige, umweltfreundliche Entwicklung zu gewährleisten, müssen erneuerbare Energie- und Biomassequellen im Mittelpunkt der Forschung stehen. Biomasse aus Müll oder nachwachsende Ressourcen kann zu Synthesegas vergast werden, welches sich hauptsächlich aus H_2 , CO_2 und CO zusammensetzt. Ebenfalls entstehende Verunreinigungen sind abhängig von der verwendeten Vergasungstechnik und der eingesetzten Biomasse. Synthesegas und andere CO -reiche Gase können auch als Nebenprodukt in der Industrie, wie zum Beispiel bei Stahlwerken, anfallen. Eine hochspezialisierte Gruppe von anaeroben, autotrophen Bakterien, bekannt als Acetogene, kann die beschriebenen Gase als Substrat für Fermentationen verwenden. In ihnen wird Synthesegas im Verlauf des reduktiven Acetyl-CoA Wegs, auch als Wood-Ljungdahl Weg bekannt, metabolisiert. Als gut erforschter und charakterisierter Modell-Acetogener wurde *Clostridium ljungdahli* für die vorliegende Arbeit als Organismus ausgewählt. *Clostridium ljungdahli* fixiert den im Substrat enthaltene Kohlenstoff in Form von Acetat und Ethanol. Mit anderen Organismen können jedoch auch andere Produkte wie Butyrate und 2,3-Butadiol erhalten werden. Diese wiederum dienen als Grundchemikalien in aktuellen Wertschöpfungsketten. Damit verwandelt die Fermentation industrieller Abgase wertlose Nebenprodukte in wertvolle Substrate und hilft die Menge des in die Atmosphäre abgegebenen CO_2 zu reduzieren. Die Vergasung von Biomasse in Kopplung mit einer Synthesegasfermentation bietet eine Möglichkeit die aktuelle „Teller versus Tank“ Debatte zu bewältigen, da Lignin enthaltende Abfälle Verwendung finden und selbst Lignozellulose umgewandelt werden kann. Gegenüber der seit Jahrzehnten erprobten Verwendung von Synthesegas in chemischen Prozessen, wie der Fischer-Tropsch Synthese (FT), sind Bakterien viel toleranter gegenüber Unreinheiten des Substrates. Ebenso findet die Umwandlung, verglichen mit den hohen Drücken (300 bar) und Temperaturen (350 °C) des FT Prozesses, bei mildereren Bedingungen statt und kann damit energieeffizienter sein.

Für den Erfolg der Synthesegasfermentation als weit verbreitete Technologie, muss sie optimiert und ihre ökonomischen und bioenergetischen Begrenzungen evaluiert werden. An erster Stelle wird ein tiefes Verständnis für die den Fermentationsausgang bestimmenden Parameter benötigt. Faktoren, die die Produktivität und die Produktverhältnisse beeinflussen können, sind die Verfügbarkeit des Substrates, welche durch den Gasfluss beeinflusst wird, die Verfügbarkeit von Nährstoffen im Medium, der pH-Wert und die Temperatur. Diese Parameter wurden in der vorliegenden Arbeit in

einem Rührkessel-Tisch-Reaktor Fed-batch Prozess getestet. Das Hauptaugenmerk lag dabei auf dem Erhöhen der Konzentrationen von Hefeextrakt und Cystein im Medium, dem Absenken des pH-Wertes und einer Kombination von gesenktem pH-Wert und reduzierter Gaszufuhr. Die Ergebnisse sind in Kapitel 4.1. nachzulesen. Es stellte sich heraus, dass nach dem Erreichen des maximalen Substratverbrauchs die Kultur unweigerlich kollabierte. Hierbei kam zunächst der H₂-Verbrauch gefolgt vom CO-Verbrauch zum Erliegen. Das Kollabieren konnte auch durch eine erhöhte Gabe von Hefeextrakt oder Cystein weder verhindert noch verzögert werden, womit ein Mangel an Nährstoffen als Grund ausgeschlossen werden kann. Das Absenken des pH-Wertes verringerte das molare Verhältnis von Acetat zu Ethanol während der Phase des maximalen Gasverbrauches der Kultur. Auf den Verlauf der gesamten Fermentation bezogen war dies jedoch nicht der Fall, da der niedrigere pH-Wert ebenfalls zu einer geringeren Biomasseproduktion und damit zu geringerer Produktivität und geringeren Produkttitern führte. Die Kombination von gesenktem pH-Wert und geringerem Gasfluss führte zu dem höchsten Verhältnis von Ethanol zu Acetat mit 0,25 Mol Ethanol pro Mol Acetat, nahezu dem Doppelten in Bezug auf die Kontrolle, jedoch auch zur geringsten Produktivität mit 0,12 g/L·h. Das benutzte Fermentationssystem erwies sich als wertvolles Werkzeug für Screening-Anwendungen, da es nicht nur in der Lage war Änderungen in der Produktbildung, sondern auch Variationen im Gasverbrauch nachzuweisen.

Der nächste Schritt für eine Kopplung von Biomassevergasung und Synthesegasfermentation ist die Bestimmung der Toleranz der verwendeten Mikroorganismen gegenüber Unreinheiten des Synthesegases, um das Ausmaß an benötigten Reinigungsschritten abzuschätzen und dadurch exzessive Kosten zu vermeiden. Hierbei muss auch die Kombination von verschiedenen Synthesegasen und ihren Unreinheiten in Betracht gezogen werden. Trotz Bekanntheit dieser Fakten legen viele Studien ihren Fokus auf reines Synthesegas ohne Unreinheiten, oder einem einzelnen inhibierenden Stoff. Mit dem oben vorgestellten Fermentationssystem als Screening-Methode wurden hier verschiedene, aus Biomasse gewonnene Synthesegase, getestet. Dies ist in den Kapiteln 4.2 und 4.3 dieser Arbeit dargestellt. In Kooperation mit Prof. Dr. Nicolaus Dahmen wurde Synthesegas aus der Bioliq-Anlage des KIT in Karlsruhe mit zwei unterschiedlichen Gasflüssen fermentiert. Im Rahmen von Ambition, eines Horizon2020 Projektes, und in Kooperation mit der TNO Energy Transition, Biomass & Energy Efficiency Unit, in Petten in den Niederlanden, wurden zwei weitere Synthesegase aus Buchenholz und Lignin getestet. Als Vergleich zu den aus Biomasse stammenden Synthesegasen, wurden Synthesegase derselben Gaszusammensetzung ohne Unreinheiten verwendet. Zusätzlich wurden vier weitere reine Synthesegaszusammensetzungen evaluiert. Zwei von diesen stammten von der Vergasungsanlage von ENEA (Italian National Agency for New Technologies, Energy and Sustainable Economic Development) im Forschungszentrum von Trisaia in Italien und von der

Vergasungsanlage von LNEG (National Laboratory of Energy and Geology) in Amadora, Portugal. Alle beschriebenen Synthesegase wurden in Fermentationen im Hinblick auf Biomassewachstum, Produktbildung und Gasverbrauch untersucht. Der direkte Vergleich der aus Biomasse stammenden und der kommerziellen, Unreinheit freien Synthesegasen offenbarte komplexe synergistische Effekte. Bei gleicher Gaszusammensetzung ließen sich die reinen Synthesegase nicht mit den aus Biomasse stammenden vergleichen, da die Unreinheiten einen größeren Einfluss auf die Fermentation hatten, als die Gaszusammensetzung. Bei Anwesenheit von Unreinheiten sanken immer sowohl die Produktivität, als auch das Acetat zu Ethanol Verhältnis — ein Zeichen für einen Wechsel zu einer höheren Ethanol Produktion. Keines der aus Biomasse gewonnenen Synthesegase inhibierte das Wachstum der Mikroorganismen, obwohl eine etwas geringere Gesamtbiomasse im Vergleich zu den Unreinheiten-freien Synthesegasen während der Fermentation erzielt wurde. Das verwendete STR Fermentationssystem erwies sich erneut als zuverlässiges Screeningwerkzeug, für eine erste Evaluation von aus Biomasse erzeugten Synthesegasen. Ein allgemeiner Überblick aller Fermentationen inklusive Substratverbrauch- und Fixierungsraten, sowie ein Vergleich der theoretisch berechneten maximalen und der tatsächlich produzierten Acetatmenge ist in Kapitel 4.4 dargestellt.

Ein weiteres Problem der Fermentation von Synthesegas sind die Limitierungen, die durch die geringe mögliche Biomassekonzentration und die geringe Produktivität entstehen. Aufgrund der gasförmigen Natur des Substrates ist dessen Bereitstellung durch den Gas-Flüssig-Massetransfer des schlecht löslichen CO und H₂ begrenzt. Bei einer STR Konfiguration wird die, für eine Erhöhung des Gas-Flüssig-Massetransfers benötigte, volumenbezogener Leistungseintrag für industrielle Anwendungen als zu hoch angesehen, weshalb andere Konfigurationen wie Blasensäulenreaktoren oder Gas-Hub-Reaktoren bevorzugt werden. Der aufgrund der Höhe dieser Systeme im industriellen Maßstab entstehende hydrostatische Druck erhöht hierbei die Löslichkeit der genannten Gase. In Kapitel 4.5 dieser Arbeit wurde der Effekt von gesteigertem Druck von Synthesegas, CO₂/H₂ und reinem CO auf *C. ljungdahlii* in einem Batch-System getestet. Des Weiteren wurden Änderungen in der relativen Genexpression der Kulturen mit CO₂/H₂ via qPCR analysiert, um die Auswirkung des erhöhten Druckes auf die transkriptionelle Regulierung der Zellen zu untersuchen. Das Kultivierungssystem wurde durch Testen verschiedener Reaktionsgefäße, Stahlflaschen und Glasrohre mit einem Manometer, an die hohen Drücke angepasst. In diesem System konnten Drücke bis 5 bar (absolut) getestet werden. Steigender Synthesegasdruck erzielte höhere Biomassekonzentrationen, wobei bei über 1 bar absoluter Druck eine Lag-Phase zu beobachten war. Gegen Ende der Fermentation nahm die Biomassekonzentration wieder ab, sodass am Ende in allen Fällen eine ähnliche Konzentration erreicht wurde. Die Acetatkonzentration stieg von 11 g/L bei 1 bar um 1 g/L bei 1,5 und 2,5 bar und um 2 g/L bei 2 bar. Der Ethanolgehalt fiel gegensätzlich von 2,6 g/L bei 1 bar auf 0,9-1,1 g/L bei erhöhten

Drücken. Bei der Fermentation von CO₂/H₂ wuchs die Kultur bei 5 bar nicht und die Acetat-Produktion war um 54 % gegenüber von 1 bar reduziert. Auf CO wuchs die Kultur sowohl bei 1 bar wie auch bei 5 bar nicht und die Acetatproduktion betrug im Verhältnis geringe 2,6 g/L. Um den Einfluss von Druck auf die Genexpression von *C. ljungdahlii* zu bestimmen, wurde die relative Expression der CO₂/H₂ Kulturen mit qPCR verglichen. In Bezug auf die Genexpression konnten keine signifikanten Unterschiede beobachtet werden, damit kann bei den getesteten Druckverhältnissen von einer dem atmosphärischen Druck äquivalenten Genexpression ausgegangen werden.

Abschließend spielt auch die anaerobe Natur von *C. ljungdahlii* eine Rolle. Eine Kontamination des Synthesegases mit Sauerstoff hat eine hemmende Wirkung auf den Organismus und damit einen negativen Einfluss auf den Prozess. In Kapitel 4.6 und in einem gemeinsamen Projekt mit Dr. Teresa Mohr konnte eine Zwei-Schritt Kultur zur acetogenen Fermentation von Sauerstoff enthaltenden Abgasen entwickelt werden. Im ersten Schritt verbrauchte der fakultativ anaerobe thermophile *Parageobacillus thermoglucosidasius* den Sauerstoff einer Mischung von 50 % Luft/50 % CO, wobei H₂ und CO₂ mit einem Rest N₂ übrigblieben. Hierauf erfolgte die Inokulation von *C. ljungdahlii* wodurch 0,52 mmol Acetat produziert werden konnten. Dies entspricht, auf die Menge des zu Beginn des Prozesses vorhandenen CO, 63 % des theoretischen Maximums.

Insgesamt wurden in der vorliegenden Arbeit folgende Themen untersucht:

- Evaluierung eines Fed-Batch Systems zum Studium des Einflusses von Medien und Prozessparametern auf die Synthesegasfermentation.
- Auswirkung von verschiedenen Unreinheiten aus Biomasse stammender Synthesegase und verschiedener Gaszusammensetzungen auf Wachstum und Produktbildung von *C. ljungdahlii*.
- Auswirkung von erhöhtem Substratdruck auf Batch-Kulturen von *C. ljungdahlii* und deren Genexpression.
- Etablierung einer Zwei-Schritte Kultur zur acetogenen Fermentation mit Sauerstoffentfernung.

TABLE OF CONTENT

Preamble	I
Acknowledgments.....	II
List of publications	IV
Abstract.....	VI
Zusammenfassung	X
Table of content.....	XIV
1 Introduction	1
2 Theoretical background	6
2.1 Acetogenic bacteria	6
2.1.1 The Wood-Ljungdahl pathway and metabolism of acetogens	7
2.1.1.1 Stoichiometry of the WLP	9
2.1.2 Energy conservation and bioenergetics during autotrophic growth.....	9
2.1.3 <i>Clostridium ljungdahlii</i>	11
2.2 Syngas fermentation.....	12
2.2.1 Biomass-derived syngas and the biorefinery concept.....	14
2.2.2 Impact of media components and process parameters.....	15
2.2.3 Impact of syngas composition and impurities	17
2.2.4 Impact of elevated pressure	18
2.2.5 Impact of oxygen and biological oxygen removal.....	19
3 Material and Methods	21
3.1 General procedures for STR experiments.....	21
3.1.1 Microorganism and Medium	21
3.1.2 Fermentation conditions.....	22
3.1.3 Analytical Methods	22
3.1.4 Calculation of product formation parameters using different metrics and at specific phases of the fermentation	23
3.1.5 Carbon balance	26
3.2 Impact of medium components and process parameters.....	26
3.3 Evaluation of beech wood and lignin derived syngas.....	28
3.4 Impact of syngas composition and impurities	28
3.4.1 Gas flow rate setting.....	29
3.5 Impact of elevated pressure	31

3.5.1	Microorganism and media	31
3.5.2	Effect of syngas overpressure	32
3.5.2.1	Experimental setup	32
3.5.2.2	Sample withdrawal, pH, optical density and pressure measurements	33
3.5.2.3	Fructose, acetic acid and ethanol determination	33
3.5.2.4	Headspace gas analysis	34
3.5.3	Effect of CO ₂ /H ₂ and CO overpressure.....	34
3.5.3.1	Experimental setup	34
3.5.3.2	Sample withdrawal, pH, optical density and pressure measurements	35
3.5.3.3	Fructose, acetic acid, ethanol, and formic acid determination	36
3.5.3.4	Specific production rate calculation	36
3.5.3.5	Headspace gas analysis	36
3.5.3.6	Relative quantification of gene expression by RT-qPCR (quantitative reverse transcription PCR)	37
3.6	Sequential cultivation for acetogenic fermentation from oxygen-containing waste gas.....	39
3.6.1	Microorganisms and media	39
3.6.2	Experimental set up	40
3.6.3	Analytical methods	40
4	Results.....	41
4.1	Impact of medium components and process parameters.....	41
4.1.1	Effect of medium components	41
4.1.2	Effect of pH	47
4.1.3	Effect of pH and gas flow	51
4.1.4	Carbon balance	53
4.2	Evaluation of beech wood and lignin derived syngas.....	55
4.2.1	Gas flow rate setting	55
4.2.2	Fermentation of TNO syngas from beech wood.....	55
4.2.2.1	Substrate usage and carbon fixation	55
4.2.2.2	Biomass, product formation, yield and productivity	60
4.2.3	Fermentation of TNO syngas from lignin.....	63
4.2.3.1	Substrate usage and carbon fixation	63
4.2.3.2	Biomass, product formation, yield and productivity	65
4.3	Impact of syngas composition and impurities	67
4.3.1	Gas flow rate setting	67

4.3.2	Comparison between biomass-derived and impurity-free syngas	69
4.3.2.1	Bioliq® syngas, setups 1 and 2	69
4.3.2.2	Bioliq® syngas, setups 3 and 4	77
4.3.2.3	TNO syngas, setups 5 and 6	79
4.3.3	Clean syngas fermentations.....	81
4.3.3.1	LNEG and ENEA based syngas, setups 7 and 8.....	81
4.3.3.2	Custom Mixtures A and B, setups 9 and 10	83
4.3.4	Productivity and product ratio comparison according to syngas type and composition	86
4.4	Overview of fermentation results.....	90
4.4.1	Overall summary of carbon fed, usage and fixation	90
4.4.2	Overall comparison between experimental and maximum theoretical yields.....	93
4.5	Impact of elevated pressure	96
4.5.1	Effect of syngas overpressure	96
4.5.2	Effect of CO ₂ /H ₂ and CO overpressure.....	100
4.5.2.1	Growth and product formation	100
4.5.2.2	Formic acid.....	104
4.5.2.3	Effect of CO ₂ /H ₂ on gene expression	106
4.6	Sequential cultivation for acetogenic fermentation from oxygen-containing waste gas...	107
4.6.1	Anaerobic growth of <i>C. ljungdahlii</i> following <i>P. thermoglucosidasius</i> cultivation.....	107
4.6.2	<i>C. ljungdahlii</i> acetate production.....	109
5	Discussion.....	110
5.1	Impact of medium components and process parameters.....	110
5.1.1	Effect of medium components	110
5.1.2	Effect of pH	111
5.1.3	Effect of pH and gas flow	112
5.1.4	Carbon balance	113
5.2	Evaluation of beech wood and lignin derived syngas.....	113
5.2.1	Substrate usage and carbon fixation	113
5.2.2	Biomass, product formation, yield and productivity	115
5.3	Impact of syngas composition and impurities	116
5.3.1	Biomass, product formation, yield and productivity	116
5.3.2	Substrate usage and carbon fixation	117
5.3.3	Product ratio comparison according to the type and composition of syngas.....	118

5.4	Overview of fermentation results.....	121
5.4.1	Overall summary of carbon fed, usage and fixation.....	121
5.4.2	Overall comparison between experimental and maximum theoretical yields.....	121
5.5	Impact of elevated pressure	122
5.5.1	Effect of syngas overpressure on growth and product formation	122
5.5.2	Effect of CO ₂ /H ₂ and CO overpressure.....	124
5.5.2.1	Growth and product formation	124
5.5.2.2	Formic acid.....	127
5.5.2.3	Effect of CO ₂ /H ₂ on gene expression	128
5.6	Sequential cultivation for acetogenic fermentation from oxygen-containing waste gas...	128
6	Conclusion.....	130
	References	132
	List of figures.....	142
	List of tables	143
	Appendix	144

1 INTRODUCTION

In the current scenario of a growing world population and decreasing resources, together with the environmental implications of fossil fuel combustion, alternatives sources for fuels and chemicals need to be found. The dependence of our society on fossil fuels is clear: a vast majority of everyday materials, as well as primary energy, are derived from fossil fuels (Edenhofer et al., 2014). (Infantes et al., 2020a). This, combined with the population growth, is causing a rise in the release of CO₂ into the atmosphere (McGlade and Ekins, 2015). At the same time, reducing the CO₂ emissions has been identified as a much needed measure to prevent the global temperature increase (Friedlingstein et al., 2014). (Infantes et al., 2020b)

In contrast, the fermentation of synthesis gas (syngas) by acetogenic bacteria can provide an environmentally-friendly and renewable alternative for the production of low-carbon fuels and chemicals, and is receiving ever more attention (Liew et al., 2013; Hu et al., 2016; Richter et al., 2016). (Infantes et al., 2020a)

Syngas consists of a mixture of mainly CO, H₂ and CO₂, and can be derived from the gasification of biomass. This is advantageous in comparison to the fermentation of biomass-derived sugar feedstocks since the lignin fraction becomes accessible (Liew et al., 2016). Carboxydrotrophic and homoacetogenic bacteria such as *Clostridium ljungdahlii* can grow by using the carbon and electrons derived from syngas, thanks to their unique carbon-fixating reductive acetyl-coenzyme A pathway, also known as the Wood-Ljungdahl pathway (WLP). Their primary end-product is acetic acid and ethanol, but other products like butyrate or butanol have also been described (Henstra et al., 2007; Bengelsdorf et al., 2018). Given the fact that these microorganisms are becoming more relevant, the understanding of the fermentation process and their product formation profile is of valuable interest. (Infantes et al., 2020a). As well, acetogenic fermentation of syngas has been lately gaining ever more attention, since commercial syngas or waste gas fermentation plants are being developed or are already operational (LanzaTech, 2018; Sun et al., 2019). (Infantes et al., 2020b)

By increasing or decreasing certain medium components, biomass, gas consumption and product formation can be affected. For instance, Abubackar et al. (2012) showed that increasing the cysteine concentration in the medium enhanced the ethanol production of *Clostridium autoethanogenum*. The work of Saxena and Tanner (2012), showed that yeast extract and trace metals were required for *Clostridium ragsdalei* to grow. (Infantes et al., 2020a). Not only nutrients affect the outcome; pH also plays an essential role in the fermentation performance: it significantly impacts the behavior of the microorganism, affecting both growth rate and product formation. A drop in the external pH might be

a way to induce the production of more reduced compounds, such as ethanol (Barik et al., 1988; Phillips et al., 1993; Abubackar et al., 2012). Taking all this into account, part of this thesis focused on assessing the ability of the existing fermenter setup to follow the effect of two selected nutrients (yeast extract and sulfur, in the form of cysteine), as well as the impact of pH and the influence of the amount of substrate fed (gas flow rate) on syngas fermentation by *C. ljungdahlii*. For this, products, biomass formation, and gas consumption were analyzed, and the obtention of a closed carbon balance was also assessed. (Infantes et al., 2020a)

Biomass is seen as an important source for renewable commodity chemicals and some liquid hydrocarbon fuels: it can be gasified, including lignocellulosic biomass, waste and non-food crops, to produce syngas. This gasification technology is well-established and has been broadly studied (Sikarwar et al., 2016). (Infantes et al., 2020b)

Due to the nature of the joint operation of the gasification of biomass for the obtention of syngas, followed by its conversion to products via fermentation by acetogenic bacteria, it has been named a “hybrid thermochemical/biochemical process” (Griffin and Schultz, 2012). Acetogenic microorganism present several advantages compared to traditional chemical catalysts, for instance, the flexibility that they possess to tolerate broad H₂/CO ratios, including a changing composition during the process. Contrasting with it, chemical catalysts cannot operate outside a fixed ratio. The conditions for syngas fermentation are, additionally, milder compared to thermochemical routes for syngas conversion, which can lead to reduced operational costs (Daniell et al., 2012; Griffin and Schultz, 2012).

The fermentation outcome is strongly influenced by the final syngas composition, as well as the impurities and inhibitory compounds present in the final syngas (Ahmed et al., 2006; Xu et al., 2011). Both factors are dependent on the feedstock and gasification technique employed (Daniell et al., 2012; Yasin et al., 2019). When assessing biomass-derived syngas fermentation, a varying biomass composition, as well as seasonal oscillations, are to be expected. The question of whether the fermentation outcome of biomass-derived syngas will mainly be affected by the CO, CO₂ and H₂ composition, as it is in the case with clean syngas, or if the impurities will play a bigger role needs to be answered if an integrated bio-refinery concept is to be established, so that the production and cleaning of the syngas can be optimized to ensure the best possible outcome. A fermentation system where a first screening can be performed, in an easy and rapid manner can definitively help tackling this matter. (Infantes et al., 2020b)

With all this in mind, part of this thesis was devoted to examining the effect of biomass-derived syngas from straw, beech wood, and lignin, and compared it to clean, commercially-prepared syngases of the same composition. As well, four different compositions of clean syngas were tested, from which two

had been mixed to match the composition of two different gasification processes. The examination of the gas usage, product formation and growth, as well as yields, productivities, and product distribution profiles allowed for a complete overview of the impact of the different syngases in this particular system. This highlights its ability to serve as a valuable assessment tool for the evaluation of biomass-derived syngases as fermentation substrate. (Infantes et al., 2020b)

A further important point of focus throughout this work was the evaluation of changes on the gas consumption profile of the culture during all fermentations in bioreactors. Not many studies can be found on the topic of syngas which show a system with the ability to track changes in the consumption of the gas substrates with on-line analytics, even if it is considered to be very relevant information (Fernández-Naveira et al., 2017). In many cases, studies focusing on the effect of medium components or gas composition are performed in batch, with serum bottles, with the limitations that this implies (difficult pH control, no continuous gas feed, no possibility of out-gas analysis). (Infantes et al., 2020a)

Gaseous substrates must first dissolve into the medium to be accessible for the bacteria. Gas-liquid mass transfer limitation is regarded as one of the biggest challenges for the commercialization of syngas fermentation, since it is the rate limiting step and a potential bottleneck (Mohammadi et al., 2011; Munasinghe and Khanal, 2011). One approach to enhance the gas-liquid mass transfer is to augment the volumetric power input (Sander, 2015). Gas diffusion and liquid-gas interaction are other important factors that affect gas-liquid mass transfer (Sun et al., 2019), and different approaches are found in literature, like different impeller designs, fluid flow patterns, baffle design and the usage of microbubble dispersers (Munasinghe and Khanal, 2011). Moreover, another parameter which is regarded as being crucial to consider is augmenting the pressure in the headspace (Asimakopoulos et al., 2018). This will improve the gas-liquid mass transfer due to the increased solubility of the gases into the liquid.

Even if applying higher pressure in acetogenic fermentations can have clear advantages, there are only a few studies which have looked at the effects of increasing the pressure of the substrate beyond 1 bar (atmospheric pressure). Some examples are outlined here: an unidentified bacterium, isolated from chicken waste, was grown on syngas (18.5 % H₂, 56.1 % CO, and 10 % CO₂, in Ar), at pressures ranging from 1.1 bar to 3.5 bar (absolute) (Vega et al., 1989b). Syngas (composition unknown) at pressures up to 11 bar (absolute) was fermented with *C. ljungdahlii* (Department of Chemical Engineering, University of Arkansas, 1993). More recently, the same microorganism has been used with different syngas compositions and the following conditions: 1.8 up to 2.8 bar (absolute) with 55 % CO, 20% H₂, and 10 % CO₂ (in Ar) (Younesi et al., 2005); 1.2 to 2.5 bar (absolute) with 30% each CO, CO₂ and H₂ (in

Ar), (Mohammadi et al., 2014); and finally, 1, 4 and 7 bar with 48 % H₂, 16 % CO, 16 % CO₂ (in N₂) (Stoll et al., 2019).

Nevertheless, most of the reports found in literature are focused on only one or two gaseous components, and not syngas. Even less studies are found where *C. ljungdahlii* was the organism of choice. For instance, *Clostridium aceticum* was grown with 78 % CO and 4 % H₂ (in Ar) at pressures from 1.8 to 2.6 bar (absolute) (Sim et al., 2007); 80 % CO and 20 % CO₂ or 25 % CO and 15 % CO₂ (in N₂) from 1.4 to 2.5 bar (absolute) were used with *Clostridium carboxidivorans* P7^T (Hurst and Lewis, 2010); *Blautia producta* (reported there as *Peptostreptococcus productus*) with 80 % CO and 20 % CO₂ at pressures from 1.3 to 3. bar (absolute) (Vega et al., 1989a). A study focusing specifically on the effects of increased CO₂/H₂ pressure (53.3 % and 26.7 %, respectively), on *C. ljungdahlii* was only recently carried out, with pressures of 1, 4 and 7 bar (Oswald et al., 2018a). No reports could be found of the effects of pure CO at elevated pressure for *C. ljungdahlii*. In order to get more insights of how the metabolism of *C. ljungdahlii* is affected by pressure, part of this work focused on using a syngas mixture to assess the influence of increased pressures from 1 to 2.5 bar (absolute). Besides, to isolate the effect of each component, pure CO, as well as a mixture of CO₂ and H₂ were tested at two extremes: 1 bar and 5 bar (absolute).

Moreover, it has been reported that under different fermentation conditions, *C. ljungdahlii* experiments a metabolic shift which is reflected by a change in the gene expression profile for genes of central enzymes of the Wood-Ljungdahl pathway (Xie et al., 2015). Despite these findings, two separate studies are not in agreement with that conclusion: firstly, the metabolic shift of *C. ljungdahlii* was found to be not caused by enzyme expression but rather by the level of acetate in the extracellular environment (Richter et al., 2016), and, secondly, that not only acetate concentration, but the maintenance of ATP homeostasis triggers the metabolic shift in acetogens (Valgepea et al., 2017a). No studies could be found on the effects of increased pressures on gene expression. Here, qPCR was used to study the gene expression profiles of central enzymes of the Wood-Ljungdahl pathway at increased pressures of CO₂/H₂. A qPCR study of the cultures grown with pure CO was planned but abandoned in light of the results obtained.

Due to *C. ljungdahlii*, and most known acetogenic organisms being classified as strict anaerobes (Ragsdale, 1991; Liew et al., 2016), the use of industrial waste gasses which contain O₂ as fermentation substrate is not directly feasible. Many of the enzymes of the WLP are described as being sensitive to even small amounts of oxygen, and the cost, and the techniques required for stripping the syngas of O₂ makes this approach unfeasible to implement in the frame of syngas fermentation: for instance, any syngas wash-system would require to use de-aerated water to prevent introducing O₂ into the

syngas. Metal based catalysts can be used to eliminate oxygen from the gas, but that would require an extra cleaning step, adding to the process costs. (Liew et al., 2016; Ramachandriya et al., 2016). Even if some acetogens have been reported to be able to withstand low amounts of O₂, it caused a lag phase and diminished optical densities, and some, like *A. woodii*, were not able to grow at all (Karnholz et al., 2002). Symbiotic-like interactions between acetogens and microaerophiles or aerotolerant organisms have been observed, with the oxygen-consuming bacterium protecting the acetogen from oxidative stress, as well as generating products that can be used by the acetogen (Drake et al., 2008). With this, a similar strategy was deployed as part of this work, in order to be able to use oxygen-containing gases for acetogenic fermentation, as a joint project with Dr. Teresa Mohr. A sequential culture system is presented as part of this thesis, where *P. thermoglucosidasius* was used to consume the O₂ from a CO/air mixture and produce CO₂ and H₂, which would then be used by *C. ljungdahlii* during the second phase of the cultivation, obtaining mainly acetate as a final product. The selection of the oxygen-consuming organism was driven by the fact that it should withstand the toxicity of CO, since it is known to be inhibitory, or at least disrupt the metabolism of most bacteria (Chin and Otterbein, 2009; Wareham et al., 2016). At the same time, *C. ljungdahlii* should be able to survive and to further ferment the products of the first O₂-consuming microorganism. For this thesis, the focus is put on the *C. ljungdahlii* cultivation part, and its final outcomes.

2 THEORETICAL BACKGROUND

2.1 Acetogenic bacteria

Acetogenic microorganisms, or acetogens, are a group of anaerobic bacteria that, through the reduction of CO₂, are capable of conserving energy and fix carbon via the acetyl-CoA pathway (Drake et al., 2008; Sun et al., 2019). This pathway is also known as Wood-Ljungdahl Pathway (WLP), as recognition of those who first described it, H. G. Wood and L. G. Ljungdahl. Acetogenic bacteria can grow autotrophically using CO₂/H₂ and/or CO as sole carbon and energy source. Historically, in naming this bacteria group, emphasis was put on their characteristic acetate production. This definition of acetogens has proved challenging, since this is not the defining trait of acetogens, nor is it their only possible product. Many other microorganisms generate acetate as end product, but for including bacteria in the acetogens group, its synthesis must happen through the WLP (Drake et al., 2006). Other products by acetogenic bacteria are mainly, organic acids and alcohols like butyrate, ethanol, and butanol. Some acetogens can also form hexanoic acid, hexanol or 2,3-butanediol (Sun et al., 2019). Acetogens capable of producing solvents (e.g. ethanol) are sometimes described as “solventogenic”; other terms, such as “carboxydobacteria”, “carboxydotrophs” or “carboxydotrophic bacteria” can be found in literature so as to emphasize the ability of using and tolerating high concentrations of carbon monoxide (Bengelsdorf et al., 2018).

As a whole, acetogenic bacteria form a very diverse group in terms of morphology, nutritional requirements and physiology (Drake et al., 2008; Bengelsdorf et al., 2018). Acetogenesis is not a phylogenetic trait, since 23 different bacterial genera are found to contain acetogens, but, from those, not all contain acetogenic species exclusively. The phylum Firmicutes (Gram-positive bacteria with low GC-content) contain most known acetogens (Schuchmann and Müller, 2014), while the majority of acetogenic species identified are comprised in the genera *Clostridium* and *Acetobacterium* (Drake et al., 2006).

The ecology of acetogens is diverse, and have been isolated from extremely varied habitats, like black sediments of estuaries, marine sources, freshwater ponds, anoxic sewage sludge, sediments from an oil-drilling site, intestinal material from animals including chicken yard waste and rabbit feces, tundra wetland soil, the gut of termites, as well as thermophilic sources, like sediments of Lake Kivu (Africa), and hot springs (Schink, 1994; Drake et al., 2006; Bengelsdorf et al., 2018).

2.1.1 The Wood-Ljungdahl pathway and metabolism of acetogens

The Wood-Ljungdahl pathway is a terminal electron-accepting process, formed by two branches: the methyl branch and the carbonyl branch, which merge to form the central intermediate acetyl-CoA. (Drake et al., 2006; Köpke et al., 2011; Bengelsdorf et al., 2018). A schematic representation of the metabolism of the model acetogen *C. ljungdahlii* is shown in Figure 2.1. If the only carbon source available is CO, one molecule will enter the carbonyl branch, forming the carboxyl group. Another molecule is oxidized to CO₂ by the carbon monoxide dehydrogenase activity of the bifunctional acetyl-CoA synthase/CO dehydrogenase (Acs/COdh), which also results in the formation of reduced ferredoxin (Diekert and Thauer, 1978; Hu et al., 1982; Drake et al., 2008). This CO₂ enters then the methyl branch. Here, CO₂ is reduced to formate by the formate dehydrogenase (Fdh). This group is then bound to the cofactor tetrahydrofolate (THF), forming formyl-THF, at the expense of ATP, by a formyl-THF synthetase (Fhs). Subsequent reduction reactions by a bifunctional methenyl-THF cyclohydrolase/formyl-THF cyclohydrolase (Mtc) (Shen et al., 1999), methylene-THF dehydrogenase (Mtd), and methylene-THF reductase (Mtr) yield methenyl-THF, methylene-THF and methyl-THF, respectively. A methyltransferase (Met) transfers the methyl group to a corrinoid iron-sulfur protein, and, finally, to a subunit of the Acs/COdh (Drake et al., 2006; Schuchmann and Müller, 2014; Bengelsdorf et al., 2018).

If, instead, CO₂ is the carbon source, one molecule will be reduced to CO by the bifunctional Acs/COdh and will enter the carbonyl branch, while a second one will enter the methyl branch directly. It has been postulated that the Acs/COdh complex contributes mainly to the oxidation of CO to CO₂, and that a different COdh could reduce CO₂ during growth on H₂/CO₂ (Richter et al., 2016). Both Acs/COdh complex and an independent COdh are described as being able to catalyze the reverse reaction as well, the oxidation of CO to CO₂ (Doukov et al., 2002; Drake et al., 2008; Fontecilla-Camps and Volbeda, 2011). Besides, the Acs/COdh merges the methyl group and the carbonyl group together with coenzyme A (CoA) to form acetyl-CoA (Ragsdale and Wood, 1985; Drake et al., 2006; Schuchmann and Müller, 2014).

This acetyl-CoA can then be directed towards cellular carbon via the anabolic pathways, or towards acetate formation. Here, two enzymes are involved: phosphotransacetylase (Pta) and acetate kinase (Ack). The reaction of Ack generates on ATP via substrate-level phosphorylation (SLP), but since one ATP is required for the formation of formyl-THF, no net ATP gain is obtained overall (Schuchmann and Müller, 2014; Bengelsdorf et al., 2018). This will be discussed in detail below, in the following section *2.1.2 Energy conservation and bioenergetics during autotrophic growth*. Ethanol can also be a product of acetogens. Undissociated acetic acid is the substrate of an aldehyde ferredoxin oxidoreductase

(Aor) to form acetaldehyde (Huber et al., 1995; Napora-Wijata et al., 2014; Richter et al., 2016), which is then transformed into ethanol by the bifunctional aldehyde/alcohol dehydrogenase (AdhE), or by an alcohol dehydrogenase (Adh). The Aor route has been found to be the main source of ethanol, while the formation of ethanol directly through the acetyl-CoA and acetaldehyde route by AdhE is regarded as being only minimal (Richter et al., 2016; Liew et al., 2017; Bengelsdorf et al., 2018).

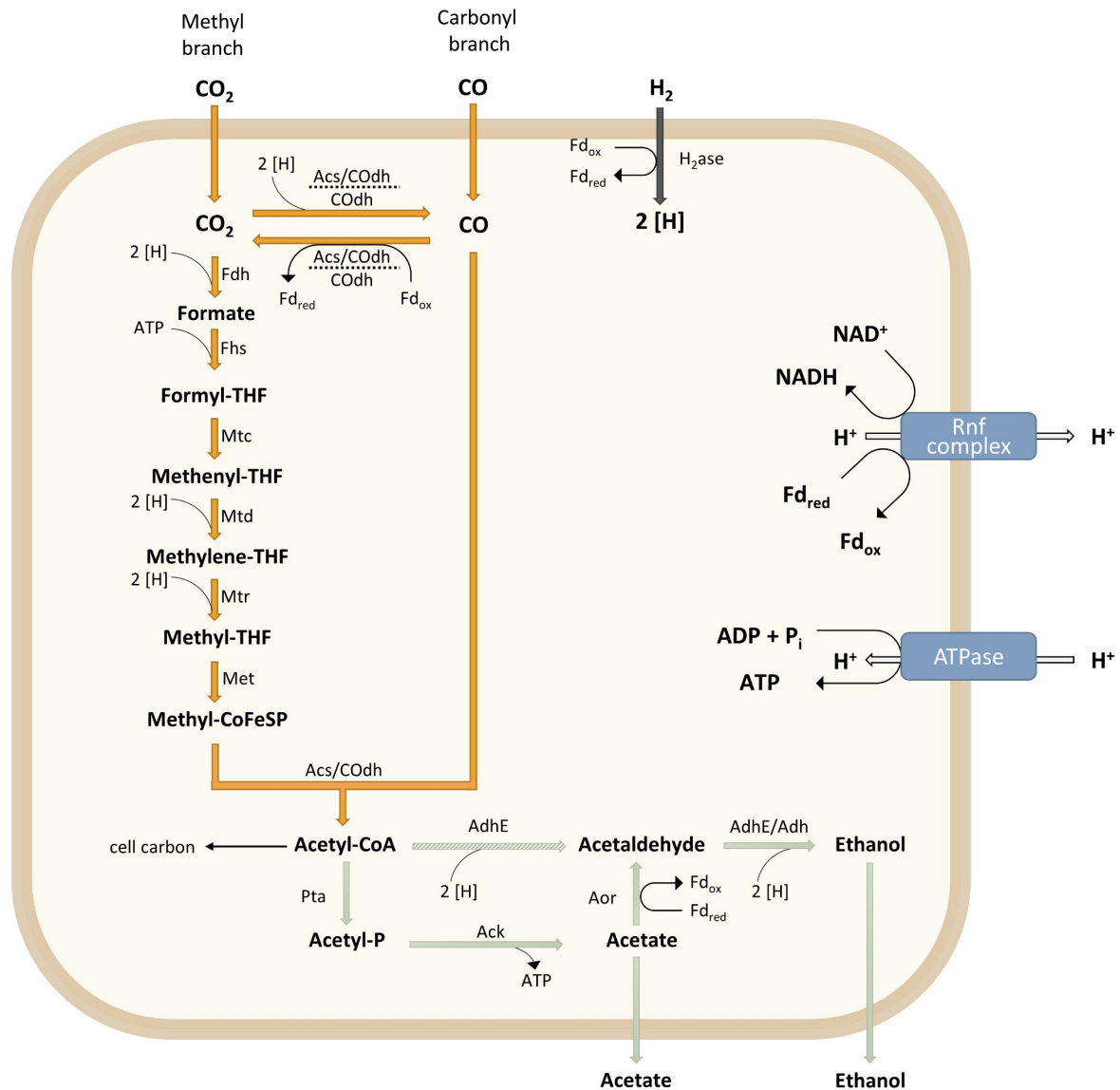


Figure 2.1 – Representation of the metabolism of the model acetogen *C. ljungdahlii*. THF: tetrahydrofolate; CODh: carbon monoxide dehydrogenase; H₂ase: hydrogenase; Fdh: formate dehydrogenase; Fhs: formyl-THF synthetase; Mtc: methenyl-THF cyclohydrolase/formyl-THF cyclohydrolase; Mtd: methylene-THF dehydrogenase; Mtr: methylene-THF reductase; Met: methyltransferase; Acs/Codh: acetyl-CoA synthase/ CO dehydrogenase; Pta: phosphotransacetylase; Ack: acetate kinase; AdhE: bifunctional aldehyde/alcohol dehydrogenase; Aor: aldehyde ferredoxin oxidoreductase; Fd_{ox}: oxidized ferredoxine; Fd_{red}: reduced ferredoxine. A dotted horizontal line between Acs/CODh or CODh shows that the reaction could be catalyzed by either enzyme. The production of acetaldehyde directly from acetyl-CoA by AdhE is considered marginal (green striped arrow), and the main route for the production of acetaldehyde is then via the Pta, Ack and Aor reactions. WLP reactions are marked by orange arrows; hydrogen uptake, by dark grey; and acetate and ethanol formation by light green ones. For full explanations, see main text.

2.1.1.1 Stoichiometry of the WLP

As already mentioned, acetate and ethanol can be produced from either pure CO, CO₂/H₂, or a mixture of those. In the first case, with CO as sole carbon and energy source, the production of acetate and ethanol follow equations (2.1) and (2.2), respectively. If the substrate is CO₂/H₂, acetate is produced according to (2.3), and ethanol according to (2.4) (Datar et al., 2004; Bengelsdorf et al., 2013; Liew et al., 2013). For syngas, a mixture of CO, CO₂ and H₂, the result of the sum of the equations which produce acetate (2.1 and 2.3) is shown in (2.5), which, simplified, leads to (2.6). The sum of the ethanol producing reactions (2.2 and 2.4) is represented in (2.7), which simplified is (2.8). The case for syngas fermentation will be discussed in more detail below, in section 2.2 *Syngas fermentation*.



2.1.2 Energy conservation and bioenergetics during autotrophic growth

As outlined above, no ATP formation, and hence, no energy conservation, is possible via SLP when acetogens grow autotrophically: even if one ATP is formed by the Ack, one ATP is required by the Fhs. A chemiosmotic mechanism is responsible for the energy conservation in this case. It involves the establishment of either a H⁺ or Na⁺ gradient through the membrane, which will then be used by the ATPase as the driving force for the synthesis of ATP (Figure 2.1) (Heise et al., 1993; Müller, 2003). Two different membrane-bound systems are described in acetogens for the generation of the ion gradient: ferredoxin-NAD⁺ oxidoreductase (Rnf complex) and energy-converting hydrogenase (Ech). The Rnf, a membrane-bound, iron-sulfur and flavin-containing electron transport complex, was first described in *Acetobacterium woodii*, and has been reported to be composed of at least six different subunits. It catalyzes the electron transfer from reduced ferredoxin to NAD⁺ (Biegel et al., 2009; Biegel and Müller, 2010). Ech hydrogenases, which couple the exergonic electron transfer from reduced ferredoxin to H⁺, producing H₂, coupled to the transport of protons (Schoelmerich and Müller, 2019) are composed by

two membrane-integral subunits, at least two hydrophilic subunits and two hydrogenase subunits, a large one containing the [NiFe]-active site, and a small one (Hedderich and Forzi, 2005). The ion specificity of Rnf differs among acetogens, and it can either be Na⁺ or H⁺ specific (Hess et al., 2016). Similarly, in different species, the Ech complex may use either Na⁺ or H⁺ as the coupling ion (Hedderich and Forzi, 2005; Schuchmann and Müller, 2014; Schoelmerich and Müller, 2020).

Thermodynamically, the reduction of two molecules of CO₂ to acetate with H₂ as the electron donor is an exergonic reaction, but this does not take into account all the intermediate steps, some of which are endergonic. The biggest thermodynamic barrier in the WLP is the first step of the carbonyl branch, i.e. the reduction of CO₂ to CO. The CO₂/CO redox pair has a more negative standard redox potential ($E_0' = -520$ mV) than H⁺/H₂ ($E_0' = -414$ mV). Reduced ferredoxin (Fd_{red}) can be the electron donor in that reaction, but there still is a large energetic barrier for the electron transfer from hydrogen to ferredoxin ($E_0' \approx -400$ to -450 mV). The physiological potential for ferredoxin (E') might be closer to -500 mV, while that of H₂ might be closer to $E' = -340$ mV. Fd_{red} is the essential electron donor for the functioning of both the Ech and the Rnf complex, as mentioned above (Schuchmann and Müller, 2014). To overcome this thermodynamic challenge, acetogens employ a recently discovered mechanism known as flavin-based electron bifurcation (Buckel and Thauer, 2018a). With it, two electrons are diverged into two different electron acceptors, one of which has a higher reduction potential than the electron donor, while the other has a lower one. In this way, the reducing power of one electron is magnified at the expense of the other (Schuchmann and Müller, 2014).

In acetogens, specifically, this energy coupling mechanism links the exergonic reduction of NAD⁺ ($E_0' = -320$ mV) to the endergonic reduction of ferredoxin with hydrogen. Another possible electron bifurcating enzyme in the WLP is the Mtr. It is not clear, though, if Mtr is NADH or NADPH dependent, and whether it is electron bifurcating in all acetogens (Bertsch and Müller, 2015; Mock et al., 2015).

If CO is the electron donor, ferredoxin can be reduced directly through the oxidation of CO to CO₂. From this reaction, one Fd_{red} is gained, and an additional Fd_{red} can be saved since the CODH is not needed to reduce CO₂ for the methyl branch. This regenerated cofactors can then be used in the WLP and by the Rnf complex (Bertsch and Müller, 2015; Wiechmann and Müller, 2019). In this case, the bifurcating mechanism could seem superfluous, but it may be used to maintain an adequate reduction equivalent ratio, as different steps of the WLP require different cofactors. (Diender et al., 2015).

An exact calculation of the ATP generated by the WLP is only partially possible, since the ATP gain depends greatly on which electron carrier is used (NADH, NADPH or ferredoxin), but the cofactor specificity for some of the enzymes are not known. Moreover, the same enzymatic reaction can use different cofactors in different species, and, as already hinted above, the amount of ATP generated

will also depend on whether CO or CO₂/H₂ are used as substrates. It has been proposed that, when growing on CO₂ and H₂, *Clostridium autoethanogenum* could form 0.14 to 1.5 mol ATP per mol ethanol (Mock et al., 2015). For *A. woodii*, its complete energy metabolism was recently described, generating 0.3 moles of ATP per mole of acetate. For *Morella thermoacetica*, it is proposed to be 0.5 mol ATP per mol of acetate. For *C. ljungdahlii*, contrasting with the two former microorganisms, the specificity of the enzymes is not known. For growth on H₂/CO₂, and with acetate as the sole product, the ATP formation can range from 0.13 to 0.63 mol ATP (Schuchmann and Müller, 2014). With CO, and again considering only acetate as product, 1.125 mol ATP have been proposed to be formed (Diender et al., 2015). Even more recently, a metabolic scheme for *C. ljungdahlii* has indicated that 0.75 mol ATP are generated per mole of acetate formed from H₂/CO₂, assuming that it is the only product. For CO as substrate, 1.7 mol ATP have been proposed to be generated per mol of product, considering that 4 mol ethanol, 1 mol acetate and 1 mol 2,3-butanediol are produced (Zhu et al., 2020).

2.1.3 *Clostridium ljungdahlii*

Clostridium ljungdahlii is one of the most studied acetogens, and its genome is completely sequenced (Köpke et al., 2010). It was first isolated from chicken yard waste (Tanner et al., 1993), but it has also been isolated from a natural waster source, in wastewater anaerobic digesters and in methane production reactors (Whitham et al., 2016). Its genome size is 4.6 Mbp, with a GC-content of 31 % (Köpke et al., 2010). Its natural products are mainly acetate and ethanol, also when grown on CO, and it has been reported to produce lower amounts of 2,3- butanediol and lactate as well (Bengelsdorf et al., 2018). Genetic analysis has shown that *C. autoethanogenum* is closely related to it (Bengelsdorf et al., 2016). *C. ljungdahlii* was characterized in 1993, with optimum growing conditions of pH 6.0 and 37°C. Growth was observed in the range between pH 4.0 and 7.0 and 30°C to 40°C. Morphologically, it is rod-shaped, with cells being 0.6 to 3 µm in size, and motile. It has the ability to form spores, although they are rarely observed (Tanner et al., 1993). Cobalamin is an important cofactor, since several proteins require it, but it can be synthesized by *C. ljungdahlii*. Cobalt transport systems were found in its genome, and it is predicted that folate, riboflavin, NAD⁺, CoA and thiamine can also be synthesized. Biotin synthesis might not be possible, since many of the genes involved were found to be missing (Köpke et al., 2010). Yeast extract is required for growth (Tanner et al., 1993; Annan et al., 2019). Growth experiments indicated that this organism is auxotrophic for pantothenate, biotin and thiamine (Annan et al., 2019). As well, gens related to molecular nitrogen fixation and ammonia assimilation are present in this strain (Richter et al., 2016). Heterotrophically, it can grow on a wide variety of substrates, like fructose, arabinose, xylose, ethanol or pyruvate, amongst others (Tanner et al., 1993; Köpke et al., 2010).

The mechanism used for energy conservation in *C. ljungdahlii* is a H⁺-dependent Rnf complex (Köpke et al., 2010; Tremblay et al., 2012). The Rnf complex is thought to export two protons per oxidized ferredoxin, while the ATPase would generate one ATP per four protons imported (Diender et al., 2015). As in *C. autoethanogenum*, another electron-bifurcating complex is present in *C. ljungdahlii*, the Nfn complex (NAD⁺-dependent reduced ferredoxin:NADP reductase). If H₂ is the electron donor, and the bifurcating hydrogenase is NADP dependent, 0.5 mole NADPH are needed for the reduction of 2 moles of CO₂ to acetate. It must be noted that the Fdh and the NADPH- specific electron-bifurcating [FeFe]-hydrogenase form a complex (Wang et al., 2013; Richter et al., 2016; Buckel and Thauer, 2018b). In this scenario, the Nfn complex ensures the supply of the needed cofactors by reducing 2 moles of NADP with 1 mole of Fd_{red} and 1 mole of NADH (Nagarajan et al., 2013). *C. ljungdahlii* was found to contain genes encoding for Aor (Köpke et al., 2010), which has been further confirmed (Richter et al., 2016; Zhu et al., 2020), so this organism has the potential to generate more ATP from the formation of ethanol than others which can only use the direct AdhE route from acetyl-CoA (Figure 2.1) (Bertsch and Müller, 2015).

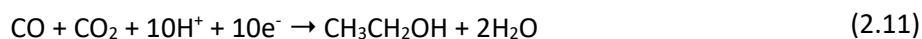
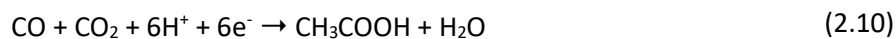
2.2 Syngas fermentation

Syngas, or synthesis gas, is composed by CO, CO₂ and H₂. It can be produced via gasification of a wide variety of sources, from waste streams, including municipal solid waste, non-food biomass and steel mill gas (Acharya et al., 2014; Chandolias et al., 2018).

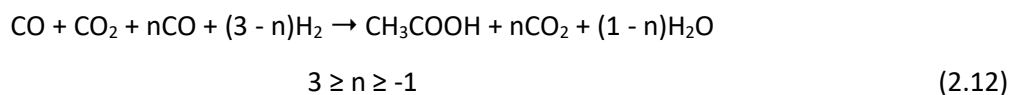
Even if the fermentation of syngas is one of the most important application of acetogens, most of the literature only cite stoichiometries for either CO or CO₂/H₂, as shown above in section 2.1.1.1 *Stoichiometry of the WLP*. When using syngas as a substrate, CO₂ seems not to be used, according to equations (2.6) and (2.8) above. In fact, it must be noted that the reducing equivalents needed for carbon fixation can be supplied by either CO or H₂, and that acetogens can reduce CO₂ to CO and oxidize CO to CO₂, mediated by ferredoxin (Figure 2.1), according to equation (2.9). This reaction is known as the water-gas shift reaction.



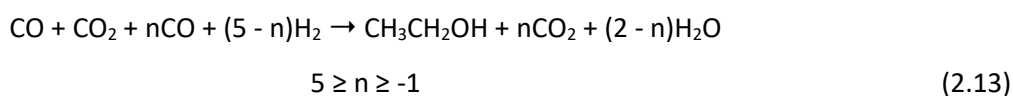
According to this, several intermediate equations are possible. Taking into account all the different combinations of CO, CO₂, H₂ and H₂O that are possible to produce either acetate or ethanol (Whitham et al., 2016; Phillips et al., 2017; Monir et al., 2020), the general stoichiometry for the production of acetic acid (Equation 2.10) and ethanol (2.11) from syngas can be given, regardless of the source of the reducing equivalents (H⁺ + e⁻) (Phillips et al., 2017):



These equations can also be written in an alternative manner, which allows for the generation of all possible stoichiometries for acetate (Phillips et al., 2017):



and for ethanol (Phillips et al., 2017):



If a negative coefficient results for CO_2 or H_2O as a product, this indicates that the species is added as a reactant instead (Phillips et al., 2017).

All possible combinations of $\text{CO}:\text{CO}_2:\text{H}_2$ ratios for the production of acetate and ethanol, derived from Equations (2.12) and (2.13) are compiled in Table 2.1. It is important to remark that the production of a single product is not usual, and a mixture will most likely be observed.

Table 2.1 – Possible stoichiometric coefficients for the production of acetate and ethanol from syngas according to Equations (2.12) and (2.13).

CO	CO ₂	H ₂	H ₂ O	→	CH ₃ COOH	CO ₂	H ₂
4			2		1	2	
3		1	1		1	1	
2		2			1		
1	1	3			1		1
	2	4			1		2
CO	CO ₂	H ₂	H ₂ O	→	CH ₃ CH ₂ OH	CO ₂	H ₂
6			3		1	4	
5		1	2		1	3	
4		2	1		1	2	
3		3			1	1	
2		4			1		1
1	1	5			1		2
	2	6			1		3

2.2.1 Biomass-derived syngas and the biorefinery concept

The linkage of the gasification process for the generation of syngas and its subsequent fermentation has been described as a hybrid thermochemical/biochemical platform (Griffin and Schultz, 2012; Phillips et al., 2017). It is also referred to as a “biorefinery”, which implies a (future) organic chemical industry where the carbon products, from food to fuel, are derived from renewable biomass (Henrich et al., 2015). A schematic representation is shown in Figure 2.2

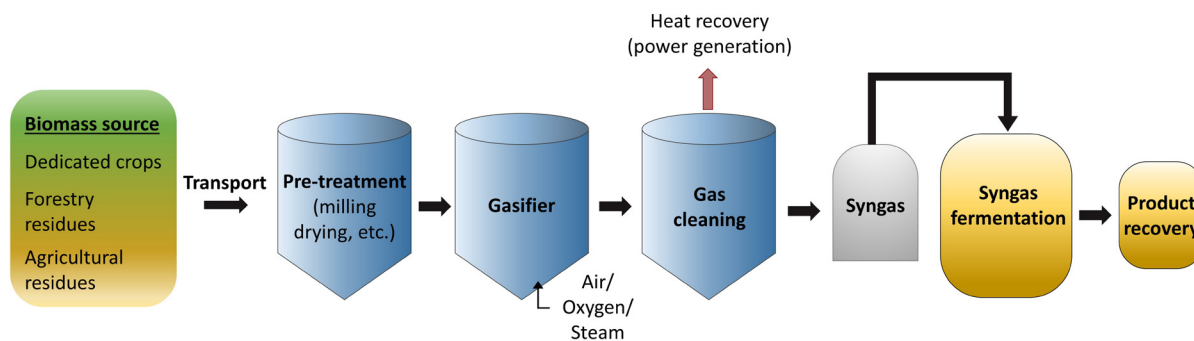


Figure 2.2 – Schematic representation of the biorefinery concept, from biomass to product via syngas fermentation.

Biomass, including the lignin fraction, and waste materials can be converted to syngas. All organic parts of the feedstock, including lignin, which can constitute up to 30 % of the biomass, are utilized, which is a significant advantage compared to the fermentation of sugary feedstocks (Ramachandriya et al., 2016). Different syngas compositions will be obtained depending on the characteristics of the feedstock, like moisture, tar content, and particle size, and the gasifier used (Munasinghe and Khanal, 2011; Kennes et al., 2016; Ramachandriya et al., 2016). The most common types of gasifiers are fixed bed, fluidized bed, and entrained bed (or entrained flow), and the type of gasification agent can be either air, oxygen, steam, or mixtures of those (McKendry, 2002; Munasinghe and Khanal, 2011; Chandolias et al., 2018). A range of usual syngas compositions obtained for oxygen and steam gasification are shown in Table 2.2. Impurities can also be present; this will be discussed further in detail in section 2.2.3 *Impact of syngas composition and impurities*.

Regarding the feasibility of the establishment of biorefineries based on biomass, it has been assessed that it is viable, even without the need for major changes to agricultural or forestry practices (Henrich et al., 2015).

Table 2.2 – Typical dry syngas composition for oxygen and steam gasification of biomass. Modified from Rauch et al., (2015)

Compound	Oxygen gasification		Steam gasification
	Entrained bed	Fluidized bed	
CO (vol %)	40 – 60	20 – 30	20 – 25
CO ₂ (vol %)	10 – 15	25 – 40	20 – 25
H ₂ (vol %)	15 – 20	20 – 30	30 – 45
N ₂ (vol %)	0 – 1	0 – 1	0 – 1

Despite the positive aspects of the integration of biomass gasification and syngas fermentation, there are still challenges that need to be addressed (Abubackar et al., 2011; Ramachandriya et al., 2016):

- Selection of appropriate feedstocks
- Selection of suitable gasification and syngas cleaning system
- Choosing the most adequate microorganism and fermentation media
- Improvement of mass transfer and scale-up
- Development of product recovery strategies
- Evaluation of production costs and market value of products

Moreover, the successful integration of a biorefinery concept must include the efficient harvesting, storage and transportation systems for the biomass and products (Munasinghe and Khanal, 2011).

2.2.2 Impact of media components and process parameters

Acetogenic bacteria growing on CO₂/H₂ and/or CO experiment a metabolic shift similar to that seen in ABE Clostridia (Liew et al., 2013), which display a biphasic fermentation profile. During the exponential growth of ABE Clostridia, carboxylic acids are produced together with H₂ and CO₂ (acidogenic phase), while during the stationary phase these acids are taken up and solvents are formed (solventogenic phase). This metabolic change is accompanied by a significant change in gene expression (Lee et al., 2008). Despite the strategy similarities of both ABE and syngas-fermenting Clostridia, no gene expression regulation could be found as the mechanism driving the shift in the syngas-fermenting microorganism (Richter et al., 2016). Physiologically, temperature, pH, acetic acid concentration, and nutrient limitation are regarded as factors that can induce a transition to non-growth conditions and solventogenesis (Mohammadi et al., 2011; Liew et al., 2013). (Infantes et al., 2020a)

By increasing or decreasing certain medium components, biomass, gas consumption and product formation can be affected. For instance, Abubackar et al. (2012) showed that increasing the cysteine concentration in the medium enhanced the ethanol production of *Clostridium autoethanogenum*. The work of Saxena and Tanner (2012), showed that yeast extract and trace metals were required for *Clostridium ragsdalei* to grow. (Infantes et al., 2020a)

Moreover, based on a proteome analysis, Richter et al. (2016) found that the genes for the sulfate reduction in the sulfur-assimilation pathway in *C. ljungdahlii* are absent. Therefore, they suggested replacing the sulfate that is usually present in the syngas fermentation medium by sulfide or cysteine. In this context, a medium containing no sulfate, but cysteine as the sulfur source has already been reported to support growth for *Clostridium autoethanogenum*, *Clostridium ljungdahlii* and *Clostridium ragsdalei* (Annan et al., 2019). (Infantes et al., 2020a)

Yeast extract is a crucial part of the medium since its removal does not support the growth of syngas-fermenting microorganisms (Barik et al., 1988). Even so, the reduction of its concentration in the medium has been shown to be beneficial in terms of ethanol production (Abubackar et al., 2012; Barik et al., 1988; Phillips et al., 1993; Vega et al., 1989). Still, the necessity for complex and not well understood medium components in the syngas fermentation medium is remarkable: one study showed that when substituting yeast extract with CSL (corn steep liquor), the supplementation with 0.5 g/L of yeast extract or trace metals, NH_4^+ and cysteine was necessary to support growth of *C. ragsdalei*. Even CSL itself could not be reduced below 10 g/L without experimenting a reduction in ethanol production (Saxena and Tanner, 2012). Cotter et al. (2009a) assessed the effect of nitrogen limitation to achieve stable resting cultures for the production of ethanol. When they removed nitrogen from the media, neither *C. ljungdahlii* nor *C. autoethanogenum* were able to maintain a stable cell density. They concluded that even non-growing cultures of *C. ljungdahlii* and *C. autoethanogenum* required organic nitrogen sources to prevent decaying cell densities. (Infantes et al., 2020a)

On the other hand, providing additional nutrients in the form of yeast extract to supports cell growth had a positive effect on acetic acid production in a study by Barik et al. (1988). This agrees with acetate being a growth-related product (Barik et al., 1988; Richter et al., 2016), since higher biomass resulted in an enhanced production. (Infantes et al., 2020a)

Certainly, not only nutrients affect the outcome; pH also plays an essential role in the fermentation performance: it significantly impacts the behavior of the microorganism, affecting both growth rate and product formation. A drop in the external pH might be a way to induce the production of more reduced compounds, such as ethanol (Barik et al., 1988; Phillips et al., 1993; Abubackar et al., 2012).

In a study with *B. methylotrophicum*, the pH was lowered from 6.8 to 6.0 only after reaching the stationary phase, which caused an increase in butyrate production (Worden et al., 1991). Similarly, Klasson et al. (1993) firstly grew a dense *C. ljungdahlii* culture at a pH of 5.0, and only then was the pH lowered between 4.0 and 4.5 to enhance ethanol production. Even so, Kundiyana et al. (2011) reported that lowering the pH below 6.0 did not produce a beneficial effect on ethanol production on *C. ragsdalei*. It must also be taken into account that acetate in its undissociated form is lipophilic and freely diffuses through the cell membrane, which results in the move of H⁺ across the transmembrane gradient, lowering the intracellular pH (Kundiyana et al., 2011). If the pH drops too low, it might negatively affect the culture since the microorganism could struggle to maintain a neutral intracellular pH (Cotter et al., 2009; Mohammadi et al., 2011; De Tissera et al., 2017). (Infantes et al., 2020a)

2.2.3 Impact of syngas composition and impurities

The stoichiometry of the WLP reactions (see section above, 2.1.1.1 *Stoichiometry of the WLP*) implies that, when using CO alone, 50 % of the carbon could be fixed into acetate, producing 0.5 mol of CO₂ per mol of CO used. Considering ethanol as the only end-product, only 33 % of the carbon would be fixed, releasing the remaining amount as CO₂. If H₂ is present at an equimolar ratio to CO, then theoretically all carbon would be fixed to acetate, or 67 % of the carbon would be converted to ethanol. For a mixture of CO₂ and H₂, complete fixation into acetate would require a 1:2 molar ratio; for ethanol, it would need to be 1:3 (Datar et al., 2004; Bengelsdorf et al., 2013; Liew et al., 2013). These stoichiometric ratios do not apply for the growing phase though, since the carbon and reducing equivalents needed for biomass increase are not contemplated. Only with resting cells can these ratios be balanced, and only in the case of homoacetogenesis. This represents a challenge of its own, since the result of a more realistic scenario of mixed products and varying gas composition cannot be directly inferred. (Infantes et al., 2020b)

As outlined above, the biomass-derived syngas can contain several impurities, such as volatile tars, ethane (C₂H₆), benzene (C₆H₆), hydrogen sulfide (H₂S), sulfur dioxide (SO₂), carbonyl sulfide (COS), ammonia (NH₃), nitrogen (N₂), hydrogen cyanide (HCN), nitrous oxide (N₂O), methane (CH₄), acetylene (C₂H₂), and ethylene (C₂H₄). Their concentration can vary depending on the biomass source, but can range from ppm to up to 15 %. (Acharya et al., 2014; Ramachandriya et al., 2016). Many studies have been conducted on the effect of syngas impurities on different acetogenic bacteria, but most of them dealt with single impurities, rather than the complex mixture found in real biomass-derived syngas (Ahmed and Lewis, 2007; Xu and Lewis, 2012; Ramachandriya et al., 2016; Oswald et al., 2018b). Some groups already performed some tests with biomass-derived syngas, although in most cases with just one type of such syngas (Datar et al., 2004; Ahmed et al., 2006; Xu et al., 2011; Xu and Lewis, 2012).

Besides, the reported impact of the impurities has been heterogeneous, thus a generalization is not straightforward (Ramachandriya et al., 2016). Since the cleaning and removal of the impurities represents an important part of the gasification costs, it is of crucial importance to assess the extent of the cleaning needed for syngas fermentation. (Chiche et al., 2013). Studies performed for the cleaning of syngas which is intended to be used in traditional chemical applications cannot be directly extrapolated in this case, due to the differences mentioned above. (Infantes et al., 2020b)

In literature, ammonia has been shown to act as a non-competitive hydrogenase inhibitor, and at 200 ppm reduced growth of *Clostridium ragsdalei* by half (Xu and Lewis, 2012). Cyanide causes a lag-phase in *Clostridium ljungdahlii* when grown on fructose, and at 1 mM it completely inhibited autotrophic growth (Oswald et al., 2018b). Nitric oxide (NO) might cause an increase in ethanol production, but reversibly inhibits the hydrogenase, with complete inhibition above 160 ppm, while at 40 to 130 ppm caused a reversible growth inhibition on *Clostridium carboxidivorans* (Ahmed and Lewis, 2007). Any inhibitor affecting the hydrogenase has the potential effect of reducing the carbon conversion efficiency of syngas fermentation, since electrons cannot be derived from H₂. These would have to be provided by CO, causing less carbon to be available for product formation, since CO₂ would be produced and released (see Equation 2.1).

2.2.4 Impact of elevated pressure

In the aqueous fermentation broth, CO₂ is 48 times more soluble than CO (at 273.15 K and 101.33 kPa), and 80 times more soluble than H₂ (at 273.15 K and 101.33 kPa). (Cardarelli, 2008). CO and H₂ are the electron and reducing equivalent supply, and are needed for producing more reduced compounds, such as ethanol (Table 2.1). The partial pressures of the gases will, hence, influence the product distribution, as well as the yield (Teixeira et al., 2018). (Infantes et al., 2020b)

According to Henry's law, the concentration of a gas species i , c_i , in the aqueous phase, is proportional to the partial pressure, p_i , of that gaseous species i (Cardarelli, 2008; Sander, 2015):

$$H_i^{cp} = \frac{c_i}{p_i} \quad (2.14)$$

here, H^{cp} is the Henry's solubility constant defined via concentration, and its SI units are mol m⁻³ Pa⁻¹, although it is also commonly expressed as M atm⁻¹ (Sander, 2015).

Applying Henry's law (Equation 2.14), the liquid mass transfer of the gaseous species i becomes proportional to the partial pressure of the substrate in the liquid phase, and is described by Equation 2.15 (Vega et al., 1989a; Phillips et al., 2017):

$$-\frac{1}{V_L} \frac{dn_i}{dt} = k_{L,i} a (c_i^* - c_{i,L}) = k_{L,i} a H_i^{cp} (p_i - p_i^*) \quad (2.15)$$

where V_L is the volume (L) of liquid into which the gas is transferred, $-dn_i/dt$ (mol i h⁻¹) is the molar rate of transfer of the gaseous substance i , being negative due to the consumption of i from the gaseous phase. The constant $k_{L,i} a$ is the volumetric mass transfer coefficient for the gas i (h⁻¹), c_i^* is the concentration of the gas component i at the gas-liquid interface in equilibrium, $c_{i,L}$ is the concentration of i in the liquid, H_i^{cp} is the Henry's solubility constant defined via concentration (mol m⁻³ Pa⁻¹), and p_i^* is the partial pressure of i (Pa) in equilibrium by Henry's law with the concentration of i dissolved in the liquid (Phillips et al., 2017).

The amount of substance that can be dissolved is, thus, controlled by the transport rate. The solubility of CO and H₂ is low, and therefore the amount of those gases available for the cells' consumption is low. When the biomass increases above a threshold, and the consumption rate equals the transfer rate (amount of substrate that can be dissolved per unit of time), the amount of substrate dissolved in the liquid becomes zero and the substrate consumption becomes a transport-controlled process. The substrate consumption rate can then only equal the transport rate of the substrate into the liquid phase (Vega et al., 1989a). Increasing the pressure of the substrate in the headspace will provide more substrate to the cells, theoretically increasing its consumption rate.

When looking at scale-up economics, increasing the pressure has the potential to lesser the need to increase the volumetric power input, making the scale-up process more economically feasible (Takors et al., 2018). As well, since the reaction rate increases linearly with respect to the gas pressure, this will lead to lower effective retention times. The volume of reactor can also be reduced when using gaseous substrates at higher pressures (Munasinghe and Khanal, 2011).

2.2.5 Impact of oxygen and biological oxygen removal

Oxygen can be present in the final stored biomass-derived syngas (Wang et al., 2006; Yan et al., 2013; Liew et al., 2016; Liakakou et al., 2019), and the maintenance of strict anaerobic conditions through the production, cleaning and transport of syngas can represent a struggle for the implementation of biomass-derived syngas fermentation (Ramachandriya et al., 2016).

One of the most toxic components to syngas fermentation is, indeed, oxygen, since it inhibits various key enzymes, like pyruvate-ferredoxin oxidoreductase hydrogenases (both Ni- and Fe- containing)

(Ramachandriya et al., 2016), the formate dehydrogenase and the acetyl-CoA synthase, these last two being regarded as the most oxygen-sensitive enzymes known (Drake et al., 2006).

Not many studies have been focused on assessing the aerotolerance of acetogens; but some have shown a limited tolerance to oxygen, most of them only to trace or low levels. Peroxidase, NADH oxidase, and superoxide dismutase are some enzymes which have been proposed to be the associated with the aerotolerance and consumption of low oxygen levels of acetogens (Küsel et al., 2001; Karnholz et al., 2002; Drake et al., 2006). *Sporomusa silvacetica* and *Clostridium magnum* were shown to tolerate up to 1.9 % O₂ in the headspace when growing heterotrophically on semisolid medium; *Moorella thermoacetica* tolerated up to 1 % O₂, while *A. woodii* and *Thermoanaerobacter kivui* did not grow with oxygen concentrations in the headspace above 0.3 and 0.5 % O₂, respectively. As well, in all cases, increasing amounts of O₂ prolonged the lag phase (Karnholz et al., 2002). In another study, the rate of acetate formation of *Sporomusa* sp. strain TmA03 decreased with increasing O₂ headspace partial pressures when growing autotrophically with H₂/CO₂. The maximum oxygen level tolerated was 1.5 kPa (1.5 % O₂) in reduced medium, and in unreduced medium, no acetate production was detected above 0.2 kPa (0.2 % O₂) (Boga and Brune, 2003). Yet another report highlights the fact that the enzymes of the WLP are indeed quite sensitive to O₂, and hence acetogenesis was much more affected by its presence than glucose fermentation in *Clostridium glycolicum*. When this microorganism was grown on H₂/CO₂ no H₂ consumption was detected above 1 % of O₂ in the headspace, while when growing on glucose it could tolerate 6 times more, if the tube was static, or 4 times more if shaken (Küsel et al., 2001). This highlights the issues which could arise for syngas fermentation systems from a continued O₂ exposition, and the importance of removing O₂, if present, from the syngas stream.

For the removal of oxygen, aside from the existing chemical/physical methods, like catalytic oxidation, adsorption/absorption, and combustion (Yan et al., 2013), a biological oxygen removal tool could be also applied to syngas, in light of the reported interaction of acetogens with other more aerotolerant, O₂-consuming, microorganisms (Drake et al., 2008). For the application of this approach, the O₂-consuming bacteria must be also tolerant to CO, which inhibits, or disrupts, the metabolism of most organisms, including bacteria (Chin and Otterbein, 2009; Wareham et al., 2016). In this scenario, *Parageobacillus thermoglucosidasius*, a facultative anaerobic thermophile, is able to grow in CO/air mixtures, producing H₂ and CO₂ (Mohr et al., 2018b, 2018a). Moreover, in preliminary studies it was shown that *P. thermoglucosidasius* did not produce any inhibiting compounds to *Clostridium ljungdahlii* (data not published).

3 MATERIAL AND METHODS

3.1 General procedures for STR experiments

3.1.1 Microorganism and Medium

C. ljungdahlii DSM 13528 was used to perform the fermentations. The strain used here was kindly provided by the group of Peter Dürre at the University of Ulm. Unless otherwise stated, all chemicals were acquired from Carl Roth GmbH + Co. KG (Germany) or Sigma-Aldrich Inc. (Germany). (Infantes et al., 2020a)

Both the pre-cultures and the fermentation media was based on the one described by Tanner (Tanner, 2007). It contained: 20 g/L 2-(*N*-morpholino) ethanesulfonic acid (MES), 0.5 g/L yeast extract (BD, USA), 2 g/L NaCl, 2.5 g/L NH₄Cl, 0.25 g/L KCl, 0.25 g/L KH₂PO₄, 0.5 g/L MgSO₄·7 H₂O, 0.1 g/L CaCl₂·2 H₂O, 10 mL trace element solution, 10 mL vitamin solution and 0.001 g/L resazurin. The pH was adjusted to 5.9 using 4 M KOH before autoclaving at 121 °C. After that, 0.6 g/L cysteine-HCl·H₂O were added to each fermenter, while the pH control was active to counteract the acidification caused. For the pre-cultures, 1 g/L was added to each serum flask, and the pH was measured and adjusted with 4 M KOH if necessary. Trace element solution contained: 2 g/L nitrilotriacetic acid, 1 g/L MnSO₄ H₂O, 0.567 g/L FeSO₄·7 H₂O, 0.2 g/L CoCl₂·6 H₂O (Riedel-de Haën, Germany), 0.2 g/L ZnSO₄·7 H₂O, 0.02 g/L CuCl₂·2 H₂O, 0.02 g/L NiCl₂·6 H₂O, 0.02 g/L Na₂MoO₄·2 H₂O, 0.02 g/L Na₂SeO₃·5 H₂O and 0.022 g/L Na₂WO₄·2 H₂O. Vitamin solution contained: 2 mg/L biotin, 2 mg/L folic acid, 10 mg/L pyridoxine (Alfa Aesar, Germany), 5 mg/L thiamine-HCl, 5 mg/L riboflavin, 5 mg/L niacin, 5 mg/L calcium-pantothenate, 5 mg/L cobalamin, 5 mg/L 4-aminobenzoic acid, and 5 mg/L lipoic acid (Cayman Chemical, USA). (Infantes et al., 2020a)

The pre-cultures for each experiment were freshly prepared, starting from a single glycerol stock. Glycerol stocks were produced from a 48 h grown culture. 5 mL of the culture was aseptically and anaerobically removed and dispensed into a sterile, anaerobised Hungate-type culture tube. The culture was then centrifuged for 5 minutes at 4 °C and 3000 g. The supernatant was then discarded, and the pellet was resuspended in 1 mL of anaerobic and sterile freezing solution, made with equal volumes of culture media and a 50 vol-% glycerol solution. (Infantes et al., 2020a)

For the pre-culture, a glycerol stock frozen at -80 °C was thawed and its entire volume was anaerobically and sterilely dispensed into a 100 mL anaerobic serum flask containing 50 mL of the Tanner medium. The carbon source used for the pre-cultures was 10 g/L of fructose. This culture was allowed to grow for 48 h at 37 °C without shaking. Two subsequent passages with the same cultivation

conditions were performed, but for the second passage, three 250 mL serum flasks, with a working volume of 150 mL, were used. In all cases, a 10 % inoculum volume was added to the serum flasks containing fresh medium. The fermenters were all inoculated simultaneously with a 10 % inoculum volume, using the full content (150 mL) of one of the 250 mL serum flask for each fermenter. (Infantes et al., 2020a)

3.1.2 Fermentation conditions

All fermentations were carried out in Minifors® bench-top stirred tank reactors (STR) (Infors-HT, Switzerland), which have a total volume of 2.5 L. The working liquid volume was 1.5 L. All experiments were performed in triplicates. (Infantes et al., 2020a)

The gas for the fermentation was supplied with a microsparger, while the gas flow rate was controlled via a mass flow controller (MFC) red-y smart series, from Vögtlin Instruments (Switzerland). The temperature of the fermenter was kept at 37 °C, pH was controlled at 5.9 with 4 M KOH, and stirring was regulated at 800 rpm. Anaerobic conditions were ensured after autoclaving by sparging the fermenters with N₂ for 2 h. Following this, the gas supply was changed to syngas with a flow rate of 50 mL/min for at least 3 h until just before inoculation, when the gas flow rate was adjusted as required. (Infantes et al., 2020a)

A detailed description of the fermenter setup can be found in Oswald et al. (2016). The gas flow rate being fed into the fermenters was controlled at 18 mL/min. For all the fermentations, a pure gas mixture was used, with the following composition: 32.50 vol-% CO, 16.00 vol-% CO₂, 32.50 vol-% H₂ and 19 vol-% N₂ (Air Liquide, France). (Infantes et al., 2020a)

3.1.3 Analytical Methods

The fermenters' off-gas were analyzed using a GC-2010 Plus AT gas chromatograph (GC) (Shimadzu, Japan), with a ShinCarbon ST 80/100 Column (2 m × 0.53 mm ID, Restek, Germany) and an Rtx-1 capillary column (1 µm, 30 m × 0.25 mm ID, Restek, Germany). The detector used was a thermal conductivity detector with helium as carrier gas. The column flow rate was 3 mL/min, with an oven temperature of 40 °C for 3 min followed by a ramp of 35 °C/min. The total analysis time was 7.5 min. Data obtained was subsequently evaluated as described in Oswald et al. (2016). (Infantes et al., 2020a)

The sampling regime was as follows: four samples of 2 mL were taken daily at 2 – 3 h intervals, with no sample collection taking place overnight. These were then used for OD (optical density) determination and left-over fructose and products (acetate and ethanol) concentration. OD (optical density) was determined at 600 nm. The sample collection, its treatment, and off-line analysis are described in detail in Oswald et al. (2016). (Infantes et al., 2020a)

The OD (optical density) and cell dry weight (CDW) correlation was determined as the average of 12 fermentations under comparable conditions (data not shown), with a resulting factor of $CDW/OD = 0.30 \pm 0.04 \text{ g/L/OD}$. (Infantes et al., 2020a)

3.1.4 Calculation of product formation parameters using different metrics and at specific phases of the fermentation

First of all, the terminology used here is clarified. A list of terms used through this work is provided below (Infantes et al., 2020a):

- Substrate: CO, CO₂ and H₂.
- Substrate fed: amount of substrate, in mol, sparged into the bioreactor.
- Substrate usage: difference between the amount of substrate fed into the reactor and the amount measured in the off-gas stream (in mol). A negative usage value indicates production.
- Carbon fixation: amount of CO and/or CO₂, in mol, that got incorporated into products or biomass.
- CO fixed: amount of CO assimilated by the cells to products or biomass and not released as CO₂.
- CO used: this comprises both the CO fixed and the amount of CO that is converted to CO₂ by the bacteria which does not get incorporated and is released with the out-gas.

For an accurate analysis, in the case of CO, it is necessary to distinguish between CO used and CO fixed. “CO fixed” refers specifically to the amount of this substance assimilated by the cells to products or biomass. “CO used” comprises both the CO fixed and the amount of CO that is converted to CO₂ by the bacteria which does not get incorporated and is released with the out-gas. Hence, in the absence of any other carbon source, if the amount of CO₂ in the off-gas is larger than the amount being fed (i.e., the CO₂ usage value is positive), it is an indication of CO being converted to CO₂. This amount of produced CO₂ from CO (in mol) must be subtracted from the “used” amount of CO (in mol) to obtain the actual amount of CO fixed. Taking this into account, two scenarios are possible: firstly, if CO₂ is indeed produced from CO, the value of the (perceived) CO usage will be higher than the actual amount of CO fixed into products and biomass. Secondly, if no CO₂ is produced, then the amount of CO fixed is equal to the amount of CO used. For clarity, a short overview of the calculation is given below: (Infantes et al., 2020a)

$$CO_{used} = CO_{fed} - CO_{out} \quad (3.1)$$

$$CO_{used} = CO_{fixed} + CO_{converted} \quad (3.2)$$

$$CO_{converted} = CO_{2, produced} \quad (3.3)$$

$$CO_{fixed} = CO_{used} - CO_{2, produced} \quad (3.4)$$

Regarding yield calculations, they are all given here in gram of product (the sum of acetate and ethanol, in grams) per gram of substrate (the sum of CO₂, CO and H₂, in grams). Three approaches were used: yield per carbon fed ($Y_{P/S, fed}$), yield per carbon used ($Y_{P/S, used}$), and yield per carbon fixed ($Y_{P/S, fixed}$). In the latter case, this includes the amount of CO fixed, the amount of H₂, and, if any, the amount of CO₂ used. (Infantes et al., 2020a)

In order to be able to analyze and compare the data between both fermentations, the product formation parameters yield and productivity, as well as the acetate to ethanol ratio were calculated for the complete run, and up to the point when maximum CO consumption stopped. (Infantes et al., 2020a)

The yield per carbon fed, ($Y_{P/S}$), was calculated according to:

$$Y_{P/S, fed} = \frac{(\Delta c_{acetic\ acid} + \Delta c_{ethanol}) V_R}{\Delta m_{sub, fed}(t)} \quad (3.5)$$

with c_i = concentration of substance i, g L⁻¹; V_R = volume of bioreactor, L;

$\Delta m_{sub, fed}$ = mass of substrates fed into the bioreactor

and:

$$\Delta m_{sub, fed} = \Delta n_{H_2, fed} M_{H_2} + \Delta n_{CO_2, fed} M_{CO_2} + \Delta n_{CO, fed} M_{CO} \quad (3.6)$$

where: $n_{i, fed}(t)$ = total amount of substance fed into the bioreactor, mol,

M_i = molar mass of substance i, g mol⁻¹;

and:

$$\Delta n_{i, fed}(t) = \dot{n}_{i, fed} \times (t - t_{-1}) \quad (3.7)$$

with t = process time, h.

The yield per carbon used was calculated as follows:

$$Y_{P/S, used} = \frac{(\Delta c_{acetic\ acid} + \Delta c_{ethanol}) V_R}{\Delta m_{sub, used}} \quad (3.8)$$

with $\Delta m_{sub, used}$ = mass of substrates used, calculated as:

$$\Delta m_{subused} = \Delta m_{fructoseused} + \Delta m_{H_2,used} + \Delta m_{CO_2,used} + \Delta m_{COused} \quad (3.9)$$

$$\Delta m_{iused} = \Delta n_{iused} M_i \quad (3.10)$$

$$\Delta n_{iused} = \Delta n_{ifed} - \Delta n_{iout} \quad (3.11)$$

$$\Delta n_{iout} = \frac{(\dot{n}_{iout}(t) + \dot{n}_{iout}(t_{-1}))}{2} \times (t - t_{-1}) \quad (3.12)$$

For the yield per carbon fixed, the calculation was:

$$Y_{P/Sfixed} = \frac{(\Delta c_{acetic\ acid} + \Delta c_{ethanol}) V_R}{\Delta m_{subfixed}} \quad (3.13)$$

with $\Delta m_{subfixed}$ = mass of substrates fixed into products and biomass:

$$\Delta m_{subfixed} = \begin{cases} \Delta m_{subused} & \text{if } \Delta n_{CO_2,used} > 0 \\ \Delta m_{fructoseused} + \Delta m_{H_2,used} + \Delta m_{COfixed} & \text{else} \end{cases} \quad (3.14)$$

$$\Delta m_{COfixed} = \Delta n_{COfixed} M_{CO} \quad (3.15)$$

$$\Delta n_{COfixed} = \Delta n_{COused} - \Delta n_{CO_2,produced} \quad (3.16)$$

$$\Delta n_{CO_2,produced} = -\Delta n_{CO_2,used} \quad \text{if } \Delta n_{CO_2,used} < 0 \quad (3.17)$$

Endpoint calculations were done using the values measured with the sample taken immediately before terminating the fermentation. The maximum CO fixation interval was determined by identifying the period where the CO fixation reached a value of 85 % or higher. Calculations were done from the starting of the fermentation to the last point when CO fixation was above 85 %. Due to limitations in the number of samples that could be withdrawn, the measurements from the sample closest to that point are used. The interval of maximum overall usage is determined according to the gas consumption profile. The sum of CO fixation and CO₂ and H₂ usage for each measured point is calculated throughout the fermentation; note that only if no CO₂ is produced then CO used equals CO fixed. The maximum value achieved is defined as the maximum overall usage. The interval of maximum overall usage is the period during which the sum of the usage value of the three gaseous substrates is ≥ 85 % of the mentioned maximum. (Infantes et al., 2020a)

The total amount of carbon fixed ($E_{C\ total}$) was calculated as:

$$E_{C_{total}(t)} = \frac{n_{C_{total,fixed}(t)}}{n_{C_{total,fed}(t)}} \times 100 \quad (3.18)$$

with $n_{C_{total,fed}(t)}$ = total amount of carbon fed, calculated as:

$$n_{C_{total,fixed}(t)} = n_{CO_{used}(t)} + n_{CO_{2,used}(t)} \quad (3.19)$$

$$n_{C_{total,fed}(t)} = n_{CO_{2,fed}(t)} + n_{CO_{fed}(t)} \quad (3.20)$$

3.1.5 Carbon balance

In order to estimate the carbon content in the dry biomass, an approximation of the elemental composition of bacterial cells was used. The total amount of carbon, in mmol, in the dry biomass was calculated by using the carbon content of *Escherichia coli* as reported by Taymaz-Nikerel et al. (2010), 44 % carbon per dry weight (in gram). (Infantes et al., 2020a)

$$C_{products+biomass} = \left(2(\Delta c_{acetic\ acid} + \Delta c_{ethanol}) + \left(\frac{0.44}{12} \times 1000 \times \Delta CDW \right) \right) V_R \quad (3.21)$$

where:

$C_{products+biomass}$ = carbon in products and biomass (mol);

c_i = concentration of substance i, mM;

CDW = cell dry weight concentration, g L⁻¹; and:

V_R = bioreactor volume, L

3.2 Impact of medium components and process parameters

Six experiments were conducted, where the effect of different gas flows, pH, initial yeast extract concentration and initial cysteine concentration were observed. Each experiment was performed as a triplicate (unless otherwise stated), and all fermentations were carried out for approximately 93 h. A detailed description of each setup can be found in Table 3.1. The optimum growing pH for *Clostridium ljungdahlii* was reported to be 6.0 (Tanner et al., 1993), but the DSMZ recommends a pH of 5.9. This is used as optimum growing pH in this study. pH 4.8 was used as lower limit since it was the lowest pH

at which cell growth was still detected. pH 5.4 was chosen as a mid-point between the optimum, 5.9, and the lowest pH where cell growth was still detected. (Infantes et al., 2020a)

Table 3.1 - Experimental setup. All fermentations were done as triplicates (n = 3), except for setup 3, where one fermenter was kept unaltered (3a), and two fermenters were treated (3b). (Infantes et al., 2020a)

Setup	Medium	pH	Gas flow
1	0.5 g/L cysteine, 0.5 g/L yeast extract	5.9	18 mL/min
2	0.5 g/L cysteine, 0.5 g/L yeast extract	No pH regulation	18 mL/min
3a	Increased cysteine to 1 g/L	5.9	18 mL/min
3b	Increased cysteine to 1 g/L	68 h at pH 5.9, then changed to 5.4	18 mL/min
4	Doubled yeast extract concentration to 1 g/L	5.9	18 mL/min
5	0.5 g/L cysteine, 0.5 g/L yeast extract	24 h at pH 5.9, then let drop to pH 4.8 and hold	18 mL/min
6	0.5 g/L cysteine, 0.5 g/L yeast extract	24 h at pH 5.9, then let drop to pH 4.8 and hold	24 h at 18 mL/min, then decreased to 12.6 mL/min

3.3 Evaluation of beech wood and lignin derived syngas

For the fermentation of beech wood syngas (BWS), the gas flow rate was controlled at 18 mL/min. For the fermentation of ligning syngas (LS), the flow rate used was 23 mL/min. Both gases were kindly obtained from TNO, Energy Transition, Biomass & Energy Efficiency Unit (Petten, the Netherlands). The composition of both gases can be found in Table 3.2.

Table 3.2 - Average composition of the gas and flow rate for TNO BWS and LS.

The bioreactors were sparged with syngas from before inoculation for at least 3 h. The values detected in the off-gas are the average of the measurements during this time, after reaching equilibrium conditions in the fermenter. All fermentations were done as triplicates (n=3), and the values given here are the corresponding averages.

		H₂	CO	CO₂	CH₄
BWS (flow rate: 18 mL/min)	%	22.35 ± 0.54	28.19 ± 0.15	19.23 ± 0.29	9.93 ± 0.02
	mmol/min	0.18 ± 0.00	0.23 ± 0.00	0.15 ± 0.00	0.08 ± 0.00
LS (flow rate: 23mL/min)	%	27.02 ± 0.09	21.31 ± 0.10	18.00 ± 0.24	10.64 ± 0.02
	mmol/min	0.28 ± 0.00	0.22 ± 0.00	0.19 ± 0.00	0.10 ± 0.00

3.4 Impact of syngas composition and impurities

All experiments were conducted in triplicates (n = 3). The fermentation time for all setups was approximately 93 h. (Infantes et al., 2020b)

The syngas used for setups 1 and 3 was derived from gasified straw, and was produced and bottled at the Bioliq® plant at KIT, Germany (Dahmen et al., 2017). Setups 2 and 4 used a commercially-mixed, clean syngas mixture which replicated the composition of the Bioliq® syngas. The impurities of the biomass-derived Bioliq® syngas were reported to be: CH₄ (0 %), CH₃OH (0 %), HCl (0 ppm), HCN (0.91 ppm), NH₃ (150 ppm), H₂S (54.1 ppb), COS (12.3 ppb). The analysis was done before CO₂ cleaning. (Infantes et al., 2020b)

Setups 5 and 6 used clean, commercially-mixed syngas. It mimicked the composition of the syngas produced from the gasification of beech wood or lignin, respectively, at the MILENA indirect gasifier at TNO Energy Transition, Biomass & Energy Efficiency Unit, the Netherlands (Liakakou et al., 2019), but no CH₄ was included in the mixture. Composition for the biomass-derived TNO gas and its impurities can be found in section 3.3 *Evaluation of beech wood and lignin derived syngas* above, and in Liakakou et al. (2020). (Infantes et al., 2020b)

The syngas used for setups 7 and 8 was clean, commercially-mixed. For setup 7, its composition was based on the syngas resulting from the gasification of lignin at 850 °C after limestone cleaning, at LNEG (National Laboratory of Energy and Geology), Portugal (data not published). For setup 8, the composition was equivalent to that of the syngas obtained by an updraft gasifier of lignin both using oxygen and steam as gasification agents, at the ENEA Research Centre of Trisaia, Italy (Cerone et al., 2017). Both the original biomass-derived syngas on which setups 7 and 8 are based contained only a small amount of N₂. This means that the standard off-gas analysis, as described elsewhere (Oswald et al., 2016), would not be possible, since N₂ is used in this fermentation system to calculate the total flow rate in the off-gas. The syngas from LNEG and ENEA contained CH₄, and since it has been proven to be inert (Liakakou et al., 2020) and can be easily detected by GC analysis, CH₄ was included in the custom-made gas mixture and used in place of N₂ to calculate the off-gas flow rate in the same manner. (Infantes et al., 2020b)

Two other theoretical, clean syngas compositions were tested in setup 9 and 10, named here “custom mixture A” and “custom mixture B”. (Infantes et al., 2020b)

3.4.1 Gas flow rate setting

Due to the differing gas composition of the gases tested, not all parameters could be kept constant simultaneously.

Table 3.3 shows the average composition and the gas flow fed into the fermenter for all syngases. The values are given as the measured off-gas composition by the on-line GC after the reactor reached equilibrium and under abiotic conditions (before inoculation). At that point, the gas flow fed into the fermenter equals to that which comes out at the off-gas. (Infantes et al., 2020b)

To enable a comparison between the different compositions, the gas flow rate was adapted in each fermentation so that the total molar flow of carbon (C_{in} , the sum of CO₂ and CO) fed into the fermenter was 0.4 mmol/min, except for setups 3 and 4 (Table 3.3). In these two fermentations, rather than the molar flow of carbon, the total gas flow was modified so that the molar flow of H₂ fed into the fermenter ($H_{2,in}$) was to 0.23 mmol/min. Both the flow of carbon or H₂ fed were established and chosen as standard conditions in previous experiments (data not shown). (Infantes et al., 2020b)

Table 3.3 – Composition of the gas, flow rate and amount of substance fed for each setup.

The bioreactors were sparged with each gas before inoculation for at least 3 h. The syngas composition is given based on the average of the values detected in the off-gas measured during this time, after reaching equilibrium conditions in the fermenter. In all cases, apart from CO, CO₂, H₂ and CH₄, the remaining component of the syngas is N₂. C_{in} refers to the sum of the amount of CO and CO₂. All fermentations were done as triplicates (n = 3), and the values given here are the correspondent averages. Superscripts a and b denote pairs of fermentations done under the exact same conditions, with equivalent gas compositions except for the presence of impurities. The syngas custom mixtures which were prepared with the same composition as biomass-derived syngas are marked as such, with the source of the syngas they were based on in brackets. TNO BW: syngas produced at TNO from beech wood; TNO LS: syngas produced at TNO from lignin; LNEG: syngas produced at LNEG, gasification at 850 °C, with lime stone treatment; ENEA: syngas produced at ENEA, gasification using O₂ and steam.

Syngas source	Bioliq® straw	Custom mixture (Bioliq®)	Bioliq® straw	Custom mixture (Bioliq®)	Custom mixture (TNO BW)	Custom mixture (TNO LS)	Custom mixture (LNEG)	Custom mixture (ENEA)	Custom mixture A	Custom mixture B
Impurities	Yes	No	Yes	No	No	No	No	No	No	No
Setup	1 ^a	2 ^a	3 ^b	4 ^b	5	6	7	8	9	10
Syngas composition [vol-%]										
CO	28.8	29.8	28.9	29.2	27.0	21.3	26.1	26.7	32.5	21.2
CO ₂	2.8	2.6	2.8	2.7	18.3	20.6	16.7	26.4	11.9	13.7
H ₂	29.5	29.1	28.4	28.3	23.3	25.4	30.4	34.5	21.9	21.9
CH ₄	-	-	-	-	-	-	18.9	5.3	-	-
Gas flow rate [mL/min]	26.3	26.3	18.0	18.0	18.0	23.0	20.0	16.0	18.0	23.0
C_{in} (CO₂ + CO) [mmol/min]	0.37	0.38	0.25	0.26	0.37	0.43	0.38	0.38	0.36	0.36
H_{2, in} [mmol/min]	0.35	0.34	0.23	0.23	0.19	0.26	0.27	0.25	0.18	0.23
CO_{in} [mmol/min]	0.34	0.35	0.23	0.23	0.22	0.22	0.23	0.19	0.26	0.22
CO_{2, in} [mmol/min]	0.03	0.03	0.02	0.02	0.15	0.21	0.15	0.19	0.10	0.14
CH_{4, in} [mmol/min]	-	-	-	-	-	-	0.18	0.04	-	-

3.5 Impact of elevated pressure

3.5.1 Microorganism and media

C. ljungdahlii DSM 13528 was used to perform the experiments. The strain was originally obtained from the DSMZ culture collection (Deutsche Sammlung von Mikroorganismen und Zellkulturen, Braunschweig, Germany). (Mohr et al., 2019)

Both the pre-cultures and the experiments' media was based on GA (General Acetogen) medium, adapted from Groher and Weuster-Botz (2016). It contained: 20 g/L 2-(N- morpholino) ethanesulfonic acid (MES), 1 g/L NH₄Cl, 0.3 g/L KCl, 0.23 g/L KH₂PO₄, 0.5 g/L MgSO₄·7H₂O, 2.25 g/L NaCl, 2 g/L yeast extract, 0.15 g/L CaCl₂·2H₂O and 0.001 g/L resazurin, 1 ml/L of trace element solution and 10 ml/L of vitamin solution. The trace element solution was composed of 4 g/L FeSO₄·7H₂O, 3 mg/L Na₂SeO₃·5H₂O, 4 mg/L Na₂WO₄·2H₂O, 3 g/L FeCl₂·4H₂O, 140 mg/L ZnCl₂, 200 mg/L MnCl₂ ·4H₂O, 12 mg/L H₃BO₃, 380 mg/L CoCl₂·6H₂O, 4 mg/L CuCl₂·2H₂O, 48 mg/L NiCl₂·6H₂O, and 72 mg/L Na₂MoO₄·2H₂O. The vitamin solution contained: 4 mg/L biotin, 4 mg/L folic acid, 20 mg/L pyridoxine, 10 mg/L Thiamine-HCl·2H₂O, 10 mg/L riboflavin, 10 mg/L nicotinic acid, 10 mg/L calcium pantothenate, 0.2 mg/L cobalamin, 10 mg/L 4-aminobenzoic acid and 10 mg/L lipoic acid. (Mohr et al., 2019)

The pH of the medium was adjusted to 6.0 with KOH and distributed in bottles. These were then closed with gas-tight butyl rubber stoppers and secured with an aluminium seal, and anaerobized. The anaerobisation process was performed as follows: a needle, which was connected to a vacuum/gas line, was inserted through the septum; then, vacuum was applied to a final pressure of 10 psi (absolute), holding for 40 seconds, followed by pressurizing the bottles to 30 psi (absolute) using a gas mixture containing 20 vol-% carbon dioxide in nitrogen (Air Liquide, France). Following this, vacuum was applied again, and the whole process was repeated for 20 cycles. The anaerobised bottles were autoclaved at 121 °C, holding time 20 min. After autoclaving, 1 g/L of cysteine HCl·H₂O and 10 g/L of fructose were aseptically dispensed to each bottle. Cysteine solution was prepared using anaerobised water, prepared by boiling and cooling under a constant flow of N₂. After dissolving the cysteine, the bottles were immediately anaerobised. The fructose stock solution was also anaerobised prior to autoclaving. (Mohr et al., 2019)

To ensure sterility and anaerobic conditions, all additions to the autoclaved bottles were done using sterile syringes and needles and piercing through the septum. All stock solutions were prepared and anaerobised as described above. (Mohr et al., 2019)

For pre-cultivation of *C. ljungdahlii* a glycerol stock (total volume 1 mL) was transferred anaerobically to a serum bottle containing 50 ml of anaerobic, sterile GA medium (prepared as above) and incubated for 48 h. The method for glycerol stock preparation was based on the one outlined by Straub (2012), and adapted by Oswald (2018). The glycerol stocks were prepared in sterile, anaerobic hungate-type tubes which were closed with gas-tight rubber septa and secured with a perforated screw cap. In order to anaerobically transfer the glycerol stock and to inoculate the following cultures, sterile syringes and needles were used. The withdrawal of the liquid and its addition to the following serum bottle was performed by piercing through the septum. (Mohr et al., 2019)

From the revived glycerol, a total of 5 mL was transferred anaerobically to 50 mL of fresh GA medium and cultivated at 37 °C and 120 rpm for 24 h. From this culture, 5 mL were dispensed into each of two fresh 50 mL bottles and were cultivated under the same conditions. (Mohr et al., 2019)

3.5.2 Effect of syngas overpressure

3.5.2.1 Experimental setup

All experiments were performed in batch, at 37 °C, with a starting pH of 6, and without shaking. Inoculation volume was, for all cases, 20 %.

The syngas used was composed of 32.50 % CO, 16.00 % CO₂ and 32.50 % H₂ (in N₂).

The cultures were subjected to three different pressures: 1.5, 2 and 2.5 bar (absolute) were applied. A control was included at atmospheric pressure (1.1 bar absolute). The slight overpressure in the control bottle (approximately 0.1 bar absolute) served as a safety measure to prevent any oxygen or contamination entering the bottles.

All experiments were done in 1 L bottles (Figure 3.1) tightly closed with a rubber stopper (item number 203045, Glasgerätebau Ochs Laborfachhandel e.K.), and a hollow plastic screwcap (item number L994.1, Carl Roth). All bottles were tested prior to the experiment to ensure gas-tightness.

All bottles were filled with 20 mL GA medium. The bottles were autoclaved and anaerobised following the same procedure explained above. After autoclaving, and immediately before starting the experiment, the gas phase was changed by creating vacuum with an electric vacuum pump up to approximately 0.3 bar absolute and holding for 5 minutes, and subsequently filling the headspace of the bottles to the desired pressure. A 0.2 µm filter was used to dispense the gas to ensure sterility. Afterwards, they were inoculated, anaerobically and aseptically.

3.5.2.2 Sample withdrawal, pH, optical density and pressure measurements

For each sample, 1 mL cultivation broth was taken from each bottle. Immediately prior to sample taking, a gentle swirl was given to each bottle to ensure homogeneity. On the 1 L bottles, a sterile syringe and needle were used to pierce through the rubber septum, and the sample was obtained by inverting the bottles.

The sample was dispensed onto an empty 2 mL plastic tube. pH and optical density (OD) were measured, and afterwards, the sample was centrifuged at 16000 g for 10 minutes. The supernatant was recovered and stored at -20 °C for product formation analysis.

The pH of each sample was measured directly after withdrawal with a pH meter (Profilab pH 597, WTW) fitted with micro electrode (SenTix® Mic, WTW).

The OD of the samples was measured at 600 nm using a UV-Vis spectrophotometer (Spectronic 200, Thermo Fisher Scientific Inc). If the measured sample OD was above 0.6, the sample was diluted with 0.9 % w/v NaCl. The sample, or the dilution if this was needed, was centrifuged at 16000 g for 10 minutes, the supernatant collected, and its OD measured. The sample OD was the result of subtracting the supernatant value from the (diluted if needed) sample OD. This procedure was performed to be able to account for any changes in the absorbance caused by the presence of resazurin in the medium.

The cell dry weight was calculated applying a conversion factor of 0.3, as explained above in section *3.1.3 Analytical Methods*.

Pressure was measured at the time of sampling. A precision hand-held manometer (GMH 3111, Greisinger) equipped with a pressure sensor (GMSD 10 BR - K31, Greisinger) ending in a Luer-Lock® connection was used. A sterile needle was attached to the Luer-Lock®, and it was used to pierce through the septum.

3.5.2.3 Fructose, acetic acid and ethanol determination

Fructose was measured using an enzymatic kit (article number 10207748035, r-biopharm). No more measurements were done after its complete consumption was detected. Acetate and ethanol content of fructose-containing samples were determined using an enzymatic kit (10148261035 for acetate and 10176290035 for ethanol, r-biopharm).

The acetate and ethanol quantification of fructose-free samples was determined by GC as described by Oswald (2018), with minor modifications. The GC device (model 6890N, Agilent), was equipped with an auto-sampler, ROTI®Cap FFAP capillary column (0.5 µm, 30 m × 0.32 mm ID, Carl-Roth) and FID, and the carrier gas was helium at 1 bar. The analytical standards consisted of a mixture of ethanol,

sodium acetate and isobutanol in 0.18 M HCl. The standards were prepared at three different final concentrations of ethanol and sodium acetate: 5 mM, 10 mM and 20 mM. Isobutanol concentration was kept unaltered at 9.09 mM for all standards. 50 μ M of an acidified internal standard (100 mM isobutanol in 2 M HCl) was added to 500 μ L of sample.

Samples were prepared by acidifying 500 μ L with 50 μ L internal standard solution, consisting of 100 mM isobutanol in 2 M HCl. The analysis was conducted by injecting 1 μ L of sample or standard. Initial temperature of the column was 60 °C, holding for 2 min, followed by 10 °C/min ramp, with a final temperature of 180 °C. Total time of the measurement was 20 minutes.

3.5.2.4 Headspace gas analysis

To verify the gas composition in the bottle's headspace at the start of the experiment, a gas sample was taken from each bottle on the first sample taking point and measured with a Micro GC gas analyzer (model 3000, Inficon).

The sample was divided by the Micro GC into two channels which simultaneously measured the gas components. In the first channel, H₂, N₂, O₂ and CO were measured with a 10 m Molsieve column preceded by a 3 m PLOT U pre-column. CO₂ was measured in the second channel by a 10 m PLOT Q column. Carrier gas was Helium. The analysis was performed at 80 °C, isothermally.

A 5 mL gas sample was withdrawn from the headspace using a syringe attached to a sterile needle, which was used to pierce through the septum. The gas-filled syringe was immediately attached to the Micro GC inlet, and the sample was manually injected.

3.5.3 Effect of CO₂/H₂ and CO overpressure

3.5.3.1 Experimental setup

All experiments were performed in batch, at 37 °C, with a starting pH of 6, and without shaking. Inoculation volume was, for all cases, 20 %.

Two different gases were used as substrate for the culture, either 100 % CO or a CO₂/H₂ mixture (26.70 % CO₂, 53.30 % H₂ and 20 % N₂).

For each gas to be tested, 8 bottles were prepared. Four served as a control and were kept at atmospheric pressure. 1 L bottles were used for this setup, prepared as described above in section *3.5.2.1 Experimental setup*.

For the pressure treatment, 4 pressure resistant bottles (item number 8649-35, Ace Glass Inc.) with a total capacity of 140 mL were used. The bottles had two ports, a #7 and a #15 Ace-Thread.

On the #7 Ace-Thread port, a pressure gauge (item number 13385-48, Ace Glass Inc.) was fitted, connected to the flask by a PTFE adapter (item number 5844-58, Ace Glass Inc.). A hollow PTFE bushing (item number 8648-19, Ace Glass Inc.) was screwed onto the #15 port. A manually cut-to-size butyl rubber septum was then tightly fitted onto the orifice. Both ports were sealed gas-tight by front-seal FETFE® O-Rings (item number 7855-707 for #7 port, I.D. 9.2 mm, wall size 2.6 mm; item number 7855-716 for #15 port, I.D. 18.6 mm, wall size 3.5 mm; Ace Glass Inc.). All flasks were tested prior to the experiment to ensure gas-tightness. Figure 3.1 shows the bottle setup here described.

All bottles contained 40 mL of GA medium, and were anaerobised and autoclaved following the same procedure explained above in section 3.5.2.1 *Experimental setup*.

3.5.3.2 Sample withdrawal, pH, optical density and pressure measurements

For each sample, 1.5 mL cultivation broth were taken from each bottle. Immediately prior to sample taking, a gentle swirl was given to each bottle to ensure homogeneity. A sterile syringe and needle were used to pierce through the rubber septum, and the sample was obtained by inverting the bottles. For the pressure flasks, to prevent the syringe plunge to escaping the syringe body due to the pressure and to facilitate the sample taking, a two-way valve with Luer-Lock® connectors was used between the needle and the syringe. The needle was inserted through the septum with the valve closed, the



Figure 3.1 – 1 L bottle (left) and Ace Glass pressure flasks with pressure gauge attached (right). 1 L bottles were used for all experiments up to 2.5 bar. The Ace Glass pressure flasks were used for the CO and CO₂/H₂ 5 bar experiments.

bottle was inverted, and the valve was slowly opened to allow for the required amount of broth to fill the syringe. After sampling, the valves were rinsed with 96 % ethanol and completely submerged in a fresh 96 % ethanol solution in a glass container. The ethanol was then discarded, the container was covered, and the whole was put to dry at 60 °C. Clean, dried valves were reused during the experiment.

Each sample was divided into two separate Eppendorf tubes for further processing. One tube contained RNeasy Protect[®] Bacteria Reagent (QIAGEN[®]) at a 2:1 reagent to sample volume ratio. 0.5 mL from the sample was added and vortexed for 5 seconds. Afterwards, it was incubated at room temperature for 5 min, followed by centrifugation at 5000 g for 10 min. The supernatant was decanted, and the pellet was stored at -80 °C.

The remaining was dispensed onto a second empty tube. Sample treatment, pH and OD measurements were performed as described above in section 3.5.2.2 *Sample withdrawal, pH, optical density and pressure measurements*. For the 5 bar treated bottles, pressure was read directly from the fitted gauge.

3.5.3.3 Fructose, acetic acid, ethanol, and formic acid determination

Fructose, acetic acid and ethanol were measured as in 3.5.1.3 *Fructose, acetic acid and ethanol determination*. Formic acid was measured using an enzymatic kit (article number 10979732035, r-biopharm).

3.5.3.4 Specific production rate calculation

Due to the limitation in the number of samples that could be taken, an approximation using the average of the CDW (cell dry weight) between two subsequent sample points was used. The specific production rate was thus calculated between two successive samples, according to the following equation:

$$\text{specific production ratio} = \frac{\rho_{i,t_2} - \rho_{i,t_1}}{\text{average}(CDW)_{t_2,t_1} \times (t_2 - t_1)} \quad (3.22)$$

with ρ_i being the concentration of substance i , and *average (CDW)* being the average (arithmetic mean) concentration of biomass, measured as cell dry weight, for times t_1 and t_2 . All results are given as average (arithmetic mean) \pm STD.

3.5.3.5 Headspace gas analysis

The same procedure as outlined in section 3.5.2.4 *Headspace gas analysis* was followed.

3.5.3.6 Relative quantification of gene expression by RT-qPCR (quantitative reverse transcription PCR)

3.5.3.6.1 Selected genes

The following genes were studied (locus tag given in brackets): *cooC2*, CODH nickel-insertion accessory protein (CLJU_c37660); *fdh*, formate dehydrogenase subunit alpha (CLJU_c08930); *pta*, phosphotransacetylase (CLJU_c12770); and *aor*, aldehyde ferredoxin oxidoreductase (CLJU_c20110). The reference genes were *gyrA*, DNA gyrase subunit A (CLJU_c00070) and *fhs* formate-tetrahydrofolate ligase (CLJU_c37650). Primers sequences for *fdh*, *pta* and *aor* were obtained from Xie *et al.* (2015). Primer sequences for *gyrA* and *fhs* were obtained from Liu *et al.* (2013). The primer sequence for *cooC2* was designed *de novo*, as shown in Table 3.4. All primers were purchased from Thermo Fisher Scientific Inc. in standard desalted form.

Table 3.4 – Primer sequence for *cooC2* (CLJU_c37660).

Gene		Primer sequences (5' – 3')
<i>cooC2</i>	forward	ATCTACACCTTGTGCTGTCC
	reverse	TTGTTTCTGCCCGAAAATG

3.5.3.6.2 RNA extraction, purification, and quantification

The frozen pellets, treated as explained above (3.5.2.2 *Sample withdrawal, pH, optical density and pressure measurements*), were used to extract the RNA. Extraction was performed with *Quick-RNA™* Fungal/Bacterial Microprep Kit (Zymo Research), as described in the manual, with in-column DNase I Digestion.

A further DNase I treatment followed the extraction. The method was based on the one described in the manual of the RNA Clean & Concentrator™-5 kit (Zymo Research), but the DNase I treatment was performed twice before clean-up. The incubation temperature for the DNase I treatment was 35 °C, for 15 minutes.

To assess the concentration of RNA in the extracted samples, a first, direct quantification was done by dispensing 2 µL of the sample on a Take3 plate. The measurement was done in an Epoch™ Microplate Spectrophotometer (BioTek), controlled with Gen5 software. For an accurate measurement, a Quant-it™ RNA assay (Invitrogen, Thermo Fisher Scientific Inc.) was used. The results from the Epoch™ measurement was used to dilute the samples so that they fell in the calibrated range of the assay. The dilutions were always done with nuclease-free water, and the assay was performed in a 96-well plate

according to its instructions. The measurement was done in a plate reader (Infinite 200 PRO, Tecan Trading AG).

3.5.3.6.3 RT-qPCR

A dye-based, quantitative reverse transcription PCR kit was used (Luna[®] Universal One-Step RT-qPCR Kit, New England Biolabs Inc.). The RNA template volume was adjusted between 1 μL and 3 μL , so that a constant amount of 10 ng of RNA was used for each reaction. If necessary, RNA samples were diluted with nuclease-free water to 10 ng/ μL , according to the concentration obtained from the Quant-it[™] assay. The amplification was performed following the protocol from the kit. No template control (NTC) and no reverse transcription control (NRT) were added to each plate, and all measurements were done at least in duplicates.

To assess target specificity, a melt curve was done at the end at the conditions recommended for the real-time detection instrument used (CFX96, Bio-Rad Laboratories GmbH): from 60 °C to 95 °C with an increment of 0.5 °C and plate read every 5 seconds, as recommended for the real-time detection instrument used.

To determine the efficiency of each of the primers, the standard curves method was used with template concentrations in the range of 10 ng - 10 pg. Each primer dilution was used for a qPCR reaction in triplicate ($n = 3$). The mean C_q (quantification cycle, also known as threshold cycle, C_t , or crossing point, C_p) obtained was plotted against the \log_{10} of the RNA amount for each dilution. The slope of the regression line was then used to calculate the efficiency E according to the following equation (Bustin et al., 2009; Riedel et al., 2014):

$$E = 10^{[-1/slope]} \quad (3.23)$$

The efficiency can also be expressed as a percentage; in this case, the formula is:

$$E (\%) = (10^{[-1/slope]} - 1) \times 100 \quad (3.24)$$

3.5.3.6.4 Relative gene expression calculations and statistical considerations

The normalization of the qPCR data was done by the geometric averaging of two reference genes. The method is based on the equation developed by (Pfaffl, 2001), but modified to include multiple reference genes (Vandesompele et al., 2002; Pfaffl, 2007; Riedel et al., 2014), according to the equation:

$$\text{Relative gene expression} = \frac{(E_{GOI})^{\Delta Cq_{GOI}}}{\text{GeoMean}[(E_{REF})^{\Delta Cq_{REF}}]} \quad (3.25)$$

and

$$\Delta Cq = \text{Control } Cq - \text{Treatment } Cq \quad (3.26)$$

where E is the efficiency, GOI is the gene of interest, and REF is a reference gene. The term *GeoMean* implies the geometric mean. The control was the culture grown at atmospheric pressure, while the treatment was the one at 5 bar.

The averaging of the replicates was done, as well, using the geometric mean, since it is less influenced by outlying values and differences in abundance between the different genes (Vandesompele et al., 2002).

3.6 Sequential cultivation for acetogenic fermentation from oxygen-containing waste gas

3.6.1 Microorganisms and media

P. thermoglucosidasius DSM 6285 and *Clostridium ljungdahlii* DSM 13528^T were obtained from the Deutsche Sammlung von Mikroorganismen und Zellkulturen (DSMZ, Braunschweig, Germany). (Mohr et al., 2019)

P. thermoglucosidasius DSM 6285 was cultivated in mLb (modified Luria-Bertani) medium (g/l): tryptone (10), yeast extract (5), NaCl (5); 1.25 mL/L NaOH (10% w/v), and 1 mL/L of each of the filter-sterilized stock solutions 1.05 M nitrilotriacetic acid, 0.59 M MgSO₄·7H₂O, 0.91 M CaCl₂·2H₂O and 0.04 M FeSO₄·7H₂O (Zeigler, 2001). A first (20 mL mLb medium) pre-culture was grown for 24 h and a second (20 mL mLb medium) pre-culture was inoculated to an absorbance (OD₆₀₀) of 0.1 from the first pre-culture and incubated for 4 h. Both pre-cultures were grown aerobically at 60 °C and 120 rpm (Infors Thermotron, Infors AG, Bottmingen, Switzerland) in 20 mL mLb. Serum bottles (Glasgerätebau Ochs, Bovenden, Germany), closed with gas-tight butyl rubber stoppers and secured with an aluminium seal were used (Carl Roth + Co. KG, Karlsruhe, Germany). (Mohr et al., 2019)

Clostridium ljungdahlii DSM 13528^T was pre-cultured in modified GA-based medium, as described above in section 3.5 *Impact of elevated pressure – microorganism and media*.

3.6.2 Experimental set up

Stoppered serum flasks (250 mL), gas-tight and prepared as above, containing 50 mL of modified Luria Bertani (mLB) medium and with an initial gas atmosphere of CO and air (50:50 ratio) were inoculated with 1 ml of second pre-culture of *P. thermoglucosidasius* and cultivated for 70 h at 60 °C and 120 rpm. Subsequently, 5 mL of the *C. ljungdahlii* pre-culture (OD₆₀₀ = 2.5) was added to the *P. thermoglucosidasius* culture. Immediately before inoculating with *C. ljungdahlii*, 50 µL of GA trace elements, to the same final concentration as the GA medium, were added to each bottle to ensure that all elements necessary for the growth of *C. ljungdahlii* were present. Incubation of the *P. thermoglucosidasius/C. ljungdahlii* cultures were performed at 37 °C and 120 rpm. The experiments were performed in quadruplicate for a duration of 240 h. (Mohr et al., 2019)

3.6.3 Analytical methods

Growth was routinely monitored by taking 1 ml culture samples twice per day and performing absorbance (OD₆₀₀) measurements using an Ultrospec 1100 pro spectrophotometer (Amersham Biosciences, USA). Acetate concentrations were similarly monitored using the Roche Yellow line enzymatic assay (Hoffmann- La Roche, Switzerland). To measure the gas composition in the bottles at each sampling point, a 5 mL gas sample was withdrawn with a syringe from the headspace of the bottle. The bottles were kept at the incubating temperature for the specific microorganism by means of a water bath. The sample was then immediately injected into a 300 Micro GC gas analyzer (Inficon, Bad Ragaz, Switzerland) with columns Molsieve and PLOT Q. Throughout the total analysis time of 180 s, the temperature was maintained constantly at 80 °C. (Mohr et al., 2019)

Pressure was measured before and after sample taking using a manometer (GDH 14 AN, Greisinger electronic, Regenstauf, Germany). Gas composition was calculated using the ideal gas law as previously described (Mohr et al., 2018a). The acetate yield was calculated based on Bengelsdorf et al. (2013). (Mohr et al., 2019)

4 RESULTS

4.1 Impact of medium components and process parameters

If not otherwise stated, all fermentations were done as triplicates ($n = 3$), and the results are presented here as the average.

4.1.1 Effect of medium components

The first fermentation (setup 1) achieved a final acetate and ethanol concentration of 20.1 g/L and 2.0 g/L, respectively, after 95 h (Figure 4.1A). At 69 h, 15.0 g/L of acetate and 0.9 g/L of ethanol had been formed. In the case of the increased cysteine, at 68 h, 13.6 g/L of acetate and 0.9 g/L of ethanol had been formed. After 95 h, the concentration of products in the reactor kept at pH 5.9 was 16.6 g/L of acetate and 2.0 g/L of ethanol. During the fermentation with 1 g/L of cysteine (setup 3), for the first 68 h, it became clear that the behavior of the culture was equivalent to that of setup 1. In two fermenters (setup 3b) the pH was lowered after 68 h, but one fermenter (setup 3a) was kept at 5.9 to corroborate that an increased cysteine concentration did also not affect the behavior of the microorganism later in the run (Figure 4.1B). (Infantes et al., 2020a)

Both setups 1 and 3 followed a remarkably similar growth pattern up to 68 h. Setup 1 reached a final and a maximum cell dry weight (CDW) of 0.8 g/L and 0.9 g/L, respectively. In this fermenter, at 67 h, the CDW concentration was 0.8 g/L. In the case of increased cysteine, the same value was achieved at 68 h. For the fermenter left unaltered, setup 3a, the CDW at 95 h of process-time and the maximum value reached were 0.7 and 0.8 g/L, respectively. (Infantes et al., 2020a)

Concerning the influence of an increased yeast extract concentration (setup 4), a comparable final amount of acetate was formed (21.5 g/L), but only 1.4 g/L of ethanol was produced (Figure 4.1C). In terms of biomass, the final reached value was lower (0.6 g/L), as well as its maximum (0.8 g/L at 48 h), resulting in a notably higher $Y_{p/x}$ value: 41 g/g compared to 29 g/g in both setups 1 and 3a. (Infantes et al., 2020a)

Substrate consumption graphs are depicted in detail in Figure 4.2. Because of the difference of the gas consumption profiles of one fermenter, it was left out for the average calculations. This will be discussed further in detail in the section below. Both medium modifications performed similarly to setup 1 as to the duration of the maximum overall usage of the substrate, but the starting and ending time did differ, with setup 4 (increased yeast extract) starting earlier. When looking solely at CO fixation, setups 3a, 3b, and 4 behaved alike, with the maximum CO fixation lasting around 10 h less compared to the conditions of setup 1 (Table 4.1). (Infantes et al., 2020a)

For the off-gas profile for setups 1, 3 and 4 please see the Appendix, Figure A.I.

Concerning the overall yields (calculated up to the end of the fermentation), the most significant difference is the $Y_{P/X}$ in setup 4, as mentioned above (Table 4.2). Moreover, this fourth experiment had the highest productivity among all fermentations, despite the reduction in the amount of ethanol produced.

For easier comparison, since all fermentations were run for approximately 93 h, but each stopped consuming the gaseous substrates at different times, yields and productivities were also calculated up to the point when maximum CO fixation came to an end, as found in Table 4.3. Setups 1, 3a, 3b, and 4 performed likewise when compared up to the point when maximum CO fixation stopped. The most noticeable difference is the lower $Y_{P/S, fed}$ achieved by setup 3b. The highest converted amount of carbon fed into products ($Y_{P/S, fed}$) was reached by the first setup (0.51), while setup 3b was the lowest (0.38). Nonetheless, the latter achieved a comparable yield of products per carbon fixed ($Y_{P/S, fixed}$). In terms of gram of product formed per gram of biomass ($Y_{P/X}$), the difference seen on the end-of-process yields is already to be found here, with setup 4 achieving the highest value. The acetate to ethanol ratio also differs slightly during this phase, with the most acetate per mol of ethanol being produced by the setup 1 fermentation, contrasting with the results seen when looking at the end-of-process values.

Table 4.1 – Gas consumption profiles. All values given as an average of a triplicate ($n = 3$), except for the following: 3a - values of the fermenter where pH was not altered; 3b - average of the two fermenters where the pH was changed after 68 h to 5.4, with superscripts c and d designating the value for each individual fermenter, due to the divergence observed. (Infantes et al., 2020a)

	Setup	Altered medium components			Altered pH		Altered pH and gas flow	
		1	3a	4	2	3b	5	6
Maximum overall usage interval	Start (h)	32.9	28.1	18.3	17.29	30.6 ^c 46.3 ^d	20.9	24.4
	End (h)	63.0	60.8	50.7	22.90	62.6 ^c 67.1 ^d	38.0	46.1
	Duration (h)	30.1	32.6	32.4	5.61	32.0 ^c 20.8 ^d	17.1	21.7
Time to end of maximum CO fixation (<85%) (h)		78.7	66.5	68.6	22.9	67.7 ^{c, d}	45.6	59.9

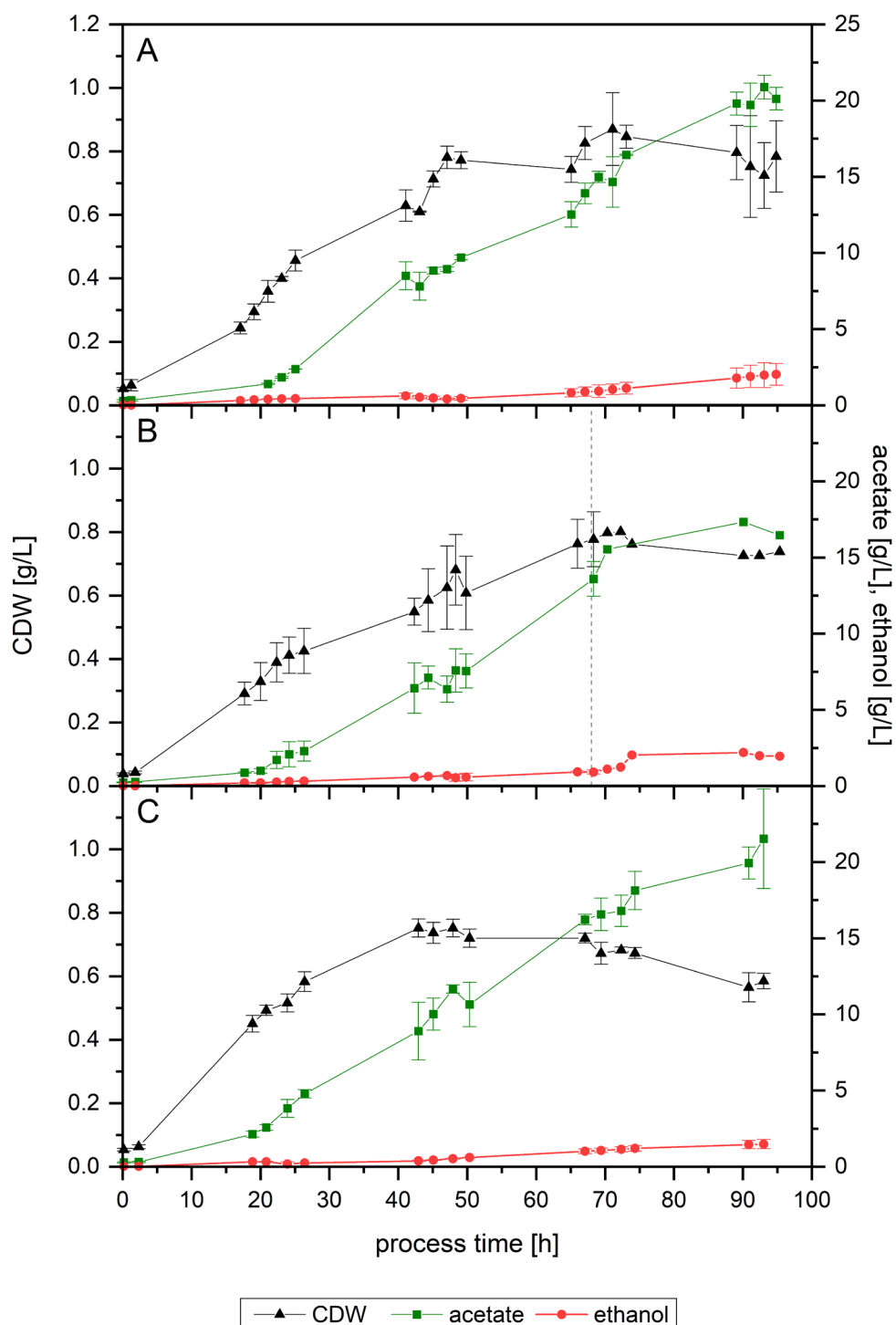


Figure 4.1 – Growth and product formation of setup 1 (A), setup 3 with increased cysteine (B) and setup 4 with increased yeast extract (C). In Figure B, the average of three fermenters is shown up to 68 h (vertical line). Afterwards, only the fermenter kept at pH 5.9 is shown (setup 3a). Average values of the triplicates ($n = 3$) with STD for cell dry weight (CDW, black triangles), acetate (green squares) and ethanol (red dots). Points indicate actual measurements. Lines are only depicted for clarity purposes. (Infantes et al., 2020a)

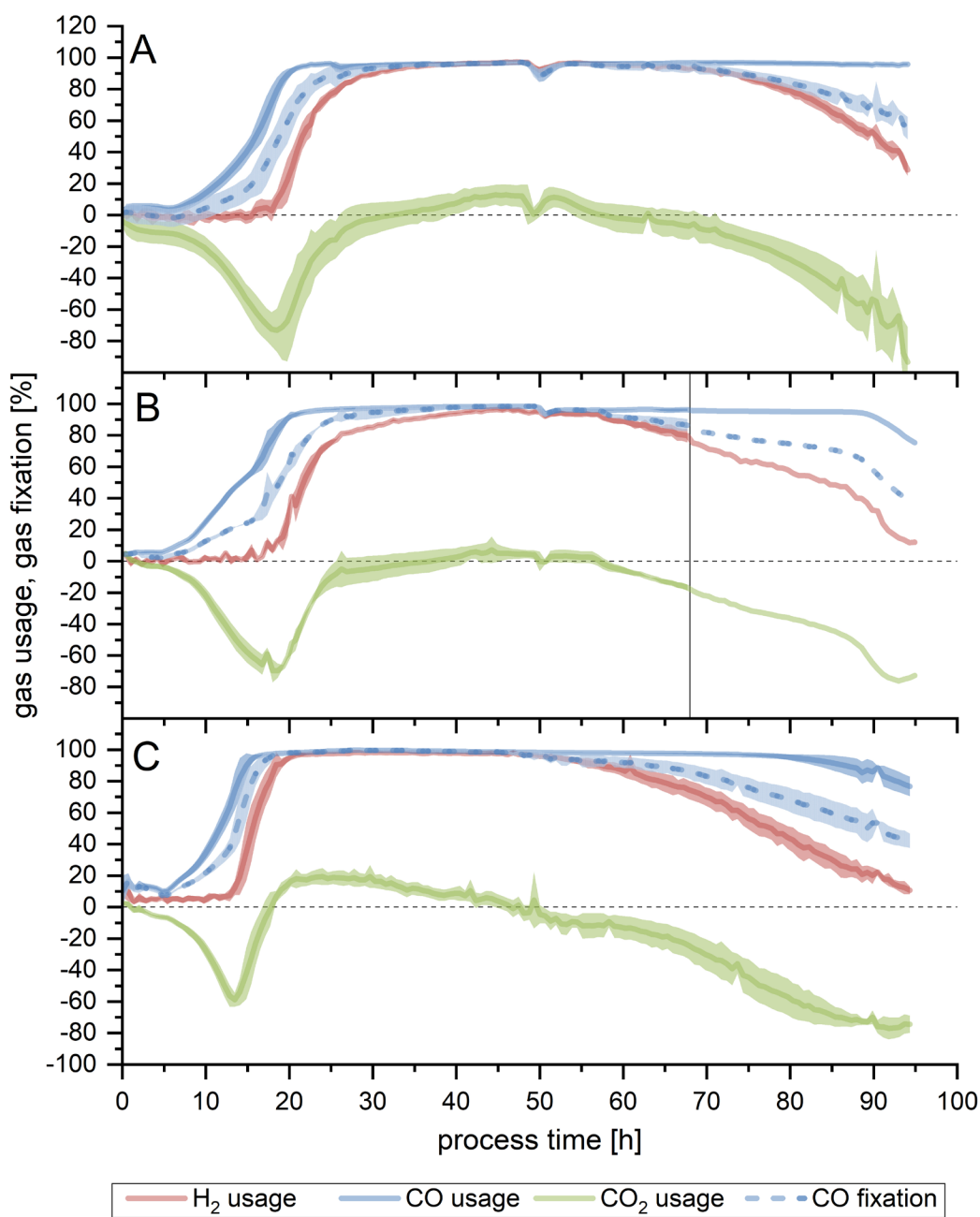


Figure 4.2 – Substrate usage or fixation for setup 1 (A), setup 3 with increased cysteine (B) and setup 4 with increased yeast extract (C). In Figure B, the average of two fermenters is shown up to 68 h (vertical line). Afterwards, only the fermenter kept at pH 5.9 is shown (setup 3a). One fermenter has been left out of the averages due to being remarkably delayed in comparison with the other two. Usage is shown for H₂ (red line), CO₂ (green line) and CO (blue line). CO fixation is depicted by the dotted blue line. Except where otherwise stated, lines show the average of a triplicate (n = 3), while the lighter colored areas depict the standard deviation (Infantes et al., 2020a)

Table 4.2 – Fermentation outcomes, yields, and productivities at the endpoint. 3a: calculated for the fermenter where pH was not altered. 3b: referring to the pair of fermenters where the pH was changed after 68 h to 5.4. $Y_{P/S}$ (g/g) = gram of products (acetate and ethanol) formed per gram of substrate. $Y_{P/X}$ (g/g) = gram of product (acetate and ethanol) per gram of biomass (cell dry weight). Values are given as the average of a triplicate (n = 3) with standard deviations, except for setup 3a, where only the values for the fermenter left unaltered at pH 5.9 are shown, and setup 3b, where the average of the two fermenters on which pH was modified is given. (Infantes et al., 2020a)

Variables		Altered medium components			Altered pH		Altered pH and gas flow	
		1	3a	4	2	3b	5	6
Setup		1	3a	4	2	3b	5	6
Total process time (h)		95	95	93	93	92	93	93
$Y_{P/S, \text{ used}}$ (g/g)		0.88 ± 0.09	0.85	0.88 ± 0.08	0.74 ± 0.02	0.80 ± 0.02	0.79 ± 0.06	0.79 ± 0.02
$Y_{P/S, \text{ fed}}$ (g/g)		0.43 ± 0.04	0.41	0.45 ± 0.04	0.13 ± 0.01	0.35 ± 0.03	0.24 ± 0.01	0.30 ± 0.01
$Y_{P/S, \text{ fixed}}$ (g/g)		0.96 ± 0.06	0.94	0.96 ± 0.09	0.97 ± 0.03	0.94 ± 0.04	0.92 ± 0.06	0.94 ± 0.04
$Y_{P/X}$ (g/g)		28.58 ± 2.02	29.25	41.10 ± 6.00	16.28 ± 1.69	25.89 ± 0.03	18.76 ± 1.61	21.26 ± 2.02
$V_{\text{gas, fed}}$ (L)		102.42 ± 0.00	102.96	99.66 ± 1.10	100.35 ± 0.00	99.77 ± 0.05	100.35 ± 0.00	99.68 ± 1.36
Acetate : Ethanol (mol)		7.80 ± 2.01	7.32	11.61 ± 2.44	11.20 ± 2.78	8.59 ± 2.15	8.96 ± 4.00	4.05 ± 1.44
Productivity (g/L·h)	Acetate	0.20 ± 0.02	0.19	0.22 ± 0.02	0.06 ± 0.01	0.17 ± 0.01	0.11 ± 0.01	0.10 ± 0.01
	EtOH	0.02 ± 0.01	0.02	0.02 ± 0.00	0.004 ± 0.00	0.02 ± 0.01	0.01 ± 0.00	0.02 ± 0.01
	Total (acetate + ethanol)	0.22 ± 0.02	0.21	0.24 ± 0.02	0.07 ± 0.00	0.19 ± 0.02	0.13 ± 0.01	0.12 ± 0.00

Table 4.3 – Fermentation outcomes, yields, and productivities calculated up to the point when maximum CO fixation stopped. 3a: calculated for the fermenter where pH was not altered. 3b: referring to the pair of fermenters where the pH was changed after 68 h to 5.4. $Y_{P/S}$ (g/g) = gram of products (acetate and ethanol) formed per gram of substrate. $Y_{P/X}$ (g/g) = gram of product (acetate and ethanol) per gram of biomass (cell dry weight). Values are given as the average of a triplicate (n = 3) with standard deviations, except for setup 3a, where only the values for the fermenter left unaltered at pH 5.9 are shown, and setup 3b, where the average of the two fermenters on which pH was modified is given. (Infantes et al., 2020a)

Variables	Altered medium components			Altered pH		Altered pH and gas flow		
	1	3a	4	2	3b	5	6	
Setup								
$Y_{P/S, \text{ used}} \text{ (g/g)}$	0.98 ± 0.00	0.95	0.91 ± 0.03	0.89 ± 0.04	0.84 ± 0.03	0.84 ± 0.00	0.81 ± 0.01	
$Y_{P/S, \text{ fed}} \text{ (g/g)}$	0.51 ± 0.08	0.44	0.46 ± 0.01	0.32 ± 0.03	0.38 ± 0.01	0.39 ± 0.00	0.33 ± 0.00	
$Y_{P/S, \text{ fixed}} \text{ (g/g)}$	0.99 ± 0.21	1.00	0.93 ± 0.03	0.93 ± 0.10	0.94 ± 0.06	0.93 ± 0.01	0.92 ± 0.03	
$Y_{P/X} \text{ (g/g)}$	23.89 ± 2.58	21.73	27.63 ± 1.44	9.06 ± 0.62	18.36 ± 2.33	11.98 ± 0.33	13.35 ± 0.56	
$V_{\text{gas, fed}} \text{ (L)}$	78.93 ± 0.00	73.80	76.02 ± 1.49	25.65 ± 0.00	73.76 ± 0.05	49.32 ± 0.00	53.84 ± 0.00	
Acetate : Ethanol (mol)	13.23 ± 2.96	11.49	11.66 ± 1.73	9.93 ± 2.15	11.69 ± 1.23	6.55 ± 1.72	5.07 ± 0.54	
Productivity (g/L·h)	Acetate	0.25 ± 0.04	0.22	0.23 ± 0.01	0.17 ± 0.01	0.19 ± 0.00	0.19 ± 0.00	0.13 ± 0.00
	EtOH	0.02 ± 0.00	0.01	0.02 ± 0.00	0.01 ± 0.00	0.01 ± 0.00	0.02 ± 0.01	0.02 ± 0.00
	Total (acetate + ethanol)	0.27 ± 0.04	0.23	0.25 ± 0.01	0.18 ± 0.01	0.20 ± 0.00	0.21 ± 0.00	0.15 ± 0.00

4.1.2 Effect of pH

When a fermentation with no pH regulation was performed (setup 2), growth slowed down after 20 h of process-time, with the pH having decreased to 5.0. After 43 h, when the pH value was already at its lowest (4.4), no significant growth or product formation could be detected. An increase in the CDW between 43 and 48 h was observed but was subsequently followed by a further decline and eventually remained mostly constant, with a final value of 0.5 g/L. The final acetate and ethanol concentration achieved were 6.2 and 0.4 g/L, respectively (Figure 4.3A). Gas consumption stopped after 40 h, with the maximum overall usage interval lasting only 5 h (Figure 4.4A and Table 4.1). The yields and productivities for this fermentation were the lowest among all the tests performed, with the exception of $Y_{P/S, \text{fixed}}$ (both end-of-process and up to the end of maximum CO fixation) and $Y_{P/S, \text{used}}$ (calculated up to the end of the maximum CO fixation), which were analogous to the rest. More detail can be found in Table 4.2 and Table 4.3. (Infantes et al., 2020a)

In setup 1, gas consumption started to decrease after approximately 70 h. After observing that for the first 68 h hours in setup 3 the gas consumption, growth, and product formation were equivalent to that of setup 1 (Figure 4.1A and Figure 4.1B, and Figure 4.2A and Figure 4.2B), the effect of lowering the pH after that point was investigated in setup 3b. Mainly, the aim was to observe the effect that a lower pH value would have in this late stage of the fermentation, especially regarding the product formation and its ratios. At 68 h, the pH was lowered in two of the fermenters by 0.5 units to 5.4, by using 4 M H_3PO_4 . As a result, maximum CO fixation came to an end, and a noticeable divergence between fermenters could be noted from this point on. In one fermenter (Figure 4.4B), immediately after the pH shift the gas consumption started to decrease for CO_2 and H_2 , and after a small delay, also for CO. Despite the declining tendency, some consumption could be detected up to 92 h: H_2 , CO and CO_2 average usage was 8, 25 and -16 %, respectively, between 80 and 92 h. CO fixation during this interval was 17 % on average. In the second fermenter (Figure 4.4C) a drop in H_2 and CO_2 usage also happened, but it eventually stabilized at around 50 % and -60 %, respectively. CO usage was still at its maximum, but as a result of the cells not using CO_2 any further, net CO fixation decreased as well, to an average of 69 % between 68 and 92 h. For the first fermenter, maximum overall usage lasted for 32 h (Table 4.1, fermenter "c"), while it was 10 h shorter in the second (Table 4.1, fermenter "d"). Looking at the CDW and product formation (Figure 4.3B), the deviation between the fermenters is apparent in the biomass yield, as indicated by the standard deviation bars, but much less remarkable in the case of product formation. The maximum CDW measured was, on average, 0.9 g/L at 74 h. After that, the amount of biomass in the fermenter fell to its final value, 0.7 g/L. Acetate was produced throughout the fermentation, even after the biomass decreased. The final concentration obtained was 15.7 g/L. Ethanol, on the other hand,

increased until 74 h of process time. Between 72 and 74 h, a somehow steeper increase of 0.4 g/L in the ethanol concentration in the fermenter was detected, from 1.1 to 1.5 g/L, value which remained constant later on. The yields and productivities achieved in this test were, in general, lower compared to setup 1, although not to such an extent as seen in the non-pH-regulated fermentation (Table 4.2 and Table 4.3). (Infantes et al., 2020a)

In the non-pH-regulated fermentation (setup 2), at 22.5 h just before gas consumption started to diminish, and when the exponential phase had already ended, but there was still cell growth detected, the measured pH was 4.8 (Figure 4.3A). This pH value was then chosen for a further test in setup 5. Here, the fermentation was carried out under standard conditions for 24 h to ensure that gas consumption was already at its highest. Changing the pH by externally adding an acid can cause a sudden shock in the culture, as well as changing the ionic strength of the medium. To prevent this, the pH was allowed to drop naturally, as the result of metabolic activity, to pH 4.8, and then the pH control was further regulated to this new value, which was reached after 55 h, as Figure 4.3C shows. In this setup, biomass concentration reached its maximum earlier than in setup 1: at 43 h, when the pH value was 5.0, the CDW measured was already 0.9 g/L – it was 0.6 g/L in setup 1. The biomass remained thus stable up to 70 h, dropping after that – 15 h after the pH of 4.8 was reached. Up to 50 h of process-time, acetate formation followed a similar profile to that of setup 1, reaching a value of 9.4 g/L in the reactor at that time. After this point, though, around the time when the lowest pH was reached and cell concentration decreased, the acetate production slowed down and eventually stopped at 11 g/L, at around 70 h. Ethanol formation also stopped at this point, reaching a final maximum concentration of 1.4 g/L. As can be seen in Figure 4.4D, during the first 24 h of cultivation the gas consumption followed a trend equivalent to that of the setup 1, although it reached its maximum 12 h earlier (Table 4.1). It can also be noted that the maximum overall usage interval was shorter, as well as the time until the end of maximum CO fixation. Yields and productivities for this fermentation were also found to be lower in relation to the setup 1, and the productivities at the end of the 93 h were almost halved (Table 4.2). (Infantes et al., 2020a)

Finally, looking at the yields and productivities up to the end of the maximum CO fixation phase (Table 4.3), the non-pH-regulated run achieved again both the lowest $Y_{P/S, fed}$ and $Y_{P/X}$. The values for the fermentation setup 1 were, in all cases, higher than the rest of the setups where pH was modified. That being said, in these runs the acetate to ethanol ratio was lower in comparison to the that first setup, indicating a shift towards more ethanol per mol of acetate produced. Productivities of setups 2, 3 (excluding the fermenter where the pH was not changed), and 5 were all similar. (Infantes et al., 2020a).

The off-gas profile for setups 2, 3b and 5 are shown in the Appendix, Figure A.II.

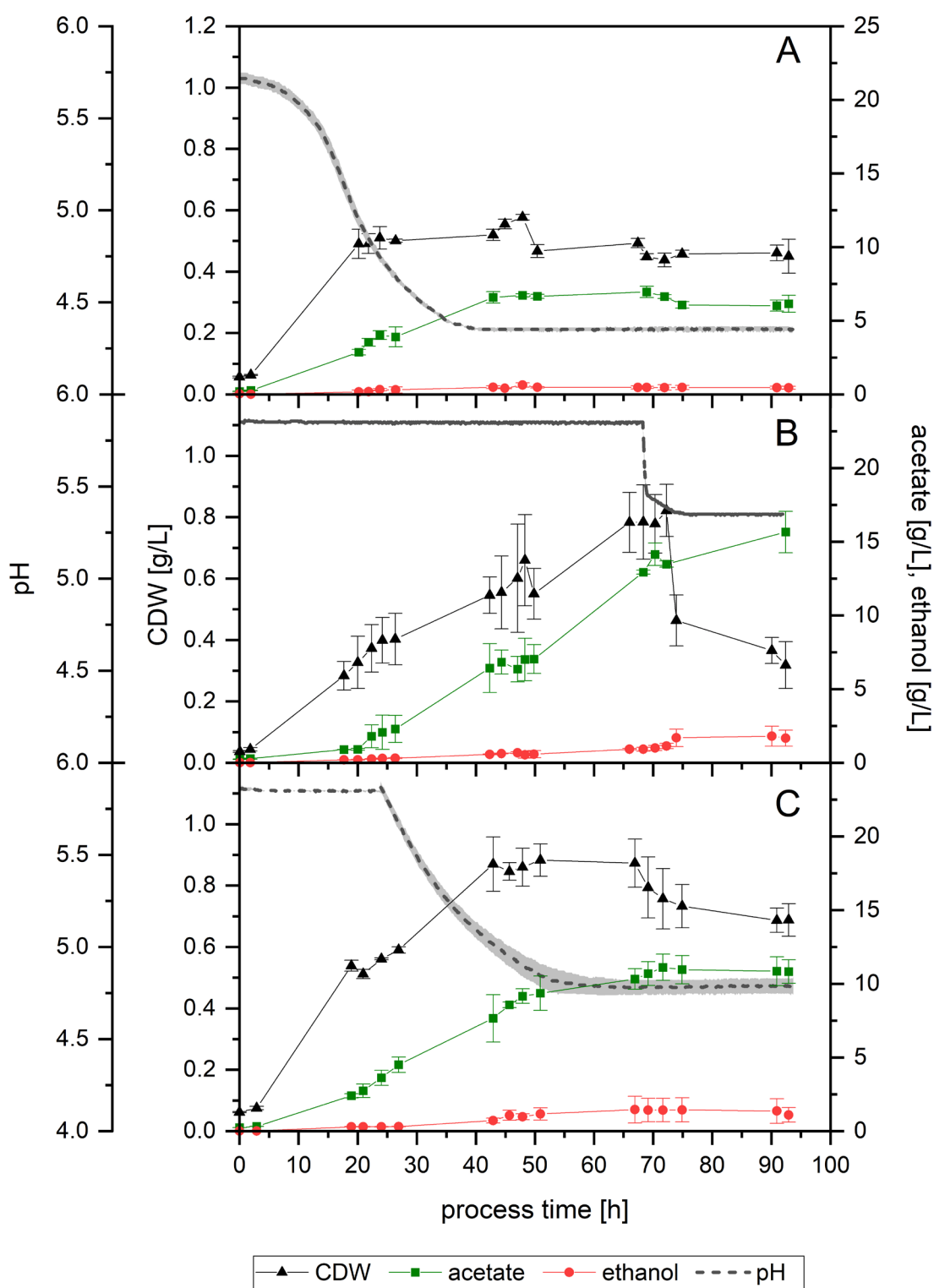


Figure 4.3 – Growth, pH profile and product formation of setup 2 without pH regulation (A), setup 3b with increased cysteine and pH change to 5.4 after 68 h (B) and setup 5 with pH allowed to drop to 4.8 after 24 h (C). Average values of the triplicates ($n = 3$) with STD for cell dry weight (CDW, black triangles), acetate (green squares), ethanol (red dots), and pH (grey dotted line). In figure (B), after 68 h, only the two fermenters where the pH was changed are plotted. The lightly colored area around the pH average represent the standard deviation. For CDW, acetate and ethanol points indicate actual measurements, lines are only depicted for clarity purposes. pH was measured on-line. (Infantes et al., 2020a)

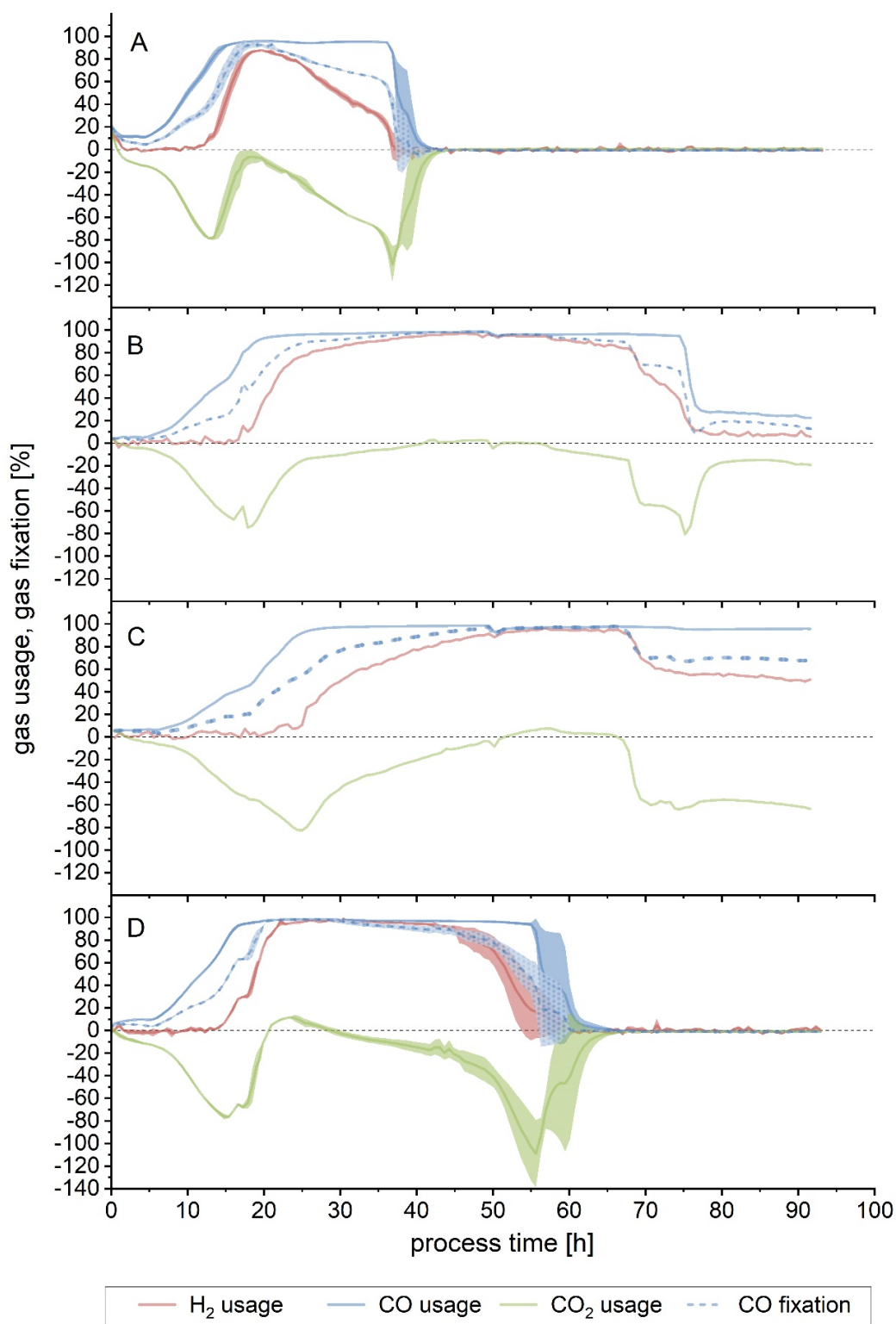


Figure 4.4 – Substrate usage or fixation for setup 2 without pH regulation (A), setup 3b with increased cysteine and pH change to 5.4 after 68 h (B and C) and setup 5 with pH allowed to drop to 4.8 after 24 h (D). Figure B and C show each of the individual fermenter profiles due to the divergence observed between them: the second fermenter (C) is remarkably delayed. Usage is shown for H₂ (red line), CO₂ (green line) and CO (blue line). CO fixation is depicted by the dotted blue line. The calculated difference between amount of substance flow rate fed into the bioreactor and the amount of substance flow rate detected in the off-gas is shown here as a percentage. For the CO fixation, if the CO₂ usage was negative, the amount of CO₂ produced was subtracted from the amount of (perceived) CO used. Except where otherwise stated, lines show the average of a triplicate ($n = 3$), while the lighter colored areas depict the standard deviation. (Infantes et al., 2020a)

4.1.3 Effect of pH and gas flow

It was noticed that in setup 5, despite the lower pH, the achieved cell growth was similar or even slightly higher than in the setup 1 fermentation, but the product formation was lower. Because of this, the focus was turned to finding out if a reduction in the gas flow, as well as in the pH, would direct the culture towards the formation of more products rather than biomass. In order to do so, setup 6 was run as setup 5 for the first 24 h, time after which the pH was allowed to drop naturally until 4.8. At the same time, the gas flow was reduced by 30 % from 18 mL/min to 12.6 mL/min. This flow was deemed adequate to avoid excessive starvation of the culture, but to provide substrate limitation. (Infantes et al., 2020a)

First of all, pH 4.8 was reached at 58 h, 3 h later than in setup 5, but in this case, and due to the configuration of the pH control, it continued to drop further until 4.7 at 69 h, value at which remained constant thereafter. Concerning cell growth, a CDW of 0.4 g/L was achieved after 24 h, contrasting with the higher CDW of setup 5 (0.56 g/L), even if the conditions in both runs were equal up to that point. The maximum biomass concentration for this fermentation was lower: 0.6 at 69 h, coinciding in time with the moment when the pH reached its final lower value. From this point on, no cell growth was detected, and the biomass concentration in the reactor eventually decreased. Acetate was produced until around this time point, as well. Its final concentration, 9 g/L, is lower than in setup 5 (11 g/L), but not so ethanol: in this last fermentation, 2 g/L could be formed (Figure 4.5). Looking at the acetate to ethanol ratio, found in Table 4.2 and Table 4.3, this is the fermentation with the lowest value achieved, that is, the product formation is clearly shifted towards ethanol. (Infantes et al., 2020a)

Gas consumption for the first 24 h was similar in both fermentation 5 and 6 (Figure 4.4D and Figure 4.6). Maximum gas usage was attained after 24 h in setup 6, similarly to setup 5 (20 h) (Table 4.1). In setup 6, due to the reduced flow, both the maximum usage interval and the time up to the end of the maximum CO fixation were prolonged (8 and 14 h longer, respectively). (Infantes et al., 2020a)

The off-gas profile for setups 6 is shown in the Appendix, in Figure A.III.

The yields achieved by lowering the flow after 24 h show that it did not have an impact on how much substrate was fixed into product ($Y_{p/S, \text{fixed}}$), given that the results achieved by this fermentation (0.94 ± 0.04 g/g for the complete run, and 0.92 ± 0.03 g/g up to the end of maximum CO consumption) are comparable to the other setups (Table 4.2 and Table 4.3). The product yield per carbon fed was lower than in setup 5 when calculating it up to the point of the end of maximum CO fixation phase, but contrarily, was improved in this last run in terms of the overall values, as a

result of a prolonged gas consumption phase and a lower substrate flow. Due to the diminished growth in setup 6, the $Y_{P/X}$ calculated at both points was higher, demonstrating that more products had been formed per gram of biomass. Nevertheless, the highest values of setup 1 were not reached. The acetate to ethanol ratio, though, was the lowest of the 6 setups, being about half of that of setup 1 (Table 4.2 and Table 4.3): all in all, this fermentation was displaced towards less growth, as well as less acetate and more ethanol per gram of biomass. Despite this, productivities for this setup were lower than for setup 5, and they were almost half of those of the setup 1 run. (Infantes et al., 2020a)

Furthermore, the percentage of carbon fixed per carbon fed can be used to determine which fermentation parameters would be more beneficial in order to fix the maximum amount of carbon fed into products. The results obtained are in line with what has been described previously here: in the altered medium experiments, with an increase in yeast extract or cysteine (setups 3a and 4, respectively), the effect observed was not as remarkable as in the lower pH fermentations, where the values are clearly lower than in setup 1. (Infantes et al., 2020a)

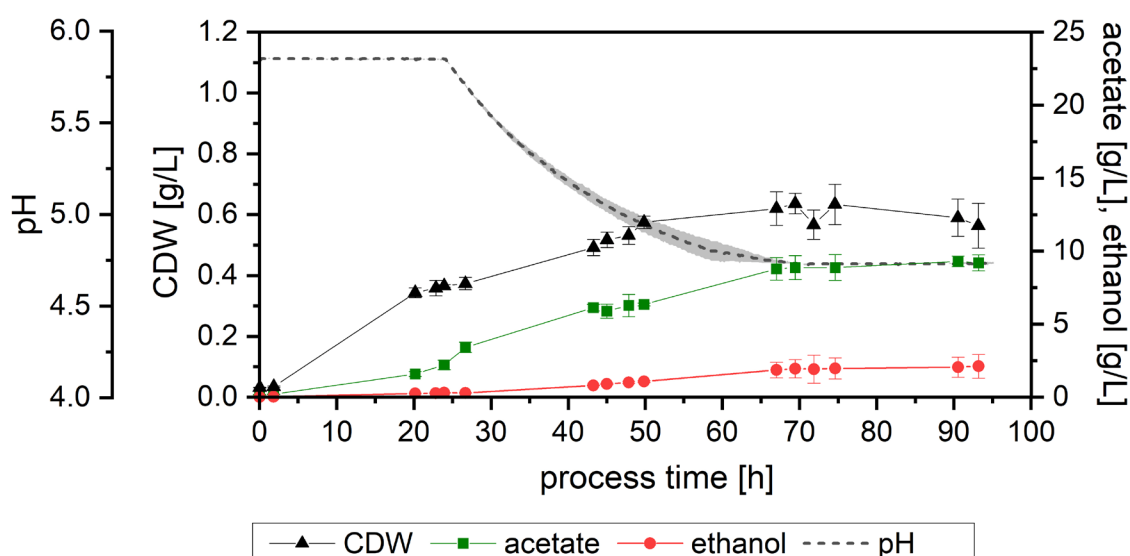


Figure 4.5 – Growth, pH profile and product formation of setup 6 with pH allowed to drop to 4.8 and gas flow decreased to 12.6 mL/min after 24 h. Average values of the triplicates ($n = 3$) with STD for cell dry weight (CDW, black triangles), acetate (green squares), ethanol (red dots), and pH (grey dotted line). The lightly colored area around the pH average represent the standard deviation. For CDW, acetate and ethanol points indicate actual measurements, lines are only depicted for clarity purposes. pH was measured on-line. (Infantes et al., 2020a)

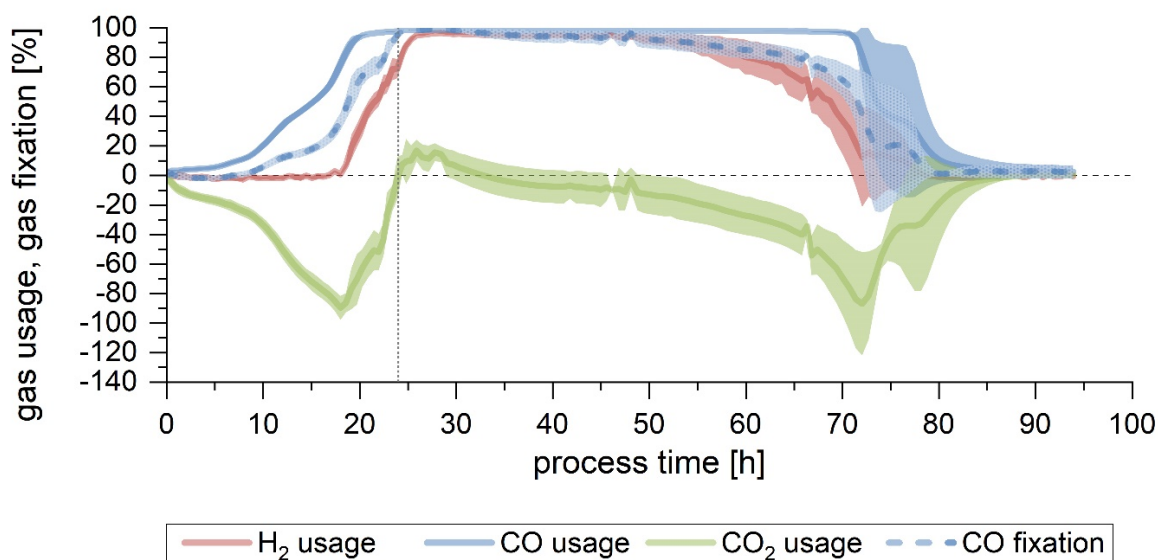


Figure 4.6 – Substrate usage or fixation for setup 6, where pH was allowed to drop to 4.8 and gas flow was decreased to 12.6 mL/min after 24 h (grey dotted vertical line). Usage is shown for H₂ (red line), CO₂ (green line) and CO (blue line). CO fixation is depicted by the dotted blue line. The calculated difference between amount of substance flow rate fed into the bioreactor and the amount of substance flow rate detected in the off-gas is shown here as a percentage. For the CO fixation, if the CO₂ usage was negative, the amount of CO₂ produced was subtracted from the amount of (perceived) CO used. Lines show the average of the triplicate (n = 3), while the lighter colored areas depict the standard deviation. (Infantes et al., 2020a)

4.1.4 Carbon balance

The ability of the system to provide a closed carbon balance, that is, to detect all carbon which has been fixed, according to the out-gas analysis, in the products, was assessed. A closed carbon balance is an important marker to determine the quality and relevance of the data, especially yields and productivities, as well as to ensure that all products were detected (Ellis et al., 2012). (Infantes et al., 2020a)

As shown in Table 4.4, in all except one case the carbon balance is closed, with values within $100 \pm 3\%$. In setup 1, an additional 6% of carbon was detected in the biomass and products, which was not accounted for as fixed. Even so, it is below 10% difference, and looking at the other carbon balance results, this discrepancy could be attributed to analytical error. (Infantes et al., 2020a)

Table 4.4 – Carbon balance for each entire run. The amount of carbon fed (the sum of the carbon content in mmol, for both carbon monoxide and carbon dioxide), the amount of carbon fixed, derived from the calculation based on the outgas analysis (the difference between the amount fed and the amount detected in the outgas, in mmol), and the amount of carbon detected in the measured products and biomass (in mmol), are shown here. The values given are the average of a triplicate ($n = 3$), with standard deviations, except for setup 3a, which is calculated for the fermenter where pH was not altered, and for 3b, which refers to the pair of fermenters where the pH was changed after 68 h to 5.4. (Infantes et al., 2020a)

Variables	Altered medium components			Altered pH			Altered pH and gas flow	
	Setup	1	3a	4	2	3b	5	6
Carbon fed (CO + CO₂) (mmol)		1968 ± 17	2131	2092 ± 2	2071 ± 1	2123 ± 0	2050 ± 2	1602 ± 8
Carbon fixed (from outgas analysis) (mmol)		1119 ± 25	1096	1150 ± 30	336 ± 11	914 ± 41	647 ± 12	606 ± 36
Carbon in products and biomass (mmol)		1190 ± 45	1086	1168 ± 43	345 ± 19	903 ± 84	634 ± 20	617 ± 25
Carbon detected in products per carbon fixed (%)		106	99	101	103	99	98	102
Carbon fixed per carbon fed (%)		57	51	55	16	43	32	38

4.2 Evaluation of beech wood and lignin derived syngas

4.2.1 Gas flow rate setting

Due to the differing gas composition of the two gases tested, not all parameters could be kept constant simultaneously. To enable a comparison between them, the gas flow rate was adapted in each fermentation so that the total amount of carbon (the sum of CO₂ and CO) fed into the fermenter was in both cases 0.4 mmol/min. This value was established and chosen as standard conditions in previous experiments (data not shown). (Liakakou et al., 2020)

As a result, the amount of H₂ fed to the fermenters differed between both experiments, being 0.2 mmol/min for the TNO (Energy Transition, Biomass & Energy Efficiency Unit, Petten, the Netherlands) beech wood-derived syngas (BWS) and 0.3 mmol/min for the TNO lignin-derived syngas (LS) (Table 4.5). (Liakakou et al., 2020)

Table 4.5 shows also the average composition of the gas flow fed into the fermenter, measured after the reactor reached equilibrium, and under abiotic conditions, i.e. before inoculation. The gas flow fed into the fermenter equals then to that coming out in the off-gas. (Liakakou et al., 2020)

Table 4.5 – Average composition of the gas and flow rate for TNO BWS and LS. The bioreactors were sparged with TNO syngas from beech wood before inoculation for at least 3 h. The values detected in the off-gas are the average of the measurements during this time, after reaching equilibrium conditions in the fermenter. All fermentations were done as triplicates (n = 3), and the values given here are the correspondent averages. (Liakakou et al., 2020)

		H ₂	CO	CO ₂	CH ₄
BWS	%	22.35 ± 0.54	28.19 ± 0.15	19.23 ± 0.29	9.93 ± 0.02
Flow rate:					
18 mL/min	mmol/min	0.18 ± 0.00	0.23 ± 0.00	0.15 ± 0.00	0.08 ± 0.00
LS	%	27.02 ± 0.09	21.31 ± 0.10	18.00 ± 0.24	10.64 ± 0.02
Flow rate:					
23 mL/min	mmol/min	0.28 ± 0.00	0.22 ± 0.00	0.19 ± 0.00	0.10 ± 0.00

4.2.2 Fermentation of TNO syngas from beech wood

4.2.2.1 Substrate usage and carbon fixation

The fermentation was performed for a total of 92.75 h. The peak observed in the off-gas graph (Figure 4.7) and the sudden decreased in substrate usage or fixation (Figure 4.8) between approximately 39 and 52 h of process time were due to an error on the setup of the pH regulation

that led to an increased fermenter volume of up to 1.7 L in all three bioreactors. The amount of products and biomass taken out from the fermenters have been taken into account in the calculations. At 43 h and 67 h of process-time the excess fermentation broth was retrieved from the vessels bringing it down to the initial volume of 1.5 L. The pH could be kept constant nonetheless during this time. The smaller peaks at around 68 h seen in both Figure 4.7 and Figure 4.8 correspond to the addition of anti-foam to the fermenter, which causes a punctual alteration on the solubility of the gases in the fermenter broth. (Liakakou et al., 2020)

During the first five hours of the fermentation, *C. ljungdahlii* mainly used up an average of 0.55 g/L of fructose carried over from the inoculation culture (data not shown). After that initial phase, CO was taken up by the culture in an ever-increasing manner, as reflected by the decreasing amount of CO detected in the waste gas stream, up to the point when at 15 h of process-time the average detected amount of substance flow rate in the off-gas ($\dot{n}_{\text{CO,out}}$) was below 0.020 ± 0.003 mmol/min (Figure 4.7). At 17 h, $\dot{n}_{\text{CO,out}}$ had already decreased to 0.012 ± 0.001 mmol/min, which corresponds to the point when the maximum CO fixation (> 85 %) started (Figure 4.8). This continued for another 21 h, that is, up to 38 h after inoculation, with an average CO fixation during this time of 91 %. Afterwards, due to the interference of the pH regulation issue, $\dot{n}_{\text{CO,out}}$ increased until process-time 44 h, signalling a decrease in its usage. Nevertheless, it eventually increased again, reaching 70 ± 2 % fixation at process-time 51 h, with an average of 79 % until 64 h. After that, the fixation of CO started to decrease, being the average from this time up to the end of the process of 70 %. From time 51 h to the end of the process, the average was 73 %. (Liakakou et al., 2020)

Looking at the CO usage (Figure 4.8), it stayed above 85 % from 14 h to 40 h, with an average of 95 %. Once more, the pH regulation glitch caused the CO usage to stay below that threshold for 10 h, until process-time 50 h. There, it increased again above the 85 % mark, staying so up to 90 h, with an average between those times of 91 %. The value at 91 h was 84 %, and it decreased to 80 % at the end of the process (93 h). (Liakakou et al., 2020)

Regarding H₂ uptake, a usage of ≥ 80 % was reached in average at 19 h after inoculation (Figure 4.8), when the off-gas analysis showed a detected gas flow rate of H₂ of 0.038 ± 0.005 mmol/min (Figure 4.7). This persisted for at least 20 h, being the average usage during this interval 86 % (Figure 4.8). Analogously to CO, the effect of the pH regulation malfunction can also be seen in the H₂ off-gas analysis. The amount of H₂ detected increased rapidly from 38 h until 45 h of process-time, but after removing excess broth it decreased to a new minimum of 0.052 ± 0.012 mmol/min at 61 h. The average between 45 h and 61 h for H₂ usage was 49 %. From this point on, and contrary to what is seen for CO, hydrogen usage did not recover its initial maximum values but rather

decreased continuously until the end of the process, with an average in this case of 48 %. (Liakakou et al., 2020)

CO₂ was not used throughout the fermentation, but rather was produced, as shown in Figure 4.8. As is the case for CO and H₂, the apparent increase in CO₂ production seen at process-time 43 h and 50 h was due to the malfunction of the pH regulation system. The maximum value measured for CO₂ outside that interval occurred at process-time 13 h, with a value of 0.219 ± 0.006 mmol/min. (Liakakou et al., 2020)

The amount of CH₄ detected in the off-gas remained almost constant throughout the fermentation (Figure 4.7). Before inoculation, an average of 0.077 ± 0.001 mmol/min was measured (Table 4.5). The average maximum was 0.086 ± 0.001 mmol/min, and the average minimum, 0.061 ± 0.001 mmol/min. The average for the whole run was 0.073 ± 0.006 mmol/min. Again, the interference caused by the pH regulation fail can also be observed here between process-times 40 h and 50 h. (Liakakou et al., 2020)

Finally, considering carbon fixation, the percentage of total carbon fixed per total carbon fed for the whole process was 42.30 ± 0.44 %. For the interval up to 38 h, when maximum fixation of CO ceased, it was 39.68 ± 1.93 % (Table 4.5 and Table 4.6) (Liakakou et al., 2020)

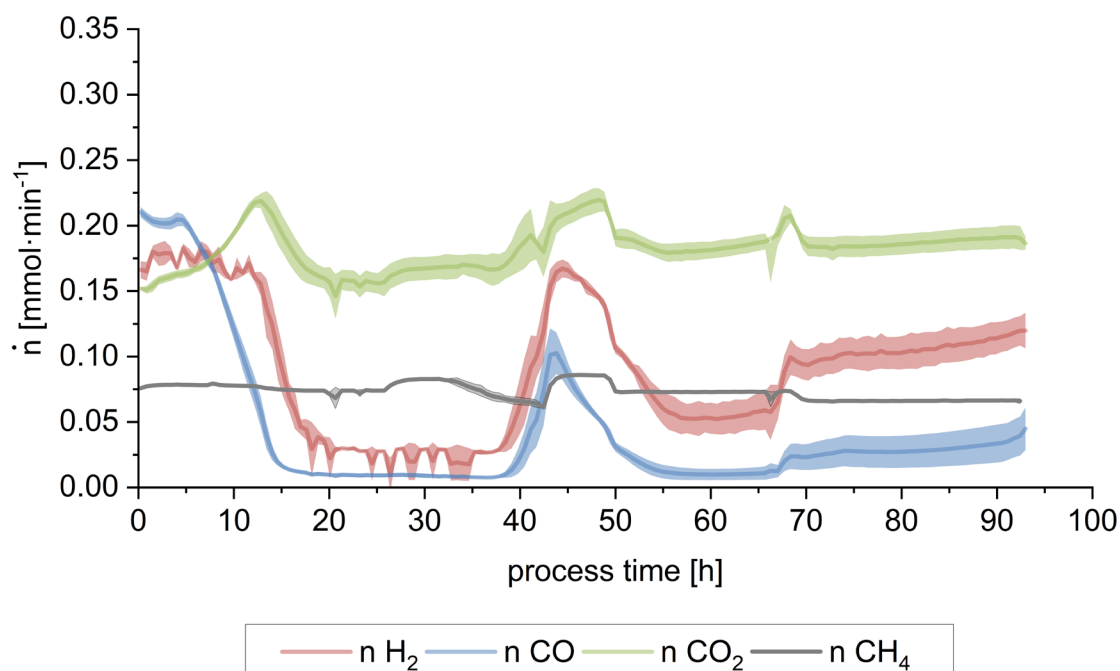


Figure 4.7 – Amount of substance flow rate in the off-gas for beech wood syngas. Average measured amount of substance flow rate (\dot{n}) for hydrogen (red), carbon monoxide (blue), carbon dioxide (green) and methane (grey). Lines show the average of a triplicate ($n = 3$), while the lighter coloured areas depict the standard deviation. A drop in the detected amount of substance in the off-gas compared to the initial starting value indicates the usage of that substance. The peaks observed between approx. 40 and 55 h are the result of a pH malfunction. (Liakakou et al., 2020)

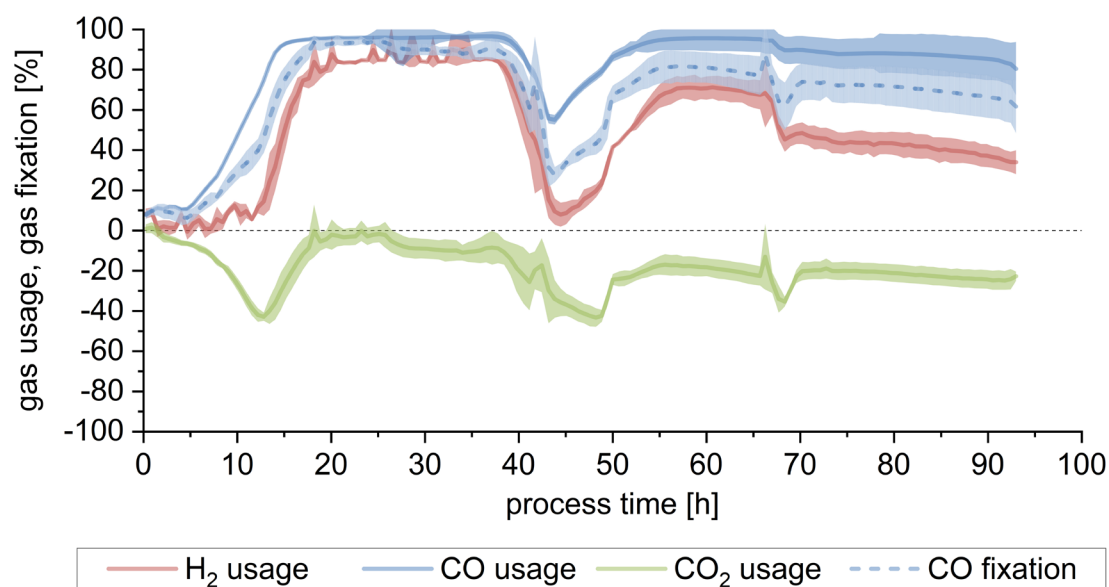


Figure 4.8 – Substrate usage or fixation for beech wood syngas. Usage is shown for H_2 (red line), CO_2 (green line) and CO (blue line). CO fixation is depicted by the dotted blue line. The calculated difference between amount of substance flow rate fed into the bioreactor and the amount of substance flow rate detected in the off-gas is shown here as a percentage. For the CO fixation, if the CO_2 usage was negative, the amount of CO_2 produced was subtracted from the amount of (perceived) CO used. Lines show the average of a triplicate ($n = 3$), while the lighter colored areas depict the standard deviation. The peaks observed between approx. 40 and 55 h are the result of a pH malfunction. (Liakakou et al., 2020)

Table 4.6 – Gas consumption profile, fermentation outcomes, yields, and productivities for the beech wood syngas. Endpoint time (h) = duration of the whole process; maximum CO fixation (h) = time elapsed from the starting of the fermentation until maximum CO fixation ended; maximum overall usage interval (h) = interval where the overall gas usage (the sum of CO, CO₂ and H₂ usage) was above 85 %. $Y_{P/S}$ (g/g) = gram of products (acetate and ethanol) formed per gram of substrate (CO, CO₂ and H₂). This has been calculated per grams of substrate fed, used and fixed. $Y_{P/X}$ (g/g) = gram of product (acetate and ethanol) per gram of biomass (cell dry weight). $E_{C, total}$ (mol %) = percentage of carbon fixed, as the sum of CO_{used} and CO_{2, used} per total carbon fed (CO_{fed} plus CO_{2, fed}). For the parameters calculated up to the end of maximum CO fixation, the sample closest to the given time point was used. Values are given as the average of a triplicate (n = 3) with standard deviations. (Liakakou et al., 2020)

Interval	Endpoint	End of maximum CO fixation	Maximum overall usage interval
Process time (h)	93	38	17 – 38
$Y_{P/S, used}$ (g/g)	0.83 ± 0.02	0.85 ± 0.09	0.96 ± 0.12
$Y_{P/S, fed}$ (g/g)	0.33 ± 0.01	0.32 ± 0.03	0.44 ± 0.05
$Y_{P/S, fixed}$ (g/g)	0.97 ± 0.05	0.94 ± 0.13	1.02 ± 0.15
$Y_{P/X}$ (g/g)	31.86 ± 1.30	13.97 ± 1.72	32.40 ± 5.23
$V_{gas, fed}$ (L)	100.17 ± 0.00	45.81 ± 0.00	25.56 ± 0.00
Acetate:Ethanol (mol)	7.79 ± 0.28	16.29 ± 3.40	14.45 ± 1.15
Acetate	0.17 ± 0.01	0.17 ± 0.02	0.26 ± 0.06
Ethanol	0.01 ± 0.00	0.01 ± 0.00	0.01 ± 0.00
Total	0.18 ± 0.021	0.18 ± 0.02	0.27 ± 0.06
$E_{C, total}$ (mol %)	42.30 ± 0.44	39.68 ± 1.93	55.39 ± 2.27

4.2.2.2 Biomass, product formation, yield and productivity

During the first 20 hours, biomass increased rapidly. Afterwards, growth slowed down and the CDW (cell dry weight) reached its maximum measured value of 0.62 ± 0.01 g/L at 66.5 h. Following that, growth stopped, and the biomass eventually decreased, with the last value recorded averaging 0.57 ± 0.01 g/L (Figure 4.9). (Liakakou et al., 2020)

With respect to product formation, acetate starts being produced immediately after inoculation, though the highest production started after 20 h, as can be seen in Figure 4.9 The final average acetate concentration reached was 15.61 ± 1.91 g/L. The ethanol concentration in the broth increased to 0.20 ± 0.03 g/L already after 19 h, reaching a value of 0.44 ± 0.08 at 50 h of cultivation, and finally reaching 1.56 ± 0.38 g/L at the end of the process. (Liakakou et al., 2020)

Product yields (acetic acid and ethanol) to total substrate fed ($Y_{P/S, \text{fed}}$), to used substrate ($Y_{P/S, \text{used}}$), and to substrate fixed ($Y_{P/S, \text{fixed}}$) are shown in Table 4.6 for each of the considered time spans: endpoint, up to the end of maximum CO fixation and during the interval of maximum overall usage. The highest $Y_{P/S}$ values were obtained during the maximum overall usage interval, with 0.44 ± 0.05 (g/g of total substrate fed), 0.96 ± 0.12 (g/g of total substrate used) and 1.02 ± 0.15 (g/g of substrate fixed). Acetate productivity was also here at its highest, with 0.26 ± 0.06 g/L·h. Ethanol productivity was 0.01 ± 0.00 for the three intervals. (Liakakou et al., 2020)

The acetate to ethanol ratio, in mol, at the endpoint, was 7.79 ± 0.28 . This, and the values for the other two relevant intervals are shown in Table 4.6. (Liakakou et al., 2020)

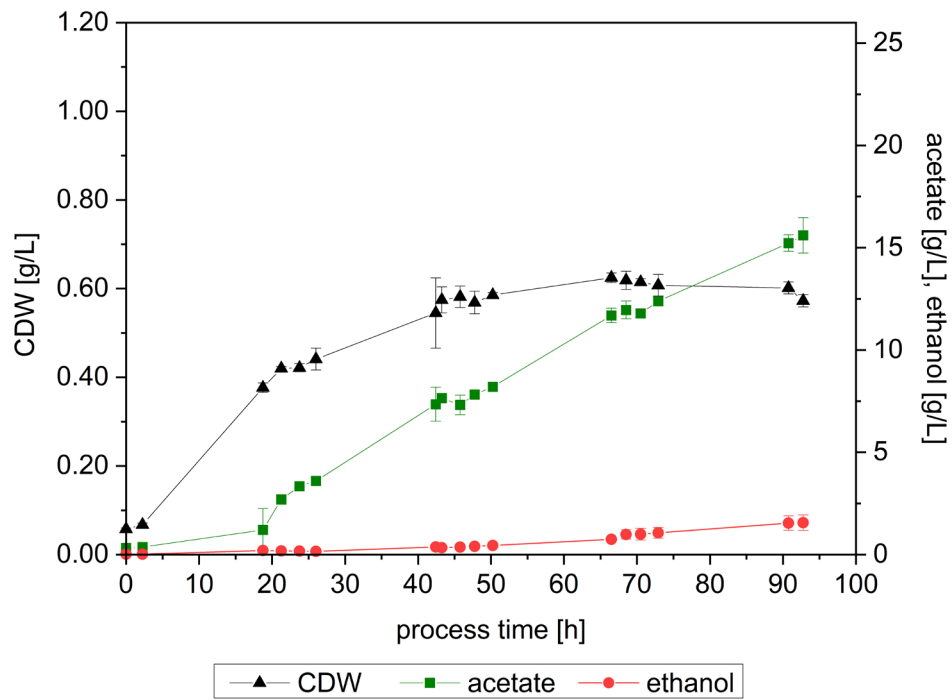


Figure 4.9 – Growth and product formation profiles for beech wood syngas. Points indicate actual samples. Lines are only depicted for clarity purposes; error bars show the standard deviation among the triplicate. CDW = cell dry weight. (Liakakou et al., 2020)

Table 4.7 – Gas consumption profile, fermentation outcomes, yields, and productivities for the lignin syngas. Endpoint time (h) = duration of the whole process; maximum CO fixation (h) = time elapsed from the starting of the fermentation until maximum CO fixation ended; maximum overall usage interval (h) = interval where the overall gas usage (the sum of CO, CO₂ and H₂ usage) was above 85 %. $Y_{P/S}$ (g/g) = gram of products (acetate and ethanol) formed per gram of substrate (CO, CO₂ and H₂). This has been calculated per grams of substrate fed, used and fixed. $Y_{P/X}$ (g/g) = gram of product (acetate and ethanol) per gram of biomass (cell dry weight). $E_{C, total}$ (mol %) = percentage of carbon fixed, as the sum of CO_{used} and CO_{2, used} per total carbon fed (CO_{fed} plus CO_{2, fed}). For the parameters calculated up to the end of maximum CO fixation, the sample closest to the given time point was used. Values are given as the average of a triplicate (n = 3) with standard deviations. (Liakakou et al., 2020)

Interval	Endpoint	End of maximum CO fixation	Maximum overall usage interval
Process time (h)	92.5	52	22 - 48
$Y_{P/S, used}$ (g/g)	0.79 ± 0.02	0.89 ± 0.02	0.84 ± 0.07
$Y_{P/S, fed}$ (g/g)	0.30 ± 0.01	0.32 ± 0.00	0.40 ± 0.02
$Y_{P/S, fixed}$ (g/g)	0.92 ± 0.07	0.94 ± 0.06	0.84 ± 0.07
$Y_{P/X}$ (g/g)	31.77 ± 2.29	18.89 ± 0.66	33.38 ± 2.78
$V_{gas, fed}$ (L)	127.65 ± 0.00	68.31 ± 0.00	35.19 ± 0.00
Acetate:Ethanol (mol)	5.24 ± 0.50	17.44 ± 2.80	16.19 ± 1.89
Productivity (g/L·h)	Acetate	0.16 ± 0.01	0.19 ± 0.00
	Ethanol	0.02 ± 0.00	0.01 ± 0.00
	Total	0.18 ± 0.01	0.20 ± 0.00
$E_{C, total}$ (mol %)	42.08 ± 4.07	45.36 ± 5.90	55.93 ± 3.64

4.2.3 Fermentation of TNO syngas from lignin

4.2.3.1 Substrate usage and carbon fixation

The total process time for this fermentation was 92.5 h. In Figure 4.10 and Figure 4.11, a small disturbance in the gas leaving the bioreactor can be seen around 45 h, which was caused by the addition of antifoam. (Liakakou et al., 2020)

As in the previous fermentation, during the first 5 h approximately the microorganism used up an average of 0.54 g/L of fructose that were left as a carry-over from the inoculation culture (data not shown). Similarly to what is seen in the BWS fermentation, CO uptake started directly afterwards (Figure 4.11), and $\dot{n}_{\text{CO, out}}$ at the out-gas decreased to below 0.020 ± 0.002 mmol/min after 15.6 h of process-time (Figure 4.10). At 18 h, $\dot{n}_{\text{CO, out}}$ reached values below 0.010 ± 0.001 mmol/min, corresponding to 87 % fixation. This is the starting point for the maximum CO fixation interval, which continued for 34 h, until process-time 52 h, as seen in Figure 4.11. The average CO fixation calculated for this time period is 95 %. At 64 h of process-time, CO fixation was 77 ± 1 %, and the average between 52 h and 64 h was 81 %. From 52 h of process-time up to the end of the fermentation the average for the percentage of carbon fixed was 73 %. The average from 64 h to the end of the process was 68 %. (Liakakou et al., 2020)

In terms of CO usage, it reached 89 ± 4 % after 15 h (Figure 4.11). CO usage was maintained from that point throughout the duration of the process, being its average 96 %. (Liakakou et al., 2020)

Concerning H₂, the threshold of 80 % usage was achieved at 23 h and lasted for 34 h, until 57 h of process-time, as Figure 4.11 shows. From that point, where the flow detected in the out-gas was 0.055 ± 0.007 mmol/min, the amount of H₂ leaving the reactor steadily increased, being 0.147 ± 0.015 mmol/min the last measured value. The average usage between 57 h and the end sample was 68 %, decreasing from 80 ± 2 % at the start of this interval to 47 ± 6 % at the end. (Liakakou et al., 2020)

As opposed to what is seen in the previous fermentation, CO₂ was used between process-time 22 h and 46 h (Figure 4.11), with an average of 6 %. Its maximum was 12 ± 8 % at 42.6 h, corresponding to a detected amount in the out-gas of 0.163 ± 0.01 mmol/min (Figure 4.10). (Liakakou et al., 2020)

Finally, CH₄ remained stable, with a minimum and a maximum substance flow rate of 0.099 ± 0.007 and 0.112 ± 0.010 mmol/min respectively. The average for the entire run was 0.107 ± 0.003 mmol/min. (Liakakou et al., 2020)

The percentage of total carbon that *C. ljungdahlii* was able to fix per carbon fed ($E_{C, total}$) during the entire fermentation (Table 4.6 and Table 4.7) was $42.08 \pm 4.07\%$. Up to 52 h, it was $45.36 \pm 5.90\%$. (Liakakou et al., 2020)

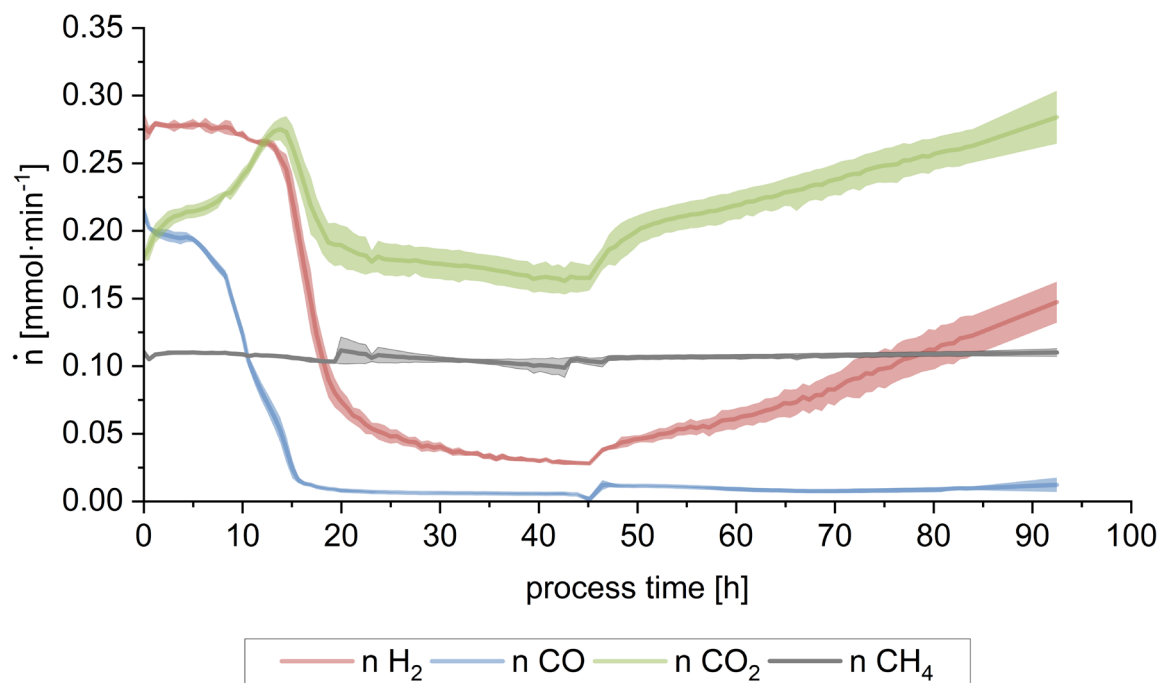


Figure 4.10 – Amount of substance flow rate in the off-gas for lignin syngas. Average measured amount of substance flow rate (\dot{n}) for hydrogen (red), carbon monoxide (blue), carbon dioxide (green) and methane (grey). Lines show the average of a triplicate ($n = 3$), while the lighter colored areas depict the standard deviation. A drop in the detected amount of substance in the off-gas compared to the initial starting value indicates the usage of that substance. (Liakakou et al., 2020)

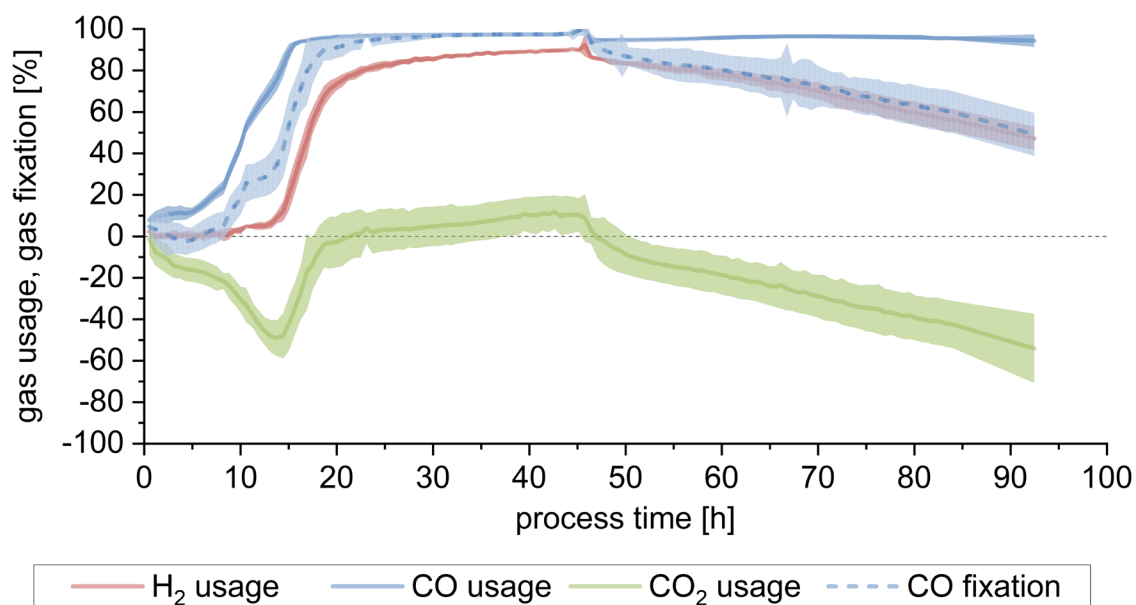


Figure 4.11 – Substrate usage or fixation for lignin syngas. Usage is shown for H₂ (red line), CO₂ (green line) and CO (blue line). CO fixation is depicted by the dotted blue line. The calculated difference between amount of substance flow rate fed into the bioreactor and the amount of substance flow rate detected in the off-gas is shown here as a percentage. For the CO fixation, if the CO₂ usage was negative, the amount of CO₂ produced was subtracted from the amount of (perceived) CO used. Lines show the average of a triplicate (n=3), while the lighter colored areas depict the standard deviation. (Liakakou et al., 2020)

4.2.3.2 Biomass, product formation, yield and productivity

The fastest increase in biomass happened during the first 19 h of fermentation. Analogous to the first fermentation, growth also slowed down afterwards, eventually coming to a stop. The maximum CDW value was 0.61 ± 0.01 g/L, reached at 66 h. At the process ending point, the value measured was 0.58 ± 0.03 g/L (Figure 4.12). (Liakakou et al., 2020)

Acetate formation could be detected already with the first samples, but, as in the preceding experiment, it was only after around 20 h that the highest production rate was achieved. Subsequently, it remained stable up to around process-time 45 h, when a slight decrease in its production could be observed. The final measured acetate concentration in the fermentation medium was 14.86 ± 0.84 g/L. The ethanol concentration in the fermenter was 0.19 ± 0.00 g/L after 19 h, and 0.42 ± 0.07 after 50 h. The maximum reached at the end of the process amounted to 2.19 ± 0.15 g/L. This can be seen in more detail in Figure 4.12. (Liakakou et al., 2020)

Also in this case the highest $Y_{P/S}$ obtained corresponded to the time interval where maximum overall usage happened: 0.40 ± 0.02 (g/g of total fed substrate) and 0.84 ± 0.07 g/g for both total used and fixed substrate. Acetate productivity also reached its maximum there: 0.23 ± 0.01 g/L·h, Ethanol productivity was highest when calculated up to the end of the process: 0.02 ± 0.00 g/L·h.

For both the maximum usage and maximum CO fixation intervals, it was 0.01 ± 0.00 g/L-h. More details can be found in Table 4.6. (Liakakou et al., 2020)

For this particular syngas, the product profile at the endpoint was shifted towards ethanol, with a ratio of acetate to ethanol of 5.24 ± 0.50 . The other two intervals, on the contrary, presented a slightly higher ratio compared to the BWS. This is shown in Table 4.6, together with the values for the other two intervals. (Liakakou et al., 2020)

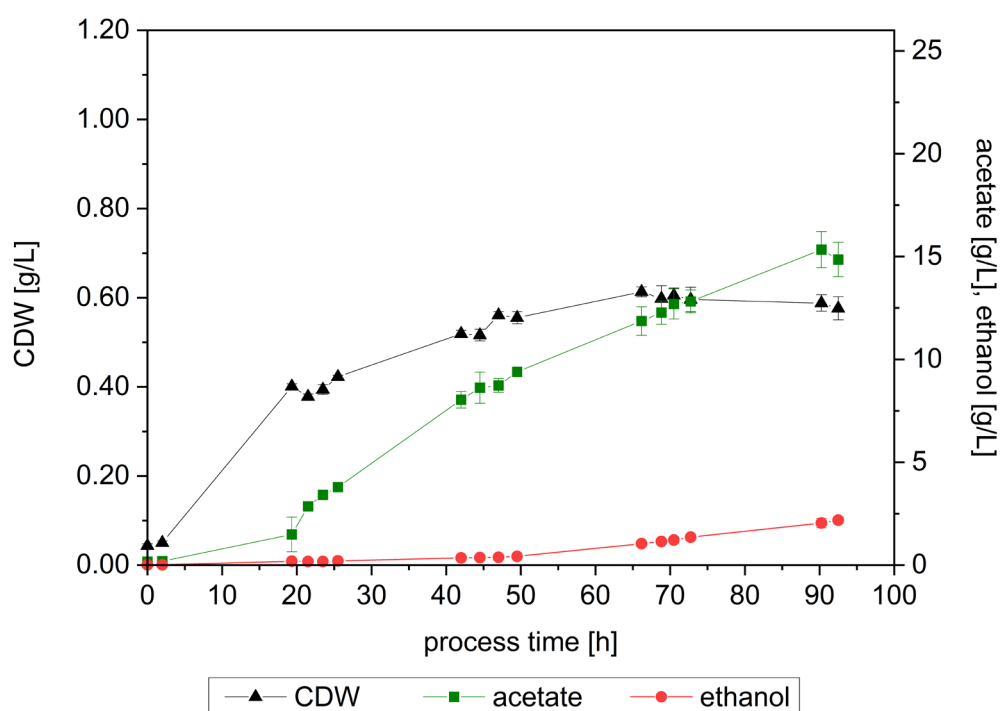


Figure 4.12 – Growth and product formation profiles for lignin syngas. Points indicate actual samples. Lines are only depicted for clarity purposes; error bars show the standard deviation among the triplicate. CDW = cell dry weight. (Liakakou et al., 2020)

4.3 Impact of syngas composition and impurities

4.3.1 Gas flow rate setting

Due to the differing gas composition of the gases tested, not all parameters could be kept constant simultaneously. To enable a comparison between them, the gas flow rate was adapted in each fermentation so that the total molar flow of carbon (C_{in} , the sum of CO_2 and CO) fed into the fermenter was 0.4 mmol/min, except for setups 3 and 4 (Table 4.8). In this two fermentations, rather than the molar flow of carbon, the total gas flow was modified so that the molar flow of H_2 fed into the fermenter ($H_{2,in}$) was to 0.23 mmol/min. Both the flow of carbon or H_2 fed were established and chosen as standard conditions in previous experiments (data not shown). (Infantes et al., 2020b)

Table 4.8 shows the average composition and the gas flow fed into the fermenter for all syngases. The values are given as the measured off-gas composition by the on-line GC after the reactor reached equilibrium and under abiotic conditions (before inoculation). At that point, the gas flow fed into the fermenter equals to that which comes out at the off-gas. (Infantes et al., 2020b)

Table 4.8 – Composition of the gas, flow rate and amount of substance fed for each setup. The bioreactors were sparged with each gas before inoculation for at least 3 h. The syngas composition is given based on the average of the values detected in the off-gas measured during this time, after reaching equilibrium conditions in the fermenter. In all cases, apart from CO, CO₂, H₂ and CH₄, the remaining component of the syngas is N₂. C_{in} refers to the sum of the amount of CO and CO₂. All fermentations were done as triplicates (n = 3), and the values given here are the correspondent averages. Superscripts a and b denote pairs of fermentations done under the exact same conditions, with equivalent gas compositions except for the presence of impurities. The syngas custom mixtures which were prepared with the same composition as biomass-derived syngas are marked as such, with the source of the syngas they were based on in brackets. TNO BW: syngas produced at TNO from beech wood; TNO LS: syngas produced at TNO from lignin; LNEG: syngas produced at LNEG, gasification at 850 °C, with lime stone treatment; ENEA: syngas produced at ENEA, gasification using O₂ and steam. (Infantes et al., 2020b)

Syngas source		Bioliq® - Straw	Custom mixture (Bioliq®)	Bioliq® - Straw	Custom mixture (Bioliq®)	Custom mixture (TNO BW)	Custom mixture (TNO LS)	Custom mixture (LNEG)	Custom mixture (ENEA)	Custom mixture A	Custom mixture B
Impurities		Yes	No	Yes	No	No	No	No	No	No	No
Setup		1 ^a	2 ^a	3 ^b	4 ^b	5	6	7	8	9	10
Syngas composition [vol-%]	CO	28.8	29.8	28.9	29.2	27.0	21.3	26.1	26.7	32.5	21.2
	CO ₂	2.8	2.6	2.8	2.7	18.3	20.6	16.7	26.4	11.9	13.7
	H ₂	29.5	29.1	28.4	28.3	23.3	25.4	30.4	34.5	21.9	21.9
	CH ₄	-	-	-	-	-	-	18.9	5.3	-	-
Gas flow rate [mL/min]		26.3	26.3	18.0	18.0	18.0	23.0	20.0	16.0	18.0	23.0
C_{in} (CO₂ + CO) [mmol/min]		0.37	0.38	0.25	0.26	0.37	0.43	0.38	0.38	0.36	0.36
H_{2,in} [mmol/min]		0.35	0.34	0.23	0.23	0.19	0.26	0.27	0.25	0.18	0.23
CO_{in} [mmol/min]		0.34	0.35	0.23	0.23	0.22	0.22	0.23	0.19	0.26	0.22
CO_{2,in} [mmol/min]		0.03	0.03	0.02	0.02	0.15	0.21	0.15	0.19	0.10	0.14
CH_{4,in} [mmol/min]		-	-	-	-	-	-	0.18	0.04	-	-

4.3.2 Comparison between biomass-derived and impurity-free syngas

All results are given as the average of a triplicate experiment ($n = 3$).

Product yields (acetic acid and ethanol) to total substrate fed ($Y_{P/S, \text{ fed}}$), to used substrate ($Y_{P/S, \text{ used}}$), and to substrate fixed ($Y_{P/S, \text{ fixed}}$) calculated up to the endpoint are shown in Table 4.9

The same parameters mentioned but calculated up to the point when maximum CO fixation ended, are given in Table 4.10.

CO, CO₂ and H₂ usage and CO fixation profiles for all setups are shown in Figure 4.13. The full gas usage and fixation profile for setups 1 to 4 can be found in the Appendix, Figure A.IV.

4.3.2.1 Bioliq® syngas, setups 1 and 2

4.3.2.1.1 Substrate usage and carbon fixation

In setup 1, which used Bioliq® syngas containing impurities at a gas flow rate of 26.3 mL/min (Table 4.8), the culture presents a lag phase lasting 8 h, after which CO usage started (Figure 4.13A).

Maximum CO usage (that is, when less than 0.05 mmol/min CO, corresponding to 85 % of CO usage, is detected in the off-gas) started 35 h after inoculation. It lasted for 34 h (Figure 4.14A). H₂ usage started only after 23 h, when the off-gas flow of CO was 0.19 ± 0.09 mmol/min. The lowest flow of H₂ detected in the off-gas was 0.13 ± 0.02 mmol/min at 47 h, corresponding to 62.20 ± 6.27 % usage. This can be seen in Figure 4.13A and Figure 4.14A. (Infantes et al., 2020b)

No CO₂ usage was detected at any point; on the contrary, it was produced throughout the fermentation (Figure 4.14A). This affected the maximum CO fixation obtained, since it stayed above 70 % for only 7 h, reaching its maximum value (74.14 ± 2.89 %) at 47 h, simultaneously to the highest consumption of H₂. The percentage of carbon fixed in products and biomass ($E_{C, \text{ total}}$) at the end of the run was 30.95 ± 2.05 mol % (Table 4.9). No maximum overall usage was detected during the fermentation. (Infantes et al., 2020b)

In setup 2, with the same composition of syngas and at the same flow rate, but without impurities, the lag phase was remarkably shorter, with CO usage starting almost immediately, after 1.5 h. Maximum CO usage (above 85 %) also happened earlier in this case, at 22 h of process-time, and lasted longer: 53 h (Figure 4.13B). The same trend is true for H₂, whose usage started after 7 h when the CO in the off-gas was 0.33 ± 0.01 mmol/min, which is higher than for the previous experiment. The lowest flow of H₂ and the corresponding maximum usage value were 0.08 ± 0.02 mmol/min and 75.99 ± 5.77 %, respectively, after 39 h (Figure 4.13B and Figure 4.14B). (Infantes et al., 2020b)

Table 4.9 – Fermentation outcomes, yields, and productivities for the complete run. $Y_{P/S}$, [g/g] = gram of products (acetate and ethanol) formed per gram of substrate (CO, CO₂ and H₂). This has been calculated per grams of substrate fed, used and fixed. $Y_{P/X}$ [g/g] = gram of product (acetate and ethanol) per gram of biomass (cell dry weight). $E_{C, total}$ [mol %] = percentage of carbon fixed, as the sum of CO_{used} and CO_{2, used} per total carbon fed (CO_{fed} plus CO_{2, fed}). Values are given as the average of a triplicate (n = 3) with STD. Total productivity includes all measured products, that is, ethanol and acetate. Superscripts “a” and “b” denote pairs of fermentations done under the exact same conditions, with equivalent gas compositions except for the presence of impurities. (Infantes et al., 2020b)

Setup	1 ^a	2 ^a	3 ^b	4 ^b	5	6	7	8	9	10
$Y_{P/S, used}$ [g/g]	0.54 ± 0.03	0.68 ± 0.03	0.77 ± 0.02	0.80 ± 0.02	0.87 ± 0.03	0.95 ± 0.01	0.85 ± 0.00	0.82 ± 0.04	0.72 ± 0.04	0.87 ± 0.07
$Y_{P/S, fed}$ [g/g]	0.29 ± 0.01	0.43 ± 0.00	0.46 ± 0.00	0.38 ± 0.03	0.38 ± 0.01	0.34 ± 0.00	0.38 ± 0.00	0.36 ± 0.01	0.38 ± 0.02	0.38 ± 0.03
$Y_{P/S, fixed}$ [g/g]	0.93 ± 0.05	0.99 ± 0.05	0.91 ± 0.03	0.98 ± 0.01	0.92 ± 0.03	0.96 ± 0.02	0.88 ± 0.02	0.82 ± 0.04	0.91 ± 0.04	0.96 ± 0.03
$Y_{P/X}$ [g/g]	20.51 ± 1.75	32.36 ± 1.99	20.23 ± 1.32	28.09 ± 2.70	34.79 ± 7.47	32.54 ± 1.50	29.29 ± 0.51	31.00 ± 1.96	29.49 ± 1.01	33.49 ± 2.30
$V_{gas, fed}$ [L]	146.56 ± 0.07	147.70 ± 0.00	100.35 ± 0.00	100.71 ± 0.00	100.35 ± 0.00	128.57 ± 0.00	112.20 ± 0.00	90.96 ± 0.00	100.44 ± 0.00	127.88 ± 1.63
Acetate : Ethanol [mol]	2.35 ± 0.31	5.25 ± 0.46	3.43 ± 0.37	15.09 ± 1.90	16.63 ± 1.71	8.29 ± 1.07	7.40 ± 0.42	9.16 ± 0.26	11.92 ± 0.85	8.00 ± 0.95
Productivity [g/L·h]										
Acetate	0.10 ± 0.01	0.18 ± 0.00	0.12 ± 0.00	0.12 ± 0.01	0.19 ± 0.01	0.20 ± 0.00	0.19 ± 0.00	0.19 ± 0.00	0.17 ± 0.01	0.18 ± 0.02
Ethanol	0.03 ± 0.00	0.03 ± 0.00	0.03 ± 0.00	0.01 ± 0.00	0.01 ± 0.00	0.02 ± 0.00	0.02 ± 0.00	0.02 ± 0.00	0.02 ± 0.00	0.02 ± 0.00
Total	0.14 ± 0.01	0.21 ± 0.00	0.15 ± 0.00	0.12 ± 0.01	0.20 ± 0.01	0.22 ± 0.00	0.21 ± 0.00	0.20 ± 0.00	0.18 ± 0.01	0.19 ± 0.02
$E_{C, total}$ [mol %]	30.95 ± 2.05	44.65 ± 2.23	52.23 ± 2.11	39.87 ± 3.14	48.79 ± 2.41	42.53 ± 0.56	51.52 ± 0.70	50.88 ± 1.71	46.61 ± 0.96	47.75 ± 1.49

Table 4.10 – Fermentation outcomes, yields, and productivities calculated up to the point when maximum CO fixation stopped. $Y_{P/S}$ [g/g] = gram of products (acetate and ethanol) formed per gram of substrate (CO, CO₂ and H₂). This has been calculated per grams of substrate fed, used and fixed. $Y_{P/X}$ [g/g] = gram of product (acetate and ethanol) per gram of biomass (cell dry weight). $E_{c, total}$ [mol %] = percentage of carbon fixed, as the sum of CO_{used} and CO_{2, used} per total carbon fed (CO_{fed} plus CO_{2, fed}). Values are given as the average of a triplicate (n =3) with STD. Total productivity includes all measured products, that is, ethanol and acetate. Setups 1 and 2 did not achieve a CO fixation above 85 % and are therefore not included here. Superscript b denotes fermentations done under the exact same conditions, with equivalent gas compositions except for the presence of impurities. A yield slightly above 1 is deemed the result of small analytical inexactitude. (Infantes et al., 2020b)

Setup	3 ^b	4 ^b	5	6	7	8	9	10	
$Y_{P/S, used}$ [g/g]	0.83 ± 0.06	0.88 ± 0.04	0.89 ± 0.01	0.95 ± 0.04	0.93 ± 0.05	0.82 ± 0.06	0.83 ± 0.01	0.87 ± 0.06	
$Y_{P/S, fed}$ [g/g]	0.44 ± 0.04	0.61 ± 0.03	0.38 ± 0.01	0.35 ± 0.01	0.41 ± 0.01	0.39 ± 0.02	0.38 ± 0.00	0.37 ± 0.014	
$Y_{P/S, fixed}$ [g/g]	0.98 ± 0.07	1.03 ± 0.04	0.93 ± 0.02	0.95 ± 0.04	0.93 ± 0.05	0.82 ± 0.06	0.99 ± 0.01	0.90 ± 0.06	
$Y_{P/X}$ [g/g]	13.82 ± 0.62	15.24 ± 0.41	21.67 ± 1.19	24.24 ± 0.77	21.34 ± 1.98	21.73 ± 0.58	15.34 ± 1.16	20.38 ± 0.89	
$V_{gas, fed}$ [L]	78.93 ± 0.00	51.57 ± 0.00	76.62 ± 1.49	102.58 ± 0.00	87.40 ± 1.41	70.80 ± 0.00	54.54 ± 0.00	92.81 ± 0.00	
Acetate : Ethanol [mol]	3.45 ± 0.54	17.20 ± 1.69	31.82 ± 2.22	11.60 ± 1.09	12.07 ± 1.37	14.90 ± 1.99	45.20 ± 7.39	12.40 ± 0.45	
Productivity [g/L·h]	Acetate	0.12 ± 0.02	0.20 ± 0.01	0.20 ± 0.01	0.21 ± 0.01	0.22 ± 0.01	0.21 ± 0.01	0.19 ± 0.00	0.18 ± 0.01
	Ethanol	0.03 ± 0.00	0.01 ± 0.00	0.01 ± 0.00	0.01 ± 0.00	0.01 ± 0.00	0.01 ± 0.00	0.003 ± 0.00	0.01 ± 0.00
	Total	0.15 ± 0.02	0.21 ± 0.01	0.20 ± 0.01	0.23 ± 0.01	0.23 ± 0.01	0.23 ± 0.01	0.19 ± 0.02	0.20 ± 0.01
$E_{c, total}$ [mol %]	49.33 ± 2.73	61.07 ± 3.59	48.04 ± 1.85	43.27 ± 0.28	52.31 ± 0.56	52.68 ± 1.49	44.72 ± 0.74	47.35 ± 1.39	

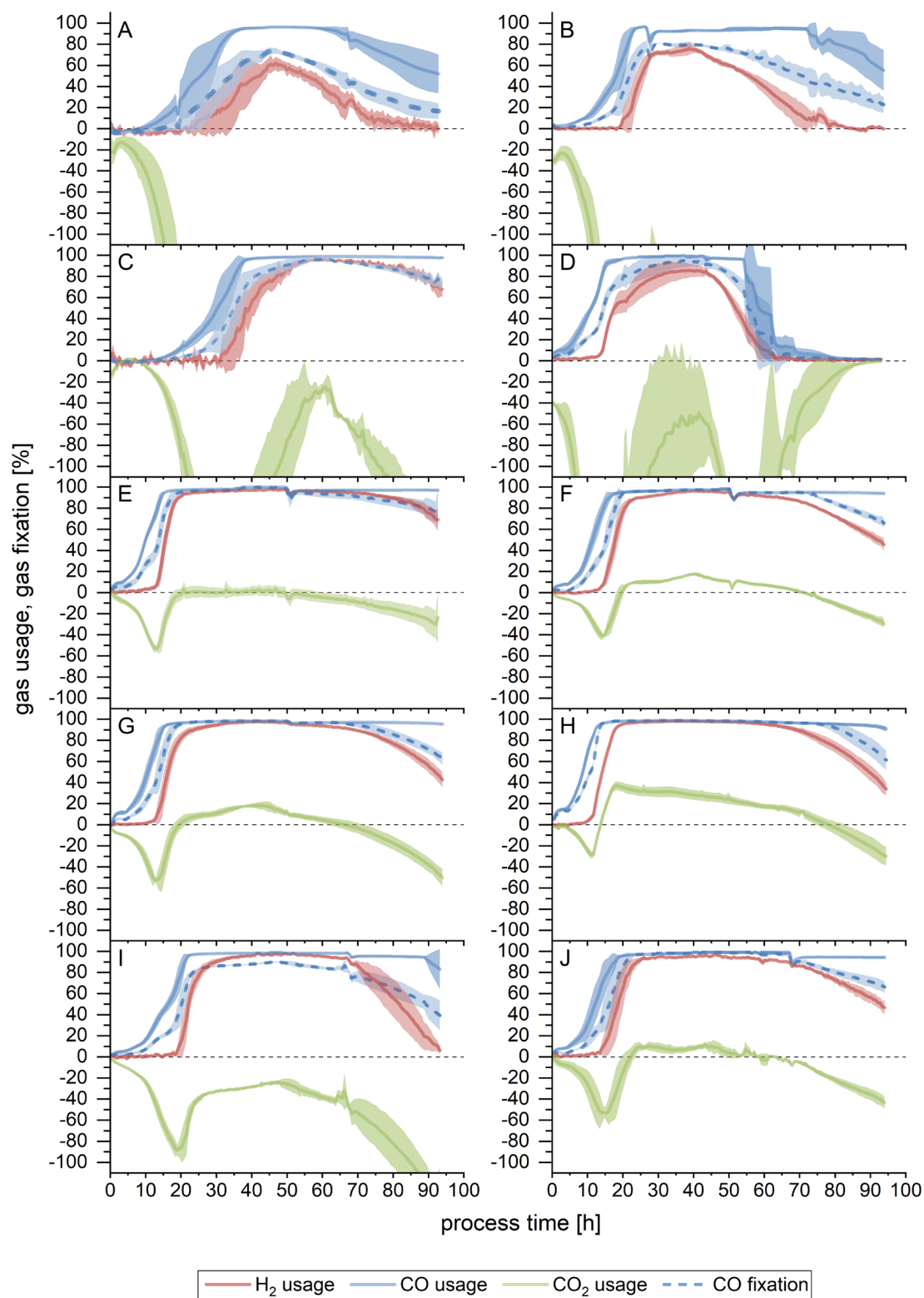


Figure 4.13 – Substrate usage and fixation for setups 1 to 10. (A) to (J), in alphabetical order, refer to each individual setup, in numerical ascending order - (A) is setup 1, (B) is setup 2, etc. Usage is for H₂ (red line), CO₂ (green line) and CO (blue line). CO fixation is depicted by the dotted blue line. The calculated difference between amount of substance flow rate fed into the bioreactor and the amount of substance flow rate detected in the off-gas is shown here as a percentage. For CO fixation, if the CO₂ usage was negative, the amount of CO₂ produced was subtracted from the amount of (perceived) CO used. Lines show the average of a triplicate ($n = 3$), while the lighter colored areas depict the standard deviation. (Infantes et al., 2020b)

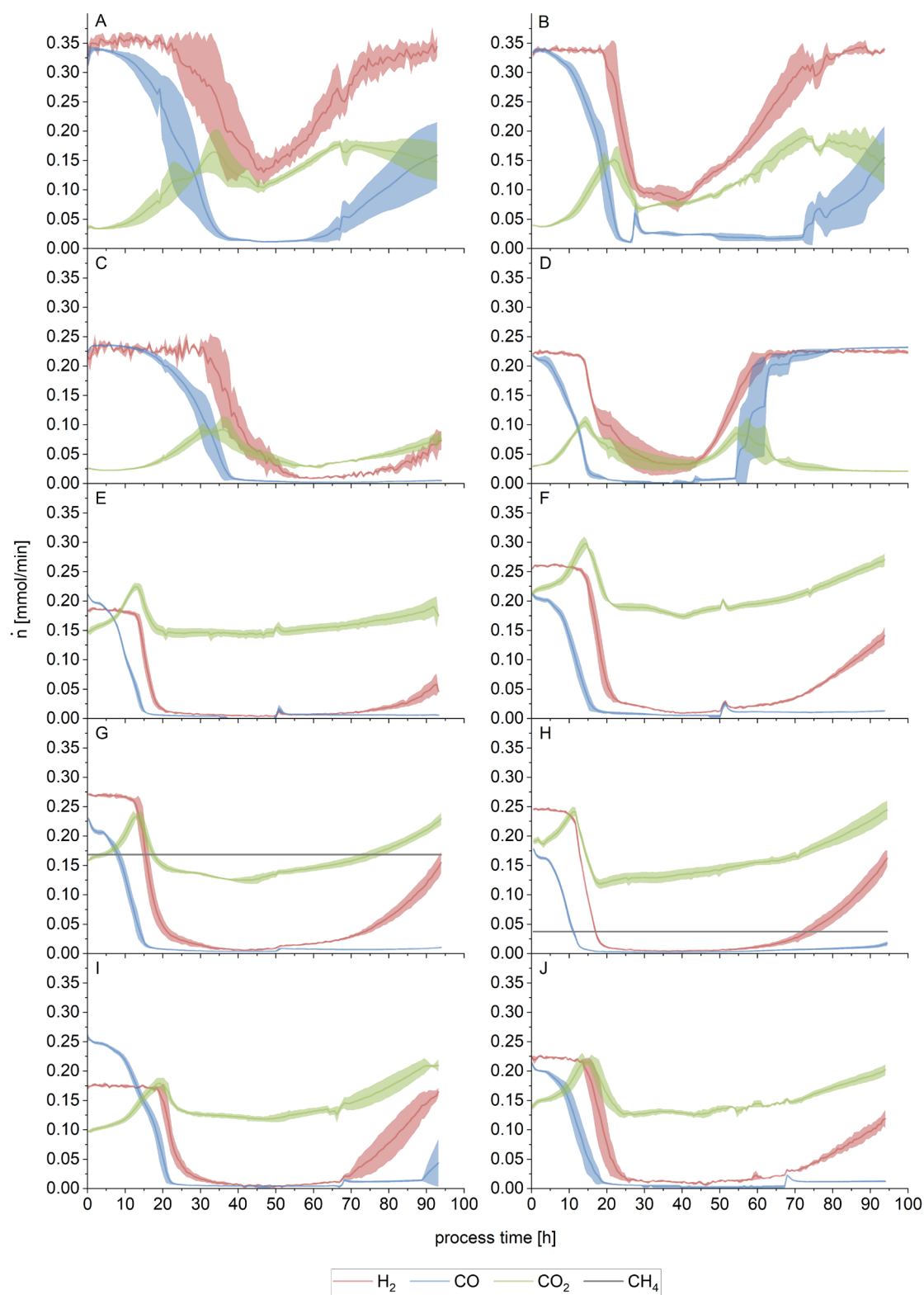


Figure 4.14 – Off-gas profile for setups 1 to 10. (A) to (J), in alphabetical order, refer to each individual setup, in numerical ascending order - (A) is setup 1, (B) is setup 2, etc. The molar flow rate is shown here, as obtained from the measurements of the on-line GC, for H₂ (red line), CO₂ (green line) and CO (blue line). Lines show the average of a triplicate (n = 3), while the lighter colored areas depict the standard deviation. (Infantes et al., 2020b)

CO₂ usage did not happen in this setup neither (Figure 4.14B). Here, though, CO fixation was above 70 % for 30.5 h, four times longer than for the former setup. Its maximum was attained earlier, at 30 h, with 81.14 ± 0.29 %, slightly before than the maximum H₂ consumption. $E_{c, total}$ was also higher, as a result of the improved CO fixation: 44.65 ± 22.23 mol % (Table 4.9). As with setup 1, neither here any maximum overall usage was observed. (Infantes et al., 2020b)

4.3.2.1.2 Biomass, product formation, yield and productivity

As can be observed in Figure 4.15A, biomass increased continuously during the first 49 h in the first setup. A CDW (cell dry weight) of 0.60 ± 0.12 g/L was achieved at that point. Afterwards, growth slowed down and eventually plateaued. Maximum CDW was reached its maximum at 69 h (0.71 ± 0.12 g/L). Acetate production happened mostly between 20 h and 73 h. (Infantes et al., 2020b)

At 25 h, the acetate concentration was 0.84 ± 0.34 g/L, and the highest concentration was detected at 91 h (10.27 ± 1.19 g/L). Ethanol production was already detected after 21 h (0.20 ± 0.12 g/L), and it continued to increase throughout the fermentation, up to 3.29 ± 0.42 g/L at the end of the run. (Infantes et al., 2020b)

As can be observed in Figure 4.15A, biomass increased continuously during the first 49 h in setup 1. A CDW (cell dry weight) of 0.60 ± 0.12 g/L was achieved at that point. Afterwards, growth slowed down and eventually plateaued. Maximum CDW was reached at 69 h (0.71 ± 0.12 g/L). Acetate production happened mostly between 20 h and 73 h. At 25 h, the acetate concentration was 0.84 ± 0.34 g/L, and the highest concentration was detected at 91 h (10.27 ± 1.19 g/L). Ethanol production was already detected after 21 h (0.20 ± 0.12 g/L), and it continued to increase throughout the fermentation, up to 3.29 ± 0.42 g/L at the end of the run. (Infantes et al., 2020b)

In setup 2, in the absence of impurities, more biomass could be generated during the first 51 h, with a CDW of 0.72 ± 0.04 g/L at that time point. At 76 h, its measured maximum was met, 0.76 ± 0.07 g/L. Thereafter, a decrease in biomass was seen (Figure 4.15B). Acetate production was faster in this case, with 2.55 ± 0.48 g/L produced after 26.5 h. The final concentration was 16.75 ± 0.34 g/L, a 63 % increase compared to setup 1. Contrarily, less ethanol was produced, with a final value of 2.47 ± 0.24 g/L, 25 % less than setup 1. (Infantes et al., 2020b)

Product yields (acetic acid and ethanol) to total substrate fed ($Y_{P/S, fed}$), to used substrate ($Y_{P/S, used}$), and to substrate fixed ($Y_{P/S, fixed}$) calculated up to the endpoint are shown in Table 4.9. No values are given up to the point when maximum CO fixation ended due to the fact that no CO fixation above 85 mol % was detected. (Infantes et al., 2020b)

It can be noted that setup 2 achieved a better performance overall, with higher yields and productivities, except for ethanol. Setup 1 presented a lower acetate to ethanol ratio (2.35 compared to 5.25 in setup 2), meaning more ethanol was produced per mol of acetate. (Infantes et al., 2020b)

$Y_{P/X}$ at the end-point is higher in setup 2: $32.36 \pm 1.99 \text{ g}_{\text{products}}/\text{g}_{\text{biomas}}$, compared to $20.51 \pm 1.75 \text{ g}_{\text{products}}/\text{g}_{\text{biomas}}$ for setup 1, indicating that more grams of product per gram of biomass were formed (Table 4.9). (Infantes et al., 2020b)

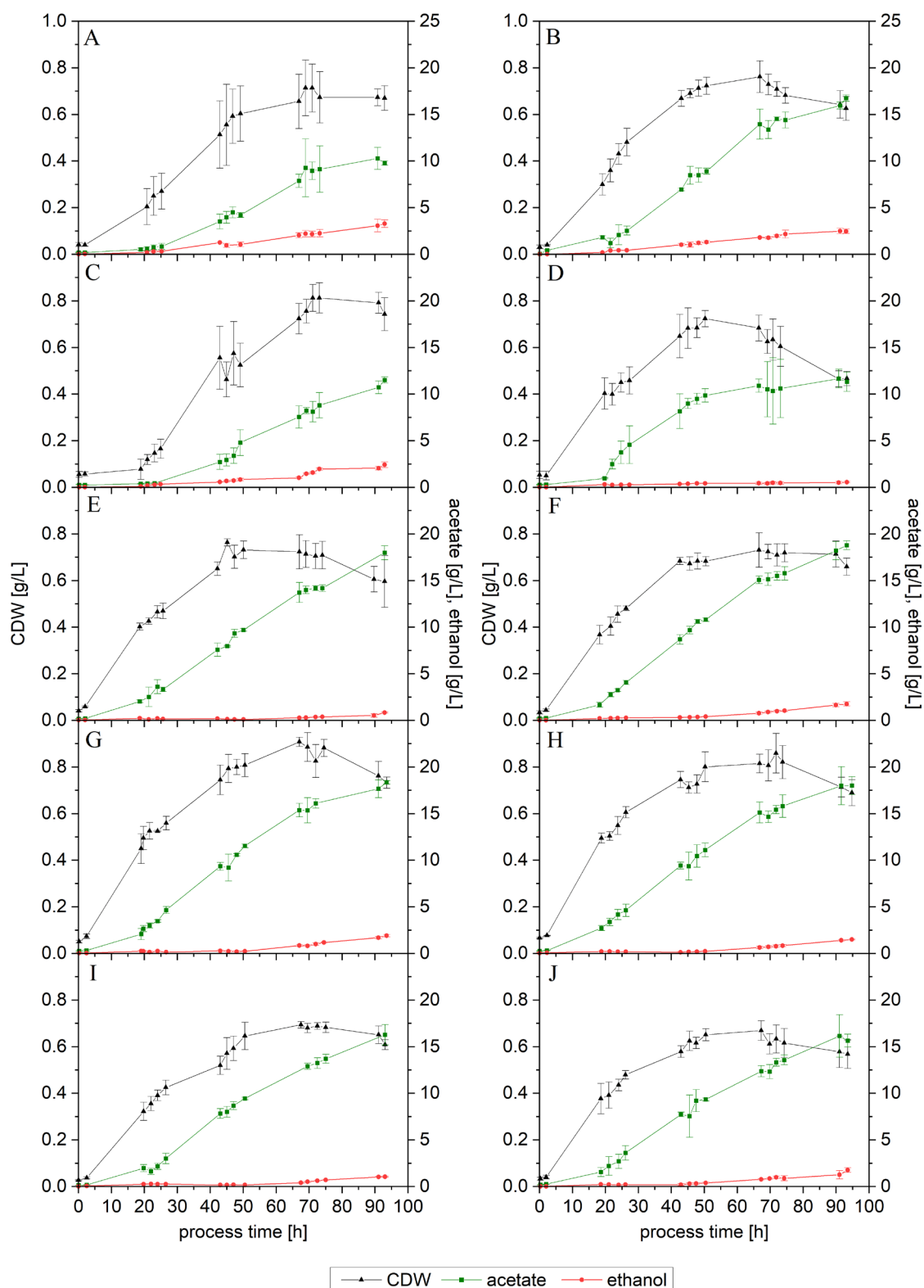


Figure 4.15 – Growth and product formation of setups 1 to 10. (A) to (J), in alphabetical order, refer to each individual setup, in numerical ascending order - (A) is setup 1, (B) is setup 2, etc. Average values of the triplicates ($n = 3$) for cell dry weight (CDW, black triangles), acetate (green squares) and ethanol (red dots), with standard deviation. Points indicate actual measurements. Lines are only depicted for clarity purposes. (Infantes et al., 2020b)

4.3.2.2 Bioliq® syngas, setups 3 and 4

4.3.2.2.1 Substrate usage and carbon fixation

In setup 3, which is analogous to setup 1 except for the reduced gas flow (18 mL/min, Table 4.8), CO usage started slightly later, at 10 h (Figure 4.13C). Maximum CO usage started after 35.8 h, similar to setup 1, but did not stop and lasted until the end of the fermentation. (Infantes et al., 2020b)

H₂ usage started, in this case, after 31.3 h, a delay of 8 h compared to setup 1. At that moment, the CO flow in the off-gas was 0.10 ± 0.05 mmol/min (Figure 4.14C). Maximum H₂ usage was remarkably higher than setup 1, 96.07 ± 0.26 % (0.01 ± 0.001 mmol/min in the off-gas), at 59.5 h. For comparison, H₂ consumption was already at 61.69 ± 13.89 % at 41 h, and 79.47 ± 9.17 % at 47 h (Figure 4.14C). (Infantes et al., 2020b)

As seen in the previous experiment with lower gas flow, no CO₂ usage was detected here either (Figure 4.14C). Nonetheless, more CO could be fixed: at 38 h CO fixation had already reached 70.91 ± 13.79 %. In contrast to setup 1, CO fixation above 85 % was detected between 44.5 h and 82.12 h (Figure 4.13C). $E_{C, total}$ at the end of the run was, therefore, increased: 52.23 ± 2.11 mol % (Table 4.9), 69 % higher than its corresponding higher-flow setup. The maximum overall usage interval, where the sum of CO, CO₂ and H₂ combined was above 85 % of the maximum achieved for the whole fermentation, lasted 9 h, from 54.4 h to 63.2 h (Table 4.11). (Infantes et al., 2020b)

The gas composition for setup 4 was the same as the one used for setup 2, emulating the Bioliq® syngas but without any impurity. The gas flow rate was the same as for setup 3 (Table 4.8). From this first group of fermentations, this was the one where CO usage started the earliest: immediately after inoculation. After 15 h maximum CO usage had been achieved, making this fermentation the fastest here as well. In this instance, though, it behaved similarly to setup 2, and decreased to 16.17 ± 7.38 % at 63.08 h, stopping altogether at 80 h (Figure 4.13D). It lasted 65 h, 12 h longer than setup 2. Some H₂ usage was observed from the start, averaging to 1.89 % for the first 9 h, reaching 20.06 ± 5.85 % at 15 h of process-time, making this the earliest of the 4 setups for Bioliq® syngas. (Infantes et al., 2020b)

Afterwards, it increased steadily, and reached higher values than its higher flow counterpart. Values above 85 % usage started at 36 h: 85.44 ± 7.98 %, corresponding to 0.03 ± 0.02 mmol/min in the off-gas (Figure 4.14D), with maximum usage lasting for 6 h (Figure 4.13D). Its maximum value was 85.73 ± 6.34 %, at 39 h. (Infantes et al., 2020b)

In line with the previous runs, no CO₂ usage was seen (Figure 4.14D). Maximum CO fixation started at 24.5 h and lasted for 24 h until process-time 49 h (Table 4.11). Even if the maximum CO fixation achieved was higher, interestingly, it stayed above 70 % during 36 h, very similar to setup 2. Its

maximum, $94.18 \pm 4.68 \%$, at 39 h, happened simultaneously to the maximum H₂ usage. $E_{C, total}$ for the complete run was $39.87 \pm 3.14 \text{ mol } \%$, lower than both setups 2 and 3 (Table 4.9). The maximum overall usage interval started 20 h earlier than in setup 3, but lasted for a similar period of time, 9.5 h, 0.7 h longer (Table 4.11). (Infantes et al., 2020b)

Table 4.11 – Gas consumption profiles. All values given as an average of a triplicate ($n = 3$). Maximum overall usage interval was calculated as the time period where an 85 % of the combined maximum total usage (CO, CO₂ and H₂) was achieved for each individual fermentation. Similarly, the maximum CO fixation for each experiment was calculated, and the last point where it was above 85 % of this maximum is given as the “time to end of maximum CO fixation”. Superscripts *a* and *b* denote pairs of fermentations done under the exact same conditions, with equivalent gas compositions except for the presence of impurities. Setups 1 and 2 did not reach a value of maximum overall usage above 85 %, nor did the CO fixation rise above that threshold. (Infantes et al., 2020b)

	Setup	1 ^a	2 ^a	3 ^b	4 ^b	5	6	7	8	9	10
Maximum overall usage interval	Start [h]	-	-	54.4	34.5	18.1	21.0	21.0	16.2	28.2	22.0
	End [h]	-	-	63.2	44.0	73.9	71.0	69.0	70.7	66.2	67.0
	Duration [h]	-	-	8.8	9.5	55.8	50.0	48.0	54.5	38.0	45.0
Time to end of maximum CO fixation (> 85 %) [h]		-	-	82.1	48.8	82.6	79.2	80.0	84.2	59.3	66.5

4.3.2.2.2 Biomass, product formation, yield and productivity

Acetate production and biomass growth started in setup 3 after 19 h, as can be seen in Figure 4.15C. After 71 h, the maximum CDW was obtained: $0.81 \pm 0.06 \text{ g/L}$, slowly decreasing after that. After the first 19 h, acetate concentration in the broth increased constantly throughout the fermentation, up to its final value of $12.25 \pm 1.59 \text{ g/L}$. Ethanol formation started also after 19 h, but its production rate increased at the same time as the growth stopped (Figure 4.15C). By the end of the fermentation, it had slowed down, reaching a final concentration of $2.43 \pm 0.01 \text{ g/L}$. (Infantes et al., 2020b)

Regarding setup 4, biomass increased faster, reaching $0.40 \pm 0.07 \text{ g/L}$ at 19 h, steadily rising to its maximum measured, $0.72 \pm 0.04 \text{ g/L}$ at 50 h. After 66.5 h, a reduction in the CDW concentration was detected, dropping to a final value of $0.47 \pm 0.03 \text{ g/L}$ (Figure 4.15D). Even if biomass had increased during the first 19 h, only $0.98 \pm 0.08 \text{ g/L}$ of acetate was produced. Subsequently, the production of acetate increased and reached the maximum measured concentration of $10.98 \pm 0.71 \text{ g/L}$ at 66.5 h, when growth had already halted. Some increase still happened up to the end of the process, albeit slower. The final concentration in the broth was $11.33 \pm 1.03 \text{ g/L}$. Contrasting with the other three setups, just $0.55 \pm 0.09 \text{ g/L}$ of ethanol was formed in this case. (Infantes et al., 2020b)

As mentioned above, in both setups 3 and 4 maximum CO consumption, above 85 %, was achieved (Table 4.11), so in this case yield and productivity are calculated for both the end-point and up to the point where maximum CO fixation stopped, and are shown in Table 4.9 and Table 4.11. (Infantes et al., 2020b)

It can be seen that, as already observed for setups 1 and 2, the fermentation with clean syngas, setup 4, resulted in a much higher acetate to ethanol ratio compared to that of setup 3, both at the end of the process (Table 4.9), and up to the point where maximum CO fixation ended (Table 4.10), being approximately 5 times higher in both cases. Concerning the yields, those of setup 4 were in all cases above the ones of setup 3. As for the end-point $Y_{P/X}$, it was higher for setup 4 ($28.09 \pm 2.70 \text{ g}_{\text{product}}/\text{g}_{\text{biomass}}$, against $20.23 \pm 1.32 \text{ g}_{\text{product}}/\text{g}_{\text{biomass}}$ for setup 3). Up to the point where CO fixation ended, even if $Y_{P/X}$ was also higher for setup 4, the difference was much smaller: 13.82 ± 0.62 for setup 3, and 15.24 ± 0.41 for setup 4. (Infantes et al., 2020b)

4.3.2.3 TNO syngas, setups 5 and 6

The results of the fermentation of two biomass-derived syngas, following the gasification of beech wood and lignin at the MILENA gasifier, TNO Energy Transition, Biomass & Energy Efficiency Unit (Netherlands), are shown above, in section 4.2 *Evaluation of beech wood and lignin derived syngas*. Here, the results for the same syngas composition but without impurities are shown. (Infantes et al., 2020b)

4.3.2.3.1 Substrate usage and carbon fixation

In setup 5, maximum CO usage was reached 14 h after inoculation (Figure 4.13E), with a detected flow of CO in the off-gas of $0.03 \pm 0.01 \text{ mmol}/\text{min}$ (Figure 4.14E). 3 h later, at 17 h of process-time, maximum CO fixation was detected. This lasted for 66 h, averaging 94 %. Maximum CO usage lasted until the end of the fermentation. (Infantes et al., 2020b)

H₂ usage started 9 h after inoculation of the fermenters, increasing thereafter, and reaching the maximum threshold ($\geq 85 \%$) after 18 h (Figure 4.13E), when the flow of H₂ detected in the off-gas had decreased to $0.03 \pm 0.01 \text{ mmol}/\text{min}$ (Figure 4.14E). This maximum usage lasted 67 h, up to 85 h of process-time, with an average of 95 %. (Infantes et al., 2020b)

Some marginal CO₂ usage was detected between 21 h and 49 h, with an average of 1 % (Figure 4.13E).

Between 18 h and 74 h, maximum overall usage was achieved (Table 4.11). $E_{C, \text{total}}$ for the overall run was $48.79 \pm 2.41 \text{ mol } \%$ (Table 4.9). (Infantes et al., 2020b)

In setup 6, maximum CO usage lasted for 79 h, between 15 h and the end of the fermentation. The maximum CO fixation interval went from 18 h to 79 h, with an average of 95 % (Figure 4.13F). (Infantes et al., 2020b)

At 22 h H₂ maximum usage started, lasting until 71 h of process-time. An average of 0.02 mmol/min, or 92 % usage, was detected between those two time points. CO₂ usage was detected starting from 20 h to 71 h, averaging 10 %. Its maximum was met at 40 h, when 0.17 ± 0.01 mmol/min of CO₂ were measured in the off-gas, representing 17.72 ± 1.50 % usage (Figure 4.13F and Figure 4.14F). (Infantes et al., 2020b)

The interval of maximum overall usage started at 21 h and ended at 71 h of process-time (Table 4.9). The $E_{C, total}$ for the complete run amounted in this case to 43.27 ± 0.28 mol % (Table 4.9). (Infantes et al., 2020b)

4.3.2.3.2 Biomass, product formation, yield and productivity

Biomass, acetate and ethanol profiles are shown in Figure 4.15E for setup 5, and Figure 4.15F for setup 6. (Infantes et al., 2020b)

On the setup 5, biomass reached 0.40 ± 0.01 g/L 19 hours after inoculation. The CDW continued to increase up to 45 h, with an average of 0.71 g/L between 42 h and 50 h. Afterwards, it started to decline, and the final recorded value was 0.60 ± 0.11 g/L. (Infantes et al., 2020b)

After the first 19 h, acetate was produced at a constant rate throughout the fermentation, reaching a final value of 18.00 ± 0.74 g/L. Ethanol, on the other hand, remained below 0.2 g/L up to 67 h, when it reached 0.28 ± 0.05 g/L. Its final concentration was 0.84 ± 0.07 g/L. (Infantes et al., 2020b)

The final molar acetate to ethanol ratio for this fermentation was 16.63 ± 1.71 (Table 4.9), while up to the end of maximum CO fixation, it was much higher, 31.82 ± 2.22 g/L (Table 4.10), as a result of the later start in ethanol formation. The total, final productivity was 0.20 ± 0.01 g/L·h, that the same value than for the productivity calculated up to the end of maximum CO fixation. Regarding the yields, $Y_{P/S, fixed}$ was very similar for the entire run and up to the end of maximum CO fixation, with values of 0.92 ± 0.03 g_{product}/g_{substrate} and 0.93 ± 0.02 g_{product}/g_{substrate}, respectively. $Y_{P/X}$ calculated at the end-point was 34.79 ± 7.47 g_{product}/g_{biomass}. Up to the end of maximum CO fixation, this was lower, 21.67 ± 1.19 g_{product}/g_{biomass}. (Infantes et al., 2020b)

Concerning setup 6, the biomass growth followed a similar trend to that of setup 5, reaching 0.68 ± 0.02 g/L 43 h after inoculation. It then slightly increased to its maximum, 0.73 ± 0.07 g/L at 67 h, remaining mostly constant until 90 h. A decrease in the cell dry weight was noticed in the last sample.

As with setup 5, acetate was produced during the whole process, but in this case, after 67 h its production slowed down slightly, coinciding to when the culture stopped growing. A noticeable ethanol production only happened after approximately 50 h, when it reached 0.41 ± 0.03 g/L. At 67 h, the ethanol formed amounted to 0.77 ± 0.11 g/L, and the final concentration measured was 1.76 ± 0.23 g/L, almost 1 g/L higher than setup 6. (Infantes et al., 2020b)

The molar ratio of acetate to ethanol at the end of the process was 8.29 ± 1.07 , half that of setup 5. Also, when looking at the ratio obtained up to the end of maximum CO fixation, on setup 6 it was almost three times lower than setup 5 (Table 4.10). The acetate and total productivities for both calculated intervals are comparable to setup 5, but is not so for ethanol, which were higher, as expected by looking at the product formation mentioned above. Both $Y_{P/S, fed}$ and $Y_{P/S, fixed}$ are comparable to those of setup 5, as can be seen in Table 4.10 and Table 4.11. $Y_{P/S, used}$, though, was higher for this run. The final $Y_{P/X}$ equated to 32.54 ± 1.50 g_{product}/g_{biomass}, very close to that of the previous setup, and so it was the calculated up to the end of maximum CO fixation, 24.24 ± 0.77 g_{product}/g_{biomass}. (Infantes et al., 2020b)

4.3.3 Clean syngas fermentations

4.3.3.1 LNEG and ENEA based syngas, setups 7 and 8

4.3.3.1.1 Substrate usage and carbon fixation

In setup 7, CO usage started directly after inoculation, reaching 85 % at 14 h. Maximum CO fixation started shortly thereafter, at 17 h, and stopped at 80 h. Maximum usage lasted up to the end of the fermentation, and during this time the average flow of CO detected in the off-gas was 0.007 mmol/min, representing a 96.97 % average usage (Figure 4.13G). (Infantes et al., 2020b)

H₂ usage started 11 h after inoculation, when the detected flow in the off-gas was 0.26 ± 0.003 mmol/min (2.47 ± 1.28 % usage). It stayed above 85 % for 53.5 h, from 21 h to 74.5 h. The average usage during that time amounted to 93.75 %. The lowest flow of H₂ detected in the off-gas was 0.006 mmol/min (97.64 % usage), between 39 h and 45 h (Figure 4.14G). (Infantes et al., 2020b)

CO₂ usage started after 20 h, and lasted until 66 h. The average usage was 10.31 %. Its maximum was 18.31 ± 3.64 %, met at 41 h (Figure 4.13G), when 0.13 ± 0.01 mmol/min were detected in the off-gas (Figure 4.14G). (Infantes et al., 2020b)

Between 21 h and 69 h, maximum overall usage was detected (Table 4.11). For the complete run, the $E_{C, total}$ was 51.52 ± 0.70 mol % (Table 4.9). (Infantes et al., 2020b)

As can be seen in Figure 4.13H, the syngas which emulated ENEA, used in setup 8, presented a very similar profile regarding CO and H₂ usage and CO fixation, but an increased CO₂ usage: in fact, the highest of all gases tested. Maximum CO usage was achieved at 12 h of process-time, while maximum CO fixation happened just one hour later. (Infantes et al., 2020b)

At 9 h of process-time, H₂ usage slowly started, and passed the 85 % usage mark at 17 h, with 0.03 ± 0.005 mmol/min in the off-gas (Figure 4.14H). At 73 h, maximum H₂ usage stopped, and it kept decreasing until the end of the fermentation. During the interval of maximum usage, its average was 95.77 %, or 0.01 mmol/min detected in the waste gas stream. (Infantes et al., 2020b)

CO₂ usage was detected at 14 h, very closely in time with the starting of maximum CO fixation. It reached its maximum, 37.08 ± 4.07 %, which corresponds to 0.12 ± 0.01 mmol/min in the off-gas (Figure 4.14H), shortly after, at 18 h. It lasted until 77.4 h, with an average of 23 %, or 0.15 mmol/min in the off-gas. (Infantes et al., 2020b)

The interval of maximum overall usage started five hours earlier than in setup 7, at 16 h, and ended at 71 h (Table 4.11). The $E_{C, total}$ for the complete run was very similar to that of setup 7, 50.88 ± 1.71 mol %. (Infantes et al., 2020b)

4.3.3.1.2 Biomass, product formation, yield and productivity

Figure 4.15G shows the profiles for CDW and products throughout the fermentation for setup 7, while for setup 8 this is depicted in Figure 4.15H. (Infantes et al., 2020b)

For the LNEG-like syngas, biomass increased up to 67 h of process-time, moment at which its maximum, 0.91 ± 0.02 g/L was measured. Afterwards, and until the end of the fermentation, it decreased continuously. Acetate formation started directly after inoculation, reaching 2.07 ± 0.60 g/L after 19 h. At 74.5 h, its concentration was 14.46 ± 1.54 g/L, and from there on, the production slowed down. Its final concentration was 18.35 ± 0.20 g/L. Up to 50 h of process-time, only 0.24 ± 0.03 g/L of ethanol could be measured. From 67 h, though, ethanol formation increased, reaching an end value of 1.91 ± 0.13 g/L. (Infantes et al., 2020b)

The end-point molar acetate to ethanol ratio was in this case 7.38 ± 0.42 (Table 4.9), while up to the point when maximum CO fixation stopped, it was 12.07 ± 1.37 (Table 4.10). The total productivities for both intervals were 0.21 ± 0.001 g/L·h (Table 4.9), and 0.23 ± 0.01 g/L·h (Table 4.10), respectively. Up to the end of maximum CO fixation, both $Y_{P/S, used}$ and $Y_{P/S, fixed}$ were 0.93 ± 0.05 . For the complete run, both yields were also similar among them, but lower than the ones obtained at the end, reflecting the slower product formation seen towards the end: 0.85 ± 0.003 g_{product}/g_{substrate} for $Y_{P/S, used}$ and 0.88 ± 0.02 g_{product}/g_{substrate} for $Y_{P/S, fixed}$. The amount of product per amount of biomass generated, $Y_{P/X}$,

at the end of the process was $29.29 \pm 0.51 \text{ g}_{\text{product}}/\text{g}_{\text{biomass}}$. Up to the end of maximum CO fixation, it was $21.34 \pm 1.98 \text{ g}_{\text{product}}/\text{g}_{\text{biomass}}$. (Infantes et al., 2020b)

The fermentation with ENEA-based syngas, setup 8, resulted in less biomass formation. During the first 26 h, a faster growth was detected. At 50 h, the measured biomass amounted to $0.80 \pm 0.06 \text{ g/L}$. Its maximum was detected at 72 h, with $0.86 \pm 0.09 \text{ g/L}$. Afterwards, a decrease in the biomass concentration was observed, with a final concentration of $0.69 \pm 0.06 \text{ g/L}$. Even so, acetate and ethanol formation presented a very similar pattern to the previous fermentation, with $2.73 \pm 0.33 \text{ g/L}$ of acetate produced after 19 h. It slowed down slightly after 69 h, similarly to what is observed in setup 8, and coinciding with the halt in growth. Nonetheless, its concentration kept rising until the end of the process, when it reached $18.02 \pm 0.43 \text{ g/L}$. Ethanol production, much like setup 7, was very low for the first 50 h, with $0.24 \pm 0.04 \text{ g/L}$ detected at that time. Afterwards, its concentration in the fermenter raised, getting to its end value of $1.51 \pm 0.05 \text{ g/L}$, lower than in the previous run. (Infantes et al., 2020b)

The obtained molar acetate to ethanol ratio at the end of the fermentation was, as expected due to the lower ethanol, somehow higher than for the previous setup, 9.16 ± 0.26 (Table 4.9). This is also true for the value obtained up to the end of the maximum CO fixation, 14.89 ± 1.99 (Table 4.10). Productivities, both calculated at the end-point or up to the maximum CO fixation point, were slightly inferior for setup 8 (Table 4.9 and Table 4.11). The total, end-point productivity was $0.20 \pm 0.004 \text{ g/L}\cdot\text{h}$. The yields obtained were also lower, especially when looking at the complete run. They were also very similar among them, with $0.82 \text{ g}_{\text{product}}/\text{g}_{\text{substrate}}$ for $Y_{P/S, \text{ used}}$ and $Y_{P/S, \text{ fixed}}$, both at the end of the process and up to the point when maximum CO fixation ended. Finally, the end-point $Y_{P/X}$ resulted in $31.01 \pm 1.96 \text{ g}_{\text{product}}/\text{g}_{\text{biomass}}$, very similar to that of setup 7. As for the resulting $Y_{P/X}$ calculated to the point of maximum CO fixation, it amounted to $21.73 \pm 0.58 \text{ g}_{\text{product}}/\text{g}_{\text{biomass}}$, equivalent to that of setup 7. (Infantes et al., 2020b)

4.3.3.2 Custom Mixtures A and B, setups 9 and 10

4.3.3.2.1 Substrate usage and carbon fixation

As illustrated in Figure 4.13I, CO usage started following inoculation on setup 9, with 85 % usage after 21 h. It reached $97.61 \pm 0.31 \%$ five hours later, at 26 h, and its maximum, $98.90 \pm 0.98 \%$ at 48 h. Average CO usage only dropped below 85 % shortly before the end of the experiment, at 92 h of process-time, but the higher standard deviation shows some discrepancy between the individual bioreactors. Concerning CO fixation, it first reached its maximum at 28 h, with $85.32 \pm 0.18 \%$, when $0.006 \pm 0.001 \text{ mmol/min}$ (Figure 4.14I) were leaving the fermenter with the off-gas. Maximum CO fixation stopped at 59 h (Figure 4.13I and Table 4.11). (Infantes et al., 2020b)

It took 19 h for H₂ usage to rise above 3 %: up to that point, it averaged 0.97 %. Afterwards, it increased rapidly, reaching 84.91 ± 4.46 % (Figure 4.13I), or 0.03 ± 0.01 mmol/min in the off-gas (Figure 4.14I), at 27 h. At 71 h it had decreased to 83.75 ± 6.04 %, and it continued to sharply decline afterwards. (Infantes et al., 2020b)

No CO₂ usage could be detected in this setup 9 fermentation. At 19 h, the amount of CO₂ detected in the waste gas stream peaked at 0.18 ± 0.01 mmol/min (Figure 4.14I), which would be -88.35 ± 4.87 % in terms of usage (or 88.35 ± 4.87 % production). (Infantes et al., 2020b)

The period between 28 h and 66 h was that of maximum overall usage (Table 4.11). The resulting $E_{C, total}$ for this setup at the end-point was determined to be 46.61 ± 0.96 mol % (Table 4.9). (Infantes et al., 2020b)

Moving on to setup 10, CO usage started, as well, directly after inoculation (Figure 4.13J). It surpassed 85 % at 16.5 h, with 85.92 ± 11.12 %, and reached its higher value, 99.18 ± 1.42 % at 47 h. From then on, and until the end of the fermentation, it remained at an average of 96.32 %, which means that an average of 0.008 mmol/min (Figure 4.15J) of CO was living the reactor. Looking at the CO fixation, it reached its maximum at 20 h, with 87.40 ± 10.59 %. At 75 h it dropped below 85 %, and continued to do so until the end-point. (Infantes et al., 2020b)

H₂ usage averaged 1.82 % during the first 13 h, starting to increase from that point on to reach 86.68 ± 5.95 % at 23 h. At 46 h its maximum was met, with 0.006 ± 0.002 mmol/min in the off-gas (Figure 4.14J), and 97.14 ± 1.01 % usage (Figure 4.13J). At 71 h, maximum usage stopped. (Infantes et al., 2020b)

CO₂ usage was first detected after 23 h, coinciding with the moment when H₂ usage reached its maximum, and lasted until 58 h of process-time. The average usage during this period was 6.93 %, with its maximum being 11.34 ± 2.99 % at 43 h, or 0.125 ± 0.005 mmol/min in the off-gas (Figure 4.14J). The maximum interval usage occurred in the period from 22 h to 67 h (Table 4.11). The $E_{C, total}$ for the complete run for setup 10 was 47.75 ± 1.49 mol % (Table 4.9). (Infantes et al., 2020b)

4.3.3.2.2 Biomass, product formation, yield and productivity

Products and biomass formation are shown in Figure 4.15I for setup 9. As can be seen, biomass increased the fastest during the first 26.5 h, when the measured concentration was 0.43 ± 0.03 g/L. Later on, growth slowed down, reaching 0.65 ± 0.06 g/L at 50.5 h and finally its maximum, 0.69 ± 0.01 g/L at 67.5 h. From that point on, biomass stagnated and eventually decreased. (Infantes et al., 2020b)

At process-time 24 h, 2.17 ± 0.34 g/L of acetate was measured. From there on, the acetate concentration increased up to 43 h, remaining constant thereafter. The final concentration measured was 16.28 ± 1.09 g/L. The detected ethanol remained very low, and practically constant, with an average of 0.22 g/L from 20 h to 50.5 h. At 67.5 h, an increase in its production was observed, reaching 0.41 ± 0.05 g/L, totaling 1.05 ± 0.07 g/L at the end of the fermentation. (Infantes et al., 2020b)

The final molar ratio of acetate to ethanol was 11.92 ± 0.85 (Table 4.9), while if calculated up to the point when maximum CO fixation ended, it was 45.20 ± 7.39 , the highest value amongst all fermentations (Table 4.10). (Infantes et al., 2020b)

The total productivity up to the end of maximum CO fixation was 0.19 ± 0.002 g/L·h (Table 4.10), and 0.18 ± 0.01 g/L·h (Table 4.9) for the complete run. (Infantes et al., 2020b)

$Y_{P/S, \text{ used}}$ and $Y_{P/S, \text{ fixed}}$ were 0.72 ± 0.04 g_{product}/g_{substrate} and 0.91 ± 0.04 g_{product}/g_{substrate}, respectively, for the entire run (Table 4.9). Up to the end of CO fixation, these were 0.83 ± 0.01 g_{product}/g_{substrate} for $Y_{P/S, \text{ used}}$ and 0.99 ± 0.01 g_{product}/g_{substrate} for $Y_{P/S, \text{ fixed}}$. The obtained end-point $Y_{P/X}$ was 29.49 ± 1.01 g_{product}/g_{biomass} while up to the point when maximum CO fixation ended was almost half, 15.34 ± 1.16 g_{product}/g_{biomass}. (Infantes et al., 2020b)

Figure 4.15J shows growth and acetate and ethanol production of setup 10. In terms of growth, this fermentation followed a very similar pattern to that of setup 9. Biomass increased at a faster rate for the first hours, reaching 0.48 ± 0.02 g/L after 26 h, slowing down afterwards, and reaching 0.65 ± 0.03 g/L at 50 h. At 67 h, it had only increased slightly to 0.67 ± 0.04 g/L, starting to decrease thereafter. (Infantes et al., 2020b)

Acetate formation also followed an equivalent trend to that of the previous setup, with a slower production for the first 19 h, followed by a continuous production, reaching a final concentration of 15.65 ± 0.89 g/L. (Infantes et al., 2020b)

Ethanol formation started earlier in this case. At 50 h 0.38 ± 0.06 g/L were detected, increasing to 0.77 ± 0.05 g/L, and finally 1.77 ± 0.24 g/L at the last sample taken, at 93.5 h. (Infantes et al., 2020b)

Regarding the productivity, taken in consideration the overall process, it was slightly higher to setup 9, 0.19 ± 0.02 g/L·h. When calculated up to the point when maximum CO fixation ended, it was 0.20 ± 0.01 g/L·h. (Infantes et al., 2020b)

Finally, the yield at the end-point equaled to 0.87 ± 0.07 g_{product}/g_{substrate} for $Y_{P/S, \text{ used}}$, while $Y_{P/S, \text{ fixed}}$ was 0.96 ± 0.03 g_{product}/g_{substrate}. $Y_{P/X}$ as calculated from the final sample, was 33.49 ± 2.30 g_{product}/g_{biomass},

and the same parameter calculated up to the point of maximum CO fixation equaled $20.38 \pm 0.89 \text{ g}_{\text{product}}/\text{g}_{\text{biomass}}$. (Infantes et al., 2020b)

4.3.4 Productivity and product ratio comparison according to syngas type and composition

The results for the fermentation of biomass-derived TNO gas from beech wood and lignin were reported above, in section 4.2 *Evaluation of beech wood and lignin derived syngas*. These are shown as stars (*) in Figure 4.16 to Figure 4.18.

As can be seen in Figure 4.16, for each pair of real and clean syngas tested under the same conditions, and for which the flow of carbon containing substrates (C_{in}) was 0.4 mmol/min (Table 4.8), the end-point productivity of the gas devoid of impurities was higher in all cases. Setups 1 and 2 present the highest difference amongst the experiments. (Infantes et al., 2020b)

For setups 3 and 4, where the gas flow was lower, with C_{in} fixed at 0.3 mmol/min and $H_{2,\text{in}}$ at 0.2 mmol/min (Table 4.8), the opposite is true: the biomass-derived syngas, containing impurities, presented a higher final productivity. (Infantes et al., 2020b)

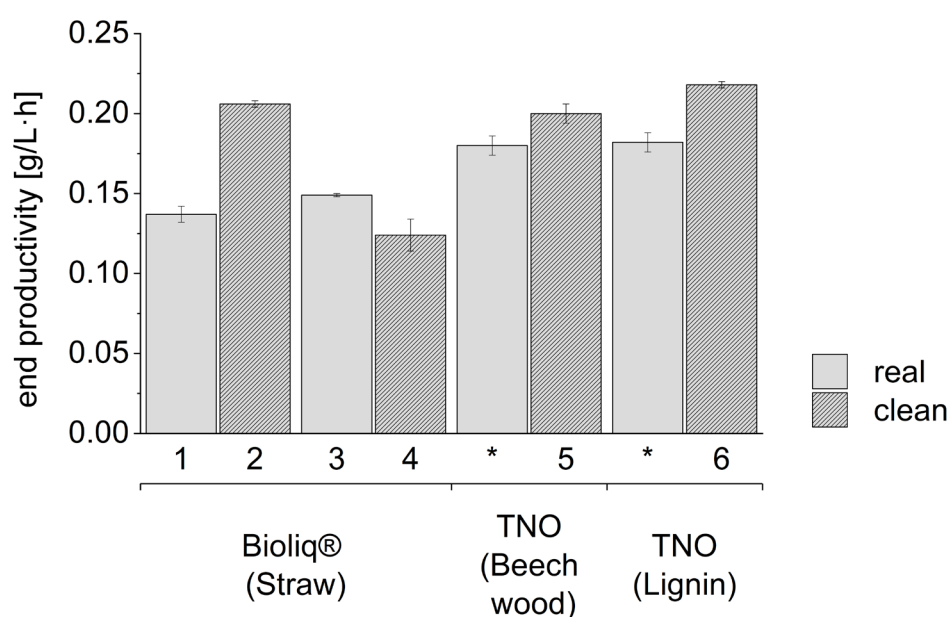


Figure 4.16 – End-point productivity for pairs of real and clean syngases. Numbers 1 to 6 indicate the setup, while stars (*) refer to TNO real gases. The productivity, as measured at the end of the fermentation, is shown by the bars. Real, biomass-derived syngases are represented by smooth light grey bars, while clean, commercially-mixed syngases are shown by diagonally striped grey bars. All values are given as the average of a triplicate, with standard deviation. (Infantes et al., 2020b)

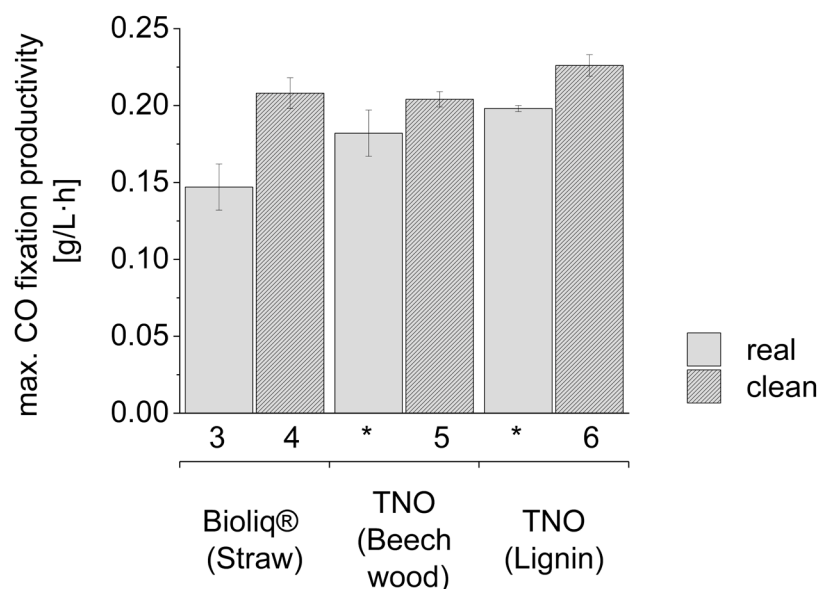


Figure 4.17 – Productivity up to the end of maximum CO fixation for pairs of real and clean syngases. Numbers 3 to 6 indicate the setup, while stars (*) refer to TNO real gases. The productivity, as measured at the end of the fermentation, is shown by the bars. Real, biomass-derived syngases are represented by smooth light grey bars, while clean, commercially-mixed syngases are shown by diagonally striped grey bars. All values are given as the average of a triplicate, with standard deviation. No values are given for setups 1 and 2 due to the fact that no maximum CO fixation occurred. (Infantes et al., 2020b)

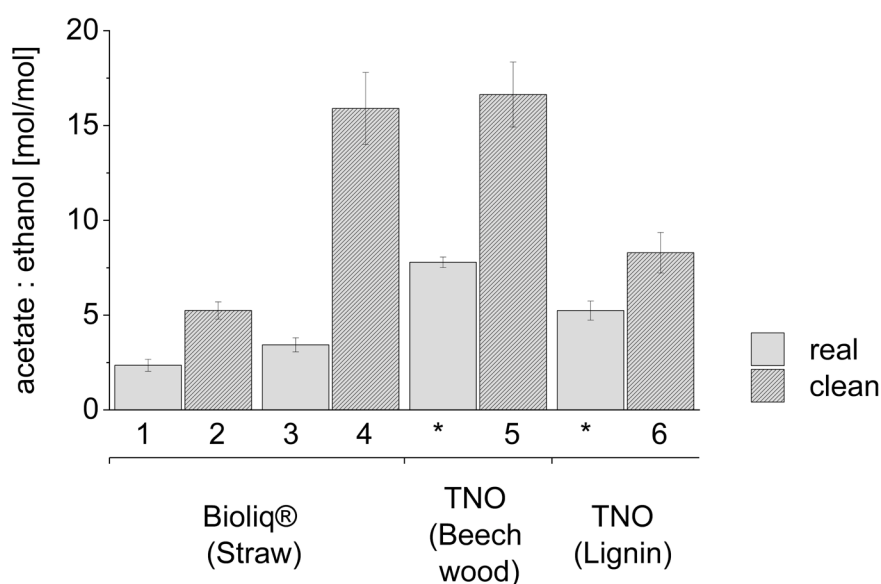


Figure 4.18 – Molar acetate to ethanol ratio for pairs of real and clean syngases. Numbers 1 to 6 indicate the setup, while stars (*) refer to TNO real gases. The ratio of acetate to ethanol, in mol, as measured at the end of the fermentation, is shown by the bars. Real, biomass-derived syngases are represented by smooth light grey bars, while clean, commercially-mixed syngases are shown by diagonally striped grey bars. All values are given as the average of a triplicate, with standard deviation. (Infantes et al., 2020b)

When the productivity is calculated up to the end of maximum CO fixation, the clean gases present a higher productivity in all cases (Figure 4.17). As mentioned above, setups 1 and 2 are not included due to the fact that no maximum CO fixation (no CO fixation above 85 %) was detected. (Infantes et al., 2020b)

Figure 4.18 illustrates the molar ratio of acetate to ethanol for the pairs of experiments comparing clean and real syngases. It can be seen that, depending on whether the syngas is “real” (biomass-derived), or clean (that is, commercially mixed and free from impurities), the product profile changes. All clean gases produce a higher acetate to ethanol ratio, while their biomass-derived counterparts generate a greater amount of ethanol per mol of acetate. (Infantes et al., 2020b)

A visual representation of the influence of the molar flow rate of each substance in the tested clean syngases on the product distribution is shown in Figure 4.19. From the eight setups which were performed with an impurity-free syngas, the ones with a lower H₂ flow, ≤ 0.23 mmol/min, appear to generate the highest acetate to ethanol ratio. There is one exception, setup 10, which had the same H₂ molar flow as setup 4, 0.23 mmol/min (Table 4.8), but did result in a much lower acetate to ethanol ratio. The molar CO flow rate was also equivalent, 0.23 mmol/min for setup 4 and 0.22 mmol/min for setup 10. The main difference here was the molar CO₂ flow, which in setup 10 was 7 times higher (0.14 mmol/min) than in setup 4, with just 0.02 mmol/min. (Infantes et al., 2020b)

The mid-range of the acetate-ethanol ratio for the syngases here tested were obtained with the higher CO₂ molar flow rates, ≥ 0.14 mmol/min, and a molar flow rate of H₂ ≥ 0.22 mmol/min. (Infantes et al., 2020b)

The lower acetate to ethanol ratio, or the fermentation which produced a higher amount of ethanol per amount of acetate, was achieved by the syngas containing the highest H₂ and CO molar flow, together with the lowest molar flow of CO₂. (Infantes et al., 2020b)

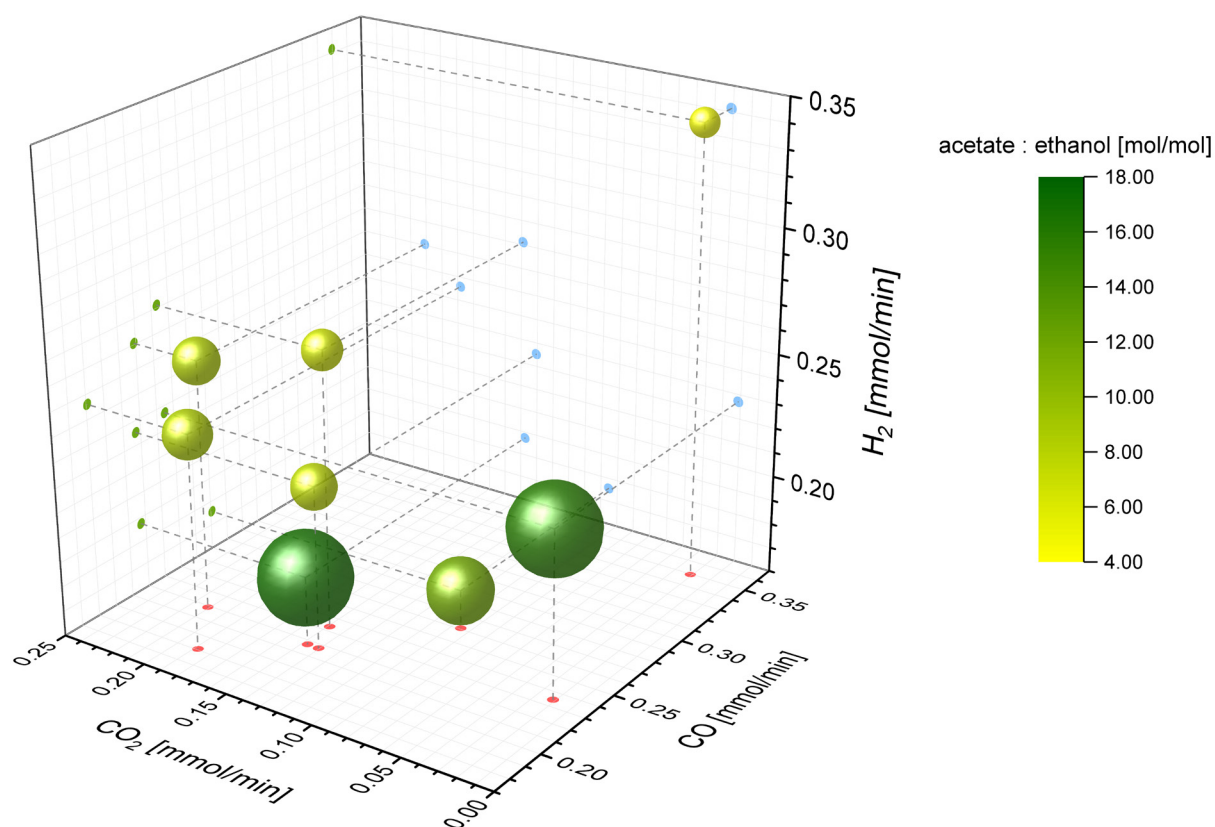


Figure 4.19 – Molar acetate to ethanol ratio obtained from each combination of tested CO, CO₂ and H₂ molar substrate flow rate for clean syngases. The acetate to ethanol molar ratio for setups 2, 4, and 5 to 10 is shown according to the molar flow rate of each substance fed into the bioreactor. The size and color of each bubble is proportional to the molar acetate to ethanol ratio. Smaller size and yellow color denote a lower acetate to ethanol ratio. Bigger bubbles, and green color, indicates a higher acetate to ethanol ratio. H₂ is represented on the Z axis, CO₂ on the Y axis and CO on the X axis. Blue dots represent the YZ projection, red dots the XY projection, and green dots, the ZX projection. Drop lines (dotted grey lines) are visual aids to assigning each bubble its value in each axis. (Infantes et al., 2020b)

4.4 Overview of fermentation results

4.4.1 Overall summary of carbon fed, usage and fixation

An overview of the amount of substance flow fed for H₂, CO₂ and CO, as well as the total amount of substance fed, used or fixed, is given in Table 4.12 for the fermentations performed for the evaluation of the impact of the medium components and process parameters, which were described above in section 4.1 *Impact of medium components and process parameters*. For the fermentations evaluating the impact of syngas impurities and composition, described in sections 4.2 *Evaluation of beech wood and lignin derived syngas* and 4.3 *Impact of syngas composition and impurities*, this is presented in Table 4.13.

It can be seen that CO₂ usage was only detected in one instance, for the ENEA syngas composition (Table 4.13). Because of this, the H₂:CO and H₂:C_{total} ratios are identical in all other cases.

Even if, as presented in Table 4.12, the amount of substance fed in all fermentations evaluating media components and process parameters was the same (except for setup 6), the H₂:CO_{used} ratios and the H₂:CO_{fixed} ratios presented a big variance. Among them, both the lowest H₂:CO_{used} and H₂:CO_{fixed} resulted from the non-pH-controlled fermentation, 0.48 ± 0.03 and 0.65 ± 0.03 , respectively; the highest were found in the standard fermentation (setup 1) (Table 4.12).

In Table 4.13 it is clear that, even when the composition of the gas was the same, but the flow was changed (setup 1 vs. setup 3 for real Bioliq gas), the H₂:CO ratios also changed significantly. The lowest H₂:CO_{used} and H₂:CO_{fixed} were those of real Bioliq gas at the highest amount of substance flow rate (setup 1), with 0.33 ± 0.04 and 0.57 ± 0.06 respectively.

Both setups 6 and 7 (synthetic impurity-free TNO lignin syngas, and synthetic impurity-free LNEG syngas) had a very similar H₂:C_{total, used}, 0.97 ± 0.01 and 0.96 ± 0.02 , respectively, which are the highest for this set of fermentations. The highest H₂:CO_{used} is found in setup 8, 1.07 ± 0.03 , and the lowest, in setup 1, with 0.33 ± 0.04 . Regarding H₂:C_{total, fixed} the highest values were those of TNO lignin syngas, setup 6 and setup 7, with 1.10 ± 0.05 , 0.99 ± 0.01 and 1.00 ± 0.02 , in that order; H₂:CO_{fixed} values are the same for those fermentations, but setup 8 was, in this case, also amongst the highest, with 1.07 ± 0.03 . The lowest value was, again, for setup 1, with 0.57 ± 0.06 (Table 4.13).

Table 4.12 – Amount of substance flow fed, and ratios of fed, used and fixed substrates for the medium components and process parameters evaluation fermentations. For setup 6, the first amount of substance flow fed value represents the first 24 h, and the second value is the one resulting after the gas flow was lowered. The results for these fermentations are presented in section 4.1.

		Setup 1	Setup 2	Setup 3a	Setup 3b	Setup 4	Setup 5	setup 6
		Standard	no pH regulation	1 g/L cysteine (2x standard); pH 5.9	1 g/L cysteine (2x standard); pH 5.40 after 68 h; pH 4.78 after 92.4 h	1 g/L yeast (2x standard)	24 h at pH 5.9, then let drop and hold at 4.78	24 h gas flow 18 mL/min, pH 5.9 - then gas flow 12.6 mL/min; let pH drop and hold at 4.78
Amount of substance flow fed (mmol/min)	H ₂	0.26	0.25	0.25	0.25	0.25	0.24	0.24 / 0.16
	CO	0.25	0.25	0.25	0.25	0.26	0.25	0.25 / 0.18
	CO ₂	0.11	0.12	0.12	0.12	0.12	0.12	0.12 / 0.08
	Total carbon (CO + CO ₂)	0.37	0.37	0.37	0.37	0.37	0.37	0.37 / 0.26
fed (mol)	CO ₂ :CO	0.45 ± 0.02	0.46 ± 0.01	0.47	0.47 ± 0.02	0.47 ± 0.01	0.46 ± 0.00	0.47 ± 0.00
	H ₂ :C _{total}	0.69 ± 0.00	0.66 ± 0.00	0.68	0.68 ± 0.00	0.67 ± 0.00	0.66 ± 0.00	0.63 ± 0.01
	H ₂ :CO	1.01 ± 0.01	0.97 ± 0.00	0.99	0.94 ± 0.01	0.98 ± 0.00	0.97 ± 0.00	0.93 ± 0.01
	H ₂ :CO ₂	2.22 ± 0.05	2.10 ± 0.03	2.12	2.12 ± 0.06	2.10 ± 0.02	2.11 ± 0.01	1.99 ± 0.02
used (mol)	CO ₂ :CO	-	-	-	-	-	-	-
	H ₂ :C _{total}	0.83 ± 0.04	0.48 ± 0.03	0.58	0.68 ± 0.05	0.74 ± 0.01	0.70 ± 0.02	0.62 ± 0.04
	H ₂ :CO	0.83 ± 0.04	0.48 ± 0.03	0.58	0.68 ± 0.05	0.74 ± 0.01	0.70 ± 0.02	0.62 ± 0.04
	H ₂ :CO ₂	-	-	-	-	-	-	-
fixed (mol)	CO ₂ :CO	-	-	-	-	-	-	-
	H ₂ :C _{total}	0.90 ± 0.03	0.65 ± 0.03	0.70	0.83 ± 0.04	0.82 ± 0.01	0.84 ± 0.04	0.75 ± 0.03
	H ₂ :CO	0.90 ± 0.03	0.65 ± 0.03	0.70	0.83 ± 0.04	0.82 ± 0.01	0.84 ± 0.04	0.75 ± 0.03
	H ₂ :CO ₂	-	-	-	-	-	-	-

Table 4.13 – Amount of substance flow fed, and ratios of fed, used and fixed substrates for the fermentations evaluating the impact of syngas composition and impurities. The results for these fermentations are presented in sections 4.2 and 4.3.

		Setup 1	Setup 2	Setup 3	Setup 4		Setup 5		setup 6	setup 7	setup 8	setup 9	setup 10
		real Bioliq® from straw	synthetic free Bioliq®	real Bioliq syngas from straw	synthetic impurity- free Bioliq	TNO beech wood	synthetic impurity- free TNO- beechwood -like	TNO lignin	synthetic impurity- free TNO- lignin-like	synthetic impurity- free LNEG	synthetic impurity- free ENEA	Custom mix A	Custom mix B
Amount of substance flow fed (mmol/min)	H ₂	0.35	0.34	0.23	0.23	0.18	0.19	0.28	0.26	0.27	0.25	0.18	0.23
	CO	0.34	0.35	0.23	0.23	0.23	0.22	0.22	0.22	0.23	0.19	0.26	0.22
	CO ₂	0.03	0.03	0.02	0.02	0.15	0.15	0.18	0.21	0.15	0.19	0.10	0.14
	Total carbon (CO + CO ₂)	0.37	0.38	0.25	0.26	0.38	0.36	0.40	0.43	0.38	0.38	0.36	0.36
fed (mol)	CO ₂ :CO	0.10 ± 0.00	0.09 ± 0.00	0.10 ± 0.00	0.09 ± 0.00	0.68 ± 0.0	0.68 ± 0.01	0.84 ± 0.01	0.96 ± 0.02	0.66 ± 0.01	0.99 ± 0.01	0.37 ± 0.01	0.65 ± 0.01
	H ₂ :C _{total}	0.93 ± 0.01	0.90 ± 0.00	0.90 ± 0.01	0.89 ± 0.00	0.47 ± 0.01	0.51 ± 0.00	0.69 ± 0.01	0.61 ± 0.01	0.70 ± 0.00	0.65 ± 0.00	0.49 ± 0.01	0.63 ± 0.01
	H ₂ :CO	1.02 ± 0.01	0.98 ± 0.00	0.98 ± 0.01	0.97 ± 0.00	0.79 ± 0.02	0.86 ± 0.00	1.27 ± 0.01	1.19 ± 0.01	1.16 ± 0.00	1.29 ± 0.01	0.67 ± 0.00	1.04 ± 0.01
	H ₂ :CO ₂	10.70 ± 0.4	11.02 ± 0.2	10.11 ± 0.2	10.71 ± 0.5	1.16 ± 0.1	1.27 ± 0.0	1.50 ± 0.0	1.24 ± 0.03	1.76 ± 0.01	1.31 ± 0.01	1.85 ± 0.07	1.60 ± 0.03
used (mol)	CO ₂ :CO	-	-	-	-	-	-	-	-	-	0.13 ± 0.04	-	-
	H ₂ :C _{total}	0.33 ± 0.04	0.40 ± 0.01	0.75 ± 0.03	0.58 ± 0.04	0.49 ± 0.01	0.77 ± 0.01	0.91 ± 0.03	0.97 ± 0.01	0.96 ± 0.02	0.95 ± 0.04	0.50 ± 0.02	0.78 ± 0.08
	H ₂ :CO	0.33 ± 0.04	0.40 ± 0.01	0.75 ± 0.03	0.58 ± 0.04	0.49 ± 0.01	0.77 ± 0.01	0.00 ± 0.03	0.97 ± 0.01	0.96 ± 0.02	1.07 ± 0.03	0.50 ± 0.02	0.78 ± 0.08
	H ₂ :CO ₂	-	-	-	-	-	-	-	-	-	9.41 ± 2.74	-	-
fixed (mol)	CO ₂ :CO	-	-	-	-	-	-	-	-	-	8.79 ± 2.62	-	-
	H ₂ :C _{total}	0.57 ± 0.06	0.60 ± 0.02	0.90 ± 0.02	0.72 ± 0.02	0.57 ± 0.01	0.81 ± 0.02	1.10 ± 0.05	0.99 ± 0.01	1.00 ± 0.02	0.95 ± 0.04	0.64 ± 0.02	0.88 ± 0.02
	H ₂ :CO	0.57 ± 0.06	0.60 ± 0.02	0.90 ± 0.02	0.72 ± 0.02	0.57 ± 0.01	0.81 ± 0.02	1.10 ± 0.05	0.99 ± 0.01	1.00 ± 0.02	1.07 ± 0.03	0.64 ± 0.02	0.88 ± 0.03
	H ₂ :CO ₂	-	-	-	-	-	-	-	-	-	9.41 ± 2.74	-	-

4.4.2 Overall comparison between experimental and maximum theoretical yields

Based on the WLP stoichiometry, the maximum amount of acetate that could be produced from both the substrate fed (H_2 , CO_2 and CO) and substrate used is presented in Table 4.14 for the for the fermentations evaluating the medium components and process parameters influence, and in Table 4.15 for the ones evaluating the impact of syngas impurities and composition. The results are given both with, and without taking into account the ethanol produced.

Overall, the average percentage of theoretical acetate actually measured, considering the ethanol produced, for all fermentations is $110 \pm 9 \%$; $107 \pm 9 \%$ for those described in Table 4.14, and $114 \pm 8 \%$ for those in Table 4.15. The percentage of acetate produced from the theoretical maximum calculated from the amount of substrate fed varies greatly, with the highest value overall being 80 % (setup 5, Table 4.15) and the lowest, 23 % (setup 2, Table 4.14).

Table 4.14 – Amount of acetate and ethanol produced, compared to the theoretical maximum, for the fermentations evaluating the medium components and process parameters influence. The theoretical maximum was calculated according to both the carbon and H₂ used, and C and H₂ fed, as well with, and without taking into account the ethanol produced. The results for these fermentations are presented in section 4.1.

	Setup 1	Setup 2	Setup 3a	Setup 3b	Setup 4	Setup 5	setup 6
	Standard	no pH regulation	1 g/L cysteine (2x standard); pH 5.9	1 g/L cysteine (2x standard); pH 5.40 after 68 h; pH 4.78 after 92.4 h	1 g/L yeast (2x standard)	24 h at pH 5.9, then let drop and hold at 4.78	24 h gas flow 18 mL/min, pH 5.9 - then gas flow 12.6 mL/min; let pH drop and hold at 4.78
Acetate produced (mmol)	477	154	391	466	498	271	230
Ethanol produced (mmol)	66	14	49	64	45	36	69
Acetate theoretical, from substrate used (mmol)	532	152	446	507	527	298	276
Theoretical maximum acetate from substrate used, considering ethanol produced (mmol)	433	130	372	411	459	244	172
% of theoretical maximum acetate measured, from substrate used	90	101	88	92	94	91	83
% of theoretical maximum acetate measured, from substrate used, considering ethanol produced	110	118	105	113	108	111	134
Theoretical maximum acetate from substrate fed (mmol)	684	681	678	703	672	674	526
% of theoretical acetate from substrate fed	70	23	58	66	74	40	44

Table 4.15 – Amount of acetate and ethanol produced, compared to the theoretical maximum for the fermentations evaluating the impact of syngas composition and impurities. The theoretical maximum was calculated according to both the substrate used, and the substrate fed, as well with, and without taking into account the ethanol produced. The results for these fermentations are presented in sections 4.2 and 4.3.

	Setup 1	Setup 2	Setup 3	Setup 4		Setup 5		Setup 6	Setup 7	Setup 8	Setup 9	Setup 10
	real Bioliq® from straw	synthetic free Bioliq®	real Bioliq syngas from straw	synthetic impurity-free Bioliq	TNO beech wood	synthetic impurity-free TNO-beechwood-like	TNO lignin	synthetic impurity-free TNO-lignin-like	synthetic impurity-free LNEG	synthetic impurity-free ENEA	Custom mix A	Custom mix B
Acetate produced (mmol)	241	418	288	283	380	449	371	469	458	450	407	391
Ethanol produced (mmol)	107	80	85	18	44	27	71	57	62	49	34	58
Acetate theoretical, from substrate used (mmol)	390	501	383	279	369	466	501	511	562	485	444	457
Theoretical maximum acetate from substrate used, considering ethanol produced (mmol)	230	380	256	252	304	425	395	425	468	428	393	371
% of theoretical maximum acetate measured, from substrate used	62	84	75	101	103	96	74	92	82	93	92	86
% of theoretical maximum acetate measured, from substrate used, considering ethanol produced	105	110	112	112	125	106	94	110	98	105	103	105
Theoretical maximum acetate from substrate fed (mmol)	561	574	386	388	552	565	689	670	790	621	609	620
% of theoretical acetate from substrate fed	43	73	75	73	69	80	54	70	58	72	67	63

4.5 Impact of elevated pressure

4.5.1 Effect of syngas overpressure

All values are given as average (arithmetic mean) \pm STD of the triplicate ($n = 3$). All pressures stated are in bar, and are given as absolute pressures, with zero being a perfect vacuum. Absolute pressure is equal to gauge pressure plus atmospheric pressure.

The pressure was stable for all conditions throughout the experiment, and no refills were deemed necessary due to the excess headspace compared to the culture volume. The pressure profile during the experiment is shown in Figure 4.20.

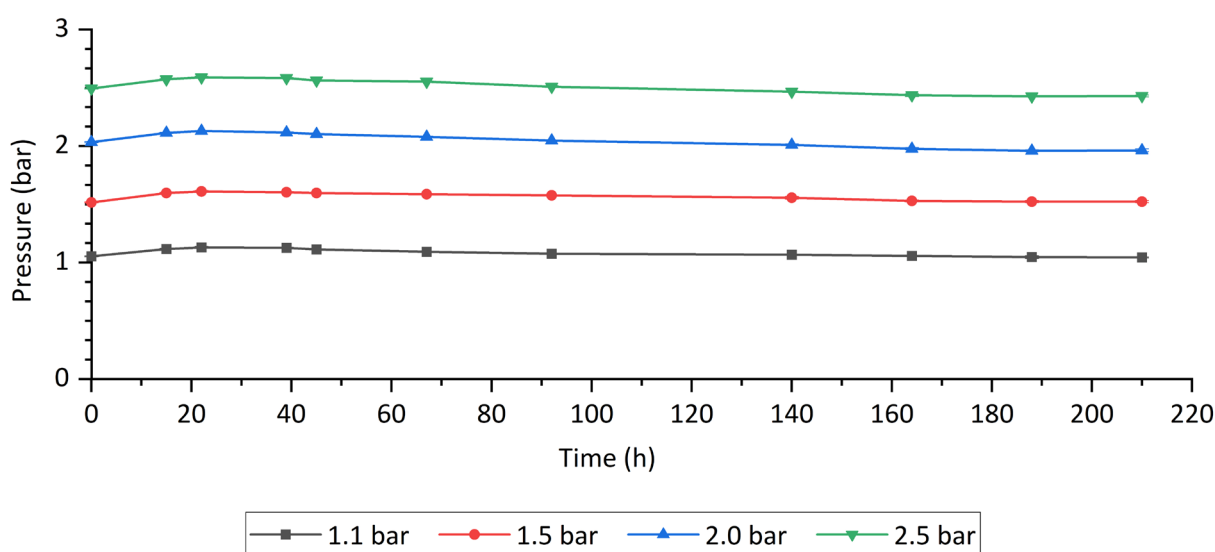


Figure 4.20 – Pressure profile for each setup throughout the experiment. Pressures are given as absolute values, referenced to zero being perfect vacuum. Values are shown as the average of the triplicate, with standard deviations (standard deviations are too small for the scale and remain thus hidden). The cultures were grown at 1.1 bar (grey squares), 1.5 bar (red circles), 2.0 bar (blue triangle) and 2.5 bar (green inverted triangle). Actual measured values at each sampling point are marked with symbols; lines are only depicted for visual purposes and do not necessarily show the actual trend.

The effect of the headspace pressure can be clearly seen in the growth profile of the different bottles (Figure 4.21A). Table 4.16 shows growth rates for each treatment at three selected intervals. The pressure-treated cultures all present a remarkably similar growth profile, with the control bottle being remarkably different. On the control culture, at atmospheric pressure, cells started growing immediately after inoculation, and its growth rate was significantly higher than any of the pressure treatments for the first 67 h. All pressure-treated cultures presented an initial lag-phase, and growth was only detected after 45 h. Even so, after that time, the specific growth rate, μ , was in all cases higher than that of the control. Between 45 h and 92 h, the growth rate of both the 1.5 bar and 2 bar treated cultures were much higher than the control, with $0.024 \pm 0.007 \text{ h}^{-1}$, and $0.026 \pm 0.005 \text{ h}^{-1}$,

respectively, compared to $0.015 \pm 0.007 \text{ h}^{-1}$ for the control. During that interval, the highest growth rate, $0.035 \pm 0.002 \text{ h}^{-1}$, was achieved at the highest pressure. After 92 h, when the CDW (cell dry weight) of the control culture reached a value of $0.57 \pm 0.05 \text{ g/L}$, growth greatly slowed down and eventually stopped, with no growth detected after 140 h. This was not the case for the pressure-treated cultures, which continued growing and achieved higher cell concentration values. Between 45 h and 140 h growth rate increased with increasing pressure, with the highest being $0.023 \pm 0.001 \text{ h}^{-1}$ in the 2.5 bar cultures. The maximum measured CDW for the control culture was $0.66 \pm 0.11 \text{ g/L}$, while for the 1.5 bar and the 2 bar pressure treatments was very similar, $0.88 \pm 0.12 \text{ g/L}$ and $0.89 \pm 0.09 \text{ g/L}$, respectively, all of them at 164 h. For the 2.5 bar treatment, the maximum CDW measured was $0.97 \pm 0.05 \text{ g/L}$ at 140 h. This was also the highest value recorded of all. In the control, the cell concentration remained stable after growth stopped, but in the pressure treated cultures the CDW dropped sharply after reaching their maximum CDW, dropping to values close to that of the control culture at the end of the experiment.

The pH profile, shown in Figure 4.21B, follows the same pattern as the observed for growth. The control culture pH dropped faster during the first 45 h, moment after which the pressure treatments presented a sharper descend. The lowest final pH, 4.41 ± 0.02 , was achieved by the cultures subjected to the highest pressures, 2 and 2.5 bar, followed by the 1.5 bar culture, with a pH of 4.50 ± 0.08 , and lastly, the control, with 4.63 ± 0.09 .

Table 4.16 – Specific growth rate μ for each syngas pressure treatment and control. The average of the triplicate is given with standard deviations. Pressures are given as absolute values, referenced to zero being perfect vacuum

Time (h)	$\mu \text{ (h}^{-1}\text{)}$			
	1.1 bar	1.5 bar	2 bar	2.5 bar
0 - 67	0.020 ± 0.004	0.012 ± 0.003	0.015 ± 0.000	0.014 ± 0.001
45 - 92	0.015 ± 0.007	0.024 ± 0.007	0.026 ± 0.005	0.035 ± 0.002
45 - 140	0.009 ± 0.004	0.018 ± 0.005	0.018 ± 0.003	0.023 ± 0.001

Regarding product formation, the acetate concentration, shown in Figure 4.21C, did not increase significantly until 45 h in any case. Up to 92 h, the acetate production for all cultures was very similar, with all pressure treated cultures reaching values close to 5 g/L (4.70 ± 0.64 g/L, 5.16 ± 0.21 g/L and 4.93 ± 0.53 g/L for the 1.5 bar, 2.0 bar and 2.5 bar, respectively), and the control reaching the highest value, 5.63 ± 2.04 g/L, albeit with a much higher difference among each single replicate. After this point, the pressure treated bottles achieved, in average, a higher acetate concentration than the control. It must be noted, though, that the standard deviation of the control and the 1.5 bar treatment overlap, and there was a big dispersion in the individual acetate production of each of the replicates. Despite this, a tendency can be observed: the cultures subjected to higher pressure produced more acetate, achieving final values of 12.16 ± 1.60 g/L, 13.09 ± 0.27 g/L and 12.10 ± 1.23 g/L for the 1.5 bar, 2.0 bar and 2.5 bar treatments, respectively, compared to 11.14 ± 1.72 g/L for the control.

All pressure-treated cultures behaved similarly regarding ethanol formation, and produced significantly lower ethanol than the control culture, as seen in Figure 4.21D. The individual replicas of the control cultures, similarly to what was seen with acetate, had the bigger differences observed amongst the difference treatment. A noticeably big variation was seen on the measured ethanol concentration, especially after 140 h. At the end point, the average ethanol concentration for the control was 2.59 ± 0.72 g/L, with individual values of the replicas ranging from 1.77 g/L to 3.11 g/L. For the pressure treated cultures, the end values were 1.13 ± 0.25 g/L, 0.86 ± 0.12 g/L, and 0.87 ± 0.06 g/L for the 1.5, 2.0 and 2.5 bar pressures.

When looking at the specific acetate production rate (Figure 4.21E), the most significant difference happened at 45 h, when the pressure-treated cultures still had a CDW below 0.2 g/L, but the acetate concentration achieved was similar to that of the control, which had a much higher CDW at that point. The specific acetate production rate for the control at that time point was 0.35 ± 0.08 $\text{g}_{\text{acetate}}/\text{g}_{\text{CDW}}\cdot\text{h}$, while the cultures grown under pressure all had similar, higher values: 0.88 ± 0.26 $\text{g}_{\text{acetate}}/\text{g}_{\text{CDW}}\cdot\text{h}$, 0.83 ± 0.02 $\text{g}_{\text{acetate}}/\text{g}_{\text{CDW}}\cdot\text{h}$ and 0.92 ± 0.11 $\text{g}_{\text{acetate}}/\text{g}_{\text{CDW}}\cdot\text{h}$ for the 1.5, 2.0 and 2.5 bar pressure treatments, respectively. No other significant difference in the specific acetate production among the various pressures could be observed throughout the experiment. As for the specific ethanol production rate (Figure 4.21F), the profile is similar to that of acetate, with the highest value at 45 h. In this case, though, no correlation between each of the pressures and the observed specific ethanol production rate could be drawn. As it can be seen in Figure 4.21F, the standard deviations at that time point overlap one another. Afterwards, the specific ethanol production rate decreases for the 2 bar and 2.5 bar cultures and does not significantly change any more. For the control culture, an increment in the specific ethanol production rate can be seen both at 92 h and 188 h, with 0.06 ± 0.04 g/g·h and 0.04 ± 0.05 g/g·h. As well, an increase at 210 h in the 1.5 bar treated culture can be seen, reaching a

value of 0.03 ± 0.06 g/g·h. At the 140 h and 164 h time points, the specific ethanol production rate stayed below 0.02 g/g·h in all cases.

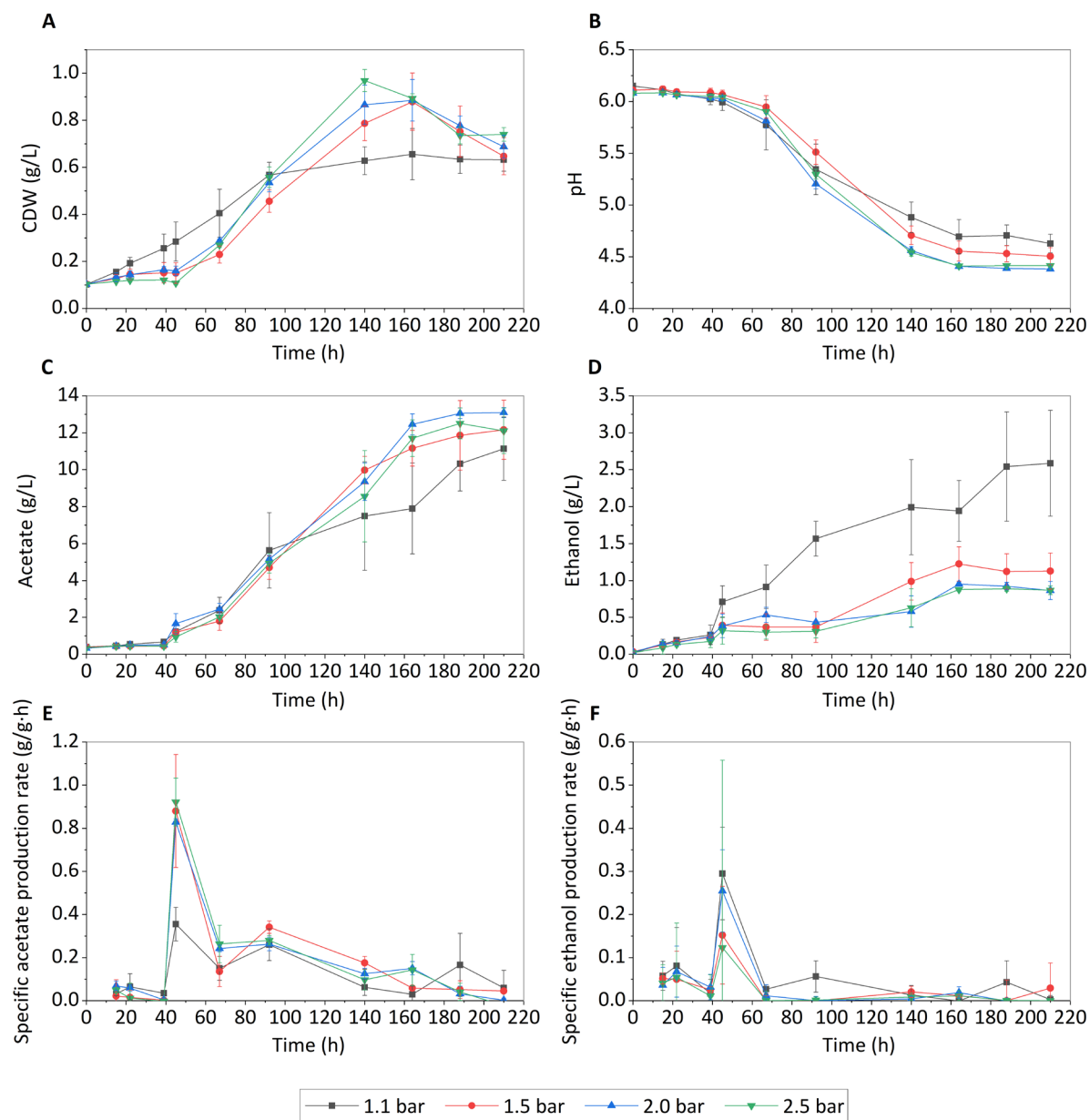


Figure 4.21 – Growth and product formation profiles at different syngas pressures. Cell dry weight, CDW (A), pH (B), acetate (C), ethanol (D), specific acetate production rate (E) and specific ethanol production rate (F) are shown as the average of the triplicate, with standard deviations. The cultures were grown at 1.1 bar (grey squares), 1.5 bar (red circles), 2.0 bar (blue triangle) and 2.5 bar (green inverted triangle). Actual measured values at each sampling point are marked with symbols; lines are only depicted for visual purposes and do not necessarily show the actual trend.

4.5.2 Effect of CO₂/H₂ and CO overpressure

4.5.2.1 Growth and product formation

All values are given as average (arithmetic mean) \pm STD of the quadruplicate (n = 4). All pressures stated are in bar and are given as absolute pressures.

4.5.2.1.1 CO₂/H₂

The pressure was monitored during the experiment, and an addition of gas was performed to keep the pressure from lowering too much at 53 h and 101 h. The pressure profile is shown in Figure 4.22.

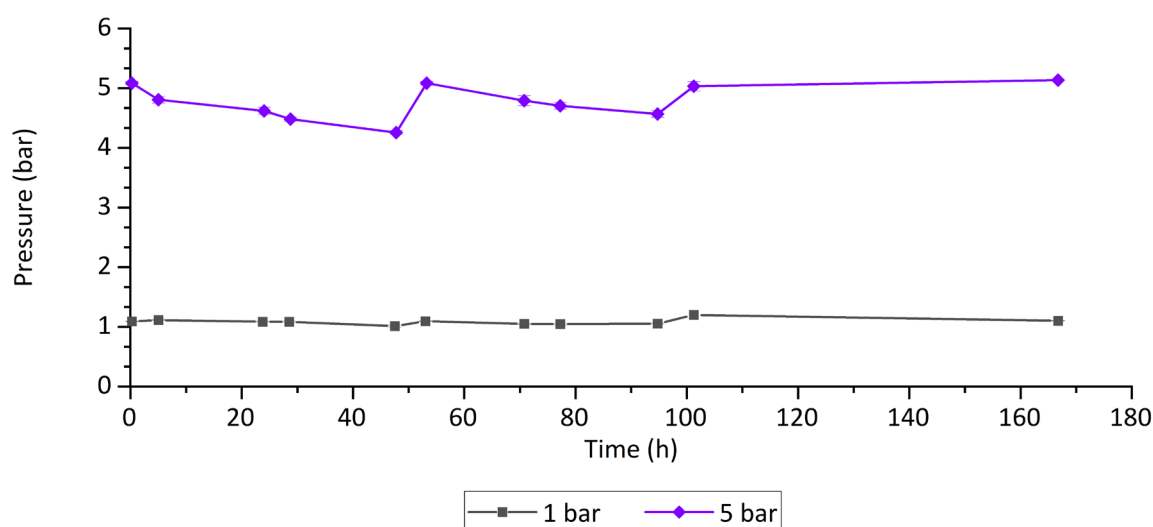


Figure 4.22 – Pressure profile for each setup grown with CO₂/H₂ throughout the experiment. Pressures are given as absolute values, referenced to zero being perfect vacuum. Values are shown as the average of the triplicate, with standard deviations (standard deviations are too small for the scale and remain thus hidden). The cultures were grown at 1.1 bar (grey squares) and 5 bar (purple diamonds). The increase in pressure seen at 53 h and 101 h corresponds to the addition of gas to the headspace to prevent the pressure from dropping too much. Actual measured values at each sampling point are marked with symbols; lines are only depicted for visual purposes and do not necessarily show the actual trend.

The growth profile of the cultures when grown on CO₂/H₂ can be seen in Figure 4.23A. Both the control and the pressure treated culture showed an initial increase in the CDW, from 0.17 g/L, measured directly after inoculation, to 0.22 g/L after 5 h. The control culture CDW remained stable for 77 h, with values between 0.24 ± 0.01 g/L and 0.22 ± 0.01 g/L. At 95 h it had increased to 0.25 ± 0.02 g/L, and its final value was 0.43 ± 0.02 g/L. Following the initial increase in biomass, the CDW of the 5 bar treated culture continuously decreased to a value of 0.15 ± 0.01 g/L at 71 h, remaining constant up to 100 h. The last measured value, at 167 h, presented a slight increase to 0.17 ± 0.01 g/L. The specific growth rate, μ , for the control culture between 5 h and 100 h can be considered zero, $(7.5 \pm 8.6) \times 10^{-4} \text{ h}^{-1}$,

while for the interval between 100 h and 167 h it was $0.009 \pm 0.001 \text{ h}^{-1}$. On the 5 bar culture a negative μ between 5 h and 101 h, $-0.004 \pm 0.001 \text{ h}^{-1}$ reflects the decrease in the biomass. Between 101 h and 167 h, μ was $0.002 \pm 0.002 \text{ h}^{-1}$. despite the biomass not increasing, a lowering in the pH could be seen in both the control and the pressure-treated culture (Figure 4.23B). It was greater in the control, where the pH decreased steadily to 5.16 ± 0.05 at 100 h. Between 100 h and 167 h the pH drop was sharper, reaching 4.46 ± 0.03 as final value. The pH in the culture grown at 5 bar fell to 5.49 ± 0.07 at 53 h. Afterwards, its decrease was slower, reaching a final value of 5.32 ± 0.07 at 167 h.

Acetate production started directly after inoculation, both in the control and the pressure-treated culture (Figure 4.23C). Up to 29 h, an equivalent acetate concentration was reached by both cultures: $1.32 \pm 0.12 \text{ g/L}$ and $1.36 \pm 0.35 \text{ g/L}$ in the control and in the 5 bar culture, respectively. At 95 h, the acetate concentration in the control had increased to $3.26 \pm 0.12 \text{ g/L}$. After that point, an increase in the acetate production ratio was seen, with the final acetate value reaching $9.19 \pm 0.62 \text{ g/L}$. The acetate concentration in the pressure-treated culture remained always lower, with $2.46 \pm 0.41 \text{ g/L}$ at 95 h, and a final value of $3.54 \pm 0.45 \text{ g/L}$.

Concerning ethanol, only very low concentrations could be detected in both cultures (Figure 4.23D). 5 h after inoculation an increase in ethanol was seen, but after 24 h it had already decreased to $0.09 \pm 0.05 \text{ g/L}$ in the control and $0.06 \pm 0.01 \text{ g/L}$ in the pressure-treated culture. After 101 h, the ethanol concentration in the control culture had increased to $0.15 \pm 0.05 \text{ g/L}$, but not so in the culture subjected to pressure, where it decreased to $0.04 \pm 0.01 \text{ g/L}$. It remained at this value until the endpoint in the pressure culture, but in the control culture it decreased to $0.12 \pm 0.02 \text{ g/L}$. The difference between the replicas was higher in the control, while the individual replicas of the pressure-treated culture behaved much more similarly. Due to the low amount of ethanol produced, the calculation of the specific production ratio did not generate meaningful results.

For the first 29 h, both cultures had a similar profile terms of specific acetate production rate, as shown in Figure 4.23E. At 48 h and 71 h, the control had a higher specific acetate production rate, $0.17 \pm 0.08 \text{ g/g}\cdot\text{h}$ and $0.10 \pm 0.08 \text{ g/g}\cdot\text{h}$, respectively, compared to the culture grown at 5 bar, which had values of $0.10 \pm 0.05 \text{ g/g}\cdot\text{h}$ and $0.03 \pm 0.11 \text{ g/g}\cdot\text{h}$, respectively, at those same times. At 77 h the 5 bar-grown culture reached a higher specific acetate production rate ($0.72 \pm 0.27 \text{ g/g}\cdot\text{h}$) than the control ($5.42 \pm 0.25 \text{ g/g}\cdot\text{h}$), but it can be seen that the difference among the triplicate increased, as implied by the higher standard deviation in both cases. After this point, both rates decreased, but towards the end, the control culture achieved higher values than the pressure-treated culture. Even so, the specific acetate production rate in the pressure-treated culture showed a tendency to increase, while the contrary was true for the control.

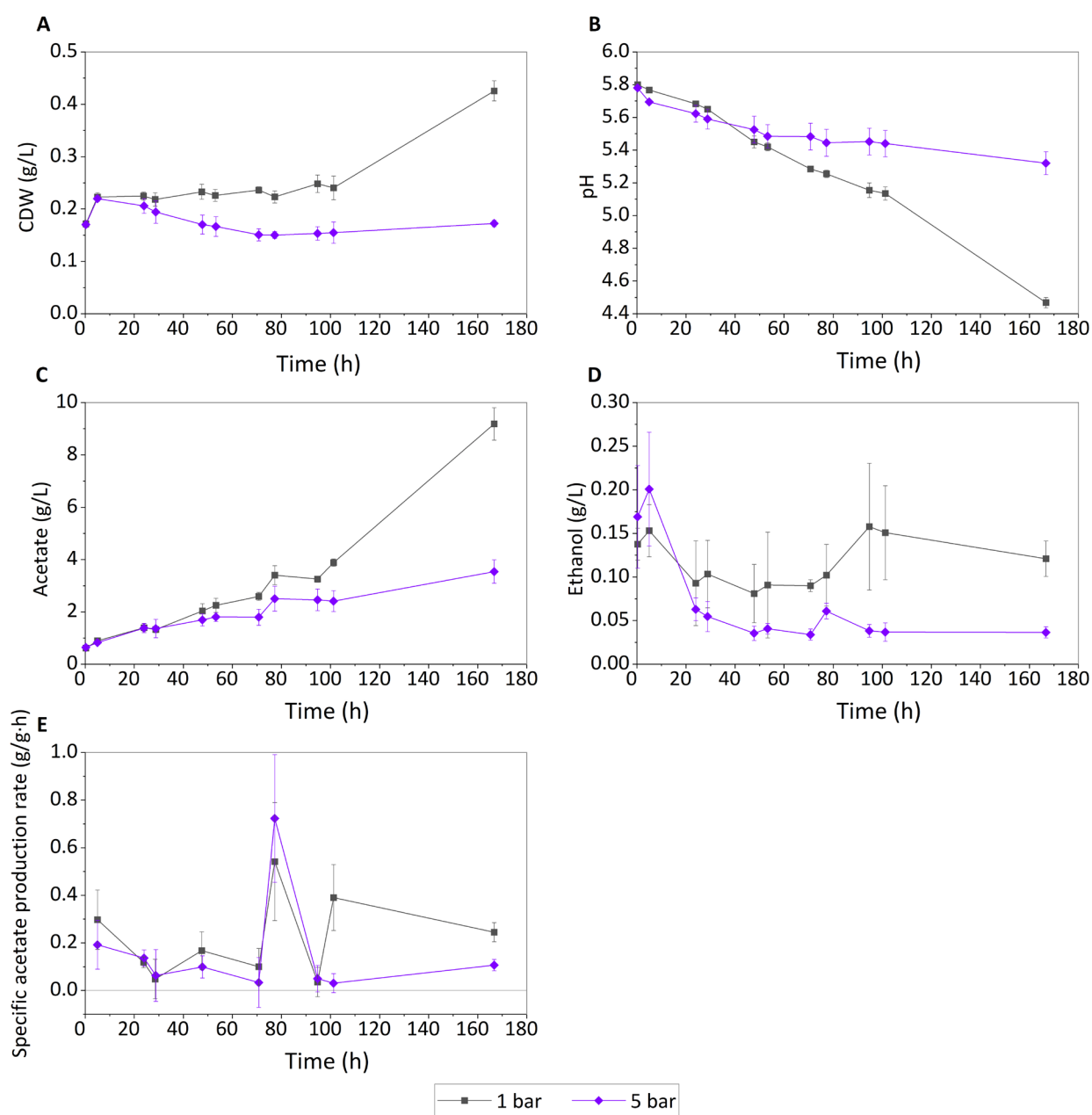


Figure 4.23 –Growth and product formation profiles at different CO₂/H₂ pressures. Cell dry weight, CDW (A), pH (B), acetate (C), ethanol (D) and specific acetate production rate (E) are shown as the average of the quadruplicate, with standard deviations. The cultures were grown at 1 bar (grey squares), and 5 bar (purple diamonds). Actual measured values at each sampling point are marked with symbols; lines are only depicted for visual purposes and do not necessarily show the actual trend.

4.5.2.1.2 CO

Pressure profiles of both setups can be seen in Figure 4.24. The pressure of the culture at 1 bar remained constant during the experiment. The pressure decrease in the 5 bar culture is due to sample withdrawal, which had a bigger impact due to the smaller size of the vessel. At 77 h a top-up of the gas in the headspace was performed to prevent an excessive pressure loss.

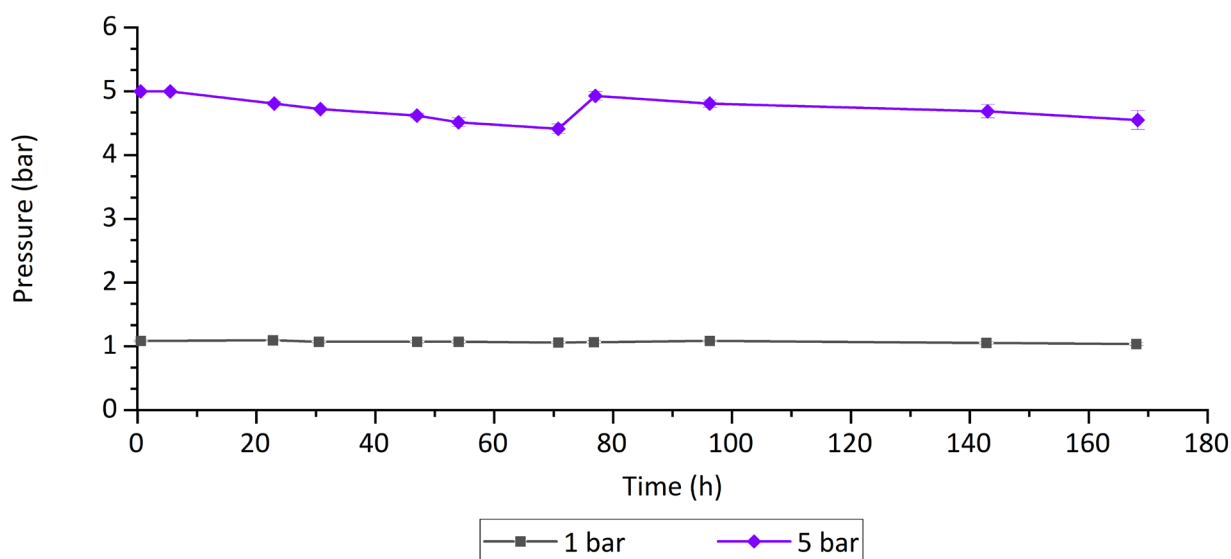


Figure 4.24 – Pressure profile for each setup grown with CO₂/H₂ throughout the experiment. Pressures are given as absolute values, referenced to zero being perfect vacuum. Values are shown as the average of the triplicate, with standard deviations (standard deviations are too small for the scale and remain thus hidden). The cultures were grown at 1.1 bar (grey squares) and 5 bar (purple diamonds). The increase in pressure seen at 53 h and 101 h corresponds to the addition of gas to the headspace to prevent the pressure from dropping too much. Actual measured values at each sampling point are marked with symbols; lines are only depicted for visual purposes and do not necessarily show the actual trend.

The growth profile of both the control and the pressure-treated culture is shown in Figure 4.25A. It can be seen that, in both cases, there was an initial increase in the CDW. The control culture rose from 0.14 ± 0.01 g/L to 0.24 ± 0.01 g/L at 23 h, and the culture grown at 5 bar, from 0.18 ± 0.02 g/L to 0.21 ± 0.02 g/L. After that, the biomass concentration in both cultures decreased following a similar profile, to increase again later. The lowest CDW measured for the control culture was 0.15 ± 0.00 g/L at 71 h, moment after which some growth was detected again, increasing to 0.19 ± 0.01 g/L at the endpoint. The pressure-treated culture reached its minimum at 54 h, earlier than the control, with 0.11 ± 0.01 g/L, and increased to a final value of 0.17 ± 0.01 g/L.

Only a minor decrease could be seen on the pH during the fermentation, especially on the control culture, as can be seen in Figure 4.25B. In that culture, from the starting value of 5.85 ± 0.01 , it

dropped to 5.67 ± 0.03 at the end of the cultivation. The pressure-treated culture started at 5.79 ± 0.02 g/L, decreasing to an end-point value of 5.55 ± 0.05 .

Acetate was produced throughout the cultivation even if at a very low rate (Figure 4.25C). Both cultures performed very similarly, with acetate increasing after 23 h to 1.06 ± 0.13 g/L in the control, and 1.28 ± 0.15 g/L in the culture grown at 5 bar. The final concentration achieved for both cultures was equivalent, being 2.15 ± 0.37 g/L in the control and 2.17 ± 0.58 g/L in the pressure-treated culture.

No significant ethanol production was observed for none of the pressure treatment (Figure 4.25D).

The average specific acetate production rate for the whole run was 0.089 ± 0.05 g/g·h for the control, and slightly lower, 0.079 ± 0.05 g/g·h, for the pressure culture. The specific acetate production rate calculated between successive samples is depicted in Figure 4.25E. As happened with CO₂/H₂, the small amount of ethanol that was produced meant that the calculation of the specific production ratio did not generate significative results.

4.5.2.2 Formic acid

Formic acid was measured for both CO and CO₂/H₂ samples, for the controls and the pressure-treated cultures, throughout the experiment, but it could not be detected in the samples. The results of the enzymatic assay were all below the detection level.

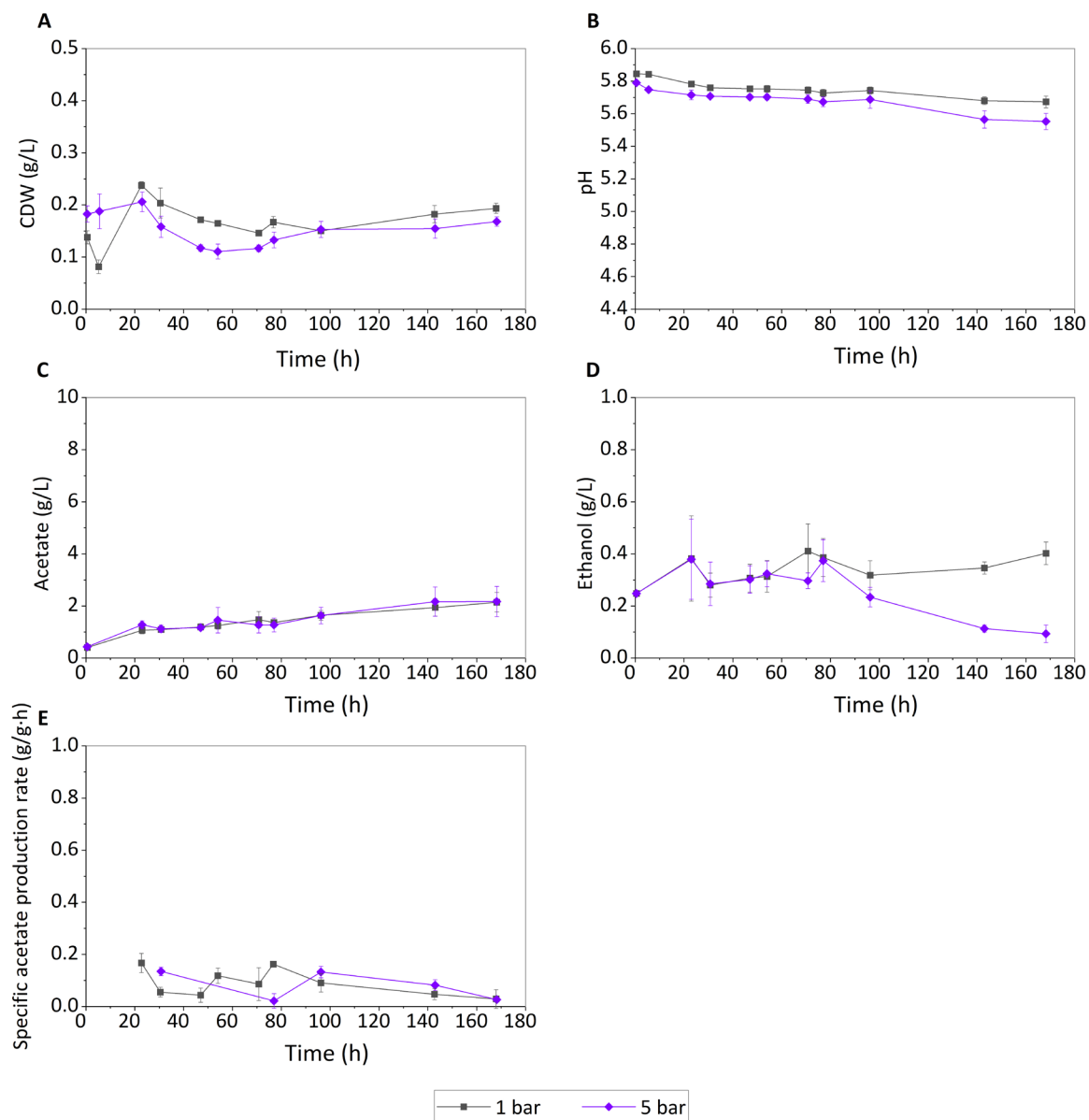


Figure 4.25 – Growth and product formation profiles at different CO pressures. Cell dry weight, CDW (A), pH (B), acetate (C), ethanol (D) and specific acetate production rate (E) are shown as the average of the quadruplicate, with standard deviations. The cultures were grown at 1 bar (grey squares), and 5 bar (purple diamonds). Actual measured values at each sampling point are marked with symbols; lines are only depicted for visual purposes and do not necessarily show an actual trend.

4.5.2.3 Effect of CO₂/H₂ on gene expression

The gene expression study was only carried out on the CO₂/H₂ cultures due to the lack of growth and the identical profile obtained for both CO pressures.

The fold change of all studied genes laid between 0.5 and 2 (Figure 4.26), meaning that no significant difference in gene expression could be detected due to the high pressure treatment. The biggest fold change observed was *cooC2* at 47 h, with a fold change of 2.0. The smallest was for *aor*, with a fold change of 0.5. For *aor*, the smallest and the biggest fold change among all the time points was 0.5 and 1.6. For *cooC2*, this was between 2.0 and 0.8, for *fdh*, 0.6 and 1.5, and for *pta*, 1.2 and 0.6. The most stable gene was, thus, *pta*, and the least, *cooC2*.

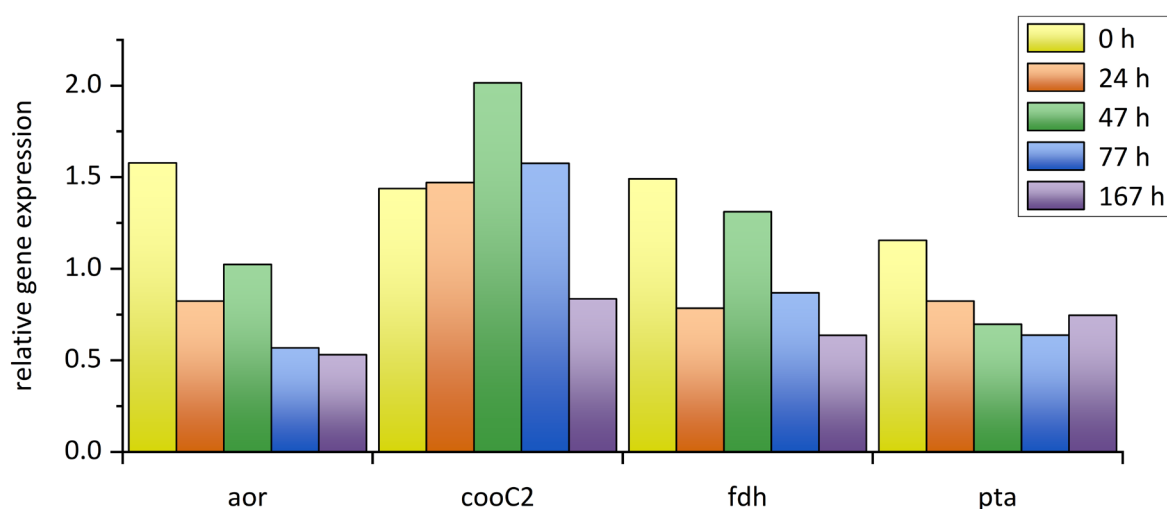


Figure 4.26 – Relative gene expression (fold change) in the pressure-treated culture at 5 bar. *aor*, aldehyde ferredoxin oxidoreductase; *cooC2*, CODH nickel-insertion accessory protein; *fdh*, formate dehydrogenase subunit alpha; *pta*, phosphotransacetylase.

4.6 Sequential cultivation for acetogenic fermentation from oxygen-containing waste gas

4.6.1 Anaerobic growth of *C. ljungdahlii* following *P. thermoglucosidasius* cultivation

In the first phase of the sequential fermentation *P. thermoglucosidasius* was grown in 50 ml modified Luria Bertani (mLB) medium with an initial gas atmosphere of CO and air (50:50) (Figure 4.27). After 70 h, when all O₂ was consumed, the culture reached an absorbance (OD₆₀₀) of 0.732 ± 0.027 and pH of 6.21 ± 0.04 (Figure 4.27). Previously we have observed that when the O₂ is consumed, the growth of *P. thermoglucosidasius* also plateaus (Mohr et al., 2018a, 2018b). To ensure that the increase of OD₆₀₀ and acetate during the second phase is not due to *P. thermoglucosidasius* on its own, a control experiment without the addition of *C. ljungdahlii* was conducted (Additional File 1). When *C. ljungdahlii* was added to the *P. thermoglucosidasius* culture 70 h after the first phase, the *P. thermoglucosidasius*/*C. ljungdahlii* sequential culture reached a maximum absorbance of 1.316 ± 0.157 approximately 23 h after the latter culture was added (Figure 4.27). This indicates that the strict anaerobe *C. ljungdahlii* is able to grow in the medium after *P. thermoglucosidasius* exhausts the O₂ from the gas atmosphere. The medium pH dropped drastically once *C. ljungdahlii* was added, from a pH of 6.20 ± 0.04 pre-addition to a pH of 5.61 ± 0.05 post-addition of the latter strain (Figure 4.27). However, the pH continued to decline throughout the experiment, which can be correlated to active metabolism and acetate production by *C. ljungdahlii*. (Mohr et al., 2019)

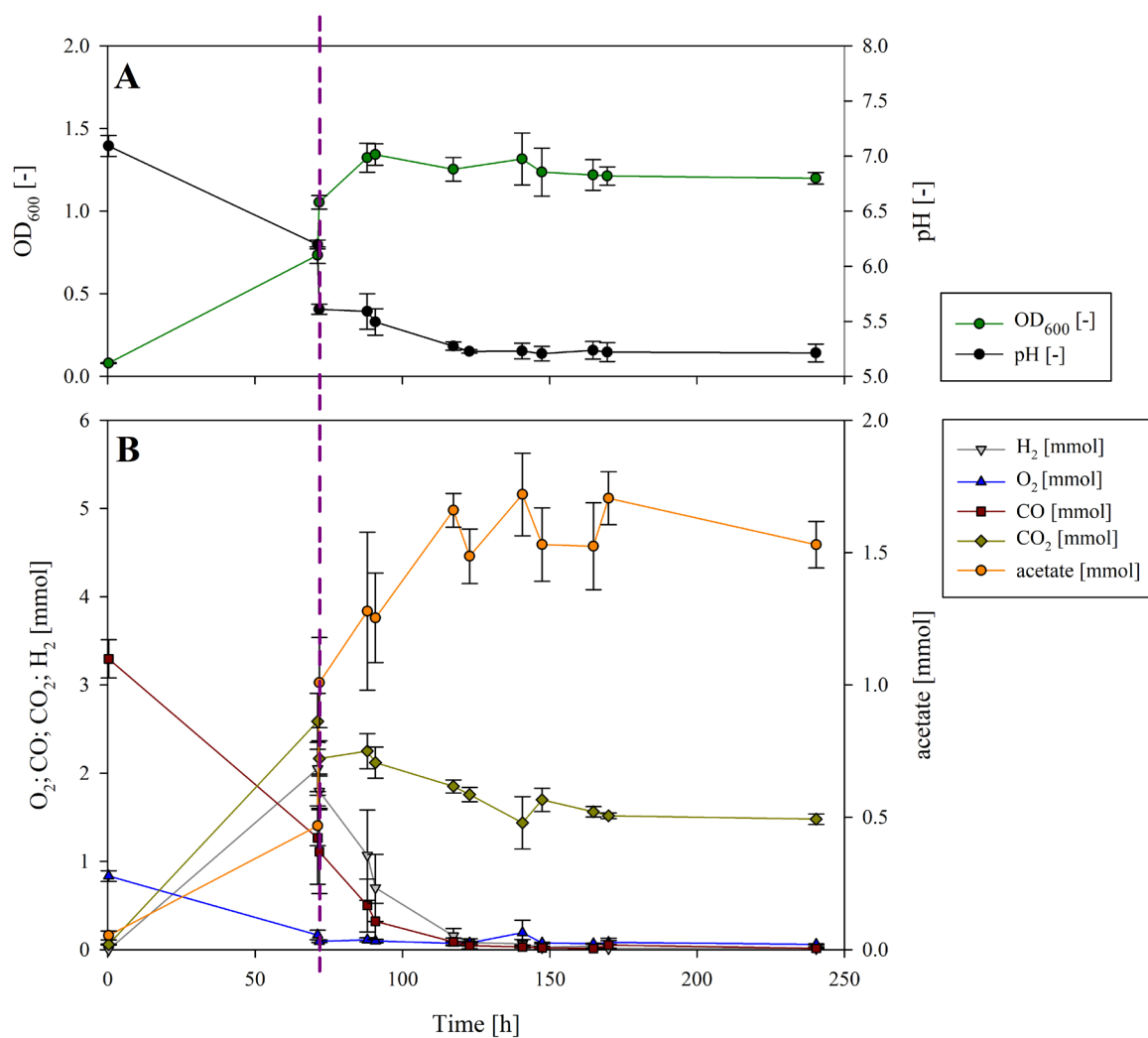


Figure 4.27 – Growth and pH (A) and gas composition and acetate production (B) of the sequential cultivation of *P. thermoglucosidasius* and *C. ljungdahlii*. The dotted line presents the inoculation of *C. ljungdahlii*. (A) The measured OD₆₀₀ (dark green) increased after 70 h, and at the same time the pH (black) decreased due to the inoculation with *C. ljungdahlii*. Growth continued until 93 h (23 h after inoculation with the second organism), and then it plateaued. As a result of the metabolic activity, the culture broth was acidified to a pH of 5.2. (B) O₂ (blue) had already been consumed before the second phase, but some CO (dark red) was still left. After inoculation with *C. ljungdahlii*, CO₂ (olive) and H₂ (grey) did not accumulate any further, since they were used as building blocks by *C. ljungdahlii* to produce acetate (orange). (Mohr et al., 2019)

4.6.2 *C. ljungdahlii* acetate production

In the post-aerobic phase *P. thermoglucosidasius* consumed 2.050 ± 0.117 mmol of CO, while 2.055 ± 0.023 and 2.646 ± 0.147 mmol of H₂ and CO₂ were produced via the water-gas shift reaction (WGS), respectively. Here, an equimolar conversion of CO to H₂ was achieved. Subsequently, both H₂ and CO decreased rapidly, being exhausted ~83 h after *C. ljungdahlii* was added. Similarly, CO₂ decreased, although 1.479 ± 0.058 mmol CO₂ were left at the end of the cultivation (after 240 h), due to the fact that 2 moles of H₂ are needed per mol of CO₂ as per the stoichiometry of the W-L pathway: $2 \text{ CO}_2 + 4 \text{ H}_2 \rightarrow \text{CH}_3\text{COOH} + 2 \text{ H}_2\text{O}$ (Ragsdale, 2008). (Mohr et al., 2019)

The decrease in the amount of these three gasses correlated with an increase in the amount of acetate. Some acetate (0.47 ± 0.07 mmol) was already observed during the first phase. This may be linked to mixed acid fermentation by *P. thermoglucosidasius* (Hussein et al., 2015). However, when *P. thermoglucosidasius* was cultivated on its own, no further increase in acetate was observed. The addition of *C. ljungdahlii* resulted in a spike in acetate (1.01 ± 0.17 mmol – an increase of 0.54 ± 0.22 mmol). This is associated with acetate production by *C. ljungdahlii* in the pre-culture in GA medium containing fructose as carbon source (Tirado-Acevedo et al., 2011). To shorten the time of inoculation of *C. ljungdahlii*, a washing step was not performed to avoid any potential lag phase due to stressing of the cells. Nevertheless, the amount of acetate increased concomitantly with H₂, CO and CO₂ consumption during the second phase, reaching a final amount of 1.53 ± 0.09 mmol of acetate. The acetate produced exclusively by *C. ljungdahlii* was, therefore, 0.52 mmol. This suggests that in the absence of additional exogenous carbon sources *C. ljungdahlii* could successfully use the H₂ and CO₂ produced by *P. thermoglucosidasius* as building blocks for acetate via the W-L pathway. (Mohr et al., 2019)

From the WLP, the theoretical maximum yield is 0.25 mol acetate/mol CO (Bengelsdorf et al., 2013). Considering the initial amount of CO in the bottles, 3.3 ± 0.216 mmol in average, a total theoretical maximum of 0.8 mmol of acetate could have been produced. The yield of acetate in the *C. ljungdahlii* phase in this study was 0.16 mol acetate/mol CO, achieving a 63 % of the theoretical maximum. (Mohr et al., 2019)

5 DISCUSSION

5.1 Impact of medium components and process parameters

The influence of the two selected medium components (yeast extract and cysteine), the different pH profiles and gas flow were successfully tracked with the fermentation system used. The effect on product formation, growth and gas consumption are discussed in this section.

5.1.1 Effect of medium components

From the results of the experiments with higher cysteine and yeast extract, it is clear that in our particular setup, none of these approaches caused any advantage, in terms of an improved gas consumption or product formation. Richter et al. (2016) reported that *C. ljungdahlii* seems unable to uptake sulfate, and recommended adding sulfide or cysteine to the medium. Since doubling the amount of cysteine did not improve the outcome of the fermentation, as mentioned before, sulfur was not a limiting component in the medium. Similarly, the original amount of yeast extract in the medium (0.5 g/L) is deemed to be sufficient, and a higher amount is not needed in this system, since the increased amount did not cause a significant improvement in biomass and product formation, or gas consumption. Thus, the original medium composition, as used in setup 1, was already enough to support the culture. (Infantes et al., 2020a)

In the case of cysteine, a study by Abubackar et al. (2012) with *Clostridium autoethanogenum* reported that an increase in the cysteine-HCl (1.2 g/L vs. 0.5 g/L) had a slightly detrimental impact on biomass, but a higher concentration of ethanol could be reached. The same negative influence on the biomass was observed on *C. acetivum* with concentrations above 0.5 g/L in another study by Sim and Kamaruddin (2008), although in that case, the product, acetic acid, was not significantly affected. Ethanol production was not reported there. In our case, the increased cysteine also had a slight detrimental effect in the biomass, with a lower final concentration of 0.8 g/L compared to 0.9 g/L in setup 1. No increase in product formation was seen, but rather the opposite: the acetate concentration with higher cysteine was 3 g/L lower than that of setup 1. The ethanol concentration did not change, though. It is possible that increasing the amount of cysteine caused an adverse effect. In order to improve the water solubility of cysteine, it is added to the reactor in the form of cysteine-HCl. The additional Cl⁻ ions that are added to the medium could be one reason for the potential adverse effect of the increased cysteine. With the available data, though, no conclusion can be drawn with certainty, and further investigation will be needed to clarify this point. (Infantes et al., 2020a)

It is important to notice, though, that the microorganisms used in the studies mentioned above were different to the one here used; besides, the study by Abubackar et al. (2012) was performed in 200 mL serum vials without pH control, and not bioreactors. The results obtained in that system are not directly comparable to the ones presented here due to the remarkable differences between the two, for instance, in the gas transfer to the liquid phase. The gas substrate differs, as well: in that study only CO was used, with no CO₂ or H₂ present, unlike in our case. (Infantes et al., 2020a)

Even if the increment of yeast extract in the medium did not translate to higher biomass formation, some changes could be observed: biomass slightly decreased, and a higher $Y_{P/X}$ was achieved. The acetate to ethanol ratio was not significantly altered, especially up to the point when maximum CO fixation stopped. Considering the complete run, only a slight increase in the acetate to ethanol ratio was detected. Besides, in this study the amount of yeast extract did not have an impact on the final acetate or ethanol concentration in our setup, contrary to what has been reported elsewhere (Barik et al., 1988; Vega et al., 1989b; Phillips et al., 1993; Abubackar et al., 2012). Similarly to what has already been discussed regarding cysteine, it is very likely that the initial, lower yeast extract concentration on setup 1 was already enough and not limiting. As well, the studies mentioned above are not directly comparable in this case neither, due to the different cultivation systems used (bottles rather than bioreactors), organisms or gas composition. Another potential argument so as to why yeast extract did not have an effect in our media could be that, since the gas mixture used contained N₂, *C. ljungdahlii* could potentially be fixing it, as proposed by Richter et al. (2016) and Tremblay et al. (2012), and thus minimizing the effect of other nitrogen sources, but this remains a controversial topic since Emerson et al. (2019) could not observe any nitrogen fixation in their experiments. (Infantes et al., 2020a)

5.1.2 Effect of pH

All fermentations performed with a lower pH had an increased amount of ethanol per acetate produced (in mol), during the maximum CO fixation phase, as it was expected and as described in literature. Even so, if the values for the whole run are taken into consideration, lowering the pH did not produce a shift of the product formation towards ethanol. A study by Kundiyana et al. (2011) reported a similar behavior, since lowering the pH below 6.0 did not produce an increase on ethanol production on *C. ragsdalei*. In our case, the effect seen might be the result of the cell culture stopping to use H₂, and eventually CO, which could lead to a slowdown of the product formation towards the end of the fermentation. It is, though, not the aim of the present study to elaborate further about this and will be analyzed in detail in the future with the system described here. The more acidic pH resulted in lower productivities as well, which could have been caused by the less favorable growing conditions.

It must also be taken into account that acetate in its undissociated form is lipophilic and freely diffuses through the cell membrane, which results in the move of H^+ across the transmembrane gradient, lowering the intracellular pH (Kundiyana et al., 2011). If the pH drops too low, it might negatively impact the culture since the microorganism could struggle to maintain a neutral intracellular pH (Cotter et al., 2009; Mohammadi et al., 2011; De Tissera et al., 2017). (Infantes et al., 2020a)

Acetate is regarded as a growth-associated product (Richter et al., 2013). Agreeing with this, in all pH-regulated experiments acetate production increased continuously, and almost parallel to biomass after around 20 h, and while cell growth happened. This is not the case only in the non-regulated experiment (setup 2) and in the one where pH was left to drop after 24 h (setup 5). In the case of setup 2 (no pH regulation), growth slowed down at approximately 20 h, moment in which acetate production was seen to increase in the pH regulated experiments. This reduced growth influenced the acetate production. In setup 5, due to the pH being regulated for the first 24 h, a higher biomass concentration could be achieved, and thus, more acetate was produced than in setup 2. (Infantes et al., 2020a)

Regarding ethanol, different studies disagree on whether ethanol might or might not be growth associated. Barik et al. (1988) and Najafpour and Younesi (2006) reported that ethanol is not associated with growth; conversely, Cotter et al. (2009) showed that *C. ljungdahlii* produced significantly less ethanol when the pH was lowered from 6.8 to 5.5 and concluded that this effect could be related to the slower growth observed. Regarding the experiments here shown, the productivity of ethanol is not constant across the different setups, and does not seem to be related to biomass formation; although when the conditions were too detrimental, as in the non-pH regulated run, both product formation and biomass were clearly affected. Again, in this case, the studies found in literature were done with various organisms, gas compositions and vessels, and none reported the gas profiles during the fermentation. (Infantes et al., 2020a)

5.1.3 Effect of pH and gas flow

The combined effect of lowering the pH and the gas flow resulted in less favorable growing conditions, and less substrate available for the cells. This caused the lower maximum CDW achieved in setup 6 compared to setup 5, as well as an increase of the ethanol ratio. This agrees with recent research on how ethanol production could be triggered, under growth-limited conditions, by the balance between intracellular and extracellular conditions, that is, total acetate concentration and extracellular pH (Richter et al., 2016). A lower amount of acetate accumulating in the culture broth, as a result of less biomass being formed, would result in less acetate being available intracellularly, and thus the microorganisms could have more time to adapt and shift towards ethanol. At the same time, the lower

pH would potentiate this effect, since more undissociated acetic acid could diffuse through the membrane to be available for further conversion into ethanol. Even so, the less favorable conditions of this experiment caused a reduction in the overall productivity. (Infantes et al., 2020a)

5.1.4 Carbon balance

A closed material balance in a fermentation system is fundamental for its characterization, and to be able to understand both the bioenergetics of the process and the amount of biomass generated. It is also an extremely valuable tool for analytical validation and detection of measurement errors (Kumara Behera and Varma, 2017). Moreover, the carbon balance is essential in order to be able to successfully undertake microbial physiology studies, predict how much carbon has successfully been fixed, and how much has been directed towards cell carbon, as well as for the consistency of the yield coefficients (Ellis et al., 2012).

The system here presented allowed to obtain a closed carbon balance, and, therefore, it can be assumed that no additional undetected product is generated, and that the analytical equipment and methods used are robust and sensitive for the purpose of this study. Both the yields and productivities obtained provide, thus, a precise description of how the process is impacted by each of the parameters here tested.

This is also proof that the diffusion of gas through tubing and connectors is minimized, thus preventing the loss of substrate. Besides, it can be concluded that the gas stripping effect of a continuous gas flow, which can potentially remove some of the produced ethanol (Perez et al., 2013) is not a critical point in this fermentation system.

5.2 Evaluation of beech wood and lignin derived syngas

5.2.1 Substrate usage and carbon fixation

Both fermentations present a first phase where *C. ljungdahlii* does not use the gas immediately, which lasted for a similar amount of time: 14 h for BWS and 15 h for the LS. This is to be expected, being the amount of fructose added with the pre-culture comparable in both cases. As well, the initial surge of CO₂ seen in Figure 4.7 and Figure 4.10, and Figure 4.8 and Figure 4.11 during that time can be thereby explained. (Liakakou et al., 2020)

When the gas consumption started, both fermentations showed a comparable trend, with similar values for $\dot{n}_{\text{CO}_2, \text{out}}$ at similar times. Hence, it can be said that the different syngas source and composition did not have an impact on the performing of the cells during this first phase. (Liakakou et al., 2020)

By looking at the CO fixation values, it can be clearly seen that the microorganism performed consistently in both experiments. Firstly, the time that was required to reach 85 % CO fixation is equivalent in both cases: 17 h and 18 h for BWS and LS respectively. Despite not being able to compare the time period during which the pH glitch happened, after that, between 51 h (BWS) or 52 (LS) h and 64 h the average was 79 % and 81 % respectively. The behavior of *C. ljungdahlii* from 52 h to the end of the process was also almost identical in both cases. (Liakakou et al., 2020)

CO and CO₂ usage, on the contrary, presented some differences. Except for the 2 first measured values, the CO₂ usage on the BWS fermentation was negative, or what is the same, was produced, during the whole run. Leaving out the first 20 h (the initial peak caused by fructose consumption), its usage value ranged from -0.05 % to -43 %. For the LS process, the variation in the range of values after 20 h was wider, from 11.7 % to -54 %. The BWS had a CO₂:CO ratio of 0.68, while the LS contained slightly more CO₂, with a ratio of 0.84. Even if the gas flow rate was adjusted so that the sum of CO₂ and CO was equivalent in both cases, and the CO₂ composition of both gases is similar (Table 4.5), only in the LS fermentation CO₂ usage was detected. After 20 h of process-time, the CO usage was constantly above 90 % during the LS fermentation, while a decrease can be seen towards the end in the BWS process. (Liakakou et al., 2020)

When looking at H₂, excluding the pH issue, both usage graphs look also similar, having a first phase where H₂ is consumed at around 80 %, and then decreasing towards the end. It is interesting to note here that the flow rate of H₂ or the H₂:C_{total} ratio does not appear to have an effect, since it was lower in the BWS, with 0.18 mmol/min and 0.47, respectively, compared to 0.28 mmol/min and 0.69, respectively, in the LS. (Liakakou et al., 2020)

CH₄ did not appear to have any effect in the process, since the microorganisms lack the ability to use it. It also did not produce any noticeable effect in growth or product formation, and can be considered, in this case, inert. This result is in line with what has been reported by Datar et al. (2004). Regarding the other major impurity in both BWS and LS, C₂H₆, Ahmed et al. (2006) showed that it also appears to not influence in any way the fermentation performance. C₂H₄ has been described as an inhibitor of methanogenic bacteria (Spratt et al., 1982), which inhibits the hydrogenases (Zorin et al., 1996). At the concentration measured in the BWS (9 ppmV), and comparing the outcome with that of LS, which did not contain any C₂H₄ in measurable amounts, it can be said it did not cause any detrimental effect. (Liakakou et al., 2020)

Considering the total carbon fixation ($E_{C, total}$), this parameter enables the comparison of the performance between different experiments. As well, it can serve as an indication of the fitness level of the cells at different stages of the fermentation. It is noticeable that not all carbon fed into the

bioreactor could be captured. In both cases the calculated endpoint value is very similar, 42.3 ± 0.44 % for BWS and 42.08 ± 4.07 % for LS. Therefore, it can be said that the different gas composition obtained from the gasification of beech wood and lignin does not influence the fermentation outcome in terms of affecting the ability of *C. ljungdahlii* to fix the carbon fed. (Liakakou et al., 2020)

The fermentation reported in section 4.1 *Impact of medium components and process parameters*, setup 1, which was performed in the same system and under the same conditions but with a clean, commercially mixed syngas containing only CO, CO₂ and H₂, has also been compared to the results obtained here. When the $E_{C, total}$ is considered, the clean syngas provided a higher carbon fixation ratio in all cases, achieving between 4 and 10 % higher carbon fixation. This difference though cannot be solely attributed to the presence of impurities, since, as mentioned above, the gas composition was also different, and it is clear that this also has an impact in the fermentation outcome (Datar et al., 2004; Bengelsdorf et al., 2013). (Liakakou et al., 2020)

5.2.2 Biomass, product formation, yield and productivity

Both the BWS and LS fermentations show an almost identical profile regarding biomass production, as can be seen in Figure 4.9 and Figure 4.12. Acetate formation started in both cases directly after inoculation, and also here the two setups performed very similarly, achieving almost the same amounts of acetate. The amount of ethanol formed was greater in the LS fermentation, although the pattern is again similar, with acetate starting after growth has slowed down, at around 50 to 60 h of process-time. End-point yields and productivities achieved are, therefore, comparable in both cases. The most noticeable difference is found during the maximum usage interval, where BWS performed better than LS. Regarding product ratios, the LS fermentation presented a higher amount of ethanol per mol of acetate at the endpoint, although it was the opposite at the other two intervals considered, suggesting that a metabolic shift happened towards the end of the fermentation. (Liakakou et al., 2020)

Looking at the standard commercially-mixed syngas (described in section 4.1 *Impact of medium components and process parameters*, setup 1), the product ratio was the same as for the BWS (7.8 mol acetate/mol ethanol), while it was lower (5.24 mol acetate/mol ethanol) for LS (indicating, thus, more ethanol per acetate). Regarding productivities, at the endpoint it was 22 % higher (0.22 ± 0.02 g/L·h) than the BWS and LS fermentations (Table 4.6); up to the point of maximum CO fixation, it was 46 % and 34 % higher (0.27 ± 0.04 g/L·h) than BWS and LS, respectively; and finally, during maximum overall usage the difference decreased, with the clean syngas being only 8 % (0.26 ± 0.02 g/L·h) above both BWS and LS. The yields achieved per substrate fed ($Y_{P/S, fed}$) at the endpoint by both the BWS and LS (Table 4.6) were also slightly worse: the clean syngas reached a value of 0.43 g/g, 0.1 and 0.13

higher than BWS and LS, respectively. Even if a negative impact of impurities was expected, as has been documented broadly in literature (Munasinghe and Khanal, 2011; Xu et al., 2011; Ramachandriya et al., 2016), the endpoint yield per carbon fixed ($Y_{P/S, \text{fixed}}$) did not change significantly and remained mainly unaltered in the three cases. (Liakakou et al., 2020)

5.3 Impact of syngas composition and impurities

5.3.1 Biomass, product formation, yield and productivity

Theoretical yield and carbon fixation calculations have to be re-considered when dealing with biomass-derived syngas. The complexity of the impurities which are present in the gas mixture highlight the necessity of having a system where each biomass-derived syngas can be tested before its implementation in a continuous, bigger-scale system. (Infantes et al., 2020b)

Besides, theoretical yields and ideal gas ratios only apply for resting cells, and it can be of interest to know how the gas composition affects the growing phase of the cells, to try and optimize this stage also: in one report it was stated that cells took up to 8 days for the OD to stabilize (Ahmed et al., 2006), and, in another study, it was reported that even with bottled, clean syngas, a lag phase of 4 days was observed (Datar et al., 2004). (Infantes et al., 2020b)

Even if the same amount of total carbon, 0.4 mol/min, was fed in all setups (except for setups 3 and 4) the different CO:CO₂:H₂ ratio of the syngases clearly had an influence. This was to be expected, as each component has a different solubility. Here, the precise impact of each syngas could be shown: gas composition had, in some cases, a marked effect in growth, but not so significant in product formation, especially up to the first half of the run. Except for setup 4, all other clean gases achieved a concentration of acetate of approximately 10 g/L at around 50 h, but this changed towards the second half of the fermentation: the product ratio and its concentration were strongly affected by the syngas composition, as shown in Figure 4.19. (Infantes et al., 2020b)

In terms of growth, all biomass-derived syngases tested could successfully be used as fermentation substrate, offering proof that the level of clean-up of the syngases is enough for syngas fermentation. This is a critical point when assessing biomass-derived syngas: cells have been reported to stop growing when biomass-derived syngas was supplied (Datar et al., 2004). As well, Ahmed et al. (2006) observed that cells stopped growing when a 0.2 µm filter was applied on the biomass-derived syngas inlet, but this was reversed when it was replaced by a 0.025 µm filter. (Infantes et al., 2020b)

When comparing each pair of clean and biomass-derived syngases, end productivities were generally not greatly affected, even if a better performance was achieved in most cases with clean syngas. The

increased production of a more valuable product, ethanol, when biomass-derived syngas was used, could counteract the lower productivity up to an extent, depending on the down-stream processing requirements and the market-value of the products. In case of setup 4, the obtained yield for $Y_{P/S, \text{fixed}}$ calculated up to the end of maximum CO fixation was slightly above 1 ($1.03 \pm 0.04 \text{ g}_{\text{product}}/\text{g}_{\text{substrate}}$); this is regarded as the result of small analytical inexactitudes, and should be interpreted as being close to 1. (Infantes et al., 2020b)

Focusing on setup 3 and 4, the total productivity at the end of the fermentation of the biomass-derived syngas (setup 3) was higher than what was obtained with clean syngas (setup 4), despite the acetate productivity of both runs being equivalent. As happened for setups 1 and 2, the ethanol productivity was higher in the setup using biomass-derived syngas. For the values obtained up to end of maximum CO fixation, the opposite is true for total and acetate productivity: setup 4 has higher values in this case. This difference can be explained because gas consumption ended much earlier in setup 4: in the calculation for the end of process values, a long time span where the culture was not active is included, lowering the resulting productivity values. (Infantes et al., 2020b)

5.3.2 Substrate usage and carbon fixation

The gas composition had a big role in how long the maximum CO fixation lasted, as well as the presence of impurities in the syngas. In all cases, clean, impurity-free syngases showed a prolonged CO fixation when compared to their biomass-derived counterpart. (Infantes et al., 2020b)

Another question encountered is whether simultaneous consumption of H_2 and CO can be achieved for a given syngas composition - the inhibition kinetics of H_2 or CO in acetogens are not well understood so far (Takors et al., 2018) - and what influence the impurities in biomass-derived syngas will have. Here, H_2 usage was observed in all biomass-derived gases, albeit each of the respective clean syngas presented a higher consumption of H_2 , except, as already explained, setups 3 and 4, the Bioliq® syngas fermentations at a lower gas flow. The successful H_2 usage is a very positive outcome for the further usage, and optimization, of the biomass-derived syngases here tested. This point is not trivial: according to Esquivel-Elizondo et al. (2017), not many studies observe concomitant H_2 and CO usage, and keeping an optimal ratio of the syngas components is key for the sustainability of the process. In some cases, biomass-derived syngas has been shown to cause H_2 consumption to stop (Ahmed et al., 2006), while in a study with *Clostridium carboxidivorans* P11, it was concluded that, at H_2 partial pressures normally occurring in biomass-derived syngas, the hydrogenase efficiency would not be at its optimum (Skidmore et al., 2013). (Infantes et al., 2020b)

The simultaneous consumption of H₂ and CO started, in all cases, after the CO consumption had increased, but in some cases, before it reached complete consumption. Due to the increasing biomass concentration, the amount of dissolved CO in the medium decreases, enabling H₂ uptake (Bertsch and Müller, 2015; Valgepea et al., 2018). This can also explain why growth and H₂ usage were linked in all cases: when growth stopped, so did H₂ usage. As less cells are metabolically active, there is less competence for CO, and each remaining active cell is exposed to a higher CO concentration, leading to a decline in H₂ consumption. This observation agrees with what has been reported by Valgepea et al. (2017), and it could be confirmed that it is valid for both, clean, and biomass-derived syngas, as long as no hydrogenase-inhibiting compound is present. (Infantes et al., 2020b)

Regarding total carbon fixation ($E_{C, total}$), it can be clearly seen that, for the same syngas composition, this was negatively impacted by impurities in biomass-derived syngas. Predicting up to which extent, is, nowadays, not possible, and it would need to be empirically determined by testing each biomass-derived syngas in a fermentation system to assess its impact. (Infantes et al., 2020b)

5.3.3 Product ratio comparison according to the type and composition of syngas

The complexity of the factors being involved in the outcome of different CO/CO₂/H₂ syngas mixtures is evident, and the obtained product ratios are not always in accordance with what is observed when gas mixtures consisting of only two components are used (CO/CO₂, H₂/CO₂, CO/H₂). There are several reports on the effect of, mostly, only pairs of these syngas constituents, however, the combined effect of CO/CO₂/H₂ blends has not been widely considered. (Infantes et al., 2020b)

Looking at the different clean, impurity-free syngases tested here, it can be seen that higher H₂ together with very low amounts of CO₂ directs the cell metabolism towards the production of ethanol: the highest H₂ and CO, with very low CO₂, produced the highest ethanol (Figure 4.19). This outcome agrees with what was reported by Valgepea et al. (2018): if CO was supplied together with H₂, more ethanol was produced. Similar results were also documented by Hurst and Lewis (2010), which used a system fed with CO₂ and CO. Different CO partial pressures were tested, and at higher P_{CO}, ethanol increased. They postulated that, when cells stop growing, less ATP is needed, and the excess electrons generated by the higher P_{CO} can be directed towards ethanol. (Infantes et al., 2020b)

Moreover, the data presented here shows that when CO₂ is supplied in higher amounts, H₂ does not seem to have such a significant impact, but if analyzing the runs with a similar CO gas flow rate (between 0.20 and 0.25 mmol/min), the highest acetate to ethanol ratios were obtained with lower H₂ and CO₂ (Figure 4.19). Looking at the findings by Phillips et al. (1994), it could be concluded that H₂ does not contribute towards the product shift to ethanol, contrary to what is found here. In that

report, when comparing two gas mixtures, H₂/CO₂ and CO/CO₂, the one containing CO resulted more favorable for growth and ethanol production. It is important to note, though, that those experiments were performed in bottles, in batch, where the gas was dispensed into the head-space without a continuous supply. In yet another set of batch experiment, different mixtures of H₂/CO were investigated. Acetate formation increased with increasing H₂ concentrations in the headspace of the serum bottles, and more ethanol was produced when the CO concentration increased. (Jack et al., 2019). This findings could also lead to assuming that lower H₂ would cause the product ratio to shift towards ethanol, contrarily to what has been shown here and in a study by Esquivel-Elizondo et al. (2017). There, both CO alone and CO/H₂ produced more ethanol than CO/CO₂ and CO/CO₂/H₂ mixtures. Yet, concluding that lower CO₂ equals, in all cases, higher ethanol production would not be accurate, as already discussed above. Syngas mixtures, composed by varying amounts of H₂/CO₂/CO, present a much more complex challenge, due to the combined effect of each component upon the others. A much more thorough study would need to be conducted, in order to better understand this, and potentially predict the outcome of different syngases. (Infantes et al., 2020b)

Comparing clean and real biomass-derived syngas, the scenario changes drastically: gas composition did not play the biggest role in terms of product distribution; rather, the nature of the syngas did. All biomass-derived syngases produced a higher ethanol to acetate molar ratio, without a direct correlation to their composition. A metabolic regulatory mechanism has been postulated for *Clostridium autoethanogenum*, an organism which is closely related to *C. ljungdahlii* (Bengelsdorf et al., 2016). In that study, Valgepea et al. (2017) reported that the increased acetic acid concentration in the medium, with the subsequent proton translocation into the cell, causes an uncoupling of the proton motive force (PMF). At higher biomass and acetate concentrations, cells try to gain more ATP by forming acetate, which causes the depletion of the acetyl-CoA pool due to the WLP not being able to function quickly enough. Eventually, this causes a “metabolic crash”, where the ability to uptake H₂ is lost while the cells try to counteract the PMF uncoupling. The subsequent result is that more CO is oxidized to CO₂ to try and maintain the amounts of reduced ferredoxin. Since less carbon is available for the WLP, the metabolism will eventually collapse. To counteract this, cells shift towards ethanol production in order to prevent the further uncoupling of the PMF, and still be able to conserve energy (Valgepea et al., 2017a). A similar mechanism could potentially also explain the behavior when other stress factors are present, like impurities in the syngas. Rather than the increased acetic acid concentration, the inhibitory effect of the impurities on the WLP enzymes could also cause a slowdown of this pathway. This would have the same outcome, that is, a depleted acetyl-CoA pool, and less ATP formation. The ATP-maintenance mechanism would then come into action, even at lower

acetate concentrations in the broth, increasing the ethanol production. This would prevent the early crash of the culture under the more challenging conditions caused by the biomass-derived syngas. (Infantes et al., 2020b)

When comparing setups 1 to 4, it can be observed that lowering the gas flow rate had some opposite effects on biomass-derived and clean syngas. Setup 1 and 3 (where biomass-derived syngas was used) show much more similarities than setups 2 and 4 (impurity-free syngas). Comparing setup 1 to setup 3, the lowering of the gas flow resulted in a higher CDW and acetate concentration in setup 3, and a slightly reduced ethanol production. One explanation for this could be that in setup 3, due to the lower gas flow, less impurities were introduced in the medium compared to setup 1. Possibly, due the impurities in the syngas, the cells in setup 1 were already limited and could not use the excess substrate being supplied with the higher flow, as the gas usage and fixation graphs show. (Infantes et al., 2020b)

In contrast, when looking at setups 2 and 4, a lower gas flow rate proved to be detrimental, with a sharp decrease in gas usage as well as CDW concentration after 55 h, and a lower final product concentration, with only traces of ethanol being produced. In setup 2, when cells reached a CDW of 0.7 g/L, the acetate concentration was still below 10 g/L. In setup 4, at the same CDW, the acetate concentration was already 10 g/L. As explained above, the crash seen in setup 4 would agree to the fact that, for the same syngas composition, at the same CDW, but with higher acetate, the ATP needs cannot be met, and the culture crashes. The reason as to why ethanol was produced in setup 2 but not in setup 4 cannot be exclusively caused by the acetate concentration, as proposed by Richter et al. (2016), since acetate production was higher in setup 4 than in setup 2. In this case, the reason behind appears to be the H₂ amount fed. The consumption of H₂ also has the effect of driving protons into the cell without ATP production (Valgepea et al., 2017a), which, again, would cause the ATP maintenance system to come into action in setup 2. This agrees with the increase in CO₂ production observed. Moreover, in a follow-up study, the same group reported that H₂ directed the metabolism towards an increased ethanol production (Valgepea et al., 2018). (Infantes et al., 2020b)

Looking at setups 3 and 4, apart from the already discussed higher ethanol, a higher CDW was achieved in the former. This observation would support the ATP maintenance mechanism coming into action in response to the impurities: due the shift in the product ratio, resulting in a lower acetate concentration and higher ethanol production, cells where able to prevent the crash, conserve energy and generate ATP, even if impurities were present. Nonetheless, this does not imply that impurities are beneficial, since the clean, impurity-free syngas achieved a higher $E_{C, total}$ as well as a higher total productivity up to the point of maximum CO fixation. The perceived better performance of setup 3

when considering the whole run is caused by the early crash of setup 4 after approximately 50 h. (Infantes et al., 2020b)

5.4 Overview of fermentation results

5.4.1 Overall summary of carbon fed, usage and fixation

From the results here obtained, it can be seen that none of the gas ratios for carbon used or fixed was constant. This was expected in the light of the results obtained, and further supports the conclusions obtained from this work mentioned above. This is further proof that the metabolic state of the cells, which is linked to the gas composition and growth conditions, has a prominent impact on which carbon and electron donor source is preferred by the bacteria, and emphasizes the fact that the requirement of growing and non-growing cells are substantially different (Richter et al., 2016).

One of the clearest cases can be found in Table 4.12, where setup 2 (without pH regulation) has the lowest H₂:CO molar ratio, both for used and fixed carbon. As has been already discussed, the lower pH causes an increase in the concentration of protons intracellularly, and thus H₂ usage is reduced (Richter et al., 2016; Valgepea et al., 2017a). In Table 4.13, when comparing setups 1 to 4, it can be seen that the same gas composition, but with or without impurities, and at two different gas flows, produces also very different results. It is, therefore, not possible to make an immediate estimation of how *C. ljungdahlii* will behave when real, impurity-containing biomass-derived syngas is used. The existing metabolic models will not help with this predictions, neither, as this aspect is not taken into account due to the models being developed with impurity-free gases (Nagarajan et al., 2013; Valgepea et al., 2017b).

5.4.2 Overall comparison between experimental and maximum theoretical yields

The stoichiometry alone cannot predict the acetate/ethanol ratio, since it is strongly dependent on the cultivation conditions, and how the different gas compositions and impurities affect the overall metabolism. Moreover, a significant fraction of the generated ATP has recently been found to be needed for cellular maintenance, which supposes a challenge for yield calculations, if only the WLP stoichiometry is considered (Valgepea et al., 2017a). This is evident when looking at the percentage of the theoretical maximum acetate produced from substrate fed for each fermentation. Even if the gas flow was adjusted to maintain the same amount of total carbon fed, the impact of the different gas compositions and impurities is clear.

In average, an excess of 10 % of the theoretical maximum acetate from substrate used (considering the ethanol formed), was detected. Here, small analytical inexactitudes are magnified, even with a closed carbon balance, which could account for the deviation observed.

5.5 Impact of elevated pressure

5.5.1 Effect of syngas overpressure on growth and product formation

The concentration of biomass, measured as cell dry weight (CDW), at the end of the cultivation time was very similar for all the different pressures tested. Nevertheless, the cultures that were subjected to pressures above atmospheric level (1.5, 2.0 and 2.5 bar, absolute) experienced a lag-phase of approximately 45 h and their maximum biomass concentration was detected considerably later. For all pressure-grown cultures, this maximum was significantly higher than the culture at 1 bar (absolute), and its value increased for each increasing treatment pressure. This agrees with the findings by Stoll et al. (2019), where an increase in the maximum cell concentration is seen at 4 bar compared to the 1 bar culture; as well, the maximum was reached later in the 4 bar experiment. At 7 bar, though, a lower CDW was achieved compared to 1 bar and 4 bar, potentially due to substrate inhibition.

In literature, diverging results can be found for *C. ljungdahlii* under increased syngas pressures. As opposed to what has been found here, enhanced growth was only seen with increasing pressure up to 2 bar (absolute), and, above that level, biomass decreased with increasing pressures of syngas (Mohammadi et al., 2014). The same trend is observed for acetic acid and ethanol formation. The cultivation time of the experiments in that study is much shorter, 40 h, than the one here, which lasted more than five times longer, 210 h. Consequently, the maximum biomass concentration achieved in that study is lower than here: 0.2 mg/L as opposed to 1 g/L, respectively; this is also true for the products, with maximum acetate and ethanol concentrations of approximately 0.5 g/L and 0.2 g/L, respectively. An increasing biomass concentration with increasing pressure was not seen neither in a study by Younesi et al. (2005). It must be noted, though, that the minimum pressure used there was 1.8 bar (absolute), so no comparison is possible to the lower pressures used here. Nevertheless, the CDW reached in that study are remarkably similar to the ones reported here. As well, the maximum CDW there was 1.15 g/L at the highest pressure, 2.8 bar, which is a similar value to what has been found here, 1 g/L at 2.5 bar. However, in most cases growth was much faster in their study: except for the cultures at 2 and 2.6 bar, all the other conditions reached maximum CDW between 40 h and 70 h. Regarding acetate, no clear influence of the increasing pressure can be seen in the mentioned study by Younesi et al. (2005). The acetate production observed was, strikingly, almost 10-fold lower than what is reported here. When looking at the study by Stoll et al. (2019), the product formation pattern is equivalent to what has been shown here when comparing 1 bar and 4 bar conditions: higher

pressure produced more acetate, but less ethanol. Conversely, this findings are not in line with the study by Younesi et al. (2005), where more ethanol was produced at the highest pressures tested (2.6 and 2.8 bar absolute). It must be noted that each study used a different syngas composition, which could account for some of the differences observed; as well, the different experiment length and fermentation systems only allow for a limited comparison.

As discussed, when higher syngas pressure was applied, more substrate became available and hence the biomass increased. The higher amount of substrate dissolved could also be the reason of a lower ethanol production in all the cultures at increased pressure, even if more acetate was present. This, at first sight, is contrary to the idea that ethanol formation becomes increasingly favorable at higher acetate concentrations (Richter et al., 2016). It must be considered, though, that at increased pressures more substrate is available for the cells, as already discussed. Valgepea et al. (2017) postulated in their study that ethanol formation happened as a response when, due to higher biomass and acetate concentrations, the ATP maintenance costs become higher, causing a complex cascade of metabolic responses and the depletion of the acetyl-CoA pool. If a higher amount of gas is dissolved in the medium, the acetyl-CoA pool could be maintained, as well as more ATP could be formed, thus eliminating the need to generate ethanol, and supporting a higher biomass concentration. This effect would stop as soon as the biomass and the acetate concentration reach a certain threshold where the cells' uptake rate of the gaseous substrates is higher than the transport rate at that certain pressure, or when the ability of the WLP to supply the Acetyl-CoA pool is no longer enough to counteract the amount of extracellular acetate. This theory would be supported by the fact that, at 1 bar, cells stopped growing much earlier, producing less acetate. Ethanol formation could be observed shortly after 45 h, with its levels increasing remarkably more than in the pressure cultures. Biomass remained constant after approximately 92 h, contrary to the pressure cultures, where it decreased after reaching their maximum. This agrees with both Valgepea et al. (2017) and observations that would point into ethanol formation having a somewhat protective effect on the cells, preventing the culture from crashing. If the biomass increases too much and only acetate is formed, the culture has been observed to crash (Infantes et al., 2020b).

In order to overcome the lag-phase observed, a step-wise pressurization of the culture would be advised in future studies. This approach was successfully applied in two instances: in the first one, the total pressure of syngas was elevated up to 11 bar, and the second one, the CO partial pressure was increased to 10 bar. Thanks to the higher biomass concentration, the culture was able to uptake the gaseous substrates, including CO, without experiencing any detrimental effects or lag-phase (Klasson et al., 1991; Department of Chemical Engineering, University of Arkansas, 1993).

5.5.2 Effect of CO₂/H₂ and CO overpressure

5.5.2.1 Growth and product formation

5.5.2.1.1 CO₂/H₂

When growing under CO₂/H₂ at 1 bar the culture did not grow for at least 100 h. At 5 bar, no significant growth was observed for the entire experiment duration. This outcome was unexpected, since *C. ljungdahlii* is a well-characterized organism, and its ability to use CO₂/H₂ mixtures is widely known (Tanner et al., 1993; Köpke et al., 2010). CO₂, when dissolved in the medium, can cause a drop in pH, as will be discussed later in more detail. This was the cause of a sub-optimal conversion rate when increasing pressures of a H₂/CO₂ mixture were applied to enhance the hydrogen-dependent carbon dioxide conversion to formic acid, using the reverse reaction of FHL in *E. coli* resting cells (Roger et al., 2018). An improved conversion was achieved once the pH was regulated. In the case here presented, any potential effect of dissolved CO₂ on the medium pH could be dismissed, since it was strongly buffered, and no sudden decrease was observed when the CO₂ was provided into the headspace at the beginning of the cultivation. Another external factor that could affect growth is different pre-culture quality. Here, all bottles used at both pressures were inoculated identically, using the same pre-culture mixture. Therefore, this dismisses any question of whether the seed culture could have influenced the growth in the 5 bar cultures. Different strategies could be employed in future studies to try and overcome this challenge: a different medium formulation could be tested, or a pre-culture grown under CO₂/H₂ could be used to inoculate the bottles. The latter was, for instance, the approach that Vega et al. (1989a) used in their study. Finally, despite the culture not growing, acetate formation could be detected under both conditions immediately after inoculation, which is proof that the cells were metabolically active.

The control culture at 1 bar performed better, producing more acetate than the pressure-treated culture, from 30 h on. As expected, a sharp acetate increase was seen after cells started growing. In the case of the 5 bar culture, even if no significant growth was seen, acetate increased continuously throughout the experiment, although at a lower rate. Ethanol was not produced at significant amounts during the fermentation, neither at 1 bar nor at 5 bar, possibly due to the diminished, or neglectable, growth of the cultures, and the excess of substrates. Even if acetate was found to be the main product when using the same H₂/CO₂ gas mixture in a 1.5 L or in a 2.5 L bioreactor at 1 bar, some ethanol could be detected in that study (Oswald et al., 2018a). This difference could be caused by the fact that the systems are not comparable, with the gas mixture being continuously sparged into the stirred fermenters, while here a true batch fermentation was performed in a closed, static system.

A possible reason for the lack of growth on the culture subjected to the higher pressure could be that the combination of an increased amount of dissolved CO₂ and H₂ caused an imbalance in the intracellular conditions, leading to a major metabolic disruption (Figure 5.1). CO₂ solubility is much higher than that of H₂ (Cardarelli, 2008), which translates into an excess of dissolved CO₂ in the medium in respect to the amount of H₂. The partial pressure for H₂ (53.3 %) and CO₂ (26.7 %) at 5 bar of total headspace pressure were 2.7 bar and 1.3 bar, respectively. Due to Henry's law constants being dependent on the temperature (Sander, 2015), the H^{cp} needs to be calculated for the experimental conditions. At 37°C, the Henry's law constant for H₂ is H^{cp} = 7.28·10⁻⁶ (Sander, 2015), and thus, the calculated dissolved concentration of H₂ at a partial pressure of 2.7 bar is 1.9 mM. CO₂ has a H^{cp} = 2.42·10⁻⁴ at 37°C (Sander, 2015), and its dissolved concentration would be 32.3 mM at a partial pressure of 1.3 bar. This represents a CO₂:H₂ molar ratio of 17. Stoichiometrically, a molar ratio of 0.5 CO₂:H₂ is needed for the conversion of those gases into acetate, so the excess of CO₂ is clear. Besides, CO₂ presents a complex behavior when dissolved into aqueous media (Carroll et al., 1991): H₂CO₃ (carbonic acid) is formed, with an hydration equilibrium constant K_h = 10^{-2.75}. The dissociation constant of carbonic acid into HCO₃⁻ (hydrogen carbonate) is pK_a = 3.6. With that, a 0.18 % of the dissolved CO₂ will form H₂CO₃ (Boyd, 2015). Even so, this will have an impact on the pH of the solution. As already discussed, acidification of the medium was prevented thanks to the buffer presence. As per Henry's law, more CO₂ will dissolve into the medium at 5 bar. CO₂ diffuses through the membrane, where the H₂CO₃ formed will dissociate into HCO₃⁻, with the consequent liberation of a proton. The intracellular pH of the cells is regulated, and is more alkaline than the extracellular medium (Terracciano and Kashket, 1986; Richter et al., 2016), although it does change as a response of metabolic activity. If the decrease of the intracellular pH is too large, it can be detrimental to the cells (Huang et al., 1986). Acetogens depend on a chemiosmotic mechanism for energy conservation (Schuchmann and Müller, 2014). Specifically, on *Clostridium ljungdahlii*, the Rnf complex is a membrane-bound, multi-subunit proton-translocating ferredoxin:NAD⁺ oxidoreductase (Tremblay et al., 2012; Hess et al., 2016), which pumps protons outside of the cell, establishing a proton motive force (PMF) which is then used by the proton-dependent ATPase for ATP synthesis. Maintenance of the ATP homeostasis has lately been pointed out as a key factor in the metabolism of acetogenic bacteria (Valgepea et al., 2017a). Under the mentioned conditions, due to the higher amount of CO₂ being taken up intracellularly, the PMF would be impaired, since, most probably, the amount and activity of the Rnf complexes is not enough to counteract the drop in intracellular pH. This would cause an extremely limited ATP production, which would prevent any increase in biomass, as it was observed here. Potentially, a step-wise pressure increase could also help here to alleviate this phenomenon by giving more time to the cells to adapt. As well, a different gas composition, with a lower amount of CO₂ could be tested, in order

to be closer to the stoichiometry of the consumption reaction with H_2 and avoid this excessive CO_2 accumulation. It must be noted, though, that an increased amount of H_2 can also have detrimental effects, since its uptake also involves a proton import not linked to ATP synthesis (Valgepea et al., 2017a), so this factor should also be taken into consideration for future studies.

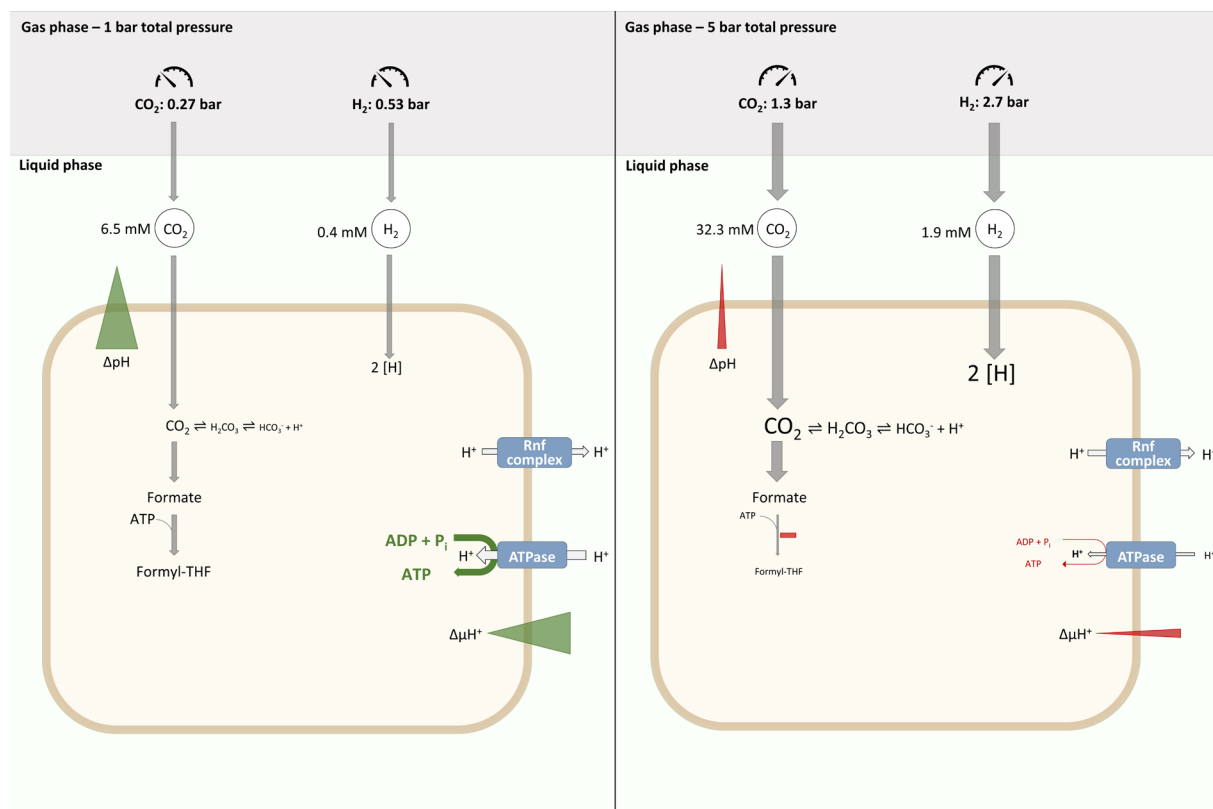


Figure 5.1 – Effect of increased CO_2 and H_2 pressure on the acetogenic metabolism. At 1 bar (left), a lower amount of CO_2 and H_2 are dissolved in the liquid, and thus, a limited amount will diffuse into the cell, as marked by the thin grey arrows. The intracellular pH of the cell is more alkali than the extracellular medium (marked as a green, wide gradient), and the Rnf complex can maintain the transmembrane potential ($\Delta\mu H^+$), which can be used by the ATPase to generate ATP (wider, green arrow, and bigger font). A small part of the CO_2 will form H_2CO_3 , which can further dissociate into $HCO_3^- + H^+$.

At 5 bar (right), a higher amount of CO_2 and H_2 will diffuse into the cell due to the increased solubility and increased concentration in the liquid, marked by thicker grey arrows. The higher amount of protons, and the increased formation of $HCO_3^- + H^+$ (depicted by a bigger font) will acidify the intracellular pH (represented as a narrower, red gradient), and will diminish the $\Delta\mu H^+$ (narrower, red gradient). If the Rnf complex cannot maintain the $\Delta\mu H^+$ necessary for the ATPase to provide enough ATP (narrower, red arrow, and smaller font), this ATP deficiency will put a stress on the necessary cell maintenance, as well as any reaction requiring ATP, such as the formyl-THF formation (marked with a red minus sign, and smaller font). Thus, the functioning of the WLP can be severely reduced.

5.5.2.1.2 CO

When pure CO was used as substrate, no growth was observed even at 1 bar, and only a marginal acetate production was observed. The fact that both conditions showed identical performances is remarkable. This could suggest that the amount of CO dissolved in the medium at 1 bar was already inhibitory for the cells, and an increase of dissolved CO due to increased pressure did not have a further impact.

Applying a kinetic model, an inhibition constant for *C. ljungdahlii* growing on syngas (30 % each CO₂, CO and H₂, in Ar) of $K_i = 0.61$ bar was obtained. The maximum inhibitory pressure, at which no growth would be apparent, was determined to be 1.75 bar (absolute) (Mohammadi et al., 2014). It is also stated there that increasing the total pressure of the reactor above 2 bar (absolute), which corresponds to $p_{CO} = 0.6$ bar, had a detrimental effect on gas uptake and cell growth. According to this kinetic model, it could be expected to see some growth with *C. ljungdahlii* growing with CO at 1 bar, since it is below the theoretical maximum inhibitory pressure. A caveat to it is the fact that the mentioned study used syngas, rather than pure CO, for the kinetic model, hence potential effects of the presence of CO₂ and H₂ cannot be underestimated. Moreover, there the medium was inoculated with cells which had already been growing on syngas, as opposed to the fructose-grown seed used in this study. This could have given an adaptative advantage to the culture which was not experienced here. As already mentioned for syngas and H₂/CO₂, performing step-wise pressure increases as well as using a lower initial p_{CO} , and the usage of a pre-culture grown on CO would be advised for future studies in order to help avoiding inhibition.

Despite all this, the fact that some acetate production was seen even under the stress of excessive CO is promising, and a testimony of the sturdiness of these bacteria, which were still able of maintaining some level of metabolic activity under that challenging condition.

5.5.2.2 Formic acid

Formic acid production was a key point in the report by Oswald et al. (2018) at 4 and 7 bar with CO₂/H₂. At the highest pressure, formic acid became the main product in detriment of acetate or ethanol. The ATP uncoupling discussed above could also explain the formation of formic acid in that case, since that reaction does not require ATP, but the following step of the Wood-Ljungdahl pathway, the formation of Formyl-THF, does (Köpke et al., 2010). Here, no formic acid formation could be observed, neither with CO₂/H₂ nor with CO. It must be noted that, since the fermentation in the study by Oswald et al. (2018) was carried out in a sparged STR bioreactor, it can be expected that the solubilized amount of CO₂ and H₂ was even higher due to the increased mass-transfer, increasing the effect of the substrates, and affecting the outcome.

In the case of CO, the metabolic activity of the cells was greatly reduced, and only a small amount of products were formed. In this case, the most likely scenario is that any formic acid that was produced from the WLP was immediately used to generate acetyl-CoA.

5.5.2.3 Effect of CO₂/H₂ on gene expression

The findings by Xie et al. (2015) could not be reproduced here. Contrary to what was reported there, no up-regulation of *aor*, *fdh* or *pta* could be identified. Despite this, the absence of a significant fold-change for the genes studied (*aor*, *cooC2*, *fdh* and *pta*) agrees with recent findings that the metabolic shift of acetogenic bacteria is not regulated by gene expression, but by environmental conditions. It is postulated that the abundance of central metabolic enzymes of the WLP is constant, and both the effect of acetic acid concentration (Richter et al., 2016), and mainly, the need for maintaining ATP formation drive the metabolic changes on acetogens (Valgepea et al., 2017a). The data shown here can provide with a first clue that, under increased pressure, it is much likely that the regulation of the metabolism of *C. ljungdahlii* is no different than at atmospheric pressure.

5.6 Sequential cultivation for acetogenic fermentation from oxygen-containing waste gas

Clostridium ljungdahlii can be used to generate sustainable value-added chemicals from waste gases, but it is a strict anaerobe, and thus, sensitive to O₂. Most anaerobes can only tolerate trace amounts of oxygen, and often it impacts their growth and product formation (Karnholz et al., 2002; Takors et al., 2018). It is necessary to ensure no oxygen can contaminate the gas stream, and removing it can suppose an impact in terms of process costs (Heijstra et al., 2017).

Here, by using the facultative *Parageobacillus thermoglucosidasius* as a tool for the removal of O₂ in a CO/air mixture, adequate conditions for the subsequent cultivation with *C. ljungdahlii* were achieved. Through the biological water-gas shift (WGS) reaction, H₂ and CO₂ are produced by the first microorganism, which are then used by the acetogen for the synthesis of acetate as a final product.

The thermophilic nature of the first organism of this sequential cultivation, *P. thermoglucosidasius*, can also alleviate the need to cool down hot flue gases. As well, due to the second organism being a mesophile, the lower cultivation temperature pertinently ensures the stopping of any remaining metabolic activity of the thermophile.

Besides, the amount of carbon lost in the formation of cellular biomass by *P. thermoglucosidasius* is almost negligible, resulting in a near stoichiometric conversion of CO into CO₂ and H₂ (Mohr et al., 2018a), making more substrate available for the acetogenic fermentation to follow. This point could be demonstrated in this study, since the biomass formation by *P. thermoglucosidasius* was indeed insignificant.

With this sequential cultivation, a total amount of 1 mmol of acetate was produced. From this, 0.47 mmol were produced by *P. thermoglucosidasius* through mixed acid fermentation (Hussein et al., 2015), and the amount of acetate generated by *C. ljungdahlii* was 0.52 mmol, which represents a 63 % of the theoretical maximum yield, and was entirely derived from the initial CO, converted to CO₂ and H₂ by the first organism.

Overall, the sequential cultivation strategy enabled the obtention of a higher yield than that obtained by other CO metabolizing organisms (King and Weber, 2007).

Finally, it could be proven that *C. ljungdahlii* can withstand such a sequential cultivation, without the need for the removal of the first organism.

6 CONCLUSION

First of all, the STR system used in this work proved to be a valuable tool for performing syngas fermentation screening experiments aimed at the study of media components and/or process parameters. It is able to show even small changes in the consumption of each of the gaseous substrates together with growth and product formation profiles. With the conditions tested, neither the supplementation with additional cysteine, nor yeast extract increased the duration of the gas consumption, and no dramatic effects on product formation could be observed. Decreasing the pH did not immediately result in higher ethanol formation and impacted the productivity negatively. When, additionally to the pH, the gas flow was also reduced, the reduction in biomass production was significant, as well as a reduction in acetate production and an increased ethanol to acetate ratio. The great variability of systems reported in literature makes a direct comparison between differing systems a challenging task. Therefore, the need to establish a system where the most common parameters, such as growth and product formation, but also substrate consumption, can be monitored in a standardized way, is high. Besides, for the proper identification of significant influences on a system, it must be highly sensitive and robust, so that the noise in the data is kept low. The experimental set up presented here proved to fulfill these requirements and will be used in further investigations on the influence of gas composition, different medium components, as well as strain comparison studies, including metabolic engineering. Finally, the obtention of a closed carbon balance provides further proof of the sensitivity of the system. (Infantes et al., 2020a)

It is evident that a number of interacting factors, including metabolic regulatory mechanisms, gas solubility and mass transfer effects all can play a role when dealing with syngas mixtures of CO/CO₂/H₂, and the extrapolation of results from one gas mixture to another is not guarantee of successfully predicting the behavior of the cells. (Infantes et al., 2020b)

Regarding the impact of syngas impurities, they have been reported to have a much greater impact in other instances described in literature. In a study by Datar et al. (2004) it was reported that the fermentation of biomass-generated, partially cleaned syngas caused both the stopping of growth and H₂ usage of *Clostridium arboxidivorans* P7. (Liakakou et al., 2020)

By partnering with both the Bioliq® plant at the KIT (Karlsruhe, Germany), and TNO, Energy Transition, Biomass & Energy Efficiency Unit (Petten the Netherlands), a further step towards the successful integration of biomass-generated syngas and its fermentation was achieved. The same syngas composition, but with different gas flows, led to opposite results for the Bioliq® syngas, showcasing

how important it is to be aware of the complexity of the synergistic effects involved. (Infantes et al., 2020b)

No cell dormancy, or substrate consumption inhibition could be observed in none of the fermentations. The ethanol/acetate ratio remained constant for the TNO beech wood syngas, but an increased ethanol production could be seen towards the end in TNO lignin syngas. With all this, it can be said that the amount of cleaning, and the composition in both TNO beech wood syngas and lignin syngas is sufficient for using the gas as fermentation substrate by *C. ljungdahlii*. Nonetheless, further optimization studies will be needed to achieve a better carbon fixation capacity, as well as to boost productivities, to improve the economical feasibility of the overall process. (Liakakou et al., 2020)

Overall, productivities and overall yields were higher when clean syngas was used, but this cannot be seen as a realistic scenario, especially considering the cost of syngas cleaning processes. Studies performed with impurity-free syngas are necessary and valuable, but it is of great importance for the advance of the syngas fermentation platform to further investigate the effect of biomass-derived syngas, if results are to be applicable in real case scenarios. (Infantes et al., 2020b)

The metabolism of *C. ljungdahlii*, and more generally, that of acetogens, has been said to exist at the thermodynamic limit of life (Schuchmann and Müller, 2014), and is extremely fine-tuned. Perturbations of that balance can have a significant impact on the behavior of the culture, as has been outlined here regarding the complex interactions of the gas pressures with the metabolism of *C. ljungdahlii*. Increasing the pressure of the gaseous substrates to increase its availability is promising, even if not a straight-forward solution. A careful consideration of the components' concentration and determination of the maximum pressure that can be applied without experiencing inhibition must be studied, as well as strategies to adapt the cultures.

Besides, the pressure-resistant bottles used for the 5 bar cultivations proved to be a straightforward system, and a valuable tool for studying the effect of pressures up to 10 bar on batch microbial cultures.

Finally, sequential fermentation as an approach to biologically remove oxygen from waste gas, so that acetogenic fermentation can be subsequently carried out, has proven to have potential for its further optimization and implementation. This system overcomes the challenges of maintaining strict anaerobic conditions throughout the process, and the acetogenic production of value-added chemicals by *C. ljungdahlii* is thus enabled. Moreover, by using *P. thermoglucosidasius*, a thermophilic organism for the first cultivation step, the risk of contamination and the need for cooling the syngas are reduced.

REFERENCES

- Abubackar, H. N., Veiga, M. C., and Kennes, C. (2011). Biological conversion of carbon monoxide: rich syngas or waste gases to bioethanol. *Biofuels, Bioprod. Biorefining* 5, 93–114. DOI:10.1002/bbb.256.
- Abubackar, H. N., Veiga, M. C., and Kennes, C. (2012). Biological conversion of carbon monoxide to ethanol: effect of pH, gas pressure, reducing agent and yeast extract. *Bioresour. Technol.* 114, 518–522. DOI:10.1016/j.biortech.2012.03.027.
- Acharya, B., Roy, P., and Dutta, A. (2014). Review of syngas fermentation processes for bioethanol. *Biofuels* 5, 551–564. DOI:10.1080/17597269.2014.1002996.
- Ahmed, A., Cateni, B. G., Huhnke, R. L., and Lewis, R. S. (2006). Effects of biomass-generated producer gas constituents on cell growth, product distribution and hydrogenase activity of *Clostridium carboxidivorans* P7^T. *Biomass and Bioenergy* 30, 665–672. DOI:10.1016/j.biombioe.2006.01.007.
- Ahmed, A., and Lewis, R. S. (2007). Fermentation of biomass-generated synthesis gas: Effects of nitric oxide. *Biotechnol. Bioeng.* 97, 1080–1086. DOI:10.1002/bit.21305.
- Annan, F. J., Al-Sinawi, B., Humphreys, C. M., Norman, R., Winzer, K., Köpke, M., et al. (2019). Engineering of vitamin prototrophy in *Clostridium ljungdahlii* and *Clostridium autoethanogenum*. *Appl. Microbiol. Biotechnol.* 103, 4633–4648. DOI:10.1007/s00253-019-09763-6.
- Barik, S., Prieto, S., Harrison, S. B., Clausen, E. C., and Gaddy, J. L. (1988). Biological production of alcohols from coal through indirect liquefaction. *Appl. Biochem. Biotechnol.* 18, 363–378. DOI:10.1007/BF02930840.
- Bengelsdorf, F. R., Beck, M. H., Erz, C., Hoffmeister, S., Karl, M. M., Riegler, P., et al. (2018). “Bacterial Anaerobic Synthesis Gas (Syngas) and CO₂ + H₂ Fermentation,” in *Advances in Applied Microbiology*, eds. S. Sariaslani and G. M. Gadd, 143–221. DOI:10.1016/bs.aambs.2018.01.002; ISBN:978-0-12-815183-9.
- Bengelsdorf, F. R., Poehlein, A., Linder, S., Erz, C., Hummel, T., Hoffmeister, S., et al. (2016). Industrial acetogenic biocatalysts: A comparative metabolic and genomic analysis. *Front. Microbiol.* 7, 1036. DOI:10.3389/fmicb.2016.01036.
- Bengelsdorf, F. R., Straub, M., and Dürre, P. (2013). Bacterial synthesis gas (syngas) fermentation. *Environ. Technol.* 34, 1639–1651. DOI:10.1080/09593330.2013.827747.
- Bertsch, J., and Müller, V. (2015). Bioenergetic constraints for conversion of syngas to biofuels in acetogenic bacteria. *Biotechnol. Biofuels* 8, 210. DOI:10.1186/s13068-015-0393-x.
- Biegel, E., and Muller, V. (2010). Bacterial Na⁺-translocating ferredoxin:NAD⁺ oxidoreductase. *PNAS* 107, 18138–18142. DOI:10.1073/pnas.1010318107.
- Biegel, E., Schmidt, S., and Müller, V. (2009). Genetic, immunological and biochemical evidence for a Rnf complex in the acetogen *Acetobacterium woodii*. *Environ. Microbiol.* 11, 1438–1443. DOI:10.1111/j.1462-2920.2009.01871.x.
- Boga, H. I., and Brune, A. (2003). Hydrogen-Dependent Oxygen Reduction by Homoacetogenic Bacteria Isolated from Termite Guts. *Appl. Environ. Microbiol.* 69, 779–786. DOI:10.1128/AEM.69.2.779-786.2003.
- Boyd, C. E. (2015). “pH, Carbon Dioxide, and Alkalinity,” in *Water Quality* (Springer, Cham). DOI:10.1007/978-3-319-17446-4; ISBN:9783319174464.
- Buckel, W., and Thauer, R. K. (2018a). Flavin-Based Electron Bifurcation, A New Mechanism of Biological Energy Coupling. *Chem. Rev.* 118, 3862–3886. DOI:10.1021/acs.chemrev.7b00707.

- Buckel, W., and Thauer, R. K. (2018b). Flavin-based electron bifurcation, ferredoxin, flavodoxin, and anaerobic respiration with protons (Ech) or NAD⁺ (Rnf) as electron acceptors: A historical review. *Front. Microbiol.* 9. DOI:10.3389/fmicb.2018.00401.
- Bustin, S. A., Benes, V., Garson, J. A., Hellems, J., Huggett, J., Kubista, M., et al. (2009). The MIQE Guidelines: Minimum Information for Publication of Quantitative Real-Time PCR Experiments. *Clin. Chem.* 55, 611–622. DOI:10.1373/clinchem.2008.112797.
- Cardarelli, F. (2008). "Gases," in *Materials Handbook* (London: Springer London), 1037–1101. DOI:10.1007/978-1-84628-669-8_19; ISBN:978-1-84628-669-8.
- Carroll, J. J., Slupsky, J. D., and Mather, A. E. (1991). The Solubility of Carbon Dioxide in Water at Low Pressure. *J. Phys. Chem. Ref. Data* 20, 1201–1209. DOI:10.1063/1.555900.
- Cerone, N., Zimbardi, F., Contuzzi, L., Prestipino, M., Carnevale, M. O., and Valerio, V. (2017). Air-steam and oxy-steam gasification of hydrolytic residues from biorefinery. *Fuel Process. Technol.* 167, 451–461. DOI:10.1016/j.fuproc.2017.07.027.
- Chandolias, K., Richards, T., and Taherzadeh, M. J. (2018). *Combined Gasification-Fermentation Process in Waste Biorefinery*. Elsevier B.V. DOI:10.1016/b978-0-444-63992-9.00005-7; ISBN:9780444639929.
- Chiche, D., Diverchy, C., Lucquin, A. C., Porcheron, F., and Defoort, F. (2013). Synthesis Gas Purification. *Oil Gas Sci. Technol. - Rev. d'IFP Energies Nouv.* 68, 707–723. DOI:10.2516/ogst/2013175.
- Chin, B. Y., and Otterbein, L. E. (2009). Carbon monoxide is a poison ... to microbes! CO as a bactericidal molecule. *Curr. Opin. Pharmacol.* 9, 490–500. DOI:10.1016/j.coph.2009.06.025.
- Cotter, J. L., Chinn, M. S., and Grunden, A. M. (2009). Ethanol and acetate production by *Clostridium ljungdahlii* and *Clostridium autoethanogenum* using resting cells. *Bioprocess Biosyst. Eng.* 32, 369–380. DOI:10.1007/s00449-008-0256-y.
- Dahmen, N., Abeln, J., Eberhard, M., Kolb, T., Leibold, H., Sauer, J., et al. (2017). The bioliq process for producing synthetic transportation fuels. *Wiley Interdiscip. Rev. Energy Environ.* 6. DOI:10.1002/wene.236.
- Daniell, J., Köpke, M., and Simpson, S. D. (2012). Commercial biomass syngas fermentation. *Energies* 5, 5372–5417. DOI:10.3390/en5125372.
- Datar, R. P., Shenkman, R. M., Cateni, B. G., Huhnke, R. L., and Lewis, R. S. (2004). Fermentation of biomass-generated producer gas to ethanol. *Biotechnol. Bioeng.* 86, 587–594. DOI:10.1002/bit.20071.
- De Tissera, S., Köpke, M., Simpson, S. D., Humphreys, C., Minton, N. P., and Dürre, P. (2017). "Syngas biorefinery and syngas utilization," in *Biorefineries. Advances in Biochemical Engineering/Biotechnology*, eds. K. Wagemann and N. Tippkötter (Springer, Cham), 247–280. DOI:10.1007/10_2017_5.
- Department of Chemical Engineering, University of Arkansas. High Pressure Synthesis Gas Conversion. Final Report (1993).
- Diekert, G. B., and Thauer, R. K. (1978). Carbon Monoxide Oxidation by *Clostridium thermoaceticum* and *Clostridium formicoaceticum*. *J. Bacteriol.* 136, 597–606. DOI:10.1128/JB.136.2.597-606.1978.
- Diender, M., Stams, A. J. M., and Sousa, D. Z. (2015). Pathways and bioenergetics of anaerobic carbon monoxide fermentation. *Front. Microbiol.* 6, 1–18. DOI:10.3389/fmicb.2015.01275.

- Doukov, T. I., Iverson, T. M., Seravalli, J., Ragsdale, S. W., and Drennan, C. L. (2002). A Ni-Fe-Cu Center in a Bifunctional Carbon Monoxide Dehydrogenase/Acetyl-CoA Synthase. *Science* (80-.). 298, 567–573. DOI:10.1126/science.1075843.
- Drake, H. L., Gößner, A. S., and Daniel, S. L. (2008). Old acetogens, new light. *Ann. N. Y. Acad. Sci.* 1125, 100–128. DOI:10.1196/annals.1419.016.
- Drake, H. L., Küsel, K., and Matthies, C. (2006). “Acetogenic prokaryotes,” in *The prokaryotes, vol. 2 (ecophysiology and biochemistry)*, eds. M. Dworkin, S. Falkow, E. Rosenberg, K.-H. Schleifer, and E. Stackebrandt (New York: Springer New York), 354–420. DOI:10.1007/0-387-30742-7_13; ISBN:978-0-387-30742-8.
- Edenhofer, O., Pichs-Madruga, R., Sokona, Y., Kadner, S., Minx, J. C., Brunner, S., et al. (2014). Technical Summary. In: *Climate Change 2014: Mitigation of Climate Change. Contribution of Working Group III to the Fifth Assessment Report of the Intergovernmental Panel on Climate Change.*, eds. O. Edenhofer, R. Pichs-Madruga, Y. Sokona, E. Farahani, S. Kadner, K. Seyboth, et al. Cambridge University Press, Cambridge, United Kingdom and New York, USA DOI:10.1017/CBO9781107415416.
- Ellis, L. D., Holwerda, E. K., Hogsett, D., Rogers, S., Shao, X., Tschaplinski, T., et al. (2012). Closing the carbon balance for fermentation by *Clostridium thermocellum* (ATCC 27405). *Bioresour. Technol.* 103, 293–299. DOI:10.1016/j.biortech.2011.09.128.
- Emerson, D. F., Woolston, B. M., Liu, N., Donnelly, M., Currie, D. H., and Stephanopoulos, G. (2019). Enhancing hydrogen-dependent growth of and carbon dioxide fixation by *Clostridium ljungdahlii* through nitrate supplementation. *Biotechnol. Bioeng.* 116, 294–306. DOI:10.1002/bit.26847.
- Esquivel-Elizondo, S., Delgado, A. G., Rittmann, B. E., and Krajmalnik-Brown, R. (2017). The effects of CO₂ and H₂ on CO metabolism by pure and mixed microbial cultures. *Biotechnol. Biofuels* 10, 220. DOI:10.1186/s13068-017-0910-1.
- Fernández-Naveira, Á., Veiga, M. C., and Kennes, C. (2017). Effect of pH control on the anaerobic H-B-E fermentation of syngas in bioreactors. *J. Chem. Technol. Biotechnol.* 92, 1178–1185. DOI:10.1002/jctb.5232.
- Fontecilla-Camps, J. C., and Volbeda, A. (2011). CO dehydrogenase/acetyl-CoA synthase. *Encycl. Inorg. Bioinorg. Chem.* DOI:10.1002/9781119951438.eibc0639.
- Friedlingstein, P., Andrew, R. M., Rogelj, J., Peters, G. P., Canadell, J. G., Knutti, R., et al. (2014). Persistent growth of CO₂ emissions and implications for reaching climate targets. *Nat. Geosci.* 7, 709–715. DOI:10.1038/NGEO2248.
- Griffin, D. W., and Schultz, M. A. (2012). Fuel and chemical products from biomass syngas: A comparison of gas fermentation to thermochemical conversion routes. *Environ. Prog. Sustain. Energy* 31, 219–224. DOI:10.1002/ep.11613.
- Groher, A., and Weuster-Botz, D. (2016). Comparative reaction engineering analysis of different acetogenic bacteria for gas fermentation. *J. Biotechnol.* 228, 82–94. DOI:10.1016/j.jbiotec.2016.04.032.
- Hedderich, R., and Forzi, L. (2005). Energy-converting [NiFe] hydrogenases: More than just H₂ activation. *J. Mol. Microbiol. Biotechnol.* 10, 92–104. DOI:10.1159/000091557.
- Heijstra, B. D., Leang, C., and Juminaga, A. (2017). Gas fermentation: cellular engineering possibilities and scale up. *Microb. Cell Fact.* 16:60, 1–11. DOI:10.1186/s12934-017-0676-y.
- Heise, R., Müller, V., and Gottschalk, G. (1993). Acetogenesis and ATP synthesis in *Acetobacterium woodii* are coupled via a transmembrane primary sodium ion gradient. *FEMS Microbiol. Lett.* 112, 261–268. DOI:10.1111/j.1574-6968.1993.tb06460.x.

- Henrich, E., Dahmen, N., Dinjus, E., and Sauer, J. (2015). The role of biomass in a future world without fossil fuels. *Chemie-Ingenieur-Technik* 87, 1667–1685. DOI:10.1002/cite.201500056.
- Henstra, A. M., Sipma, J., Rinzema, A., and Stams, A. J. (2007). Microbiology of synthesis gas fermentation for biofuel production. *Curr. Opin. Biotechnol.* 18, 200–206. DOI:10.1016/j.copbio.2007.03.008.
- Hess, V., Gallegos, R., Jones, J. A., Barquera, B., Malamy, M. H., and Müller, V. (2016). Occurrence of ferredoxin:NAD⁺ oxidoreductase activity and its ion specificity in several Gram-positive and Gram-negative bacteria. *PeerJ* 4. DOI:10.7717/peerj.1515.
- Hu, P., Chakraborty, S., Kumar, A., Woolston, B., Liu, H., Emerson, D., et al. (2016). Integrated bioprocess for conversion of gaseous substrates to liquids. *Proc. Natl. Acad. Sci.* 113, 3773–3778. DOI:10.1073/pnas.1516867113.
- Hu, S., Drake, H. L., and Wood, H. G. (1982). Synthesis of Acetyl Coenzyme A from Carbon Monoxide, Methyltetrahydrofolate, and Coenzyme A by Enzymes from *Clostridium thermoaceticum*. *J. Bacteriol.* 149, 440–448.
- Huang, L. I., Forsberg, C. W., and Gibbins, L. N. (1986). Influence of External pH and Fermentation Products on *Clostridium acetobutylicum* Intracellular pH and Cellular Distribution of Fermentation Products. *Appl. Environ. Microbiol.* 51, 1230–1234.
- Huber, C., Skopan, H., Feicht, R., White, H., and Simon, H. (1995). Pterin cofactor, substrate specificity, and observations on the kinetics of the reversible tungsten-containing aldehyde oxidoreductase from *Clostridium thermoaceticum*. Preparative reductions of a series of carboxylates to alcohols. *Arch. Microbiol.* 164, 110–118. DOI:10.1007/BF02525316.
- Hurst, K. M., and Lewis, R. S. (2010). Carbon monoxide partial pressure effects on the metabolic process of syngas fermentation. *Biochem. Eng. J.* 48, 159–165. DOI:10.1016/j.bej.2009.09.004.
- Hussein, A. H., Lisowska, B. K., and Leak, D. J. (2015). The Genus *Geobacillus* and Their Biotechnological Potential. *Adv. Appl. Microbiol.* 92, 1–48. DOI:10.1016/bs.aambs.2015.03.001.
- Infantes, A., Kugel, M., and Neumann, A. (2020a). Evaluation of media components and process parameters in a sensitive and robust fed-batch syngas fermentation system with *Clostridium ljungdahlii*. *Fermentation* 6, 61. DOI:10.3390/fermentation6020061.
- Infantes, A., Kugel, M., Klaus R., and Neumann, A. (2020b). Side-by-side comparison of clean and biomass-derived, impurity-containing syngas as substrate for acetogenic fermentation with *Clostridium ljungdahlii*. *Fermentation* 6, 84. DOI: 10.3390/fermentation6030084.
- Jack, J., Lo, J., Maness, P. C., and Ren, Z. J. (2019). Directing *Clostridium ljungdahlii* fermentation products via hydrogen to carbon monoxide ratio in syngas. *Biomass and Bioenergy* 124, 95–101. DOI:10.1016/j.biombioe.2019.03.011.
- Karnholz, A., Küsel, K., Gößner, A., Schramm, A., and Drake, H. L. (2002). Tolerance and metabolic response of acetogenic bacteria toward oxygen. *Appl. Environ. Microbiol.* 68, 1005–1009. DOI:10.1128/AEM.68.2.1005-1009.2002.
- Kennes, D., Abubakar, H. N., Díaz, M., Veiga, M. C., and Kennes, C. (2016). Bioethanol production from biomass: Carbohydrate vs syngas fermentation. *J. Chem. Technol. Biotechnol.* 91, 304–317. DOI:10.1002/jctb.4842.
- King, G. M., and Weber, C. F. (2007). Distribution, diversity and ecology of aerobic CO-oxidizing bacteria. *Nat. Rev. Microbiol.* 5, 107–118. DOI:10.1038/nrmicro1595.
- Klasson, K. T., Ackerson, M. D., Clausen, E. C., and Gaddy, J. L. (1993). Biological conversion of coal and coal-derived synthesis gas. *Fuel* 72, 1673–1678. DOI:10.1016/0016-2361(93)90354-5.

- Klasson, K. T. T., Ackerson, M. D. D., Clausen, E. C. C., and Gaddy, J. L. L. (1991). Bioreactor design for synthesis gas fermentations. *Fuel* 70, 605–614. DOI:10.1016/0016-2361(91)90174-9.
- Köpke, M., Held, C., Hujer, S., Liesegang, H., Wiezer, A., Wollherr, A., et al. (2010). *Clostridium ljungdahlii* represents a microbial production platform based on syngas. *Proc. Natl. Acad. Sci.* 107, 13087–13092. DOI:10.1073/PNAS.1004716107.
- Köpke, M., Mihalcea, C., Bromley, J. C., and Simpson, S. D. (2011). Fermentative production of ethanol from carbon monoxide. *Curr. Opin. Biotechnol.* 22, 320–325. DOI:10.1016/j.copbio.2011.01.005.
- Kumara Behera, B., and Varma, A. (2017). *Material-Balance Calculation of Fermentation Processes BT - Microbial Biomass Process Technologies and Management*. DOI:10.1007/978-3-319-53913-3_5; ISBN:978-3-319-53913-3.
- Kundiyan, D. K., Wilkins, M. R., Maddipati, P., and Huhnke, R. L. (2011). Effect of temperature, pH and buffer presence on ethanol production from synthesis gas by “*Clostridium ragsdalei*”. *Bioresour. Technol.* 102, 5794–5799. DOI:10.1016/j.biortech.2011.02.032.
- Küsel, K., Karnholz, A., Trinkwalter, T., Devereux, R., Acker, G., and Drake, H. L. (2001). Physiological Ecology of *Clostridium glycolicum* RD-1, an Aerotolerant Acetogen Isolated from Sea Grass Roots. *Appl. Environ. Microbiol.* 67, 4734–4741. DOI:10.1128/AEM.67.10.4734-4741.2001.
- LanzaTech (2018). World’s First Commercial Waste Gas to Ethanol Plant Starts Up | LanzaTech. Available at: <https://www.lanzatech.com/2018/06/08/worlds-first-commercial-waste-gas-ethanol-plant-starts/> [Accessed February 27, 2020].
- Lee, S. Y., Park, J. H., Jang, S. H., Nielsen, L. K., Kim, J., and Jung, K. S. (2008). Fermentative Butanol Production by Clostridia. *Biotechnol. Bioeng.* 101, 209–228. DOI:10.1002/bit.22003.
- Liakakou, E. T., Infantes, A., Neumann, A., and Vreugdenhil, B. J. (2020). Connecting lignin gasification with syngas fermentation. (Submitted). PREPRINT *enrXiv*. DOI:10.31224/osf.io/9f5pj.
- Liakakou, E. T., Vreugdenhil, B. J., Cerone, N., Zimbardi, F., Pinto, F., André, R., et al. (2019). Gasification of lignin-rich residues for the production of biofuels via syngas fermentation: Comparison of gasification technologies. *Fuel* 251, 580–592. DOI:10.1016/j.fuel.2019.04.081.
- Liew, F., Henstra, A. M., Köpke, M., Winzer, K., Simpson, S. D., and Minton, N. P. (2017). Metabolic engineering of *Clostridium autoethanogenum* for selective alcohol production. *Metab. Eng.* 40, 104–114. DOI:10.1016/j.ymben.2017.01.007.
- Liew, F. M., Köpke, M., and Simpson, S. D. (2013). Gas Fermentation for Commercial Biofuels Production. *Liq. Gaseous Solid Biofuels - Convers. Tech.*, 125–173. DOI:10.5772/52164.
- Liew, F. M., Martin, M. E., Tappel, R. C., Heijstra, B. D., Mihalcea, C., and Köpke, M. (2016). Gas Fermentation – A Flexible Platform for Commercial Scale Production of Low-Carbon-Fuels and Chemicals from Waste and Renewable Feedstocks. *Front. Microbiol.* 7:694. DOI:10.3389/fmicb.2016.00694.
- Liu, J., Tan, Y., Yang, X., Chen, X., and Li, F. (2013). Evaluation of *Clostridium ljungdahlii* DSM 13528 reference genes in gene expression studies by qRT-PCR. *J. Biosci. Bioeng.* 116, 460–464. DOI:10.1016/j.jbiosc.2013.04.011.
- McGlade, C., and Ekins, P. (2015). The geographical distribution of fossil fuels unused when limiting global warming to 2 °C. *Nature* 517, 187–190. DOI:10.1038/nature14016.
- McKendry, P. (2002). Energy production from biomass (part 3): gasification technologies. *Bioresour. Technol.* 83, 55–63. DOI:10.1016/S0960-8524(01)00120-1.

- Mock, J., Zheng, Y., Mueller, A. P., Ly, S., Tran, L., Segovia, S., et al. (2015). Energy conservation associated with ethanol formation from H₂ and CO₂ in *Clostridium autoethanogenum* involving electron bifurcation. *J. Bacteriol.* 197, 2965–2980. DOI:10.1128/JB.00399-15.
- Mohammadi, M., Mohamed, A. R., Najafpour, G. D., Younesi, H., and Uzir, M. H. (2014). Kinetic studies on fermentative production of biofuel from synthesis gas using *Clostridium ljungdahlii*. *Sci. World J.* 2014. DOI:10.1155/2014/910590.
- Mohammadi, M., Najafpour, G. D., Younesi, H., Lahijani, P., Uzir, M. H., and Mohamed, A. R. (2011). Bioconversion of synthesis gas to second generation biofuels: A review. *Renew. Sustain. Energy Rev.* 15, 4255–4273. DOI:10.1016/j.rser.2011.07.124.
- Mohr, T., Aliyu, H., Küchlin, R., Polliack, S., Zwick, M., Neumann, A., et al. (2018a). CO-dependent hydrogen production by the facultative anaerobe *Parageobacillus thermoglucosidasius*. *Microb. Cell Fact.* 17:108. DOI:10.1186/s12934-018-0954-3.
- Mohr, T., Aliyu, H., Küchlin, R., Zwick, M., Cowan, D., Neumann, A., et al. (2018b). Comparative genomic analysis of *Parageobacillus thermoglucosidasius* strains with distinct hydrogenogenic capacities. *BMC Genomics* 19:880. DOI:10.1186/s12864-018-5302-9.
- Mohr, T., Infantes, A., Biebinger, L., de Maayer, P., and Neumann, A. (2019). Acetogenic Fermentation From Oxygen Containing Waste Gas. *Front. Bioeng. Biotechnol.* 7, 433. DOI:10.3389/fbioe.2019.00433.
- Monir, M. U., Yousuf, A., and Aziz, A. A. (2020). "Syngas fermentation to bioethanol," in *Lignocellulosic Biomass to Liquid Biofuels*, eds. A. Yousuf, D. Pirozzi, and F. Sannino (Academic Press), 195–216. DOI:10.1016/b978-0-12-815936-1.00006-x; ISBN:9780128159361.
- Müller, V. (2003). Energy Conservation in Acetogenic Bacteria. *Appl. Environ. Microbiol.* 69, 6345–6353. DOI:10.1128/AEM.69.11.6345-6353.2003.
- Munasinghe, P. C., and Khanal, S. K. (2011). Biomass-derived syngas fermentation into biofuels: Opportunities and challenges. *Biofuels* 101, 79–98. DOI:10.1016/B978-0-12-385099-7.00004-8.
- Nagarajan, H., Sahin, M., Nogales, J., Latif, H., Lovley, D. R., Ebrahim, A., et al. (2013). Characterizing acetogenic metabolism using a genome-scale metabolic reconstruction of *Clostridium ljungdahlii*. *Microb. Cell Fact.* 12:118. DOI:10.1186/1475-2859-12-118.
- Najafpour, G., and Younesi, H. (2006). Ethanol and acetate synthesis from waste gas using batch culture of *Clostridium ljungdahlii*. *Enzyme Microb. Technol.* 38, 223–228. DOI:10.1016/j.enzmictec.2005.06.008.
- Napora-Wijata, K., Strohmeier, G. A., and Winkler, M. (2014). Biocatalytic reduction of carboxylic acids. *Biotechnol. J.* 9, 822–843. DOI:10.1002/biot.201400012.
- Oswald, F. (2018). Upgrading the toolbox for fermentation of crude syngas: Process characterization for complete carbon usage, cyanide adaption and production of C₄ components. Dissertation. Karlsruhe Institute for Technology, BLT II: Technical Biology.
- Oswald, F., Dörsam, S., Veith, N., Zwick, M., Neumann, A., Ochsenreither, K., et al. (2016). Sequential Mixed Cultures: From Syngas to Malic Acid. *Front. Microbiol.* 7, 1–12. DOI:10.3389/fmicb.2016.00891.
- Oswald, F., Stoll, I. K., Zwick, M., Herbig, S., Sauer, J., Boukis, N., et al. (2018a). Formic Acid Formation by *Clostridium ljungdahlii* at Elevated Pressures of Carbon Dioxide and Hydrogen. *Front. Bioeng. Biotechnol.* 6. DOI:10.3389/fbioe.2018.00006.
- Oswald, F., Zwick, M., Omar, O., Hotz, E. N., and Neumann, A. (2018b). Growth and product formation of *Clostridium ljungdahlii* in presence of cyanide. *Front. Microbiol.* 9:1213. DOI:10.3389/fmicb.2018.01213.

- Perez, J. M., Richter, H., Loftus, S. E., and Angenent, L. T. (2013). Biocatalytic reduction of short-chain carboxylic acids into their corresponding alcohols with syngas fermentation. *Biotechnol. Bioeng.* 110, 1066–1077. DOI:10.1002/bit.24786.
- Pfaffl, M. W. (2001). A new mathematical model for relative quantification in real-time RT-PCR. *Nucleic Acids Res.* 29, 45e – 45. DOI:10.1093/nar/29.9.e45.
- Pfaffl, M. W. (2007). “Relative quantification,” in *Real-time PCR*, ed. M Tefvik Dorak (London: Taylor & Francis), 63–82. DOI:10.4324/9780203967317; ISBN:10.4324/9780203967317.
- Phillips, J. R., Clausen, E. C., and Gaddy, J. L. (1994). Synthesis gas as substrate for the biological production of fuels and chemicals. *Appl. Biochem. Biotechnol.* 45–46, 145–157. DOI:10.1007/BF02941794.
- Phillips, J. R., Huhnke, R. L., and Atiyeh, H. K. (2017). Syngas Fermentation: A Microbial Conversion Process of Gaseous Substrates to Various Products. *Fermentation* 3, 28. DOI:10.3390/fermentation3020028.
- Phillips, J. R., Klasson, K. T., Clausen, E. C., and Gaddy, J. L. (1993). Biological production of ethanol from coal synthesis gas - Medium development studies. *Appl. Biochem. Biotechnol.* 39, 559–571. DOI:10.1007/BF02919018.
- Ragsdale, S. W. (1991). Enzymology of the Acetyl-coA pathway of CO₂ fixation. *Crit. Rev. Biochem. Mol. Biol.* 26, 261–300. DOI:10.3109/10409239109114070.
- Ragsdale, S. W. (2008). Enzymology of the Wood-Ljungdahl pathway of acetogenesis. *Ann. N. Y. Acad. Sci.* 1125, 129–136. DOI:10.1196/annals.1419.015.
- Ragsdale, S. W., and Wood, H. G. (1985). Acetate biosynthesis by acetogenic bacteria. Evidence that carbon monoxide dehydrogenase is the condensing enzyme that catalyzes the final steps of the synthesis. *J. Biol. Chem.* 260, 3970–3977.
- Ramachandriya, K. D., Kundiyana, D. K., Sharma, A. M., Kumar, A., Atiyeh, H. K., Huhnke, R. L., et al. (2016). Critical factors affecting the integration of biomass gasification and syngas fermentation technology. *AIMS Bioeng.* 3, 188–210. DOI:10.3934/bioeng.2016.2.188.
- Rauch, R., Hrbek, J., and Hofbauer, H. (2013). Biomass Gasification for Synthesis Gas Production and Applications of the Syngas. *WIREs Energy Environ.* 3. DOI:10.1002/wene.97.
- Richter, H., Martin, M. E., and Angenent, L. T. (2013). A two-stage continuous fermentation system for conversion of syngas into ethanol. *Energies* 6, 3987–4000. DOI:10.3390/en6083987.
- Richter, H., Molitor, B., Wei, H., Chen, W., Aristilde, L., and Angenent, L. T. (2016). Ethanol production in syngas-fermenting *Clostridium ljungdahlii* is controlled by thermodynamics rather than by enzyme expression. *Energy Environ. Sci.* 9, 2392–2399. DOI:10.1039/C6EE01108J.
- Riedel, G., Rüdrieh, U., Fekete-Drimusz, N., Manns, M. P., Vondran, F. W. R., and Bock, M. (2014). An Extended Δ CT-Method Facilitating Normalisation with Multiple Reference Genes Suited for Quantitative RT-PCR Analyses of Human Hepatocyte-Like Cells. *PLoS One* 9. DOI:10.1371/journal.pone.0093031.
- Roger, M., Brown, F., Gabrielli, W., and Sargent, F. (2018). Efficient Hydrogen-Dependent Carbon Dioxide Reduction by *Escherichia coli*. *Curr. Biol.* DOI:10.1016/j.cub.2017.11.050.
- Sander, R. (2015). Compilation of Henry’s law constants (version 4.0) for water as solvent. *Atmos. Chem. Phys.* 15, 4399–4981. DOI:10.5194/acp-15-4399-2015.
- Saxena, J., and Tanner, R. S. (2012). Optimization of a corn steep medium for production of ethanol from synthesis gas fermentation by *Clostridium ragsdalei*. *World J. Microbiol. Biotechnol.* 28, 1553–1561. DOI:10.1007/s11274-011-0959-0.

- Schink, B. (1994). "Diversity, Ecology, and Isolation of Acetogenic Bacteria," in *Acetogenesis. Chapman & Hall Microbiology Series (Physiology / Ecology / Molecular Biology / Biotechnology)*, ed. H. L. Drake (Boston, MA: Springer), 197–235. DOI:10.1007/978-1-4615-1777-1_7.
- Schoelmerich, M. C., and Müller, V. (2019). Energy conservation by a hydrogenase-dependent chemiosmotic mechanism in an ancient metabolic pathway. *Proc. Natl. Acad. Sci. U. S. A.* 116, 6329–6334. DOI:10.1073/pnas.1818580116.
- Schoelmerich, M. C., and Müller, V. (2020). Energy-converting hydrogenases: the link between H₂ metabolism and energy conservation. *Cell. Mol. Life Sci.* 77, 1461–1481. DOI:10.1007/s00018-019-03329-5.
- Schuchmann, K., and Müller, V. (2014). Autotrophy at the thermodynamic limit of life: a model for energy conservation in acetogenic bacteria. *Nat. Rev. Microbiol.* 12, 809–821. DOI:10.1038/nrmicro3365.
- Shen, B. W., Dyer, D. H., Huang, J.-Y., D'Ari, L., Rabinowitz, J., and Stoddard, B. L. (1999). The crystal structure of a bacterial, bifunctional 5,10 methylene-tetrahydrofolate dehydrogenase/cyclohydrolase. *Protein Sci.* 8, 1342–1349. DOI:10.1110/ps.8.6.1342.
- Sikarwar, V. S., Zhao, M., Clough, P., Yao, J., Zhong, X., Memon, M. Z., et al. (2016). An overview of advances in biomass gasification. *Energy Environ. Sci.* 9, 2939–2977. DOI:10.1039/c6ee00935b.
- Sim, J. H., and Kamaruddin, A. H. (2008). Optimization of acetic acid production from synthesis gas by chemolithotrophic bacterium – *Clostridium acetivum* using statistical approach. *Bioresour. Technol.* 99, 2724–2735. DOI:10.1016/j.biortech.2007.07.004.
- Sim, J. H., Kamaruddin, A. H., Long, W. S., and Najafpour, G. (2007). *Clostridium acetivum* - A potential organism in catalyzing carbon monoxide to acetic acid: Application of response surface methodology. *Enzyme Microb. Technol.* 40, 1234–1243. DOI:10.1016/j.enzmictec.2006.09.017.
- Skidmore, B. E., Baker, R. A., Banjade, D. R., Bray, J. M., Tree, D. R., and Lewis, R. S. (2013). Syngas fermentation to biofuels: Effects of hydrogen partial pressure on hydrogenase efficiency. *Biomass and Bioenergy.* DOI:10.1016/j.biombioe.2013.01.034.
- Sprott, G. D., Jarrell, K. F., Shaw, K. M., and Knowles, R. (1982). Acetylene as an inhibitor of methanogenic bacteria. *J. Gen. Microbiol.* 128, 2453–2462. DOI:10.1099/00221287-128-10-2453.
- Stoll, K. I., Boukis, N., and Sauer, J. (2019). Syngas Fermentation At Elevated Pressure - Experimental Results. *Biomass Convers. Technol. Energy Carriers, Chem. Mater.*, 1255–1261. DOI:10.5071/27thEUBCE2019-3CV.3.4.
- Straub, M. (2012). Fermentative Acetatproduktion durch Homoacetat-Gärung bzw. Acetatbildung. Dissertation. University of Ulm, Institute for Microbiology and Biotechnology.
- Sun, X., Atiyeh, H. K., Huhnke, R. L., and Tanner, R. S. (2019). Syngas fermentation process development for production of biofuels and chemicals: A review. *Bioresour. Technol. Reports* 7. DOI:10.1016/j.biteb.2019.100279.
- Takors, R., Kopf, M., Mampel, J., Bluemke, W., Blombach, B., Eikmanns, B., et al. (2018). Using gas mixtures of CO, CO₂ and H₂ as microbial substrates: the do's and don'ts of successful technology transfer from laboratory to production scale. *Microb. Biotechnol.* 11, 606–625. DOI:10.1111/1751-7915.13270.
- Tanner, R. S. (2007). "Cultivation of Bacteria and Fungi," in *Manual of Environmental Microbiology, Third Edition*, eds. C. Hurst, R. Crawford, J. Garland, D. Lipson, A. Mills, and L. Stetzenbach (ASM Press, Washington, DC), 69–78. DOI:10.1128/9781555815882.ch6.

- Tanner, R. S., Miller, L. M., and Yang, D. (1993). *Clostridium ljungdahlii* sp. nov., an acetogenic species in clostridial rRNA homology group I. *Int. J. Syst. Bacteriol.* 43, 232–236. DOI:10.1099/00207713-43-2-232.
- Taymaz-Nikerel, H., Borujeni, A. E., Verheijen, P. J. T., Heijnen, J. J., and van Gulik, W. M. (2010). Genome-Derived Minimal Metabolic Models for *Escherichia coli* MG1655 With Estimated In Vivo Respiratory ATP Stoichiometry. *Biotechnol. Bioeng.* 107, 369–381. DOI:10.1002/bit.22802.
- Teixeira, L. V., Moutinho, L. F., and Romão-Dumaresq, A. S. (2018). Gas fermentation of C1 feedstocks: commercialization status and future prospects. *Biofuels, Bioprod. Biorefining* 12, 1103–1117. DOI:10.1002/bbb.1912.
- Terracciano, J. S., and Kashket, E. R. (1986). Intracellular conditions required for initiation of solvent production by *Clostridium acetobutylicum*. *Appl. Environ. Microbiol.* 52, 86–91. DOI:10.1128/aem.52.1.86-91.1986.
- Tirado-Acevedo, O., L. Cotter, J., S. Chinn, M., and M. Grunden, A. (2011). Influence of carbon source pre-adaptation on *Clostridium ljungdahlii* growth and product formation. *J. Bioprocess. Biotech.* 01, 1–5. DOI:10.4172/2155-9821.s2-001.
- Tremblay, P.-L., Zhang, T., Dar, S. A., Leang, C., and Lovley, D. R. (2012). The Rnf Complex of *Clostridium ljungdahlii* Is a Proton-Translocating Ferredoxin:NAD⁺ Oxidoreductase Essential for Autotrophic Growth. *MBio* 4, 1–8. DOI:10.1128/mBio.00406-12.
- Valgepea, K., de Souza Pinto Lemgruber, R., Abdalla, T., Binos, S., Takemori, N., Takemori, A., et al. (2018). H₂ drives metabolic rearrangements in gas-fermenting *Clostridium autoethanogenum*. *Biotechnol. Biofuels* 11, 1–15. DOI:10.1186/s13068-018-1052-9.
- Valgepea, K., de Souza Pinto Lemgruber, R., Meaghan, K., Palfreyman, R. W., Abdalla, T., Heijstra, B. D., et al. (2017a). Maintenance of ATP Homeostasis Triggers Metabolic Shifts in Gas-Fermenting Acetogens. *Cell Syst.* 4, 505-515.e5. DOI:10.1016/j.cels.2017.04.008.
- Valgepea, K., Loi, K. Q., Behrendorff, J. B., Lemgruber, R. de S. P., Plan, M., Hodson, M. P., et al. (2017b). Arginine deiminase pathway provides ATP and boosts growth of the gas-fermenting acetogen *Clostridium autoethanogenum*. *Metab. Eng.* 41, 202–211. DOI:10.1016/j.ymben.2017.04.007.
- Vandesompele, J., De Preter, K., Pattyn, I., Poppe, B., Van Roy, N., De Paepe, A., et al. (2002). Accurate normalization of real-time quantitative RT-PCR data by geometric averaging of multiple internal control genes. *Genome Biol.* 3. DOI:10.1186/gb-2002-3-7-research0034.
- Vega, J. L., Clausen, E. C., and Gaddy, J. L. (1989a). Study of Gaseous Substrate Fermentations: Carbon Monoxide Conversion to Acetate. 1. Batch Culture. *Biotechnol. Bioeng.* 34, 774–784. DOI:10.1002/bit.260340608.
- Vega, J. L., Prieto, S., Elmore, B. B., Clausen, E. C., and Gaddy, J. L. (1989b). The Biological Production of Ethanol from Synthesis Gas. *Appl. Biochem. Biotechnol.* 20–21, 781–797. DOI:10.1007/BF02936525.
- Wang, D., Wright, H. A., Ortego, B. C., Trinh, S., and Espinoza, R. (2006). Selective Removal of Oxygen from Syngas. US006992112B2.
- Wang, S., Huang, H., Kahnt, H. H., Mueller, A. P., Köpke, M., and Thauer, R. K. (2013). NADP-specific electron-bifurcating [FeFe]-hydrogenase in a functional complex with formate dehydrogenase in *Clostridium autoethanogenum* grown on CO. *J. Bacteriol.* 195, 4373–4386. DOI:10.1128/JB.00678-13.

- Wareham, L. K., Jesse, H. E., Beilen, J. W. A. Van, Ali, S., Svistunenko, D., Begg, R., et al. (2016). Carbon Monoxide Gas Is Not Inert, but Global, in Its Consequences for Bacterial Gene Expression, Iron Acquisition, and Antibiotic Resistance. *Antioxid. Redox Signal.* 24, 1013–1028. DOI:10.1089/ars.2015.6501.
- Whitham, J. M., Pawlak, J. J., and M. Grunden, A. (2016). *Clostridium ljungdahlii*: A Review of the Development of an Industrial Biocatalyst. *Curr. Biotechnol.* 5, 54–70. DOI:10.2174/2211550105666151208211335.
- Wiechmann, A., and Müller, V. (2019). “Synthesis of Acetyl-CoA from Carbon Dioxide in Acetogenic Bacteria,” in *Biogenesis of Fatty Acids, Lipids and Membranes. Handbook of Hydrocarbon and Lipid Microbiology.*, ed. O. Geiger (Springer, Cham), 25–42. DOI:10.1007/978-3-319-50430-8_4; ISBN:9783319504308.
- Worden, R. M., Grethlein, A. J., Jain, M. K., and Datta, R. (1991). Production of butanol and ethanol from synthesis gas via fermentation. *Fuel* 70, 615–619. DOI:10.1016/0016-2361(91)90175-A.
- Xie, B. T., Liu, Z. Y., Tian, L., Li, F. L., and Chen, X. H. (2015). Physiological response of *Clostridium ljungdahlii* DSM 13528 of ethanol production under different fermentation conditions. *Bioresour. Technol.* 177, 302–307. DOI:10.1016/j.biortech.2014.11.101.
- Xu, D., and Lewis, R. S. (2012). Syngas fermentation to biofuels: Effects of ammonia impurity in raw syngas on hydrogenase activity. *Biomass and Bioenergy* 45, 303–310. DOI:10.1016/j.biombioe.2012.06.022.
- Xu, D., Tree, D. R., and Lewis, R. S. (2011). The effects of syngas impurities on syngas fermentation to liquid fuels. *Biomass and Bioenergy* 35, 2690–2696. DOI:10.1016/j.biombioe.2011.03.005.
- Yan, Q., Wan, C., Street, J., Yan, D. W., Han, J., and Yu, F. (2013). Catalytic removal of oxygen from biomass-derived syngas. *Bioresour. Technol.* 147, 117–123. DOI:10.1016/j.biortech.2013.08.036.
- Yasin, M., Cha, M., Chang, I. S., Atiyeh, H. K., Munasinghe, P., and Khanal, S. K. (2019). “Syngas Fermentation Into Biofuels and Biochemicals,” in *Biofuels: Alternative Feedstocks and Conversion Processes for the Production of Liquid and Gaseous Biofuels*, eds. A. Pandey, C. Larroche, C.-G. Dussap, E. Gnansounou, S. K. Khanal, and S. Ricke (Cambridge, Massachusetts: Academic Press), 301–327. DOI:10.1016/b978-0-12-816856-1.00013-0; ISBN:9780128168561.
- Younesi, H., Najafpour, G., and Mohamed, A. R. (2005). Ethanol and acetate production from synthesis gas via fermentation processes using anaerobic bacterium, *Clostridium ljungdahlii*. *Biochem. Eng. J.* 27, 110–119. DOI:10.1016/j.bej.2005.08.015.
- Zeigler, D. R. (2001). “Volume 3: The Genus *Geobacillus*,” in *Bacillus Genetic Stock Center Catalog of Strains* (Ohio: The *Bacillus* Genetic Stock Center).
- Zhu, H.-F., Liu, Z.-Y., Zhou, X., Yi, J.-H., Lun, Z.-M., Wang, S.-N., et al. (2020). Energy Conservation and Carbon Flux Distribution During Fermentation of CO or H₂/CO₂ by *Clostridium ljungdahlii*. *Front. Microbiol.* 11, 416. DOI:10.3389/fmicb.2020.00416.
- Zorin, N. A., Dimon, B., Gagnon, J., Gaillard, J., Carrier, P., and Vignais, P. M. (1996). Inhibition by Iodoacetamide and Acetylene of the H-D-Exchange Reaction Catalyzed by Thiocapsa Roseopersicina Hydrogenase. *Eur. J. Biochem.* 241, 675–681. DOI:10.1111/j.1432-1033.1996.00675.x.

LIST OF FIGURES

Figure 2.1 – Representation of the metabolism of the model acetogen <i>C. ljungdahlii</i>	8
Figure 2.2 – Schematic representation of the biorefinery concept, from biomass to product via syngas fermentation.....	14
Figure 3.1 – 1 L bottle (left) and Ace Glass pressure flasks with pressure gauge attached (right).....	35
Figure 4.1 – Growth and product formation of setup 1 (A), setup 3 with increased cysteine (B) and setup 4 with increased yeast extract (C).....	43
Figure 4.2 – Substrate usage or fixation for setup 1 (A), setup 3 with increased cysteine (B) and setup 4 with increased yeast extract (C).....	44
Figure 4.3 – Growth, pH profile and product formation of setup 2 without pH regulation (A), setup 3b with increased cysteine and pH change to 5.4 after 68 h (B) and setup 5 with pH allowed to drop to 4.8 after 24 h (C).	49
Figure 4.4 – Substrate usage or fixation for setup 2 without pH regulation (A), setup 3b with increased cysteine and pH change to 5.4 after 68 h (B and C) and setup 5 with pH allowed to drop to 4.8 after 24 h (D).....	50
Figure 4.5 – Growth, pH profile and product formation of setup 6 with pH allowed to drop to 4.8 and gas flow decreased to 12.6 mL/min after 24 h.	52
Figure 4.6 – Substrate usage or fixation for setup 6, where pH was allowed to drop to 4.8 and gas flow was decreased to 12.6 mL/min after 24 h (grey dotted vertical line).	53
Figure 4.7 – Amount of substance flow rate in the off-gas for beech wood syngas.	58
Figure 4.8 – Substrate usage or fixation for beech wood syngas.	58
Figure 4.9 – Growth and product formation profiles for beech wood syngas.	61
Figure 4.10 – Amount of substance flow rate in the off-gas for lignin syngas.	64
Figure 4.11 – Substrate usage or fixation for lignin syngas.	65
Figure 4.12 – Growth and product formation profiles for lignin syngas.	66
Figure 4.13 – Substrate usage and fixation for setups 1 to 10.	72
Figure 4.14 – Off-gas profile for setups 1 to 10.	73
Figure 4.15 – Growth and product formation of setups 1 to 10.....	76
Figure 4.16 – End-point productivity for pairs of real and clean syngases.....	86
Figure 4.17 – Productivity up to the end of maximum CO fixation for pairs of real and clean syngases.	87
Figure 4.18 – Molar acetate to ethanol ratio for pairs of real and clean syngases.	87
Figure 4.19 – Molar acetate to ethanol ratio obtained from each combination of tested CO, CO ₂ and H ₂ molar substrate flow rate for clean syngases.	89
Figure 4.20 – Pressure profile for each setup throughout the experiment.....	96
Figure 4.21 – Growth and product formation profiles at different syngas pressures.....	99
Figure 4.22 – Pressure profile for each setup grown with CO ₂ /H ₂ throughout the experiment.	100
Figure 4.23 –Growth and product formation profiles at different CO ₂ /H ₂ pressures.	102
Figure 4.24 – Pressure profile for each setup grown with CO ₂ /H ₂ throughout the experiment.	103
Figure 4.25 – Growth and product formation profiles at different CO pressures.....	105
Figure 4.26 – Relative gene expression (fold change) in the pressure-treated culture at 5 bar.	106
Figure 4.27 – Growth and pH (A) and gas composition and acetate production (B) of the sequential cultivation of <i>P. thermoglucosidasius</i> and <i>C. ljungdahlii</i>	108
Figure 5.1 – Effect of increased CO ₂ and H ₂ pressure on the acetogenic metabolism.....	126

LIST OF TABLES

Table 2.1 – Possible stoichiometric coefficients for the production of acetate and ethanol from syngas according to Equations (2.12) and (2.13).....	13
Table 2.2 – Typical dry syngas composition for oxygen and steam gasification of biomass.	15
Table 3.1 – Experimental setup.	27
Table 3.2 – Average composition of the gas and flow rate for TNO BWS and LS.....	28
Table 3.3 – Composition of the gas, flow rate and amount of substance fed for each setup.....	30
Table 3.4 – Primer sequence for cooC2 (CLJU_c37660).	37
Table 4.1 Gas consumption profiles.....	42
Table 4.2 – Fermentation outcomes, yields, and productivities at the endpoint.	45
Table 4.3 – Fermentation outcomes, yields, and productivities calculated up to the point when maximum CO fixation stopped.	46
Table 4.4 – Carbon balance for each entire run.	54
Table 4.5 – Average composition of the gas and flow rate for TNO BWS and LS.....	55
Table 4.6 – Gas consumption profile, fermentation outcomes, yields, and productivities for the beech wood syngas.....	59
Table 4.7 – Gas consumption profile, fermentation outcomes, yields, and productivities for the lignin syngas.....	62
Table 4.8 – Composition of the gas, flow rate and amount of substance fed for each setup.....	68
Table 4.9 – Fermentation outcomes, yields, and productivities for the complete run.....	70
Table 4.10 – Fermentation outcomes, yields, and productivities calculated up to the point when maximum CO fixation stopped.	71
Table 4.11 – Gas consumption profiles.....	78
Table 4.12 – Amount of substance flow fed, and ratios of fed, used and fixed substrates for the medium components and process parameters evaluation fermentations.	91
Table 4.13 – Amount of substance flow fed, and ratios of fed, used and fixed substrates for the fermentations evaluating the impact of syngas composition and impurities.	92
Table 4.14 – Amount of acetate and ethanol produced, compared to the theoretical maximum, for the fermentations evaluating the medium components and process parameters influence.	94
Table 4.15 – Amount of acetate and ethanol produced, compared to the theoretical maximum for the fermentations evaluating the impact of syngas composition and impurities.	95
Table 4.16 – Specific growth rate μ for each syngas pressure treatment and control.....	97

APPENDIX

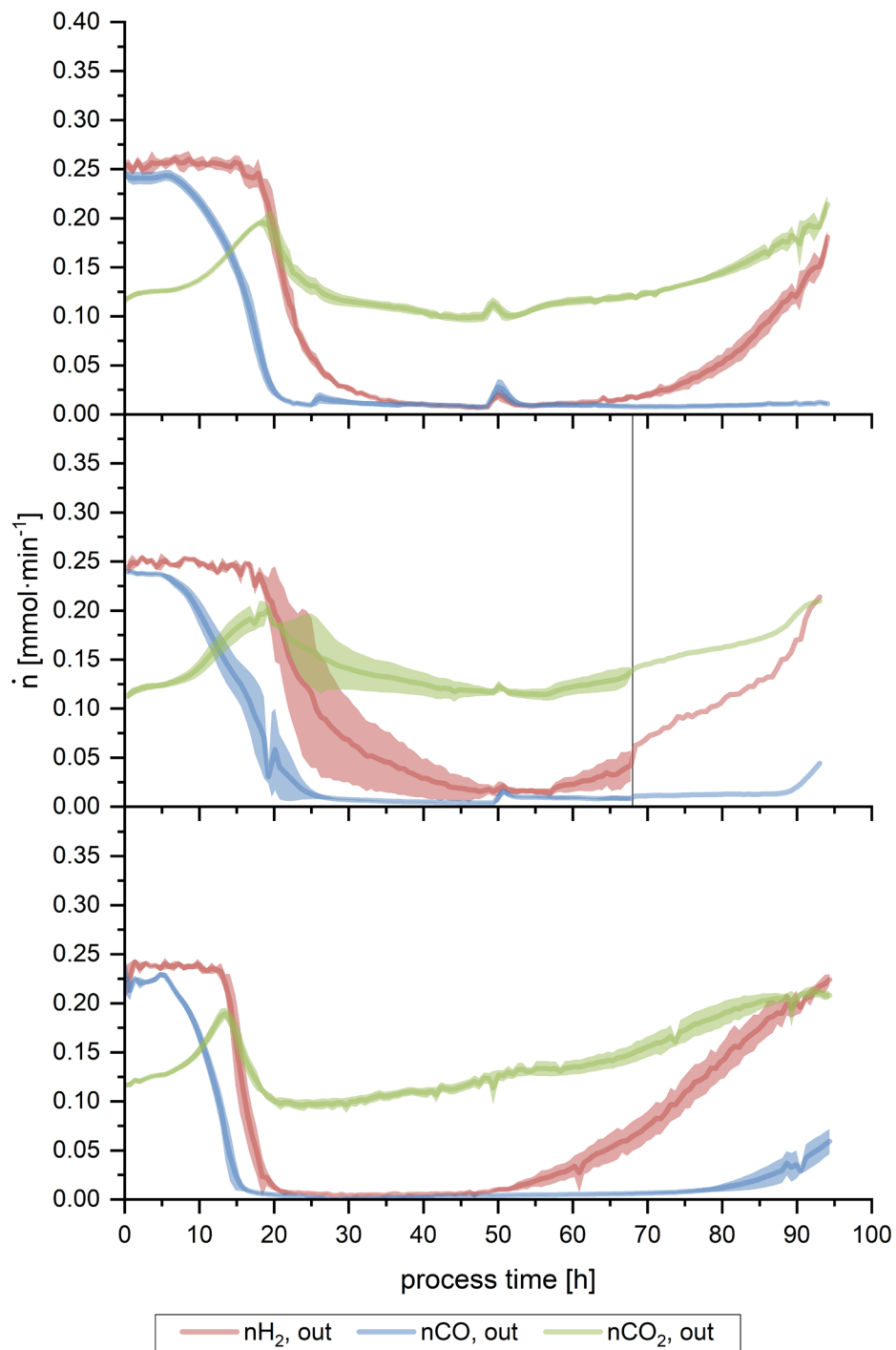


Figure A.I – Off-gas profile for the standard setup 1 (A), setup 3 with increased cysteine (B) and setup 4 with increased yeast extract (C). Figure B shows setup 3b up to 68 h (point where pH was changed, marked with vertical line). One fermenter has been left out of the averages due to being remarkably delayed in comparison with the other two. After 68 h, it shows setup 3a, where one fermenter was kept at pH 5.9.. The amount of substance flow rates is shown here, as obtained from the measurements of the on-line GC, for H₂ (red line), CO₂ (green line) and CO (blue line). Lines show the average of a triplicate (except for Figure B), while the lighter colored areas depict the standard deviation. (Infantes et al., 2020a)

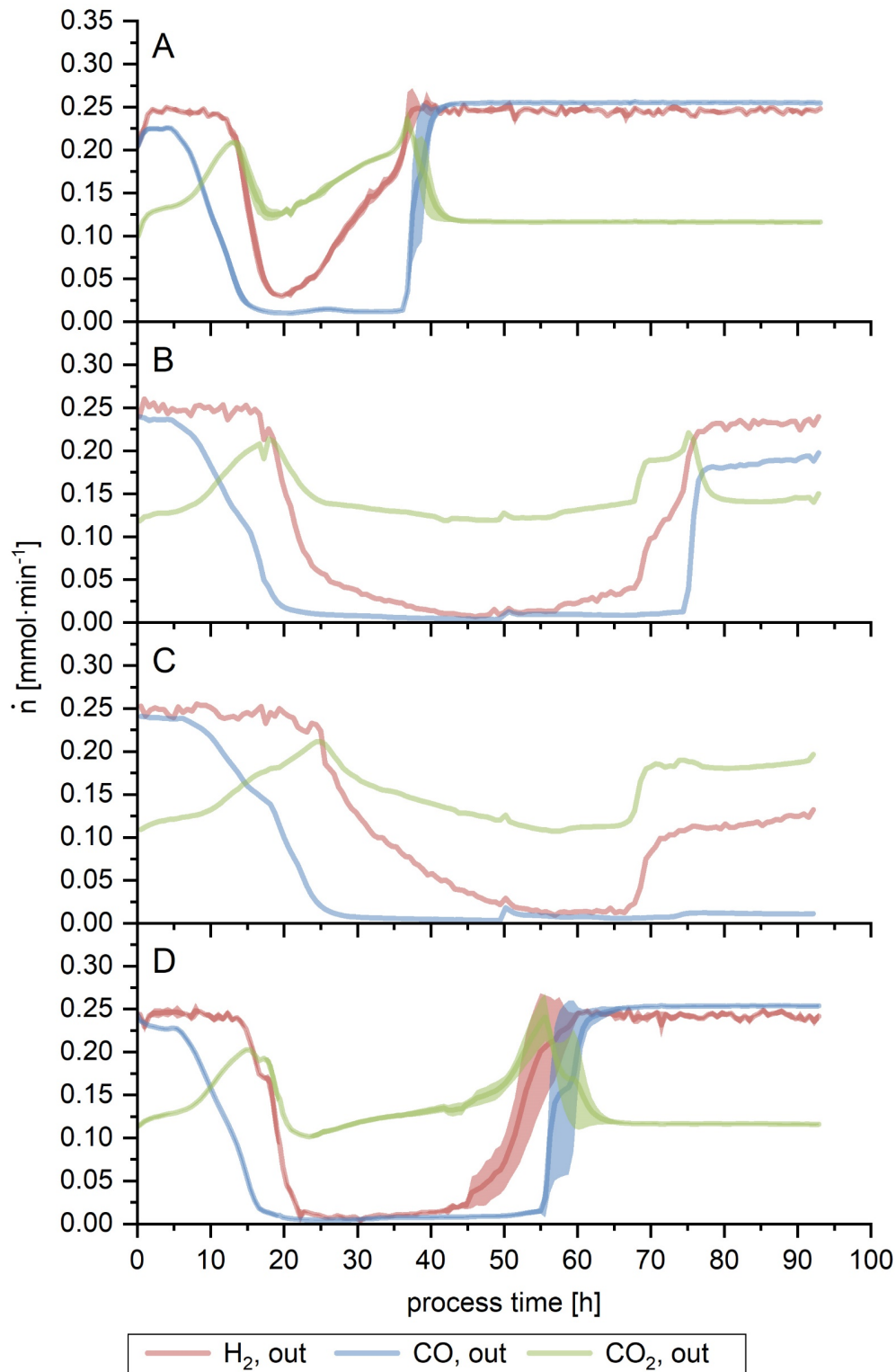


Figure A.II – Off-gas profile for setup 2 without pH regulation (A), setup 3b with increased cysteine and pH change to 5.4 after 68 h (B and C) and setup 5 with pH allowed to drop to 4.8 after 24 h (D). Figure B and C show each of the individual fermenter profiles due to the divergence observed between them: the second fermenter (C) is remarkably delayed. The amount of substance flow rates is shown here, as obtained from the measurements of the on-line GC, for H_2 (red line), CO_2 (green line) and CO (blue line). Lines show the average of a triplicate (except for figures B and C), while the lighter colored areas depict the standard deviation. (Infantes et al., 2020a)

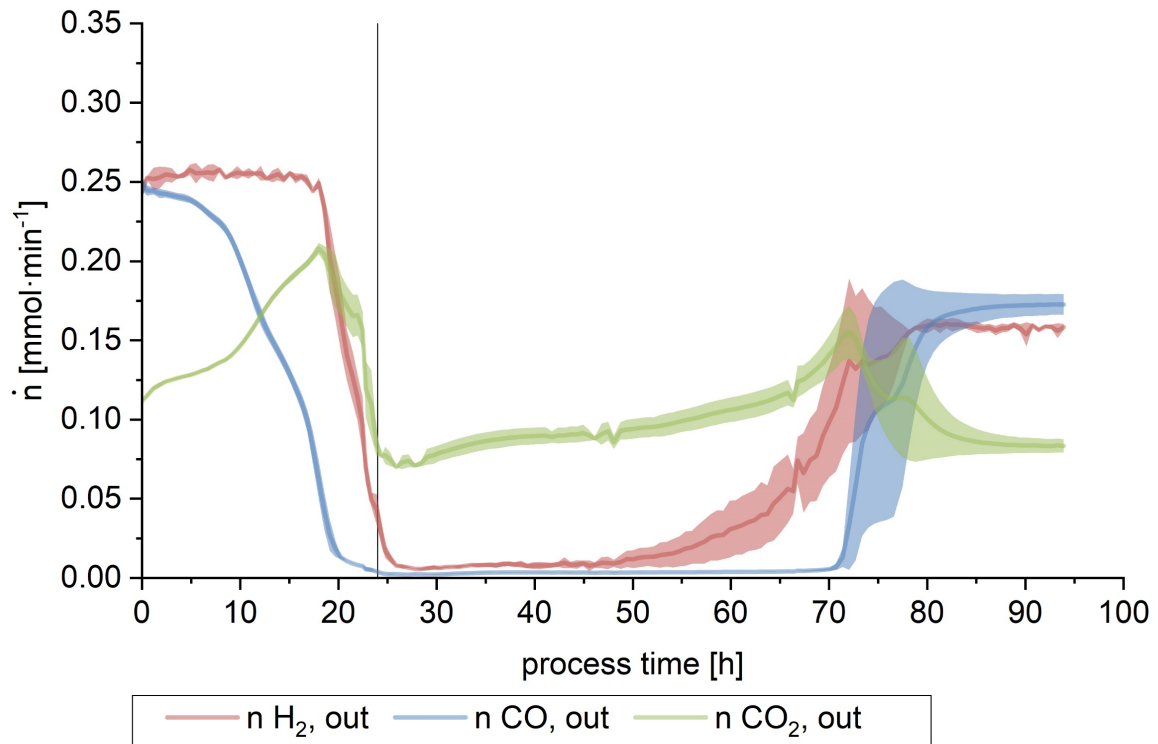


Figure A.III – Off-gas profile for setup 6, where pH was allowed to drop to 4.8 and gas flow was decreased to 12.6 mL/min after 24 h (vertical line). The amount of substance flow rates is shown here, as obtained from the measurements of the on-line GC, for H_2 (red line), CO_2 (green line) and CO (blue line). Lines show the average of a triplicate, while the lighter colored areas depict the standard deviation. (Infantes et al., 2020a)

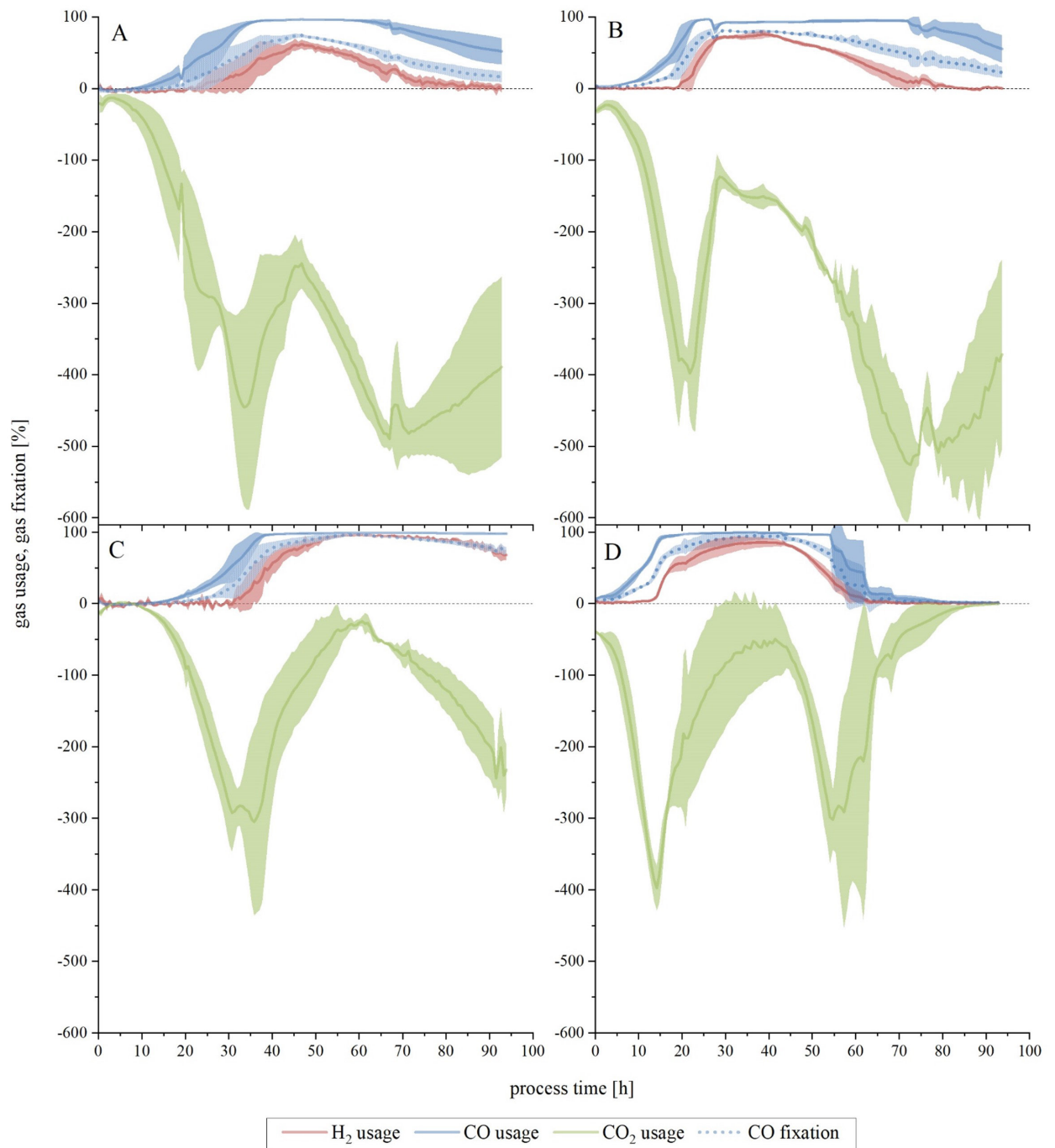


Figure A.IV – Complete substrate usage or fixation for setups 1 to 4. (A) to (D), in alphabetical order, refer to each individual setup, in numerical ascending order - (A) is setup 1, (B) is setup 2, etc. Usage is for H₂ (red line), CO₂ (green line) and CO (blue line). CO fixation is depicted by the dotted blue line. The calculated difference between amount of substance flow rate fed into the bioreactor and the amount of substance flow rate detected in the off-gas is shown here as a percentage. For CO fixation, if the CO₂ usage was negative, the amount of CO₂ produced was subtracted from the amount of (perceived) CO used. Lines show the average of a triplicate (n = 3), while the lighter colored areas depict the standard deviation. (Infantes et al., 2020a)